Tensile Properties of Loblolly Pine Strands Using Digital Image Correlation and Stochastic Finite Element Method

Gi Young Jeong

Dissertation submitted to the faculty of Virginia Polytechnic Institute & State University in partial fulfillment of the requirements for the degree of

Doctor of Philosophy
In
Wood Science and Forest Products

Dr. Daniel P. Hindman, Chair
Dr. Joseph R. Loferski
Dr. Audrey Zink-Sharp
Dr. Layne T. Watson
Dr. Surot Thangjitham

30 October, 2008
Blacksburg, VA

Keywords: earlywood, latewood, wood strands, digital image correlation (DIC), stochastic finite element method (SFEM)

Tensile Properties of Loblolly Pine Strands Using Digital Image Correlation and Stochastic Finite Element Method

Gi Young Jeong

ABSTRACT

Previous modeling of wood materials has included many assumptions of unknown mechanical properties associated with the hierarchical structure of wood. The experimental validation of previous models did not account for the variation of mechanical properties present in wood materials. Little research has explored the uncertainties of mechanical properties in earlywood and latewood samples as well as wood strands. The goal of this study was to evaluate the effect of the intra-ring properties and grain angles on the modulus of elasticity (MOE) and ultimate tensile strength (UTS) of different orientation wood strands and to analyze the sensitivity of the MOE and UTS of wood strands with respect to these variables.

Tension testing incorporating digital image correlation (DIC) was employed to measure the MOE and UTS of earlywood and latewood bands sampled from growth ring numbers 1-10 and growth ring numbers 11-20. A similar technique adjusted for strand size testing was also applied to measure the MOE and UTS of different orientation wood strands from the two growth ring numbers. The stochastic finite element method (SFEM) was used with the results from the earlywood and latewood testing as inputs to model the mechanical property variation of loblolly pine wood strands. A sensitivity analysis of the input parameters in the SFEM model was performed to identify the most important parameters related to mechanical response.

Modulus of elasticity (MOE), Poisson ratio, and ultimate tensile strength (UTS) from earlywood and latewood generally increased as the growth ring number increased except for the UTS of latewood, which showed a slight decrease. MOE and UTS from radial, tangential, and

angled grain orientation strands increased as the growth ring numbers increased while MOE and UTS from cross-grain strands decreased as the growth ring number increased. Shear modulus of wood strands increased as the growth ring number increased while shear strength decreased as the growth ring number increased. Poisson ratio from radial and angled grain strands decreased as the growth ring number increased while Poisson ratio from tangential and cross grain orientation strands increased as the growth ring number increased.

The difference of average MOE from different grain strands between experimental results and SFEM results ranged from 0.96% to 22.31%. The cumulative probability distribution curves from experimental tests and SFEM results agreed well except for the radial grain models from growth ring numbers 11-20. From sensitivity analysis, earlywood MOE was the most important contributing factor to the predicted MOE from different grain orientation strand models. From the sensitivity analysis, earlywood and latewood participated differently in the computation of MOE of different grain orientation strand models. The predicted MOE was highly associated with the strain distribution caused by different orientation strands and interaction of earlywood and latewood properties. In general, earlywood MOE had a greater effect on the predicted MOE of wood strands than other SFEM input parameters.

The difference in UTS between experimental and SFEM results ranged from 0.09% to 11.09%. Sensitivity analysis showed that grain orientation and growth ring number influenced the UTS of strands. UTS of strands from growth ring numbers 1-10 showed strength indexes (X_t, Y_t, and S) to be the dominant factors while UTS of strands from growth ring numbers 11-20 showed both strength indexes and stress components (σ_1, σ_2, and τ_{12}) to be the dominant factors. Grain orientations of strands were a strong indicator of mechanical properties of wood strands.

Acknowledgements

I am glad to have had this great opportunity provided during my Ph.D. time. I have met many great scholars and had priceless courses. I have also met incredible people in Virginia, especially Blacksburg, who have shown their hospitality and kindness. I feel a great jump that I could pretend to be a modest researcher. The wonderful experiences I have cannot be assembled into words and the piece of acknowledgement I am trying to make here.

Dr. Hindman, I do not know where I have to start. Your unstoppable guidance and patience has changed my learning behavior and attitude as a scholar. I realized every comment you have made turns out to improve my writing skills, logic, and generalizing problems that I have often faced. Your kindness and patience has helped to improve my English skills. During the over three years of my Ph.D. you have been a great mentor for me. I thank you for your generality on flexible working time, which boosted my capacity so that I could adjust my mood for taking classes, writing papers, testing specimens, organizing thoughts, and reading literature. You have been friendly to me and I sometimes consider you a close buddy of mine, who helped me share my thoughts freely. I believe your door has been open every day, which allowed me to talk to you as I needed. I thank you for giving me inspiration in every way.

Dr. Zink-Sharp, I thank you for your guidance on the digital image correlation technique and lending me your equipment which was an essential part of digital image correlation set-up. You have spent a great deal of time to encourage me to finish testing. I probably bother you too much. You have inspired me in the way how a scholar should be. Dr. Loferski, I would like to thank you for sharing with me your great experiences on wood mechanics and engineering. Your insight and wisdom impacted me greatly. I respect your kindness and care in personal relationships. Dr. Watson, I must thank you for sharing with me your academic knowledge on

numerical analysis. I thank you for your participation in every committee meeting eventhough you are busy and on sabbatical. I was impressed with your critical comments on my method and writing. Dr. Thangjitham, I thank you for sharing your comments on my method. The unique contribution from each committee member has helped me complete my Ph.D. work.

I must also thank the Brooks Center People, Angie, Will, Rick, and Kenny. You are kind and my friends. I always wanted to have brothers and sisters. You are my American brothers and sisters. Angie always greeted me with a smile and refreshed me with a cup of coffee. Will, you are my younger brother. Rick, I probably bother you too much on testing set up. You have always been kind to me and helped me to finish testing. Kenny Albert, you are such a gentle and nice man. I feel you are my American father. Your free hugs lighten my spirit and refresh me from tiredness.

I would like to thank my friends in Korea; Byung Hyn, Gwang Su, Ji Young, Ji Hoon, and Jong Sik. You are my good old friends who have the same soul and dwell in other bodies. You welcomed me whenever I would go back to Korea so that I would not feel remote.

Mom and Dad, you are my shadow that I always feel and the fact of your presence gives me energy to be mature. As an only child, I should have contacted and spent time with you more. I appreciate your patience and forgiveness.

I want to thank my wife, Yeonjeong. You have made our house feel like a real home so that I could rest after work. Even though you are a Ph.D. student and busy with many things, you have sacrificed your time to encourage me. Thank you for trusting in me and supporting me. I love You, Yeonjeong in every moment I feel.

Table of Contents

List of Figures

(Unless otherwise noted, all images are property of the author)

List of Tables

List of Symbols

Acronyms

BVS = Broadband Viscoelastic Spectroscopy

CCM = Concentric Cylindrical Model

CML = Compound Middle Lamella

CLT = Classical Laminate Theory

COV = Coefficient of Variance

CPT = Classical Plate Theory

DIC = Digital Image Correlation

DMA = Dynamic Mechanical Analysis

DSP = Digital Speckle Photography

ESEM = Environmental Scanning Electron Microscope

EW = Earlywood

EWP = Engineered Wood Products

FEM = Finite Element Method

FFT = Fast Fourier Transform

GMC = Generalized Methods of Cells

HM = Honeycomb Model

IB = Internal Bonding

LW = Latewood

LSL = Laminated Strand Lumber

LVL = Laminated Veneer Lumber

MC = Moisture Content

MCS = Monte-Carlo Simulation

MFA = Microfibril Angle

MOE = Modulus of Elasticity

MPM = Material Point Method

MOR = Modulus of Rupture

OSB = Oriented Strand Board

OSL = Oriented Strand Lumber

PSL = Parallel Strand Lumber

ROM = Rule of Mixture

SCL = Structural Composite Lumber

SFEM = Stochastic Finite Element Method

SG = Specific Gravity

TLT = Thick Laminate Theory

Chapter 1. Introduction and Background

Many natural and man-made materials exhibit different structure characteristics at different magnifications. In hierarchical structure materials, smaller structural elements combine to build larger structures. This structural hierarchy plays a major part in determining the bulk material properties. Understanding the effects of hierarchical structures can guide the synthesis of new materials with mechanical properties tailored for specific applications.

Fundamental characteristics of the structure of wood are arise from the existence of several hierarchical levels. The hierarchical structure of wood from nano to macro scale is displayed in Figure 1.1. At the nano-scale, three main chemical components (cellulose, hemicellulose, and lignin) build the fundamental structure of the wood cell wall. At the micro-scale, the wood cell wall can be largely differentiated into microfibril and matrix. Microfibrils are composed of cellulose and hemicelluloses, while the matrix is mainly composed of lignin. The wood cell wall includes different layers having different orientations of a filament-wound microfibril embedded in a matrix of hemicelluloses and lignin. Earlywood and latewood can be distinguished at this level by the different thicknesses of cell walls. Earlywood is the layers where wood grows during the early growing season, characterized by thiner cell walls and larger lumens. Latewood is the layer where wood grows during the late growing season, characterized by thicker cell walls and smaller lumens (Panshin and Zeeuw 1980). At the macro-scale, due to the earlywood and latewood, or intra-ring characters, a distinctive ring pattern can be noticed. Different cell wall characteristics are also found at different growth ring positions within a tree. Juvenile wood located near the pith has a higher microfibril angle and a thinner cell wall while

mature wood located near the bark has a lower microfibril angle and a thicker cell wall (Larson et al. 2001).

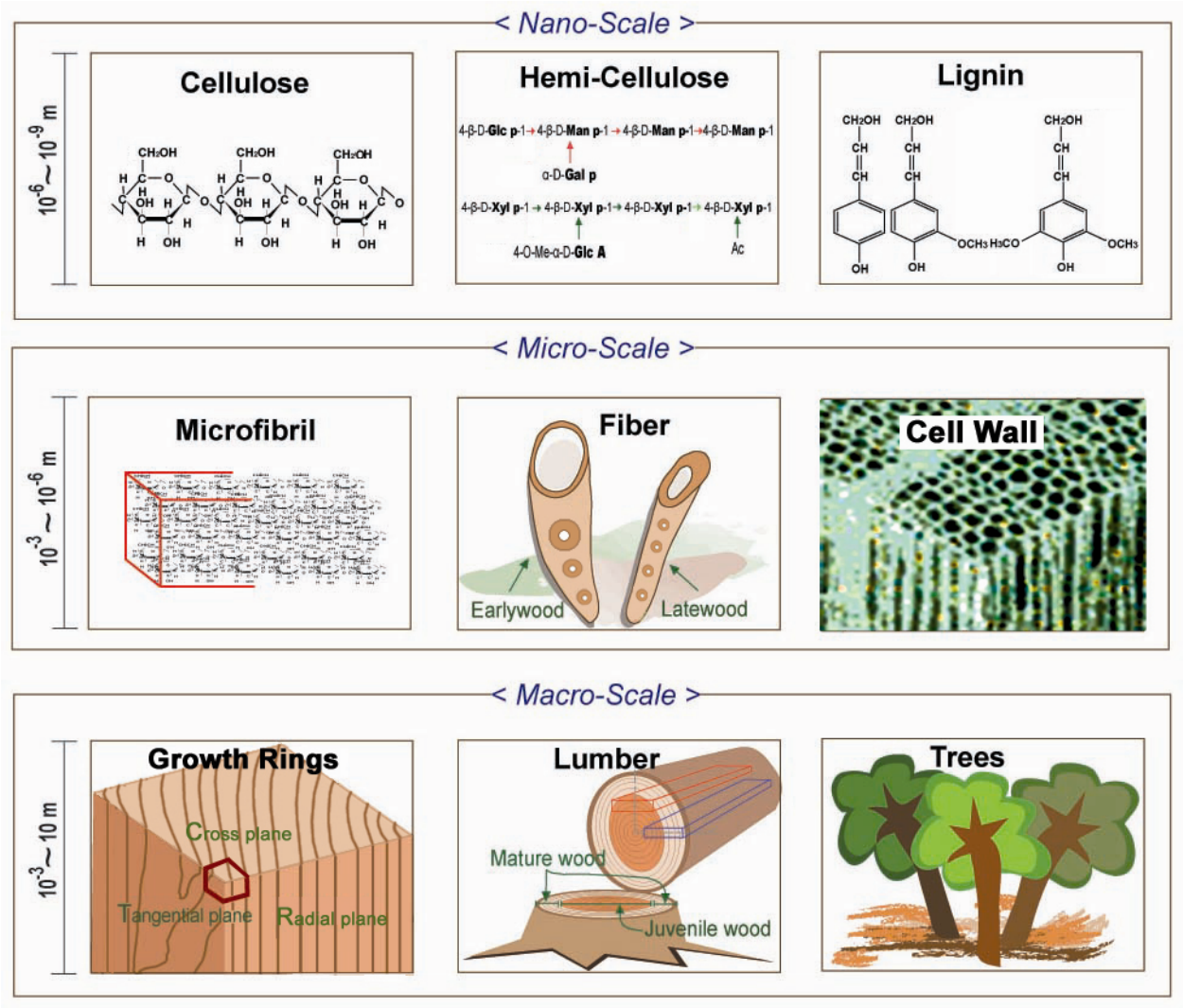

Figure 1.1 Hierarchical structure of wood showing wood characteristics at the macro, micro, and nano scale.

The hierarchical structure of wood has a large effect upon the mechanical properties of wood. Therefore, an understanding of wood structure characteristics at the different hierarchical

levels would help to use wood more efficiently. Detailed knowledge of these wood properties is not fully available for expanding the modeling of the mechanical behavior of wood continuously from the nano to the macroscale level at the current time. Many mechanical properties at the micro and nano scale levels are assumed for the wood structure. Most existing wood fiber models do not account for variation of chemical composition in the cell wall and different geometries of the wood cell wall. Models to predict mechanical properties of wood at the macro scale level could be improved by including the intra-ring characteristics.

In the U.S., the use of strands in oriented strand board (OSB) and structural composite lumber (SCL) production has increased. The modeling of wood strands can produce a better understanding of the mechanical properties of wood products. Properties of wood strands are related to the hierarchical composition of wood. This hierarchical structure varies throughout the different growth ring positions. Growth rings closer to the pith contain higher proportions of juvenile wood than growth rings closer to the bark. Juvenile wood differs from mature wood in that it has a higher microfibril angle, a greater percentage of compression wood, distorted grain patterns, and a less percentage of latewood (Larson et al. 2001). The deleterious effect of juvenile wood on the properties of wood strands is not well known. Understanding the wood strand as a fiber composite can help scientists understand the effects of juvenile wood on the mechanical behavior of wood strands.

Previous modeling of wood materials has included many assumptions of unknown mechanical properties associated with the hierarchical structure of wood. Also, experimental validation of those models did not account for the variation of mechanical properties. Little research has explored the uncertainties of mechanical properties at the earlywood, the latewood and at the strand sizes.

The goal of this study is to analyze the effect of the intra-ring properties and grain angles on the MOE and UTS of different orientation wood strands and to analyze the sensitivity of the MOE and UTS of wood strands with respect to these variables.

The objectives of this study include:

1) Evaluate the MOE and UTS of earlywood and latewood specimens from different growth ring numbers within one loblolly pine (*Pinus taeda*)
2) Evaluate the MOE and UTS of loblolly pine strands with different grain orientations (radial, tangential, and angled grain orientations)
3) Construct and validate stochastic finite element models (SFEM) of the wood strands incorporating three different grain orientations
4) Evaluate the sensitivity of the input parameters on MOE and UTS from the SFEM models

Digital image correlation (DIC) was employed to measure the MOE of earlywood and latewood bands and wood strands sampled from different growth ring positions. MOE and UTS of earlywood and latewood were measured by tension testing. A similar technique adjusted for strand size testing was also applied to measure the MOE and UTS of different orientation wood strands from the two growth ring numbers. Stochastic finite element method (SFEM) used the results from the DIC testing as input values to account the mechanical property variation of loblolly pine wood strands. A sensitivity analysis of the input parameters in the SFEM model was performed to identify the most important parameters related to mechanical response.

This dissertation is composed of eight chapters. Chapter 1 includes the introduction for

the entire project. Chapter 2 includes a comprehensive literature review on wood structure and mechanical properties of wood at different length scales. Chapter 3 evaluates the earlywood and latewood properties from growth ring numbers 1-10 and growth ring numbers 11-20 using digital image correlation (DIC). Chapter 4 reports on the longitudinal tensile properties of different orientation of loblolly pine strands from different growth ring numbers. Chapter 5 reports on the shear and transverse properties of loblolly pine strands from different growth ring numbers. Chapter 6 discusses the effective elastic properties of different orientation wood strands (radial, tangential, angled grain orientation strands) from different growth ring positions using stochastic finite element method (SFEM). Chapter 7 discusses the ultimate tensile strength (UTS) of different orientation wood strands from the different growth ring numbers using SFEM. Chapter 8 provides the conclusions of the disseration, including the summary, limitation of the study, and recommendations for future research.

Chapter 2. Literature Review

Use of strands in engineering wood products

This section discusses market growth, wood species, strand sizes, manufacturing methods, applications, and expected stresses under the service conditions for strand-based wood composite products. The use of wood in construction has changed over the last 25 years due to the development and production of engineered wood products (EWP). Specifically structural composite lumber (SCL) and oriented strand board (OSB) utilize a greater portion of the wood fiber in production compared to solid-sawn lumber. The OSB and SCL products are used as building members such as sheathing, headers, rimboards, columns, floor joists, and beams. According to the service conditions, strands are exposed to different stresses.

OSB is increasing in market share as a result of its lower cost compared to plywood. Since OSB is a newer product than plywood, there has been a steady improvement in processing methods, quality control, and performance (Smulski 1997). I-joist production in North America has grown 160% from 2000 to 2004 (Adair 2005). Schuler and Adair (2000) proposed that the main force driving the growth of these products in North America could be reasoned by prevalence of wood frame construction. The growth of these products in North American construction is very strong, and is expected to continue (Lam 2001). Figure 2.1 shows the growth of OSB and I-joist in North America from 2000 to 2004. The market growth of 0.95 cm (3/8 inch) OSB (million square feet) shows an increase 45% while I-joist (million linear feet) increases 160%. This tremendous growth shows the adaptability of these products for residential construction.

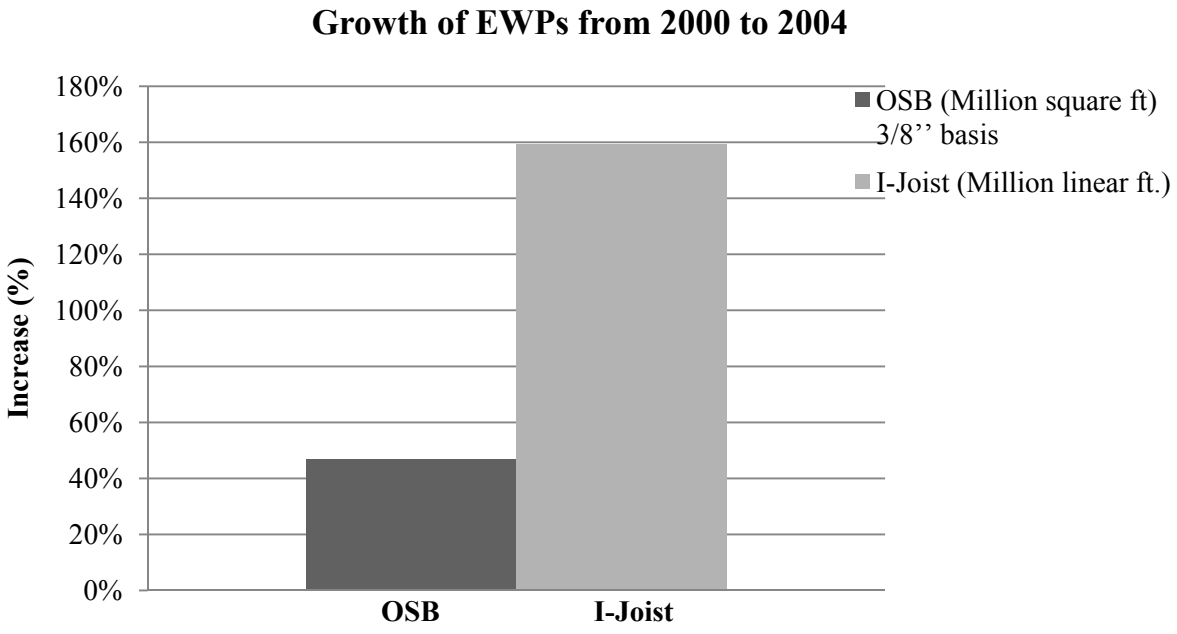

Figure 2.1 Growth of engineered wood products (Adair 2005)

OSB is commercially produced from various species including aspen (*Populus spp*.), Southern pine (*Pinus spp*.), and yellow-poplar (*Liriodendron tulipifera*). Strand sizes for OSB range from 8 to 15 cm in length and less than 0.8 mm in thickness. OSB typically has 3 or 5 layers of oriented strands. In OSB production, strands are mechanically oriented in pre-specified directions. Forming heads create distinct layers oriented perpendicularly with respect to each other. The mat is trimmed and sent to either a multi-opening press or a continuous belt press. Curing takes place at elevated temperatures. In some newly developed processes, boards are cooled prior to trimming and packaging (Smulski 1997). OSB typically has a density variation through the thickness direction. The density of face layer and core layer are 130% and 70%, respectively, of the average board density (Lam 2001). Through-thickness shear strength is approximately twice as high with OSB compared to that of plywood. OSB competes with plywood in applications such as I-joist web material, single-layer flooring, sheathing, and

underlayment in light-frame structures.

Green (1998) reported that the impetus for the development of a variety of SCL products has been the decreasing access to larger high quality logs, and industry commitments to better utilization of harvests. The development of SCLs has many advantages, such as using smaller trees, using waste wood from other processing, removal of defects, and creating more uniform components. Most composites have improved some mechanical properties compared to solid wood, and can be manufactured into different shapes. Compared to a 40% yield for solid sawn lumber from a log with bark, SCLs have higher yield than solid lumber. PSL, LSL, and OSB have 65%, 75%, and 80-90% yield, respectively (Schuler and Adair 2000 and Balatinecz and Kretschmann 2001).

Three types of SCL products are laminated strand lumber (LSL), oriented strand lumber (OSL), and parallel strand lumber (PSL). These products are produced using wood strands as the primary constituent material. Stranding slices the entire log into 7.62 cm to 30.48 cm strands. The strands are dried in a large rotary drum, where resin is applied. The strands are then dropped into a forming bin and pressed together to form the individual products. These products can be thin and flat sheets, like plywood, or long and wide, like lumber.

PSL is made from yellow-poplar (*Liriodendron tulipifera*) and Southern pine (*Pinus spp*.). PSL is sold commercially under the product name Parallam. Strand size for PSL is 3 mm thickness veneers cut to 100-300 mm long and 20 mm wide (Berglund and Rowell 2005). The strands are generally taken from veneers peeled from the outermost section of the logs, where stronger wood fibers are located. Veneers are dried to relative low moisture content and graded for strength before chopping into strands. The veneers are then aligned parallel to one another, coated with a waterproof adhesive, then pressed and cured using a radio frequency process to

form a rectangular billet up to 28 cm wide, 48 cm deep, and 20 m long. The varied profiles accommodate several applications, which include 45 mm wide piles to serve as built-up headers similar to LVL. Wider widths (65 mm, 133 mm and 178 mm) are well suited to longer span beams and headers. The even distribution of small defects in the individual strands allows for a considerably higher strength than is available from normally available solid timbers of the same cross section. The main application of PSL is for columns and beams (Smulski 1997). Due to the application of PSL, the significant portion of the stress exposed to strands is compression stress parallel to grain and bending stress.

Laminate strand lumber (LSL) is similar to OSB; however, compared to OSB, longer and slender strands (30 cm in length and 0.76~1.3 mm in thickness) are cut directly from whole logs (Berglund and Rowell 2005). LSL is sold commercially under the product name Timber Strand. LSL was produced from low grade logs (aspen, *Populus spp.* and yellow-poplar, *Liriodendron tulipifera*) that would not normally be used for conventional wood products. Manufacturing technique for LSL is similar to that used to produce OSB but using a polymeric diphenylmethane diisocyanate. The billet could be up to 140 mm thick, 2.4 m wide and 14 m long, after sanding, a large number of sizes are cut to suit applications such as headers, rimboard for floor systems, columns, joists, and studs (Smulski 1997). When LSL is used for headers, strands are mainly exposed to compression perpendicular to the grain and horizontal shear stress. However, LSL is used for rimboards, columns, joists, and studs, strands are exposed to other stresses such as crushing, compression parallel to grain, and bending stress.

Oriented strand lumber (OSL) is another type of strand composites whose strands are oriented in the length direction of the lumber. The strand size for OSL is 15.24 cm in length and less than 0.8 mm in thickness. OSL is mainly used for rimboards. The least dimension of the

board is less than 0.635 cm and the average length of OSL is between 75 and 150 times of the least dimension (Adair 2005). Since the rimboards are required to carry vertical load and to be able to transfer loads imposed by earthquake or winds, the board should be designed for preventing from crushing.

Prefabricated I-Joists, also known wood composite I-joists, are manufactured to optimize the bending stiffness of SCLs, similar to a steel I-beam. Wood I-joists are composed of a web connecting two flanges. Flanges can be solid sawn lumber, LVL or LSL. Webs use OSB or plywood. The length of the I-joist is limited by transportation restrictions which is about 20 m. The depth of the I-joist for residential applications can range from 24.1 cm to 40.6 cm (Adair 2005). Wood I-joists are used for floor joists and roof joists in residential and commercial constructions. The flanges are designed for bending stress and a good fastening surface for the sheathing. The web is designed to transfer shear stress from the flange.

In summary, the size of strands used in SCL and OSB varies from 8 cm to 30 cm long and from 0.8 mm to 3.2 mm thick. The strands used in SCL and OSB are exposed to different stress conditions. Therefore, optimization of strand size and geometry for different material may improve mechanical performance. In processing wood strands, understanding the effect of the geometry on the mechanical properties is crucial to maximizing the properties for the end use. Based on understanding, segregation into discrete categories can maximize the benefit of the wood strands for specific applications. The knowledge of wood strand geometry can lead to optimization in processing and utilization.

Hierarchical structure of wood

In contrast to most man-made composites, wood hierarchal structural levels span from

the nano-scale to the macro-scale. A wood fiber or tracheid shows a complex structure, which can be described as different layers with specific orientations of a filament-wound microfibril embedded in a matrix of amorphious or paracrystalline polymers-hemicellulose and lignin. From the viewpoint of material science, wood can be considered as a natural fibrous and cellular composite that is extremely heterogeneous and anisotropic. Navi et al. (1994) mentioned "the physical and mechanical behavior of wood can be best understood by reference to its microstructure and its chemical constituents". The following sections discuss important characteristics of wood at the different scales which affect the mechanical behavior of wood.

Nano-scale properties of wood

The nano-scale level is defined as the range of size from 1×10^{-6} to 1×10^{-9} m which includes the chemical composition of wood cells. Cellulose, hemicellulose and lignin are the main components of the composite cell wall layers. Even though their individual structure is well known, there is still a lack of information regarding their arrangement (Salmen 2004).

Cellulose is the main constituent of wood. Cellulose is a homopolysaccharide composed of β-D-glucopyranose units which are linked together by (1→4)-glycosidic bonds (Panshin and Zeeuw 1980). Approximately 40-50% of the dry substance in most wood species is cellulose, located predominantly in the secondary cell wall. The cellulose is highly crystallized and hydrophobic. Cellulose is also the main component of the microfibrils, which provides stiffness of wood in both the longitudinal and transverse directions.

Hemicelluloses are amorphous carbohydrates made of a group of heterogeneous polymers. Hemicelluloses make up about 20-30% of the dry weight of wood. The hemicellulose is highly hydrophilic. Hemicellulose may act as an adhesive between cellulose and lignin. In the cell wall,

hemicelluloses are closely associated with both cellulose and lignin. Hemicelluloses serve as the matrix (or skeletal framework) in which the cellulose microfibrils are embedded. Hemicellulose also provides support for the cell wall but to a much lesser degree than cellulose (Panshin and Zeeuw 1980). Hemicelluloses influence significantly the moisture absorption behavior of wood because of the high hydroxyl content and amorphous character. Without the presence of hemicellulose, there would be no interaction between the lignin and cellulose in wood, making a poor composite. The same is true for wood fiber plastic composites, where a coupling agent is needed to improve the interface between the fiber and plastic, which otherwise would not associate well with one another (Sjostrom 1993 and Fengel and Wegner 1983). The mechanical function of hemicellulose is to act as a buffer to recover the elastic properties even beyond yield point (Keckes et al. 2003).

Lignin is a heterogeneous three-dimensional polymer that constitutes approximately 30% of the dry weight of wood. Lignin limits the penetration of water into the wood and makes the wood compact. Lignin serves as a cementing material in the wood cell wall. It is primarily found in the middle lamella and the secondary wall. In the secondary wall, lignin acts as a matrix surrounding the cellulose fibers. Moreover, because of its high rigidity, lignin imparts strength and stiffness in compression and in shear.

The mechanical properties of cellulose, hemicelluloses, lignin composed in wood cells are tabulated in Table 2.1. Elastic properties of three main components were studied by different researchers using various methods. Sakurada et al. (1962) and Matsuo et al. (1990) determined longitudinal elastic modulus of ramie cellulose using x-ray diffraction. Mark (1967) estimated longitudinal elastic modulus of cellulose using a cellulose chain model. Mark (1967) and Cave (1978) estimated transverse elastic modulus of cellulose using cellulose model. Cousins (1976)

and Cousins (1978) determined the elastic modulus of hemicelluloses and lignin from extracted radiata pine (*Pinus radiate*). Bergander and Salmen (2002) estimated the shear modulus of hemicelluloses and transverse elastic modulus of lignin assuming the ratio of longitudinal elastic modulus (E_L) to transverse elastic modulus (E_T) was 2.0 for hemicelluloses and lignin. As shown in Table 2.1, cellulose and hemicellulose were treated as a transverse isotropic material while lignin was treated as an isotropic material. Cellulose has a much higher stiffness than hemicellulose and lignin. All three chemicals have a higher longitudinal modulus (E_L) than transverse modulus (E_T) and shear modulus (G_{LT}). The elastic ratio of cellulose is calculated to be E_L: E_T: G_{LT} = 25.2-30.6: 4.0-6.0: 1.0. The elastic ratio of hemicellulose is calculated to be E_L: E_T: G_{LT}=4.6: 0.8-2.0: 1.0. The elastic ratio of lignin is calculated to be E_L: E_T: G_{LT} = 2.6-4.6: 1.3-2.6: 1.0. Poisson ratio of three chemical components has similar trends with the elastic ratio. For cellulose Poisson ratio, the ratio of υ_{TR} (tangential-radial) to υ_{LR} (longitudinal-radial) ranged from 5.2 to 11.0. For hemicellulose Poisson ratio, the ratio of υ_{LR} to υ_{TR} ranged from 1.3 to 2.0. For lignin Poisson ratio, the ratio of υ_{LR} to υ_{TR} was 1.0. Compared to the average elastic ratio assumed for solid sawn lumber of E_L: E_T: G_{LT} = 20.0: 0.875: 1.0 (Bodig and Jayne 1992), the main chemical components elastic ratio was quite different because the different percentage of these chemical components in the cell wall affected the elastic properties of the cell wall. Most wood fiber modeling has used elastic properties of the chemical components and the percentage of the chemicals in the cell wall to calculate the elastic properties of the wood cell wall.

Table 2.1 Elastic properties of cellulose, hemicellulose, and lignin at 12% moisture content

Constituent	E_L (Gpa)	E_T (Gpa)	G_{LT} (Gpa)	ν_{LR}	ν_{TR}
Cellulose	134[a], 113.5[b], 120-135[c], 138[d]	27.2[b], 18[e]	4.5[b]	0.1[b], 0.047[e]	0.52[e]
Hemicellulose	8[f]	3.5[e], 1.4-3.5[g]	1.75[g]	0.3[e], 0.2[g]	0.4[h]
Lignin	2.0-3.5[h], 2[i]	1[g], 2[i]	0.76[b]	0.3[h]	0.3[h]

[a]Sakurada et al. (1962), [b]Mark (1967), [c]Matsuo et al. (1990), [d]Nishino et al. (1995), [e]Cave (1978), [f]Cousins (1978), [g]Bergander and Salmen (2002), [h]Persson (2000), [i]Cousins (1976)

Wood can be thought of as a reinforced composite, similar to reinforced concrete. The cellulose microfibrils act as rebar, lignin acts as the aggregate, and hemicellulose acts as the portland cement binder. The microfibril (cellulose) provides the tensile strength parallel to its length while the matrix provides the compression and shear resistance. The mechanical behavior of wood is a combination of high elasticity of the cellulose under short-term loads and plastic flow of the hemicellulose and lignin under long-term loads, which is different from most other structural materials.

Since the mechanical behavior of wood is related to the arrangement of chemical components in the wood cell, many researchers developed models to represent the arrangement of cellulose, hemicelluloses, and lignin to understand physical and mechanical behavior of wood better. Bonart et al. (1960) proposed the cable model of cellulose describing several crystallites and the non-crystal monomers in one microfibril. Frey-Wyssling and Muhlethaler (1965) suggested the microfibril concept describing perfectly crystalline elementary fibrils fastened to make purely crystalline microfibrils. Hearle (1963) suggested a fringed model describing microfibrils consist of extended chains, folded chains, fringed fibrils, or fringed micelles all having different strength and elastic properties from one another.

Fengel (1984) described a unit cell model that the six of the crystalline polymer of cellulose (β-D glucose) were located with or without some occasional substitutions of mannose for glucose residues (hemicelluloses) in random or periodic form. The hemicellulose associated with the microfibrils exhibits some degree of orientation and introduces crystal order defects in cellulose. The rest of space is filled by mainly lignin. Any unit volume of wood cell wall on the size order shown in the model can be described as a filament reinforced composite. Since the fiber wall is built up of layers of such filament reinforced matter, it is also accurate to describe it as a laminated composite.

Kerr and Goring (1975) have concluded on the basis of electron microscope studies that the cell wall has an interrupted lamella structure where the dimension of a given lignin or carbohydrate entity is greater in the tangential direction of the fiber wall than in the radial direction. The hemicellulose not only exists as a matrix around the microfibrils but is present in the lignin-containing entities. One of the most important aspects of the cell walls is the angle that the cellulose microfibrils make with the long axis of the cells known as microfibril angle (MFA). This is now generally acknowledged as one of the main determinants of stiffness in wood.

Salmen and Olsson (1998) used a dynamic mechanical analysis (DMA) to analyze the effect of hemicelluose on softening wood pulp. The main conclusion was that hemicelluloses were associated with both cellulose and lignin. Xylan was associated with lignin and glucomannan was associated with cellulose. Akerholm and Salmen (2003) used polarized infrared measurement to show the orientation of lignin. The conclusion was lignin had preferred orientation with the other orientated cell wall components.

Xu et al. (2007) used dual-axis electron tomography to analyze the cellulose microfibrils from the delignified cell wall of radiata pine (*Pinus radiate*) earlywood. Cellulose microfibrils in

the S_2 layer were measured at 3.2 nm in diameter, which appears to be an unstained core 2.2 nm and ~0.5 nm outer layer of residual hemicelluloses and lignin.

Many researchers have syudied the arrangement of three main chemical components of wood cells using experiments and modeling at the nano-scale level. Although the exact arrangements of three chemical components in wood cell have not been found yet, more sophisticated models for the association of three components have developed. Bergander and Salmen (2002) used an improved model for the chemical association as inputs to the analytical models for wood fibers. These results proved that more realistic chemical arrangements for modeling of wood cells provided more accurate predictions of mechanical properties. However, more information on the modeling of wood at this scale is needed for more reliable results.

Micro-scale properties of wood

The micro-scale level is defined as the range of 1×10^{-3} to 1×10^{-6} m including the wood cell wall and earlywood and latewood fibers. Cellulose microfibrils constitute the main structural elements of tracheid cell walls. Microfibrils are arranged into organized layers within each cell wall layer distinguished by different helical arrangements of their microfibrils. Microfibril angle (MFA) was considered one of the main determinants of wood quality (Cave and Walker 1994). MFA was also known to influence the fracturing properties of wood with small angles favoring transwall as opposed to intrawall fracturing on tangential longitudinal surfaces under transverse shear (Donaldson 1996). The MFA within individual tracheids showed little variability along the length of the tracheid, with variation being less in latewood tracheid than in earlywood tracheids (Susan et al. 2002).

Figure 2.2 shows the ultrastructure of a single wood cell wall with different layers. There

are five main layers consisting of the middle lamella, the primary layer, and three secondary layers (S_1, S_2, and S_3). The middle lamella is mainly composed of lignin and acts as a bond between the fibers. The primary wall is thin and its components are not considered structurally functional. Therefore these two layers are often combined and called compound middle lamella (CML). The thickness of CML is from 0.5 to 1.6 micrometers thick. The secondary wall layers, S_1, S_2, and S_3 are all mechanically important. Each layer in secondary wall has different microfibril angle adapted to environmental conditions.

The most obvious difference in the layers of the secondary wall is the angle of the microfibrils. The S_1 is only 0.1 to 0.35 micrometers thick and the average angle of 60 to 80 degrees. The S_2 layer is 1 to 10 micrometers thick and the average angle about 5 to 30 degrees. The S_3 layer is only 0.5 to 1.1 micrometers thick and the average angle of 60 to 90 degrees (Plomion et al. 2001).

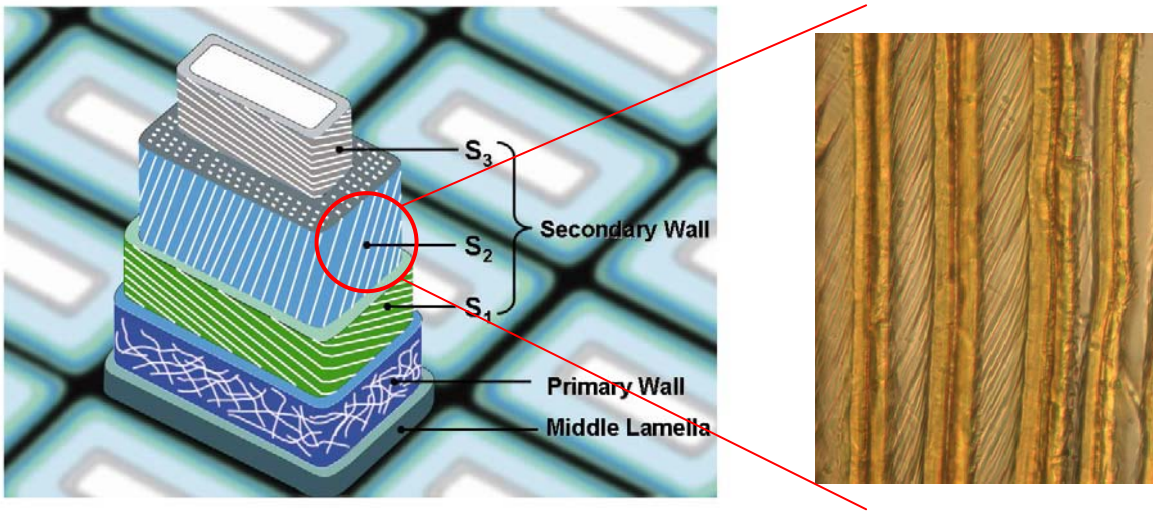

Figure 2.2 Ultrastructure of wood cell wall showing middle lamella, primary wall and secondary wall (S_1, S_2, and S_3)

Since the S_2 layer is much thicker than other cell wall layers, the physical and chemical properties of the cell wall is dominated by S_2 layer (Watson and Dadswell 1964, Cave 1968, 1969, Wood and Goring 1971, Siddiqui 1976, and Evans et al. 1996). In contrast, the S_1 and S_3 layers are very thin; nevertheless, the S_1 and S_3 layers are thought to have a crucial role in strengthening the cell against deformation by water tension forces in the living tree, as well as contributing to the hardness and crushing strength of timber (Booker 1993, Booker and Sell 1998). The MFA of the S_2 layer in the tracheid cell wall is considered to be a significant factor influencing the mechanical properties of wood, especially the modulus of elasticity (Harris and Meylan 1965). The distribution of the main chemical compositions through the cell layers are shown in Table 2.2. Many analytical models have used different chemical proportions in different cell wall layers to calculate the modulus of individual cell wall layers.

Table 2.2 Composition of the S_1, S_2, and S_3 layers expressed as weight fractions (%) of wood constituents from Fengel and Wegener (1983)

Constituent	S_1	S_2	S_3	CML
Lignin	30%	27%	27%	71%
Hemicellulose	35%	15%	15%	20%
Cellulose	35%	58%	58%	9%

Figure 2.3 shows three sections of Southern pine (*Pinus spp*.). Two distinctive diameters of wood cells, cell walls, and lumen sizes or interior cell areas can be seen in the cross section. Thin cell walls and large lumens can be seen from the upper half in the cross section, normally called earlywood. Thick cell walls and small lumens can be seen from the lower half in the cross section, normally called latewood. Because of the anatomical structural differences, the mechanical properties of these two are also different.

Tracheids with an oval shaped bundle of ray cells and resin canals can be seen from the tangential section. The cross section of ray cells is shown in that tangential section since the ray cells are aligned perpendicular to the tangential plane. In a radial section, one or more rows of cells run cross tracheids. These cells are called ray cells. The rays are composed of parenchyma cells storing food and conducting fluid radially, reinforcing the stiffness of the radial section.

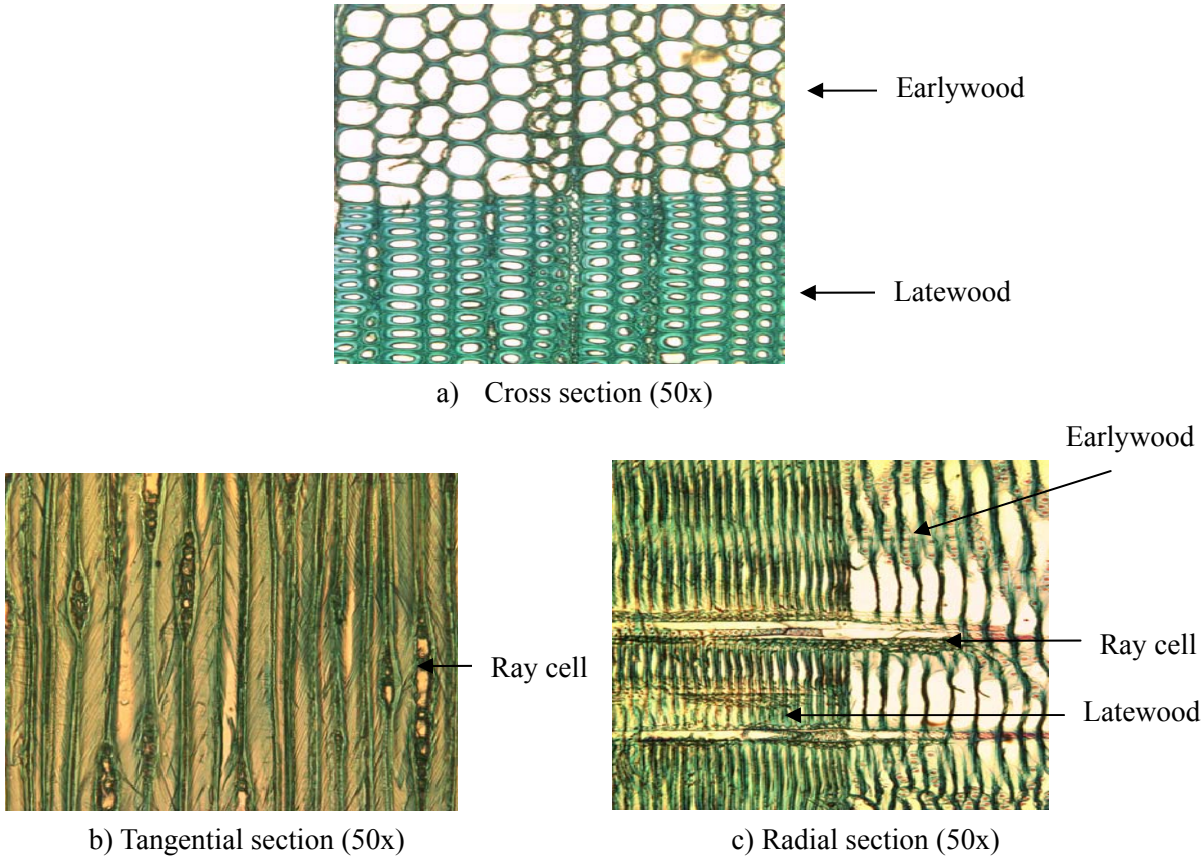

Figure 2.3 Three sections of Southern pine (*Pinus spp*).

a) cross section showing earlywood and latewood b) tangential section showing tracheids with the cross section of ray cells c) radial section showing the earlywood and latewood layers

Taylor and Moore (1980) studied the growth effects of loblolly pine (*Pinus taeda*) on the radial tracheid diameter and cell wall thickness from earlywood and latewood. These results are

summarized in Table 2.3. Radial tracheid diameter of earlywood increased 4.7% as growh ring numbers increased from 1-10 to 11-20. Radial tracheid diameter of earlywood increased 7 % as growth ring numbers increased from 1-10 to 21-30. Radial tracheid diameter of latewood only increased 2.4% as growh ring numbers increased from 1-10 to 11-20. Radial tracheid diameter of latewood only increased 3% as growh ring numbers increased from 1-10 to 21-30. The cell wall thickness of earlywood increased 4.4% as growth ring numbers increased from 1-10 to 21-30. The cell wall thickness of latewood increased 6.3% as growth ring numbers increased from 1-10 to 21-30.

Table 2.3 Radial tracheid diameter and cell wall thickness of loblolly pine as a function of growth ring (Taylor and Moore 1980)

Growth Ring		Radial tracheid diameter (μm)	Wall thickness (μm)
1-10	EW[1]	52.8	4.5
	LW[2]	32.8	9.4
11-20	EW	55.3	4.6
	LW	33.6	9.4
21-30	EW	56.7	4.6
	LW	33.8	10.0

EW[1]: earlywood, LW[2]: latewood

Growth increments stand out in wood to varying degrees because of growth intensity, and consequently the cell size, arrangement and density of the wood produced are not uniform throughout the growing year. Earlywood has a density of about 280 kg/m^3. Latewood has a density of about 600 kg/m^3 (Larson et al. 2001). The transition between the earlywood and latewood may be gradual or abrupt, giving rise to differentiations between wood species. The different density of earlywood and latewood are related to different cell wall diameters and cell wall thickness. The elastic properties of earlywood and latewood were highly related to density

and MFA (Cramer et al. 2005). From the results of linear regression analysis by Cramer et al. (2005), specific gravity and MFA explained 75% of the accuracy of the elastic modulus value for latewood, but less than 50% of the accuracy for earlywood. The mechanical properties of the wood cell wall, therefore, are highly dependent upon MFA, cell wall diameter, and wall thickness.

Macro-scale properties of wood

The macro-scale level is defined as the range of about 1×10^{2} m to 1×10^{-3} m including the intra-ring level composed of earlywood and latewood, strand level and full-size composites. Because of the manner of the tree growth and the arrangement of wood cells within the stem, wood has three orthogonal axes. These three axes are used to construct the radial (R), the tangential (T), and the longitudinal axes (L) shown in Figure 2.4. The orthogonal axes form three planes known as the cross section, radial section, and tangential section. The cross section is the plane formed by R,T directions that is exposed when wood is cut or sawed at right angles to the longitudinal axis of the tree stem. The radial section is exposed plane of L, R axes when the cut follows a radius of the cross section of the lumber, and along the axis of the lumber. Lumber cut so that the wide face of the board is principally radial is called quarter-sawn or edge-grained. The tangential section of wood is exposed plane of L,T axes when the bark is peeled from a tree. In a log this surface is curved. In sawn or sliced material, when the cut is made tangentially, the exposed surface is flat, representing a chord of the curved surface under the bark. The section is so aligned that the central part of the wide surface of the board is approximately tangent to the growth rings. Lumber cut so that the wide face of the board is tangential is said to be plain or flat-sawn. Rotary-cut veneers from the surface of the log are tangential at most points on their faces.

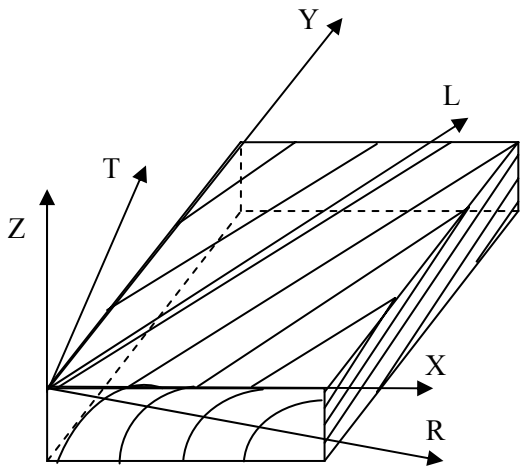

Figure 2.4 The schematic illustration to define the global coordinate axis (X, Y, Z) and material principal axis of wood (R, L, T).

The longitudinal direction is parallel to the direction of the fibers (tracheids) and has the highest elastic stiffness and strength. The wood is somewhat stronger and stiffer in the radial direction compared to the tangential direction. These strength differences are related to the ultrastructure of wood (Bergander and Salmen 2002). However, the fibers are rarely aligned with the main direction of the tree growth. Therefore it is important to define the material coordinate system and global coordinate system (X, Y, Z) for the determination of mechanical properties of wood in Cartesian coordinate system (Figure 2.4). Figure 2.4 shows grain orientations are defined as material principal directions-R, L, T. Hermanson et al. (1997) transform the global coordinates (X, Y, Z) to material principal axis (R, L, T) to analyze the effect of three surface angles on the orthotropic properties of a cross grain lumber. From numerical analysis, the elastic properties were significantly changed by change of the ring angles. The stresses were also affected by different grain angles. The failure behavior of the material would expect to be affected by the different grain angles.

As a material formed by nature, wood has a complex mechanical behavior. Natural differences in properties are caused by genetics and dissimilar growth conditions such as climate, type of soil and growth terrain. The density of the wood is affected by those same factors (Larson et al. 2001). From the micro-scale section, the differences in cross-sectional cell wall thickness between earlywood and latewood fiber also result in density variations affecting the mechanical properties.

Table 2.4 shows the average earlywood and latewood fiber lengths according to growth increments of loblolly pine from Taylor and Moore (1980). The growth increment of both earlywood and latewood fiber lengths were 38.3% and 31.8% from the fifth growth increment to fifteenth growth increment. Earlywood and latewood fiber lengths decreased from 4.6% to 0.2%, respectively, as the growth ring position was from fifth to fifteenth. Table 2.4 shows differences in fiber length not only between latewood and earlywood, but also between growth ring positions. The mechanical properties could be varied across growth ring positions due to different fiber lengths (Larson et al. (2001), Bentdsen and Senft (1986), Taylor and Moore (1980)).

Table 2.4 Average earlywood and latewood fiber length, and specific gravity in the fifth growth and fifteenth increment of a loblolly pine (Taylor and Moore 1980)

	Earlywood tracheid length (mm)	Latewood tracheid length (mm)	Difference of earlywood and latewood fiber length[2] (%)
Specific gravity	0.28	0.6	
Fifth growth increment	3 mm	3.14 mm	4.6%
Fifteenth growth increment	4.15 mm	4.14 mm	0.2%
Difference of fiber from different growth ring position[1] (%)	38.3%	31.8%	

[1]%Diff = (Fifteenth growth increment-fifth growth increment)/fifth growth increment×100%
[2]%Diff = (Earlywood fiber length-latewood fiber length)/earlywood fiber length×100%

Cramer et al. (2005) proposed that specific gravity and MFA were strong indicators of elastic properties of earlywood and latewood. The average E_L and G_{LT} of earlywood were 4.34 and 0.77 GPa, respectively. The average E_L and G_{LT} of latewood were 9.88 and 1.59 GPa, respectively. The modulus of elasticity increased with the increment of ring number and height while shear modulus increased with ring number but decreased with height. Table 2.5 shows the average ratio of LW/EW in E_L was 2.3 and the average ratio of LW/EW in G_{LT} was 2.0. Within-ring variation in E_L was as large as within-bolt variation. The coefficient of variance (COV) of E_L of LW/EW from upper bolts (6m) and lower bolts (1m) were 52% and 47%, respectively. The coefficient of variance (COV) of E_L of LW/EW from ring 3 and ring 18 were 42% and 34%, respectively.

Table 2.5 Variation of mechanical properties of earlywood and latewood of loblolly pine from different growth ring number and height (Cramer et al. 2005)

	E_L (COV)	G_{LT} (COV)	SG (COV)	MFA (COV)
LW/EW all specimen	2.3 (51%)	2.0 (38%)	1.9 (26%)	1.0 (29%)
LW/EW: upper bolts (6m)	2.7 (52%)	2.3 (35%)	2.1 (25%)	1.1 (37%)
LW/EW lower bolts (1m)	2.1 (47%)	1.8 (37%)	1.8 (25%)	1.0 (25%)
LW/EW ring 3	1.6 (42%)	1.6 (41%)	1.6 (34%)	1.1 (25%)
LW/EW ring 18	2.7 (34%)	2.0 (29%)	2.0 (11%)	1.0 (24%)

Mature wood and juvenile wood

Wood properties can vary widely from pith to bark. The first 10-20 growth rings from the pith are termed juvenile wood, while the portion of wood near the bark is called mature wood (Zobel and Sprague 1998). Large differences in the chemical content could be found in a single tree. Juvenile wood had a high xylose content while mature wood had a high lignin content. The content of extractives, lignin and pentosan decreased with increasing distance from pith while cellulose content increased (Uprichard 1971). Sugar analyses showed that the xylan and mannan content of the juvenile wood was higher, while mature wood contained more cellulose (Harwood 1971). The schematic location of juvenile wood and mature wood is described in Figure 2.5.

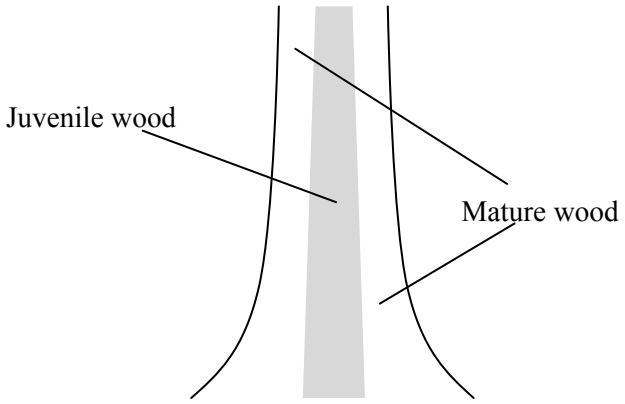

Figure 2.5 Schematic description for the location of juvenile and mature wood in a tree

Many researchers have studied the effect of juvenile wood on mechanical properties of wood and wood-based composites. Values for tensile strength, bending modulus of rupture (MOR), and bending modulus of elasticity (MOE) of juvenile wood were less than mature wood due to higher MFA, shorter tracheid length, and lower specific gravity (Bendtsen 1978, Panshin and de Zeeuw 1980, Smith and Briggs 1986, Cave and Walker 1994). Moody (1970) found that the tensile strength of juvenile wood from southern pines was 34% lower than mature wood. MacDonald and Hubert (2002) found the elastic modulus of the fibers from juvenile wood was

less than that of the fibers from mature wood. From the shape of the stress-strain curve, the fibers from mature wood linearly increase until failure, while the fibers from juvenile wood showed a nonlinear behavior (Rowland and Burdon 2004). Table 2.6 shows the SG, MOE, and MOR from two different aged trees. As ring number increases, the modulus of rupture (MOR), modulus of elasticity (MOE), and specific gravity (SG) increase. The differences of MOE and MOR of two different age groups are as large as 37% and 24%, respectively, demonstrating that there is a large effect of using wood fiber from different aged trees and from different ring positions.

Table 2.6 Comparison of the average specific gravity, MOE, and MOR from the average number of rings of two different age trees (Pearson and Ross 1984).

Number of rings from pith	Specific gravity		MOE (GPa)		MOR (MPa)	
	15 year old tree	25 year old tree	15 year old tree	25 year old tree	15 year old tree	25 year old tree
0	0.38	0.4	4.4	6.06	50.05	62.60
2	0.39	0.43	7.17	9.03	61.91	73.08
5	0.44	0.47	9.37	10.55	78.6	90.32
10	0.517	0.5	11.3	14.34	95.84	115.14

Bentdsen and Senft (1986) reported that the average MOE of mature wood (23 + years) was five times higher than that of juvenile wood and the average MOR of mature wood was three times higher than that of juvenile wood. Pearson (1988) found that MOE and crushing strength of nominal 2 by 4 in. lumber from juvenile wood were 37% and 52% less, respectively, compared to mature wood. McAlister et al. (1997) investigated bending and tensile properties of different ages (22, 28, and 40 years) of loblolly pine lumber. The stiffness, strength, and specific gravity of loblolly pine lumber increased with increasing age, but only the tension stiffness values were statistically significant at an α of 0.05. Kretschmann (1997) studied the effect of ring orientation and percentage of juvenile wood of loblolly pine on shear parallel to grain and

compression perpendicular to grain strength. The shear and compression strength decreased with an increase in percentage of juvenile wood.

In mature loblolly pines, the MFA of the S_2 layer is small, averaging about 5 to 10 degrees as measured by deviation from the vertical. In juvenile wood, the MFA is large, averaging 25 to 35 degrees and often up to 50 degrees in rings next to the pith, then decreasing outward in the juvenile core. Ying et al. (1994) found that MFA in tracheids of fast grown loblolly pines decreased from 33 degrees at age 1, to 23 degrees at age 10, and to 17 degrees at age 22. Bendtsen and Senft (1986) reported that loblolly pines had not yet attained stable MFA at age 30. Figure 2.6 shows the change of MOR, MOE, and MFA by year. While the MOR and MOE increased 1.6 and 4 times respectively from 1 year to 15 years, MFA was generally decreased 40%. Therefore, there is an inverse relationship between mechanical properties and MFA.

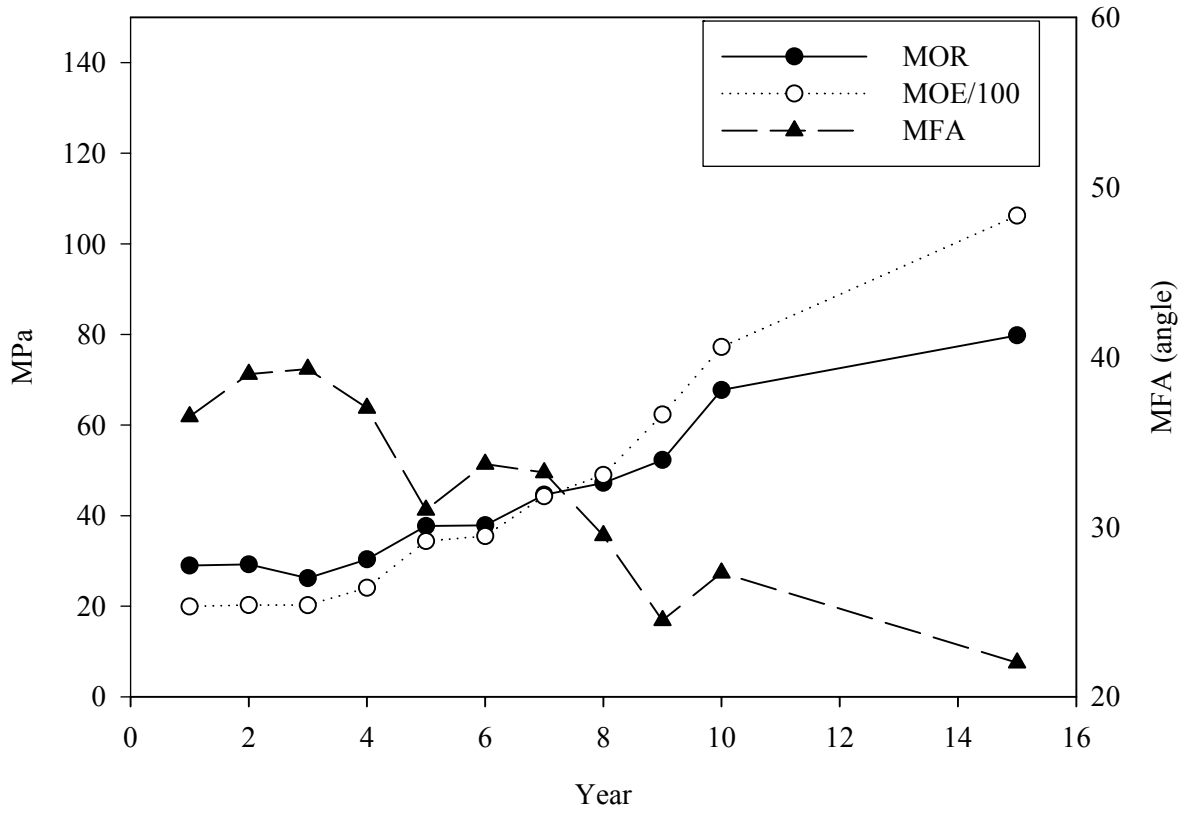

Figure 2.6 The average properties of loblolly pine by age (Bentdsen and Senft 1986)

Geimer and Crist (1980) studied mechanical properties of flake board manufactured from short-rotation trees. The bending stiffness and strength of randomly distributed flakeboard was 3.1 GPa and 27.0 MPa, respectively. Alignment of face flakes increased MOE and MOR in the direction of alignment to maximum values of 6.55 GPa and 48.0 MPa, respectively. Geimer et al. (1997) studied the effect of juvenile wood on linear expansion, water adsorption, and thickness swell of flakeboard. Boards made from juvenile wood had lower adsorption and thickness swell. Geimer (1986) found boards made from seven years old wood material had higher internal bond properties compared to boards made from six years old wood material. Wasnewski (1989) identified a 10% increment of the bonding stiffness and strength as the age of wood increased

from 1 to 50 years. The effect of packing density and horizontal density grades was associated with thicker flakes and lower density of the younger material. A 30 to 40% increase of stiffness and strength was found with lumber as the wood age increased from 1 to 50 years. Pugel et al. (1990) and Pugel et al. (1989) manufactured composite boards from loblolly pine of different ages. Composite boards made from juvenile wood had similar mechanical properties (MOE, MOR, and interal bond strength) to boards made from mature wood. Thickness swell and linear expansion of boards made from fast-grown tree were significantly higher than those of boards made from mature wood. However, the compaction ratio was higher in boards made from juvenile wood compared to boards made from mature wood to achieve the same mechanical properties. Board properties are determined by wood properties (age and anatomical properties) and manufacturing properties (compaction ratio, density grade, and particle size). Reduction in selected mechanical properties of parallel laminated veneer made from larch containing juvenile wood was reported by Jo et al. (1981). Members fabricated with 100% juvenile wood had 90% of the compression strength, 70% of the bending strength, and 70% to 80% of the block shear strength of members made with 100% mature wood. Juvenile wood could have ten times higher shrinkage compared to maturewood due to the higher MFA.

This section presented the hierarchical structure of wood, which varies between different growth ring positions. The mechanical properties of wood and wood-based composites are affected by the structure characteristics of wood. This research focused on the effect of the intra-ring properties and grain orientations of strands on the mechanical properties of wood strands. The following sections provide modeling work on wood at different hierarchical scales considering some of the hierarchical structure of wood.

Previous mechanical models of wood

Many previous researchers have studied the mechanical behavior of wood at different hierarchical scales using different methods. Micromechanics, laminate theories and finite element methods (FEM) have been used to determine the mechanical properties of wood. Failure theory has been incorporated to determine the strength of wood at the various scales. Most modeling work has bridged the different scales of wood. For instance, Bergander and Salmen (2000 and 2002) used chemical composition as an input for the models to predict the elastic behavior of the wood cell. Based on the chemical composition in cell wall layers, the stiffness of individual cell wall layers can be calculated using the rule of mixtures at the nano scale of wood. The stiffness of individual cell walls can be transformed according to MFA in each layer. The effective modulus, stress, and strain can be calculated using laminate theory at the micro scale. Most previous analytical models followed these steps.

However, analytical models of wood fiber suffer from limited information on the irregular shape of wood cells and approximations of both the chemical composition in cell walls and the MFA in each cell wall. To overcome the irregular shape of wood fibers, numerical methods were employed such as finite element method (FEM) and material point method (MPM) at the macro scale. However, many assumptions are required to model wood at this scale. For instance, transverse properties of cell wall stiffness must be assumed because of a lack of measurement capability. Many previous researchers assumed boundary conditions of cell walls in their laminate analogy model for predicting wood fiber properties. Previous finite element models for wood fibers could not represent the elliptical shape of wood fibers and different geometries of wood fibers.

Therefore, the results of these models were limited by the previously described

assumptions to predict mechanical properties of wood strands and strand-based composites. The variability of mechanical properties of wood also must be considered in modeling. As previously mentioned in the hierarchical structure of wood section, there can be a large variability in the mechanical properties of wood. Model results accounting for mechanical property variability are more reliable. The next section summarizes modeling efforts at different hierarchical scales of wood.

Previous modeling work on wood fibers

Previous analytical modeling of wood fibers has included a flat plane laminate, tube like composite, and honeycomb model with different angle layers. Muench (1938) emphasized the helical winding of microfibrils in the cell wall, considered the cell wall to be composed of several sets of helical springs embedded in a matrix of nanocrystalline material. One of the earliest mechanical models for wood fiber was suggested by Mark (1967) and Schinewind (1966). These models considered the different layers in the tracheid cell wall and developed a cell-wall model based on the concept of a laminated structure. Adaptation of laminate theory to predict the mechanical behavior of wood cell was done by Salmen and de-Ruvo (1985). The effect of different wood polymers on the wood cell walls included the longitudinal and transverse properties. Table 2.7 provides the summary of previous modeling on mechanical behavior of wood at the micro scale.

Table 2.7 Summarized previous studies on mechanical behavior of wood at the micro scale

Researcher	Theory	Objective	Result/Conclusion
Mark (1967)	CLT[1] ROM[2]	Development of tracheid cell wall model.	Failure occured at S_1 or S_1-S_2 layer due to high stress concentration.
Salmen and de-Ruvo (1985)	CLT Halpin-Tsai	The effect of different wood polymers on wood cell walls.	S_1 and S_3 layer played an important role in determining the elastic constants when microfibril angle of S_2 layer was high.
Bergander and Salmen (2002)	CLT Halpin-Tsai	The effect of cellulose, hemicellulose and lignin on elastic modulus of cell wall properties.	This model considered the orthotropic properties of hemicelluloses and lignin and showed a better fit with the results from experimental tests. The thickness and fibril angles of the S_1 and S_3 layers were also found to be important parameters for the transverse properties of the fiber.
Gassan et al. (2006)	TLT[5]	Consideration of the elliptic geometry and hollow structure of the cross section of fiber to calculate elastic properties of natural fibers.	A more realistic cross section of fiber was taken into account and provided more accurate results.
Tang and Hsu (1973)	CCM[3]	The relationship between microstructure and elastic constants of cell walls to describe mechanical behavior of Virginia pine wood fiber.	If all the properties of MFA, ratio of filament, and matrix are similar between species, the spacing of microfibrils in each layer would affect the mechanical properties of wood fiber. Not only the MFA of the S_2 layer, but also the MFA of the S_3 layer affected the strength of wood fiber.
Neagu et al. (2006)	CCM	Model incorporating ultrastructural morphology to analyze stiffness and stress distributions in the cell wall of spruce fiber.	Micromechanical modeling and analytical modeling were combined to predict the effect of the ultrastructure on the mechanical behavior of wood fibers.

Gibson and Ashby (1988)	HM[4]	Link the physical properties of cellular solids to their density and complex microstructure.	At low densities, experimental results indicated that the Young's modulus (E) of cellular solids is a function of their density (ρ) through the relation $E=C\rho^n$. However, the Poisson ratio was independent of density.
Watanabe (1999)	HM	The determination of geometries for earlywood for seven species of softwood.	Bending and stretching of wood cells showed agreement between the prediction from the model and results from experimental test.
Persson (2000)	FEM[7]	A single fiber behavior under tension.	Twisting-extension coupling and coupling between in-plane shear and out-of-plane rotation were increased with higher MFA in S_2 layer.
Perre (2005)	FEM	Development of a meshpore software.	Capability of generating image-based mesh for heterogeneous or porous media.
Wilhelmsson et al. (2006)	FEM	Imported geometrical data of tracheids of Norway spruce into the finite element method.	The difference of mechanical behavior of models was highly dependent upon the irregularity of the cell wall structure. The difference of the results was mainly induced that analytical model doesn't count the irregularity of the wood fiber and twisting-extension coupling by MFA.
Nairn (2005)	MPM[8]	The effect of anatomy features on deformation and elastic-plastic properties of different wood species.	MPM had an advantage over foam theory because foam theory could not take into account the irregular geometry of wood cell.

[1]CLT: Classical laminate theory, [2]ROM: Rule of mixture, [3]CCM: Concentric cylinder model, [4]HM: Honeycomb model, [5]TLT: Thick laminate theory, [6]TOE: Theory of elasticity, [7]FEM: Finite element method, and [8]MPM: Material point method

Tang and Hsu (1973) studied the relationship between microstructure and elastic constants of the cell wall using composite theory. Wood cell walls were modeled as cylindrical shapes with different layers to describe Virginia pine (*Pinus virginiana)* wood fibers. The ratio of microfibril to matrix in each cell wall was assumed. If the properties of microfibril, ratio of filament, and matrix were similar between species, the spacing of microfibrils in each layer was

the main factor in the mechanical properties of wood fiber. Tang and Hsu (1973) concluded that not only the microfibril angle of the S_2 layer but also the microfibril angle of the S_3 layer affected the strength of wood fiber. A larger extensibility was found for fibers with larger MFA. A remarkable increase occurred in maximum strain and a decrease in the elastic moduli with increasing MFA was found. (Reiterer, Lichtenegger, Tschegg, and Fratzl 1999).

Bergander and Salmen (2000) studied the transverse mechanical properties of wood. Ray cells were found to have an important role in transverse mechanical properties of the cell wall. The S_1 and S_3-layer and partly S_2-layer affected the transverse modulus which was found to have a large variation. Even in the transverse direction, the S_2 layer plays an important role in determining the elastic constant with high microfibril angle of the S_2 layer (Mark 1972, Salmen and de Ruvo 1985). Bergander and Salmen (2002) investigated the effect of cellulose, hemicelluloses, and lignin on elastic modulus of cell wall properties using two different sets of input data. One model assumed isotropic properties while the other model assumed orthotropic properties. Comparison of results from these two models showed little difference in longitudinal modulus evaluation, while the model including the orthotropic elastic constants of hemicellulose and lignin gave a more accurate transverse modulus.

Gassan et al. (2006) suggested a thick laminate tube model to represent cell walls. The thick laminate tube model considered the elliptic geometry and hollow structure of the cross section of a wood fiber to calculate elastic properties. Elastic properties in the axial direction decreased as the spiral angle increased. The stiffness of fiber linearly increased with the increase of cellulose content. The results of this model were more accurate when a realistic cross section of fiber was taken into account.

A honeycomb model was suggested by Gibson and Ashby (1988). The shape of the

model can be modified by changing the angle between the radial cell wall and tangential cell wall, and radial cell wall length and tangential cell wall length. The model was used by Moden (2006) to simulate transverse loading. Classical beam theory was used to describe in-plane mechanical properties of the honeycomb model. However, this model was not able to provide different properties of each layer of the wood cell wall (S_1, S_2, and S_3). The honeycomb model assumed that a uniform stress occurred through the transverse direction, which is not true for the wood cell wall. The honeycomb model was modified by adjusting the angle according to experimental data by Kahle and Woodhouse (1994). Determination of geometries for earlywood for seven species of softwood was conducted by Watanabe (1999). The model presented the behavior of bending and tension, and the agreement between the model predictions and results from experimental testing was good.

Persson (2000) used the finite element method (FEM) to model a single fiber under tension. Twisting-extension coupling and coupling between in-plane shear and out-of-plane rotation increased with higher MFA in the S_2 layer. A three-dimensional finite element model for wood cell wall was developed by Magistris (2005). Perre (2005) developed a meshpore software which has the capability of generating an image-based mesh for heterogeneous or porous media. Wilhelmsson et al. (2006) imported geometrical data from Norway spruce (*Picea abies*) tracheids into the finite element software and created a solid model and a shell model. Comparing these models with analytical model results, Wilhelmsson et al. (2006) found that the difference of mechanical behavior between the models was highly dependent upon the irregularity of the cell wall structure. The analytical model does not account for the irregularity of the wood fiber and twisting-extension coupling by MFA. Angeles et al. (2006) suggested a theoretical model to predict the elastic properties of *Urticaceae* wood using its chemical

composition. ASTM D 143 bending for small clear samples was used to verify this model, with good agreement. Neagu et al. (2006) used a composite cylinder assemblage model incorporating ultrastructural morphology to analyze the stiffness and stress distribution in the cell wall of a spruce fiber. This analytical model was compared to results from the FEM and stress function approach based on the theory of Lekhnitskii (Lekhnitskii 1963). Combining micromechanical modeling and analytical modeling to predict the effect of the ultrastructure on mechanical properties of wood is fruitful if confident understanding of the mechanical behavior of wood fiber is not achieved.

A two dimensional material point method (MPM) was applied to analyze transverse crack propagation in wood (Nairn 2005). This numerical method falls into the category of meshless methods. Algorithms were applied to digitized images of wood to separate earlywood and latewood layers. After creating a fixed grid to track the deformation of the image, stress and strain could be calculated based upon cellular movement. The disadvantages of this method were that the hierarchical structure of wood was not considered and wood is not treated as an orthotropic material. Nairn (2005) studied the transverse compression behavior of loblolly pine (*Pinus taeda*), ponderosa pine (*Pinus ponderosa*) and yellow poplar (*Liriodendron tulipifera)* using the material point method (MPM). The biggest advantage of MPM was the ability to accurately describe the complex geometry of wood anatomy. Radial and tangential loading were applied to evaluate the effect of deformation on anatomical features and the elastic-plastic properties of different wood species. MPM results were compared with results from a foam theory model. Overall, Nairn (2005) concluded that MPM had an advantage over the foam theory model because foam theory cannot account for the irregular geometry of a wood cell.

Wood strand modeling

Although several models have bridged the nano-scale to micro-scale of wood, only one article was found to link from the micro-scale to the macro-scale of wood. Hindman and Lee (2007) studied the stiffness of three different geometries of strands from loblolly pine (*Pinus taeda*) using the finite element method (FEM) and the rule of mixtures. Experimental measurements of earlywood and latewood elastic stiffness were used to generate inputs for strand models. Both a cellular model and a solid finite element model were used to represent wood strands. Tension and bending loading were conducted to verify the models. The model incorporating the intra-ring properties produced a better fit with the results from experimental tests compared to the homogeneous model. A cellular model showed less stress concentration occurs between intra-rings compared to the solid model. FEM models using earlywood and latewood properties from experimental results increased the accuracy of the prediction of strand properties compared to considering earlywood and latewood sections as homogeneous.

Wood strand based board modeling

Many previous models for wood strand-based composites were found. The main approaches included the finite element method (FEM), the Monte Carlo simulation, and classical laminate theory (CLT). Input variables for models included dimensions of strands, strand orientation, and other manufacturing parameters such as drying simulation and hot-pressing characteristics. The main results were effective modulus and strength of strand based composite material. Previous research on strand-based composite models was summarized in Table 2.8. However, no model was accounted for the effect of intra-ring properties on stiffness and strength of the composite.

Table 2.8 Summary of previous research on wood-based composite modeling

Researchers	Theories	Variables	Outputs	Main Results
Wang and Lam (1998)	FEM, Monte Carlo, Weibull weakest-link theory	Length of strands	Probability of tensile strength of parallel aligned strand board	A strength modification factor and the number of layers of multiple ply veneer composite
Lu (1999)	Monte Carlo	Distribution of strands and void area	Mat formation	Simulation of flake orientation, distribution and location of void sizes, number of strand crossings and horizontal density distribution
Clouston and Lam (2002)	FEM, Monte Carlo, Tsai-Wu failure criteria with flow rule	Strength and stiffness properties of material	Probability of effective elastic modulus and strength	Stochastic strength modeling of strand-based composites.
Lee and Wu (2003)	CLT, Von-Mises probability density function	Flake alignment distribution, flake weight ratio	Effective engineering constants	The effect of processing variables on mechanical properties of OSB.
Yadama et al. (2006)	Fiber undulation theory	In-plane and out-of-plane strand orientation	Elastic properties	Strand undulation angles degrades the MOE of laminate in both tension and compression.
Shu et al. (2006)	CLT, Tsai-Wu failure criteria, probability distribution theory	Dimension of strands, drying parameters, pressing parameters	Mat formation, pressure distribution during pressing, stress and strain distribution through thickness	Integrated modeling on wood-based composite simulations.

Wang and Lam (1998) used a three dimensional nonlinear stochastic finite element method to simulate strength distribution of parallel aligned strand board. The main variable for the model was the length of the strands. The effects of resins, pressing, and other factors on the strength of strand-based composites were defined using a non-linear least square fitting process associated with the stochastic finite element method. From this nonlinear fitting process, a strength modification factor was calibrated to adjust model results. Tensile strength from experimental tests agreed well with the results from multilayer models.

Lu (1999) used a simulation program (*Winmat*) based on the Monte-Carlo simulation technique to compute the mat formation of strands. In modeling the mat formation, the horizontal distribution of overlap and density, free flake length, distribution of void sizes, and the degree of orientation of flakes were considered. Computer simulations, robot mat formation, and X-ray scanning techniques were used to verify the model. Similar works related to mat formation can be found in Dai and Steiner (1994), Suginori and Lam (1999), Kruse et al. (2000), Zhang et al. (2005).

Goel et al. (1999) invented a wood based composite simulation (WBCSIM) environment to enhance the manufacturing process for wood-based composites based on strength. The program includes rotary dryer simulation (RDS), radio-frequency pressing (RFP), oriented strand board mat formation (MAT), hot compression, and composite material analysis (CMA). Since then, other researchers have been involved in further development of WBCSIM. Shu et al. (2006) described the improved WBCSIM and future work to create a better manufactured wood-based composite.

Lee and Wu (2003) used the classical laminate theory combined with Von-Mises probability functions to predict the mechanical properties of OSB. For both single and three-

layer OSB, the random orientation of flakes were simulated using transformation of certain invariant components (Tsai and Pagano 1968) to evaluate laminate elastic modulus, Poisson ratio, and linear expansion coefficients. Experimental tests were conducted to verify these results.

Clouston and Lam (2001, 2002) constructed a three dimensional stochastic finite element model to predict the strength of strand based wood composites. Random stiffness and strength were used as inputs for the finite element model that were incorporated with the orthotropic plastic failure theory, the Tsai-Wu failure criteria, and plastic flow rule. The numerical results agreed well with the results from experimental tests.

Yadama et al. (2006) studied the effect of undulation angle on the elastic properties of wood-strand composites made of yellow-poplar. Undulation angle was represented using a Fourier series. While compression test results were only 2-4% different from the result of the compression models for maximum undulatory angles of 4 and 8 degrees, tension test results showed 12 % greater than the result of the corresponding the tension model. In general, the model results showed that as undulation angle increases, effective modulus of laminate decreases.

Mechanical property evaluation methods of wood materials

This section summarizes the experimental tests to measure the elastic properties of wood fiber and wood strands. The study of mechanical properties of natural cellulosic fibers has largely focused on testing of macromechanical properties of stress and strain. There is a need for measurement of the strain within wood strands to improve the mechanical analysis of wood composites. Also, the measurement of mechanical properties is used for validation of many mechanical models from the previous section. Lee and Wu (2003) mentioned that “without full understanding of the properties of strands with dimensions similar to those used in strand

composite manufacturing, there is no reliable prediction of mechanical and physical properties of the strand composite". Deomano and Zink-Sharp (2004) proposed that "quality of any wood composite product depends heavily upon the quality of the raw materials used". Cramer et al. (2005) emphasized that the variation of mechanical properties of earlywood and latewood ultimately affected the mechanical behavior of the wood product. The knowledge of mechanical properties of the earlywood and latewood fibers and strands can lead to better strength and performance of strand based wood composites.

Mechanical properties measurement of earlywood and latewood fibers.

Strength properties of single wood fibers have gained interest in recent years. Details of sample preparation and test-set up can be found in the previous studies (Groom et al. 2002, Mott et al. 2001, Mott et al. 2002). Table 2.9 lists previous research showing differences in mechanical properties of earlywood and latewood from micro-tensile testing results. Although some previous works on evaluation of mechanical properties of earlywood and latewood fiber from different species were found, Table 2.9 is limited to pine and spruce species. While the present values from Navi et al. (1994), Mott et al. (2002), Groom et al. (2002), and Burgert et al. (2003) are the average longitudinal elastic modulus (E_L) of earlywood and latewood fiber and the average strength (σ_y) of earlywood and latewood fiber, the mechanical properties of a small specimen of earlywood and latewood were presented from Cramer et al. (2005)

Table 2.9 Previous works on wood fiber test showing test conditions and results

Researchers	Species	Loading speed [μm/min]	Average E_L (earlywood) [GPa]	Average σ_y (earlywood) [MPa]	Average E_L (latewood) [GPa]	Average σ_y (latewood) [Mpa]
Navi et al. (1994)	Sitka spruce (*Picea sitchensis*)	10-4	1.2-1.9	4.23-6.65	3.3-4.1	8.44-11.03
Mott et al. (2002)	Lobolly pine (*Pinus taeda*)	80	14.8	604	N/A	N/A
Groom et al. (2002)	Loblolly pine (*Pinus taeda*)	80	N/A	N/A	6.55-27.5	410-1,422
Burgert et al. (2003)	Spruce fiber (*Picea abies*)	30-150	10 [1]	530[1]	N/A	N/A
Cramer et al. (2005)	Loblolly pine (*Pinus taeda*)	N/A	4.34	N/A	9.88	N/A

[1]Transition zone between earlywood and latewood in mature wood portion

Navi et al. (1994) performed microtensile testing with a cyclic loading to measure the stiffness and strength of earlywood and latewood fibers of Sitka spruce (*Picea sitchensis*). The loading speed was 4-10 μm/min. The load-extension curve showed three distinctive behaviors. Linear elastic behavior was observed at first stage of loading. Beyond yield point, the specimen became less stiff and underwent a large, irreversible deformation. Finally, as the load increased further, the load-deformation curve exhibited the third stage shown by a significant change in slope.

Mott et al. (2002) studied mechanical properties of earlywood fibers of loblolly pine (*Pinus taeda*) using a 5N capacity load cell with a loading speed of 80 μm/min. Mature earlywood fibers were much stiffer than juvenile earlywood fibers. The MOE and ultimate strength of juvenile earlywood fibers were 11.7 GPa and 496 MPa while those of mature earlywood fibers were 17.2 GPa and 648 MPa respectively. MFA for juvenile was from 25 to 30 degrees and MFA for mature wood was from 5 to 10 degrees. Based on the results, Mott et al. (2002) concluded that MOE and strength were dependent upon MFA.

Groom et al. (2002) measured the stiffness and strength of latewood tracheids of loblolly pine (*Pinus taeda*) in different growth ring position and height of the tree. The stiffness of latewood fiber is increased with the ring number. The stiffness of latewood increased from 6.55 GPa to 27.5 GPa as the ring number increased from the pith to mature area. The strength of latewood increased from 410 MPa to 1,422 MPa as the growth ring position switched from pith to mature portion.

Burgert et al. (2002) combined a video extensometry with a micro tensile tester to determine the stiffness and strength of mature spruce fiber (*Picea abies*) in transition zones. Displacement was measured using a video extensometer instead of cross head deflection as specimen displacement. This method provided a more reliable MOE value. The MOE and UTS were 10 GPa and 530 MPa, respectively.

Cramer et al. (2005) used a broadband viscoelastic spectroscopy instrument (BVS) to measure the MOE and shear modulus of earlywood and latewood of six loblolly pine (*P. taeda*) trees. Samples with the size of 1 mm × 1 mm × 30 mm were obtained from different growth ring numbers and heights (1.5 m and 6 m). The MOE of earlywood increased from 3.5 GPa to 5.1 GPa as the height of tree increased from 1.5 m to 6 m. The MOE of latewood increased from 8.1 GPa to 13.0 GPa as the height of tree increased from 1.5 m to 6 m. Shear modulus increased with growth ring number, but decreased with height.

Eder et al. (2006) conducted micro-tensile testing using environmental scanning electron microscopy (ESEM) to analyze the fracture behavior of latewood fibers of spruce (*Picea abies*). A 500 mN load cell was used with test speed of 0.5 μm/s. The fiber had a tendency to twist even though torsional deformation was restricted by fixation to the test device.

Axial elastic modulus of wood strands.

Previous studies showed different testing set-ups to evaluate the longitudinal elastic modulus and strength of strands from different species. The dimension of specimen and loading speed were also not identical. Since the test set-up and sample species were different, the comparison of test results from different researchers is difficult. Table 2.10 shows the previous research on strand testing with wood species, dimensions, loading speed, moisture content, specific gravity, ultimate strength, and elastic modulus (E_L). As can be seen from Table 2.10, the loading speed and dimension of the specimens are different from previous studies.

Table 2.10 Previous research on the evaluation of mechanical properties of wood strands from different species

Researcher	Species	Dimension (cm×cm×cm)	Loading speed (cm/min)	Moisture content (%)	Specific gravity	Ultimate strength (MPa)	Modulus of elasticity (GPa)
Price (1975)	sweetgum (*Liquidambar styraciflua L.)*	7.62×0.95×0.038	0.0063-0.016	7	0.58	89.5	11.3
Geimer et al. (1985)	Douglas-fir (*pseudotsuga menziesii*)	5.71×1.27×0.038	0.0127	12	0.46	36.8	6.16
Hunt et al. (1989)	Yellow-poplar (*Liriodendron tulipifera L.)*	30.48×1.27×0.079	0.19	6.0-8.0	0.50	70.3	11.8
Deomano and Zink-Sharp (2004)	Southern Yellow Pine, sweetgum, and yellow-poplar	2.5×0.5×0.06	0.254	10.3^1 12.0^2 9.5^3	0.58^1 0.64^2 0.58^3	66.0^1 78.6^2 89.0^3	4.1^1 4.4^2 5.8^3
Wu et al. (2005)	Southern Pine (*Pinus spp*.)	15.24×2.54× 0.38	N/A	11	0.58	49.98	12.84
Zink-Sharp and Price (2006)	sweetgum (*Liquidambar styraciflua L.*), yellow-poplar,	0.4×0.1×0.1	0.0029	12.4^2 12.2^3 11.9^4	0.48^2 0.44^3 0.51^4	39.2^2 33.5^3 41.6^4	N/A

	(*Liriodendron tulipifera L.*), soft maple (*Acer rubrum*)						
Cai et al. (2007)	Yellow-poplar (*Liriodendron tulipifera L.*), loblolly pine (*Pinus taeda*), willow (*Salix spp.*), and red oak (*Quercus spp.*)	15.24×2.54×0.105	0.0127	6.97[3] 5.66 5.95[5] 5.83[6]	0.46[3] 0.54 0.39[5] 0.59[6]	48.5[3] 58.7 22.7[5] 40.7[6]	8.71[3] 8.60 5.04[5] 7.89[6]
Hindman and Lee (2007)	loblolly pine (*Pinus taeda*)	6.0×0.507×0.066	N/A	N/A	0.55	43.3	4.91
Jeong et al. (2008)	Southern pine (*Pinus spp.*)	13.97×2.54×0.381	0.0254	7.8	0.55	37.3	11.4

[1]Southern Yellow Pine, [2]sweet gum (*Liquidambar styraciflua L.*), [3]yellow-poplar (*Liriodendron tulipifera L.),* [4]red maple (*Acer rubrum*), [5]Willow (Salix spp.), and [6]red oak (*Quercus spp*)

Price (1975) studied the effect of gage length on the modulus of elasticity (MOE) and ultimate tensile strength (UTS) of sweetgum (*Liquidambar styraciflua L.*) flakes using a tensile test with a strain rate of 0.005 cm/cm/min. Four different gage lengths (1.27, 1.90, 2.54 and 3.17 cm) were used in this study. UTS increased with increased gage length while the MOE decreased with increased gage length. The MOE of flake was less than that of solid wood specimens.

Geimer et al. (1985) performed tensile testing to determine the MOE and UTS of two different grades of strands from Douglas-fir (*Pseudotsuga menziesii*). The grade of strands was determined by damage conditions. The test set-up had a 3.81 cm span and used cross head movement to calculate strain in the flakes. The test speed was 0.019 cm/min. Boards made from higher grade strands had 55% higher tensile strength compared to boards made from lower grade strands. UTS and MOE of the strands were 28% and 50% of the reported value for northern

interior Douglas-fir (*Pseudotsuga menziesii*).

Hunt et al. (1989) conducted tensile testing to determine MOE and UTS of yellow-poplar strands (*Liriodendron tulipifera L.*) with a 2224N load cell with a cross head speed of 0.190cm/min. The average MOE and UTS were 11.8 GPa and 70.3 MPa, respectively. Using stress wave velocity and strand density, the MOE was also predicted. Simple linear regression analysis showed the different MOE results had a R^2 of 0.69.

Deomano and Zink-Sharp (2004) conducted the three point bending test to calculate MOE and MOR of 25 mm by 5.0 mm by 0.6 mm flakes from three different species (southern yellow pine (*Pinus spp.*), sweet gum (*Liquidambar styraciflua L.*), and yellow-poplar (*Liriodendron tulipifera L.*)) with different test conditions including three different temperatures and two cutting directions. The loading rate was 2.54 mm/min. Higher drying temperature lowered mechanical properties of flakes. Tangentially cut specimens had higher mechanical properties compared to radially cut specimens. The MOE of southern pine, sweet gum, and yellow-poplar was 4,086.9, 4,430.6, and 5,829.4 N/mm^2, respectively. The MOR of southern pine, sweet gum, and yellow-poplar was 66.0, 78.6, and 89.0 N/mm^2, respectively. The average of MOE of radial and tangential cutting direction specimen was 4,308.0 and 5,256.6 N/mm^2. The MOR of radial and tangential cutting direction specimen was 69.1 and 86.7 N/mm^2.

Wu et al. (2005) studied the mechanical and physical properties of strands from southern pine. MOE and UTS of wood strand with thickness of more than 0.38 cm were similar to that of solid wood while the linear expansion of wood strands was much larger than that of solid wood. After pressing strands under 200 °C degree temperature for seven minutes, the MOE of the strands located in face layer significantly increased by 23% while the MOE of strands in the core layer remained same. The UTS of strands located in both layers increased about 26%. Cai et al.

(2007) extended the work of Wu et al. (2005) by testing willow (*Salix spp*.), yellow-poplar *Liriodendron tulipifera L*.), red oak (*Quercus spp*.), and loblolly pine (*Pinus taeda*) strands using the same methods as Wu et al. (2005).

Zink-Sharp and Price (2006) performed compression tests to determine the strength of sweetgum (*Liquidambar styraciflua L.*), yellow-poplar (*Liriodendron tulipifera L*.), and red maple (*Acer rubrum*). The size of specimens was 1 mm by 1mm by 4mm and the test was conducted at 12% moisture content (MC) with a loading speed of 0.029 mm/min. The load cell capacity was 445.2 N. The maximum compression strengths of yellow-poplar (*Liriodendron tulipifera L.*), sweetgum (*Liquidambar styraciflua L.)* and soft maple were 33.5, 39.2, and 41.6 MPa, respectively. Compression strength was weakly correlated with specific gravity and was not correlated with growth rate.

Hindman and Lee (2007) tested three different orientations of loblolly pine (*Pinus taeda*) strands for MOE and UTS using tension and bending tests. Both MOE and UTS were different depending on wood strand orientations. For MOE and UTS from tension test, the highest values were found from straight grain orientation strands, while the lowest values were found from the arbitrary grain orientation strands. For MOE and UTS from bending tests, the highest values were found from straight grain orientation strands while the lowest values were found from angle grain strands.

Although many researchers have measured MOE and ultimate strength of wood at different scales, the results are not directly comparable because of different loading conditions and different wood species. Specific guidelines for testing at both wood fiber and wood strand scales would be useful for future work. Dimension of the specimen, loading speed, and accurate strain measurement should be refined to have reliable results.

Jeong et al. (2008) evaluated the effect of loading rate and thickness of strands on MOE and UTS of southern pine (*Pinus spp*.) strands. Strand thickness varied 0.381 mm, 0.794 mm, 1.91 mm, and 3.81 mm. The different loading rates were 0.102 mm/min, 0.254 mm/min, and 0.406 mm/min. With a constant strand thickness of 0.794 mm, changes in the loading rate in the range of 0.102 mm/min to 0.406 mm/min did not produce significantly different MOE and UTS values at a level of α=0.05. Over the range of strand sizes tested, the MOE and UTS values were significantly different. Using Tukey's HSD comparisons, the MOE and UTS values were not significantly different for strand thicknesses of 0.0794 cm and 0.191 cm. Based upon these results, the authors recommend testing strands at 0.254 mm/min (0.005 cm/cm/min) and between a thickness of 0.794 mm and 1.91 mm to reduce variability.

Digital image correlation (DIC)

Improved characterization of the constitutive behavior of wood strands with varying microstructure would allow a more complete assessment of the resulting local stresses and make a more precise characterization of the material properties. Previous work to characterize the wood properties at the micro-scale level has used the constitutive properties of a representative cell wall, relative volume fractions, and a generalization of the microstructure of wood fibers (Bergander and Salmen 2000, Bergander and Salmen 2002, and Hindman and Lee 2007). These assumptions, to some extent, are valid when examining average stress and strain for evaluating the macro-scale behavior of wood. Failure of wood typically initiates from stress concentrations induced by local variations due to inhomogeneities of the wood microstructure. Therefore, the characterization of local material properties of wood is important to determine the mechanical behavior of wood at various scales. One method for measuring the local material properties of

wood uses digital image correlation (DIC). DIC is a powerful method for analyzing small specimens that cannot be attached to any extensometers or strain gauges to measure the strain. The strain field can also be characterized since DIC is a non-contact method and only needs the image of the surface of the specimens. However, DIC is sensitive to specimen characteristics and requires a sophisticated testing set up to achieve reliable results. Currently, a guideline for application of DIC to wood material is not well established. The fundamental knowledge of DIC and previous research on application of DIC to wood material are summarized in the following section. Details of the testing set-up and guidelines for the application of DIC to earlywood and latewood bands, and wood strands are also mentioned.

Principles of digital image correlation

Digital image correlation (DIC), which has been used to process experimental stress analysis results, began in the 1980s and has been broadly applied to different disciplines in science and engineering (Jin and Bruck 2005). DIC was developed to resolve the displacement on the surface of a specimen by correlating subimages of a sequence of images-one before loading and several images during loading (Sun et al. 2005). Spatial domain image correlation is the processing of digitizing images directly from the pixels of the image.

Deformation of the material can be achieved by tracking the displacement of markers on the sample's surface. The advantage of the DIC technique is the ability to track the change in position of a point in the field under study. Figure 2.7 demonstrates the general scheme of tracking the displacement of the window on the sequence of images. The first step is to locate the point of interest, P, in the image of the reference configuration before loading by generating a grid. The fixed grid on the image has information of the exact location of the point, P. After

loading, the change in the location of point P is tracked by image correlation using a pattern matching technique. Eight subsets of pixels surrounding the point P in the reference image, called a template or window, are matched with similar sized subsets of pixels within a search window determined by the maximum expected inter-image displacement without marker.

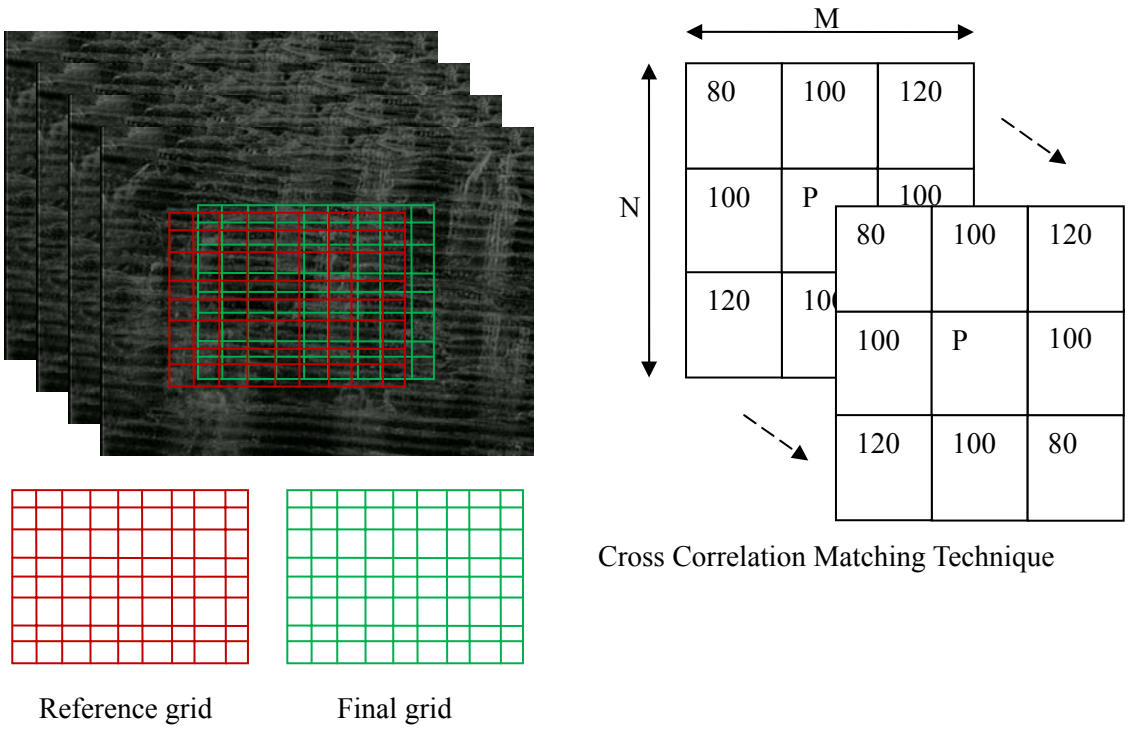

Figure 2.7 Schematic explanation of cross correlation techniques using DIC

The digital image correlation in the spatial domain is applied to obtain the displacements of a point when a subimage with the point in the center on the reference image tracks another subimage on the deformed image. The tracking of a subimage can be achieved by maximizing the cross correlation coefficient between grey value patterns of two images. Equation 2.1 shows the calculation of the cross correlation coefficient, C(p).

$$C(p) = \frac{\sum_{y=y0-N/2}^{y0+N} \sum_{x=x0-M/2}^{x0+M/2} g(x,y)h(x+u(x,y,p), y+v(x,y,p))}{\sqrt{\sum_{y=y0-N/2}^{y0+N/2} \sum_{x=x0-M/2}^{x0+M/2} g^2(x,y) \sum_{y=y0-N/2}^{y0+N/2} \sum_{x=x0-M/2}^{x0+M/2} h^2(x+u(x,y,p), y+v(x,y,p))}} \quad \textbf{(2. 1)}$$

Where,

x_0: the center point x of the subimage in the coordinate

y_0: the center point y of the subimage in the coordinate

with the size of M by N pixels in the coordinate.

g(x,y): the pixel values at the point (x,y) in the reference image

h(x+u(x,y,p),y+v(x,y,p)): the grey values in the deformed image at the mapping position of the point (x,y).

The pixel values at a sub-pixel position are obtained by using a cubic spline interpolation scheme. The coefficients C(p), where p is the mapping point, are determined from the grey values of pixel locations. The variables u(x,y,p) and v(x,y,p) are displacement functions which define how each of the subimage points located in the reference image at (x,y) is mapped to that in the deformed image.

In order to detect a small strain, the conventional DIC considered homogeneous deformations on the surface of the specimens which were dependent upon sub-pixel accuracy. A sub-set based correlation used the scheme of matching the sub-set of pixel intensity from the undeformed image with the subset of pixel intensity after loading using interpolation. If the material is not homogeneous, higher order interpolation is required while homogeneous materials only require zero or first order interpolation to approximate the variation of the displacement

field (Jin and Bruck 2005). In this study, cubic spline interpolation scheme was employed to represent the displacement field of wood.

A defined representative window size for generalizing mechanical properties of material

Baxter and Graham (2000) proposed a moving window generalized method of cells (MW-GMC) to characterize material properties of composite materials based on digitized images of local microstructure of the material. The statistical variability of material properties of composite material is dependent upon the window size. Larger window sizes produced smaller variance of material properties. However, if the window sizes become too large, the variability of material properties approaches zero. A smaller window size produces noisier fields. Also, a smaller window size required a higher computational effort which made it harder to analyze the field statistically.

Baxter et al. (2001) extended MW-GMC to three dimensions to predict more accurate material properties because of a three dimensional microstructure. The choice of window size was emphasized to represent the local material properties. Therefore, the proper window size for wood and wood-based materials should be calibrated to represent the local material properties. Such a calibration can be done by checking the relationship between different window sizes and calculated material properties at each window size. If the results converged from a certain window size, the window size would be chosen for the test.

Application of DIC to wood and wood-based material

Many previous studies have applied DIC to wood and wood-based materials. The DIC technique was introduced to measure the strain distribution of wood and paper material by Choi

et al (1991). The fundamental concept of DIC was well explained. The main objective of application of DIC of wood material was to measure the strain distribution and quantify the mechanical properties such as Poisson ratio and stress intensity factor. A summary of previous work is presented in Table 2.11.

Table 2.11 Summary of objectives, main results and conclusions from previous researches on DIC to wood and wood-based material

Researchers	Objective	Result/Conclusion
Choi et al. (1991)	Measured strain of wood and paper	The general concept of DIC and application of the method to wood mechanics were introduced.
Zink et al. (1995)	Measured the strain distribution of wood and wood-based composite	The stress concentration area can be captured and used to predict the eventual failure mode.
Zink et al. (1997)	Measured Poissons's ratios for yellow-poplar	The magnitude of Poissons ratio (υ_{LT}) decreased by increasing load level because the tangential strains were fairly uniform but longitudinal strains increased with increasing load.
Mott et al. (1996)	Measured micro-strain distribution from wood pulp fiber	Non-uniform micro strain was observed. Poisson effect and failure mechanism were estimated.
Stelmokas et al. (1997)	Displacement beneath the bolts in multiple-bolted wood connections	DIC was an effective method for describing surface displacement fields and for detecting failure beneath a bolt
Muszynski et al. (2000)	Measured interlaminar shear strains in fiber reinforcement polymer composite	DIC was capable of characterizing interlaminar shear behavior of laminated composite.
Samarasinghe and Kulasiri (2000)	Displacement fields of rubber and wood in parallel and perpendicular tension loading	While uniform stress distribution occured within the lignin matrix under tension loading perpendicular to the grain, parallel to the grain loading had a complex displacement pattern including internal shear and slippage.
Danvind (2002)	Measured the strain of wood during drying	DIC was capable of calculating two dimensional shrinkage strain field.
Samarasinghe and Kulasiri (2004)	Stress intensity factor of radiate pine (*Pinus radiata*) in tangential-longitudinal	A strong correlation between the critical stress intensity factor and the angle between the original crack plane and the radial-

	opening mode	longitudinal plane was found.
Serrano and Enquist (2005)	Strain distribution around wood adhesive bond line	The results were agreed well with the results from FEM.
Considine et al. (2005)	Measured the full-field deformation of paper and paperboard	Smaller window (16 by 16) did not give a good correlation between the deformed images due to large deformations. The higher variation of the strain region was a precursor to failure
Penneru et al. (2005)	A grid strain analysis at the macro and micro scale of wood	A similar strain pattern was observed at the both scale from compression test.
Ljungdahl et al. (2006)	The mechanical behavior of European Oak (*Quercus robur* L.) under radial and tangential compression	Multiseriate ray cells were the critical reinforcement controlling radial strength in radial tension of European oak.
Konnerth et al. (2006)	Deformation of wood in finger joint area	Further development required for the number of pixels to cover the bond lines and for the refinement of measurement of different strains and stress concentration around the bond-line.

Zink et al. (1995) applied DIC to wood and wood-based composites to measure the strain distribution. Using DIC, the stress concentration area was captured and predicted the eventual failure mode. Samarasinghe and Kulasiri (2004) calculated the stress intensity factor of radiate pine (*Pinus radiata*) in a tangential-longitudinal opening mode using DIC. Zink et al. (1997) measured Poisson ratios of yellow-poplar. The experimental results agreed well with published data. Ljungdahl et al. (2006) studied mechanical behavior of European oak (*Quercus robur* L.) under radial and tangential compression test using DIC. Strain and effective Poisson ratio were determined from earlywood and latewood. Stelmokas et al. (1997) investigated displacement beneath the bolts in multiple-bolted wood connections using DIC. DIC was an effective method for describing surface displacement fields and for detecting failure beneath a bolt. Muszynski et al. (2000) applied DIC to measure the interlaminar shear strains in fiber reinforcement polymer composites, showing the shear strain profiles over the specimen depth. Interlaminar shear

behavior of laminated composite was successfully characterized.

Samarasinghe and Kulasiri (2000) measured displacement fields of rubber and wood in parallel and perpendicular tension loading. Danvind (2002) used digital speckle photography (DSP) and X-ray computerized tomography (CT) to measure the strain of wood during drying. A method was presented for calculating the two dimensional shrinkage strain field.

Many authors emphasized precautions for the application of DIC to wood and wood based materials. Zink et al. (1997) found a loading effect on strain behaviors of different sections of wood. Considine et al. (2005) mentioned the window size for correlation of deformed images. Four different window sizes (128 by 128, 64 by 64, 32 by 32, and 16 by 16 pixels) were used. Smaller window sizes (16 pixels by 16 pixels) did not correlate well with large deformation. Mott et al. (2002) applied cyclic loading every five seconds to prevent distortion of the surface image of the specimen from suspended scanning. Lopez-Anido et al. (2004) applied 3-D DIC to characterize mechanical behavior of composite materials. DIC with four different test set-ups according to ASTM D3039 tension for composites, ASTM D638 tension for plastics, ASTM D6641 compression for composites, and ASTM D695 compression for plastics were investigated. Guidelines of the use of DIC for each test methods were presented.

DIC was also applied to measure the strain distribution of wood at the micro-scale level. Mott et al. (1996) set up a MINIMAT tester inside an environmental scanning electron microscopy (ESEM) to measure micro-strain distribution from wood pulp fiber. Murata and Masuda (2001) used a confocal microscopy incorporated with DIC to measure the swelling behavior of the cross section of cells from Douglas-fir (*Pseudotsuga menziesii*). Penneru et al. (2005) introduced a grid strain analysis at the macro and micro scale of wood. A similar strain pattern was observed at the both scale from compression test. Ljungdahl et al. (2006) studied the

mechanical behavior of European Oak (*Quercus robur* L.) under radial and tangential compression using digital speckle photography (DSP). Multiseriate ray cells were the critical reinforcement controlling radial strength in radial tension. The rays were the main microstructural factor controlling transverse anisotropy in European oak.

Konnerth et al. (2006) investigated the deformation of wood in finger joint area using electronic speckle-pattern interferometry (ESPI). Machine graded Norway spruce (*Picea abies*) was used for the finger joint specimens and glued by two different types of adhesives; melamine-urea-formaldehyde (MUF) and polyurethane (PUR). Further development was required for the number of pixels to cover the bond lines and for the refinement of measurement of different strains and stress concentrations around the bond-line. Serrano and Enquist (2005) investigated the strain distribution around wood adhesive bond lines. The results agreed well with the results from FEM.

Stochastic finite element method (SFEM)

The strength of wood strands originates from the intra-ring properties and grain angle. However, the intra-ring properties and the orientation of grain are uncertain factors. The material properties of wood are random in nature and the grain angle of strands can be random due to indeterminate cutting. Therefore, it is desirable to investigate the effect of the uncertain variables of intra-ring properties and grain angle on the mechanical behavior of wood strands under various loading conditions.

Random properties and grain angles affect the strain and stress distributions of wood strands because the mechanical behaviors are functions of the material properties. Under the condition of the indeterminate properties of wood strands, the load-displacement relations of

wood strands are influenced by the variability of the intra-ring properties and grain angles. Random properties of wood strands affect not only the stiffness of wood strands, but also the evaluation of strains and stresses in the principal material directions, which are important for failure estimation. These problems have not been elaborated in previous studies of wood science area.

The SFEM can combine the existing finite element method (FEM) for deterministic problems with uncertainty variables. The computation of the stochastic field of nodal displacements (u) from the random stiffness matrix (K) is the main objective of the SFEM. There are many representative methods to generate the stochastic finite element stiffness including perturbation, Monte Carlo simulation, Neumann expansion, and Karhunen-Loeve decomposition. The fundamental principle of the SFEM technique fits well with the uncertainty of wood structure. The stiffness and grain variation in strands can be used as an input for SFEM. Unfortunately, there are only a few SFEM applications specifically related to wood and wood based materials in the research literature. Therefore, the literature review is limited to the application of composite materials with similar structure to wood and fundamental knowledge of SFEM.

Comparison of conventional FEM and SFEM

Conventional finite element methods (FEM) are widely used to solve many practical problems in wood and wood-based composites (Mackerle 2005). The finite element solution is an approximation of the actual continuous domain using a number of finite elements. FEM results can achieve a high accuracy as the number of elements becomes large and converges to a single solution. There are numerous practical problems in FEM due to many uncertainties that

can influence the results (Kleiber and Hien 1992). Conventional FEM assumes deterministic or representative material properties and geometry of material. The nodal displacement {U} of the system is deterministic corresponding to both the deterministic global stiffness [K] and loading {F} (Equation 2.4).

$$\boldsymbol{KU = F} \qquad (\mathbf{2.4})$$

Where

K: the global stiffness matrix

U: global displacement vector

F: the deterministic load vector

While the conventional FEM uses a deterministic stiffness matrix [K] and a deterministic loading {F} to obtain a deterministic nodal displacement {U}, SFEM uses random stiffness matrices [K] and random loadings {F} to solve the corresponding set of nodal displacement vectors. Although the governing equation of SFEM is similar to the conventional FEM, SFEM needs additional functions to generate random properties and corresponding response vectors.

As shown in Table 2.12, the general procedure of the SFEM is similar to that of FEM. However, there are differences in each procedure. In pre-processing stage, SFEM generates random material properties in each element. In the analysis part, SFEM deals with a set of coefficients to generate responding displacements. In the post-processing part, SFEM produces statistical stress and strain distribution. In this study, the random material properties ($E(x,\theta)$) was implemented using Monte-Carlo simulation (MCS) with known probabilities of material

properties and the corresponding nodal displacement was analyzed.

Table 2.12 Comparison of the FEM and SFEM procedures

Procedure	FEM	SFEM	Difference[1]
Pre-processing	Discretize the element with determined element stiffness	Discretize the element with random element properties	Determined material properties/Random material properties
Analysis	Element stiffness matrices are computed, assembled to form global stiffness matrix for the system, applied boundary conditions.	The unknowns of this system are the set of nodal displacement vectors which describe the probabilistic nodal displacement of the system.	Mean displacemet/the set of nodal displacement vector
Post-processing	Mean displacement and stress distribution of the system can be calculated	Statistical analysis of stress distribution of the system based on the set of nodal displacement	Mean stress and strain distribution/ Statistical distribution of stress and strain

[1]FEM/SFEM

Relevant SFEM applications to composite materials.

SFEM has been applied to solve many different physical problems where uncertainty of geometry, material property or boundary conditions exists. The accuracy and validity of SFEM has been proven by previous work. However, since only a few SFEM applications have been applied to wood based composite, similar applications to composite materials are also listed.

Wang and Lam (1998) applied a nonlinear SFEM to estimate the tensile strength of parallel aligned wood strand composites. The input variables for the individual strands were elastic properties and strength from the experimental test. Clouston and Lam (2002) extended the study of Wang and Lam (1998) to predict the mechanical behavior of wood strand composites with strands of different grain angles using Monte-Carlo simulation based SFEM. The simulation results agreed well with the experimental test.

Chkraborty and Dey (2000) used the Neumann expansion technique based SFEM to analyze uncertain structure parameters under seismic induced random ground motion. A direct Monte Carlo simulation was performed to check the accuracy of the results from the SFEM. The results showed that Neumann expansion solution could handle up to 20% coefficient of variation of uncertain input parameters. Reliable results could be expected with less than 15 % coefficient of variation of the random inputs.

Kaminski (2000) applied perturbation-based SFEM to simulate interface defects in fiber-reinforced composites. The SFEM used real composite structures with various fictitious interface percentages. A Monte Carlo simulation approach used homogenized elastic properties and three different interface sizes to calculate the effective stiffness for a composite. The results from the SFEM showed a greater horizontal displacement occurred at a larger percentage of interface defects. Caution was emphasized using the perturbation-based SFEM in a larger percentage of the interface defects due to the significant variation of the elastic characteristics of the interface. The results from Monte-Carlo simulation showed a greater percentage interface defects had a lower elastic constant. Among three different interface sizes, the largest interface had the highest coefficient variation of the elastic constant.

Chung et al. (2005) used SFEM incorporated with a moving window generalized methods of cells (GMC) to characterize the interface of fiber metal laminates. The results from the GMC showed the variability of mean displacement was not influenced by different window size while the variability of displacement was proportional to the window size. Based on the results from the GMC, Karhunen-Loeve expansion was applied to generate the random material properties. For the response displacement, Hermite polynomial expansion was applied. The SFEM results showed the strain variability in the fiber-metal interface zone was in good

agreement with the experimental results. The largest strain variability in the interface zone was likely to have the initiation of failure.

Eiermann et al. (2005) overviewed computational implementation of SFEM. K-L expansion could produce a good random field with a large correlation length and a small number of expansion terms. An efficient solution algorithm could be achieved from the Galerkin discretization. The conclusion was an efficient implementation of SFEM and improvement of generation of random field saved computational efficiency.

From this literature review, Most SFEMs were validated their accuracy by comparing the results from the MCS based SFEM. Also Monte-Carlo simulation based SFEM has been applied to wood material. Therefore, in this study Monte-Carlo simulation based SFEM was applied to analyze the effect of the intra-ring properties and different grain angles on mechanical behavior of wood strands.

Summary and Conclusion

SCL and OSB are manufactured from wood strands of various sizes. The use of SCL and OSB products place strands in different stress conditions. Optimization of strand size and geometry would improve the mechanical performance of SCL and OSB. In the processing of wood strands, the effect of the wood strand geometry on the mechanical properties is crucial to optimize the properties for end uses. The strength of wood strands originates from the intra-ring properties and grain angles. However, the intra-ring properties and the orientation of grain are uncertain factors. The material properties of wood are random in nature and the grain angle of strands can be random due to indeterministic cutting. Therefore, it is desirable to investigate the effect of the uncertain variables of intra-ring properties and grain angles on the mechanical behavior of wood strands under various loading conditions.

Understanding the hierarchical structure of wood at different scales is important to develop high strength materials. The nano-scale contains the mechanical functions of cellulose, hemicelluloses, and lignin in wood cells. The micro-scale contains the different microfibril angles and cell wall thickness in the cell wall layer. The macro-scale contains the different characteristics of earlywood and latewood along with juvenile wood and mature wood. All of these hierarchical structures affect the mechanical properties of wood and wood-based composites.

The knowledge of mechanical properties of the earlywood and latewood bands and strands can lead to better predictions of stiffness and strength of strand-based composites. Improved characterization of the constitutive behavior of wood strands with random microstructures would allow a more complete assessment of the resulting local stresses and make

a more precise characterization of the material properties. Failure of wood typically initiates from stress concentrations induced by local variations due to inhomogeneities of the wood microstructure. Therefore, the characterization of local material properties of wood is important to determine the mechanical behavior of wood at various scales. The digital image correlation (DIC) method is chosen to measure MOE of earlywood and latewood bands, and MOE of strands.

Many previous researchers have developed different models to predict the mechanical behavior of wood at different scales using micromechanics, laminate theories and finite element methods. Although many methods of modeling wood fiber and strand based composites were found, there was a lack of research on modeling of wood strands. Analytical and numerical models for wood fiber and strand based composites, however, suffer from limiting information on input properties for the models. Most models used averaged material properties or assumed material properties that may cause an error or a variable result. Therefore, prior to model wood strands, the variation of input parameters that affect the mechanical properties of wood strands should be included.

Random intra-ring properties and grain angles affect the strain and stress distributions of wood strands because the mechanical behaviors are functions of the material properties. Under the condition of the undetermined properties of wood strands, the stiffness-displacement relations could be considered as random equations. The motivation of using stochastic analysis stems from the variability of the intra-ring properties of the wood strands. Stochastic finite element method (SFEM) can solve this variability as the known probabilities of material properties. The SFEM can take advantage of the existing FEM for deterministic problems combined with uncertainty variables. The fundamental principle of the SFEM technique fits well with the high uncertainties of wood structure. The stiffness and grain variation in strands are

used as inputs for the SFEM.

Based on the understanding of the effect of the intra-ring properties and different grain angles of the wood strands, segregation into discrete categories (earlywood, latewood, and certain grain angle strands) can maximize the benefits of a certain geometry of wood strands for specific uses. The knowledge of the effect of the intra-ring properties and grain angles of wood strands can lead to optimization in processing and utilization. This process can begin with cutting different angles of a wood block, experimentally determining intra-ring properties, and using the properties to simulate models to analyze the mechanical behaviors of wood strands.

References

Adair, C. 2005. Structural panels and engineered wood yearbook, APA. The engineered wood association E171.

Åkerholm, M. and L. Salmén 2003. The mechanical role of lignin in the cell wall of spruce tracheids. Holzforschung 57(5): 459–465.

Angeles, G., R. Davalos-Sotelo, and R. Sanjuan-Duenas. 2006. Micromechanical analysis of Urticaceae wood. 5th Plant Biomechanics Conference-Stockholm, August 28-September 1.

Anagnost, S. E., R. E. Mark, and R.B. Hanna. 2002. Variation of microfibril angle within individual fibers. Wood and Fiber Sci. 34: 337–349.

Baxter, S. C., M. I. Hossain, and L. L. Graham. 2001. Micromechanics based random material property fields for particulate reinforced composites. Int. J. Solids Struct. 38: 9209–9220.

Baxter S. C. and L. L. Graham. 2000. Characterization of random composites using a moving window technique. ASCE J. Eng. Mech. 126 (4):389–404.

Bendtsen, B. A. and J. Senft. 1986. Mechanical and anatomical properties in individual growth rings of plantation-grown Eastern cottonwood and loblolly pine. Wood and Fiber Sci. 18: 23–38.

Bergander A. and L. Salmén. 2002. Cell wall properties and their effects on the mechanical properties of fibers. J. Mater. Sci. 37 (1):151–156.

Booker, R. E. 1993. The importance of the S3 cell wall layer incollapse prevention and wood hardness. 24th Forest Products Research Conference 15–18 November, CSIRODiv. of Forest

Products, Clayton, Victoria, Australia 3(17):1–13.

Booker, R. E. and J. Sell. 1998. The nanostructure of the cell wallof soft woods and its function in a living tree. Holz Roh-Werkstoff 56:1-8.

Balatinecz, J. J. and D. E. Kretschmann. 2001. Properties and utilization of poplar wood. In Poplar Culture in North America. Part A, Chapter 9. Edited by D.I. Dickmann, J.G. Isebrands, J.E. Eckenwalder, and J. Richardson. NRC Research Press, National Research Council of Canada, Ottawa, ON KIA OR6, Canada. 277-291 pp.

Bendtsen, B.A. 1978. Properties of wood from improved and intensively managed stands. Forest Prod. J. 28(10):61-72.

Bendtsen, B. A. and J. Senft. 1986. Mechanical and anatomicalproperties in individual growth rings of plantation grown eastern cottonwood and loblolly pine. Wood Fiber Sci. 18:23–38.
Pearson, R. G. 1988. Compressive properties of clear and knotty loblolly pine juvenile wood. Forest Prod. J. 38(7/8):15-22.

Bergander, A. and L. Salmén. 2000 Variations in transverse fibre wall properties: relations between elastic properties and structure. Holzforschung 54(6): 654-600

Bergander, A. and L. Salmén. 2002. Cell wall properties and their effects on the mechanical properties of fibers. J. Materials Sci. *37*(1), 151–156.

Burdon, R. D., R. P. Kibblewhite, J. C. F. Walker, R. A. Megraw, R. Evans, and D. J. Cown. 2004. Juvenile versus mature wood: a new concept, orthogonal to corewood versus outerwood, with special reference to *Pinus radiata* and *P. taeda*. Forest Sci. 50:399-415.

Burgert, I. and J. Keckes. 2002. A comparison of two techniques for wood fibre isolation evaluation by tensile tests on single fibres with different microfibril angle. Plant Biology. 4(1): 9-12.

Burgert, I. and K. Fruhmann. 2003. Microtensile testing of wood fibers combined with video extensometry for efficient strain detection. Holzforschung. 57(6): 661-664.

Cave, I.D. 1968. The Anisotropic Elasticity of the Plant Cell Wall. Wood Science and Technology. 2(4): 268–278.

Cave, I. D. 1969. The longitudinal Young's modulus of Pinus radiata. Wood science and technology. 3(1): 40-48.

Cave, I. D. 1978. Modeling Moisture-Related Mechanical-Properties of Wood .1. Properties of Wood Constituents. Wood Science and Technology 12(1): 75-86.

Cave, I. D. and Walker, J. C. F., 1994. Stiffness of wood in fast grown plantation softwoods: the influence of microfibril angle. Forest Products J. 44(5): 43–48.

Chakraborty S. and S. S. Dey 2000. Stochastic finite element simulation of uncertain structures subjected to earthquake. Shock and Vibration. 7(5):309 -320.

Choi, D., J. L. Thorpe, and R. B. Hanna. 1991. Image Analysis to Measure Strain in Wood and Paper. Wood Science and Technology 25(2): 251-262.

Chung, D. B., M. A. Gutiérrez and R. D. Borst. 2005. Object-oriented stochastic finite element analysis of fibre metal laminates. Computer Methods in Applied Mechanics and Engineering 194(12-16):1427-1446.

Clouston, P. and F. Lam. 2001. Computational Modeling of Strand-based Wood Composites. ASCE Journal of Engineering Mechanics, 127(8): 844-851.

Clouston, P. and F. Lam. 2002. A Stochastic Plasticity Approach to Strength Modeling of Strand-based Wood Composites. Composites Science and Technology, 62:1381-1395.

Cousins, W. J. 1976. Elastic modulus of lignin as related to moisture content. Wood Sci. and Technology. 10, 9–17.

Cousins, W. J. 1978. Young's modulus of hemicellulose as related to moisture content. Wood Sci. and Technology. 12(3): 161-167.

Cramer, S.M., D. E. Kretschmann, R. Lakes, and T. Schmidt. 2005. Earlywood and latewood elastic properties in loblolly pine. Holzforschung. 59(5):531-538.

Dai C and P. R. Steiner. 1994. Spatial structure of wood composites in relation to processing and performance characteristics. Part III. Modeling the formation of multi-layered random flake mats. Wood Sci. Technol 28:229–239.

Danvind, J. 2002. Methods for Collecting and Analysing Simultaneous Strain and Moisture Data During Wood Drying; Licenciate Thesis in the Division of Wood Physics, Skelleftea Campus: Skelleftea, Sweden, Lulea University of Technology, 2002.

Deomano, E. C. and A. Zink-Sharp. 2004. Bending properties of wood flakes of three southern species. Wood and Fiber Sci. 36(4): 493-499.

Deomano E. C. and A. Zink-Sharp. 2005. Effect of species, cutting direction, dimensions, and temperature on flake drying. Forest Prod. J. 55(9): 31-36

Donaldson, L. A. 1996. Effect of physiological age andsite on microfibril angle in Pinus radiata. IAWA Journal 17: 421–429.

Eiermann M., O. G. Ernst, and E. Ullmann. 2005. Computational aspects of the stochastic finite element method. Proceeding of algoritmy. pp. 1-10.

Evans, R., S. Stuart, and J. Van der touw. 1996. Microfibrilangle scanning of increment cores by X-ray diffractometry. Appita Journal 49, 411–414.

Fengel, D. and G. Wegener. 1983. Wood—Chemistry, Ultrastructure, Reactions (De Gruyter, Berlin).

Frey-wyssling, A. and K. Muhlethaler. 1965. Ultrastructural Plant Cytology with an Introduction to Molecular Biology New York, Elsevier Publishing Co., First Edition.

Gassan J., A. Chate and A. K. Bledzki. 2001. Calculation of elastic properties of natural fibers. Journal of Materials Sci. 36:3715-3720.

Geimer R. L. and J. B. Crist. 1980. Structural flakeboard from short-rotation intensively curtured hybrid populous clones. Forest Prod. J. 30(6):42-48.

Geimer, R. L. 1986. Properties of structural flakeboard manufactured from 7-year-old intensively cultured poplar, tamarack, and pine. Forest Prod. J. 36(4):42-26.

Geimer, R. L., V. L. Herian, and D. Xu. 1997. Influence of juvenile wood on dimensional stability and tensile properties of flakeboard. Wood and Fiber Sci. 29(2): 103-120.

Geimer, R. L., R. J. Mahoney, S. P. Loehnertz, and R. W. Meyer. 1985. Influence of processing-induced damage on the strength properties of oriented strand wood products. Forest Prod. J. 50(11/12):33-42.

Ghanem R. G. and P. D. Spanos. 1991. Stochastic Finite Elements: A Spectral Approach, Springer-Verlag.

Ghanem R. 1999. Higher order sensitivity of heat conduction problems to random data using the spectral stochastic finite element method, ASME Journal of Heat Transfer, 121:290–299.

Goel A, C. Phanouriou, F. A. Kamke, C. J. Ribbens, C. A. Shaffer, and L. T. Watson. 1999. WBCSim: a prototype problem solving environment for wood-based composites simulations. EngComput 15:198–210.

Groom, L. and L. Mott. 2002. Mechanical properties of individual southern pine fibers. Part I. Determination and variability of stress-strain curves with respect to tree height and juvenility. Wood and Fiber Sci. 34(1): 14-27.

Groom, L., S. Shaler, and L. Mott. 2002. Mechanical properties of individual southern pine fibers. Part III. Global relationships between fiber properties and fiber location within an individual tree. Wood and Fiber Sci. 34(2): 238-250.

Gutierrez, M. A and S. Krenk 2004. Stochastic finite element methods. In E. Stein,R. de Borst, and T. J. R. Hughes (Eds.) Encyclopedia of Computational Mechanics. John Wiley & Sons, Ltd. in press.

Harwood, V.D. 1971. Variation in carbohydrate analyses in relation to wood age in Pinus radiata. Holzforschung. 25 (3):73–77.

Harris, J. M. and B. A. Meylan. 1965. The influence of microfibril angle on longitudinal and tangential shrinkage in Pinus radiata. Holzforschung. 19:144–153.

Hearle, J. W. S. 1963. The fine structure of fibers and crystalline polymers. III. Interpretation of the mechanical properties of fibers Journal of Applied Polymer Science, 7:1207 – 1223.

Hindman D. P. and J. N. Lee. 2007. Modeling wood strands as multi-layer composites: bending and tension loads. Wood and Fiber Sci. 39(4):516-526.

Hunt, M. O., M. H. Triche, G. P. McCabe, and W. L. Hoover. 1989. Tensile properties of yellow-poplar veneer strands. Forest Prod. J. 39(9).

Jeong, G. Y., D. P. Hindman, D. Finkenbinder, J. N. Lee, and Z. Lin. 2008. Effect of loading rate and thickness on the tensile properties of wood strands, Forest product J. 58(10):33-37.

Jin, H. and H. A. Bruck. 2005. Theoretical development for pointwise digital image correlation. Optical Engineering, Volume 44, pp.

Jo, J. M., B. J. Chung, Y. D. Lee, D. H. Kang, D. J. Chung, and S. G. Chung. 1981. Developing multiple utilization of larch wood. Forest Research Institute, No. 28. Seoul, Korea.

Jones, R. M. 1975. Mechanics of composite materials. McGraw-Hill, New York.

Kahle, E. and J. Woodhouse. 1994. The infuence of cell geometry on the elasticity of soft xylem tissue. Journal of Material Science 29:1250-1259.

Kaminski, M. 2002. Stochastic problem of fiber-reinforced composite with interface defects. Engineering computations. 19 (7) :854-868

Keckes, J., I. Burgert, K. Fruhmann, M. Muller, K. Kolln, M. Hamilton, M. Burghammer, S. V. Roth, S. Stanzl-Tschegg and P. Fratzl. 2003. Cell-wall recovery after irreversible deformation of wood. Nature Materials 2(12): 810-814

Kerr, A.J.,and D.A.I. Goring. 1975. The ultrastructural arrangements of the wood cell wall, Cellul. Chem. Technol. 9: 536–573.

Kleiber, M., T. Hien. 1992. The Stochastic Finite Element Method. Basic Perturbation Technique and Computer Implementation. John Willey & Sons.

Konnerth, J., W. Gindl, W., and U. Mueller. 2006a. Elastic properties ofadhesive polymers. Part I: Polymer films by means of electronic speckle pattern interferometry. J. Appl. Polym. Sci Vol. 103, 3936–3939.

Konnerth, J., A.Valla , W. Gindl , and U. Muller. 2006b. Measurement of strain distribution in timber finger joints Wood Sci Technol 40:631–636.

Kretschmann, D. E., H. A. Alden, and S. Verrill. 1997. Variations of microfibril angle in loblolly pine: comparison of iodine crystallization and X-ray diffraction techniques. In: Butterfield, B.G. (Ed.), Proceedings of the IAWA/IUFRO International Workshop on the Significance of Microfibril Angle to Wood Quality. Westport, New Zealand, pp. 157–176.

Lam, F. 2001. Modern structural wood products. J. Progress in Structure Engineering Material 3:(3)238-245.

Larson, P. R., D. E. Kretschmann, A. Clark III, and J. G. Isebrands. 2001. Juvenile Wood Formation and Properties in Southern Pine. General Technical Report FPL-GTR-129. Madison, Wisconsin: US Department of Agriculture, Forest Service, Forest Products Laboratory.

Lee, J. N. and Q. Wu. 2003. Continuum modeling of engineering constants of oriented strand board. Wood and Fiber Sci. 35(1):24-40.

Lekhnitskii, S. G. 1963. Theory of elasticity of an anisotropic elastic body, Holden-Day, San Francisco.

Liu, J. Y. 2002. Analysis of off-axis tension test of wood specimens. Wood and Fiber Sci. 34(2):205-211.

Ljungdahl, J. L. A. Berglund, and M. Burman. 2006. Transverse anisotropy of compressive failure in European oak-a digital speckle photography study. Holzforschung, 60: 190-195.

Lopez-Anido, R., L. Muszyñski,H. J. Dagher. 2004. Composite Material Testing Using a 3-D Digital Image Correlation System COMPOSITES 2004 Convention and Trade Show American Composites Manufacturers Association October 6-8, 2004 Tampa, Florida USA.

Lu C. 1999. Organization of wood elements in partially oriented flakeboard mats. PhD Dissertation. Dept. of Forestry, University of British Columbia, Vancouver, BC

Macdonald E. and J. Hubert2002. A Review of the Effects of Silviculture on the Timber Quality of Sitka Spruce. Forestry, 75 (2).

Mackerle, J. 2005. Finite element analyses in wood research: a bibliography. Wood Sci Technol 39: 579–600.

Mark, R.E. 1967. Cell Wall Mechanics of Tracheids. Yale University Press, New Haven, USA, 2 edition.

Mark, R. E. and P. P. Gillis. 1973. The relationship between fiber modulus and S2 angle. Tappi 56:164-167.

Matsuo M. and C. Sawatari, and Y. Iwai, and F. Ozaki. 1990. Effect of orientation distribution and crystallinity on the measurement by X-ray diffraction of the crystal lattice moduli of cellulose I and II Biomacromolecules, 23: 3266 - 3275.

McAlister, R. H., A. Clark III, and J. R. Saucier. 1997. Effect of initial spacing on mechanical properties of lumber sawn from unthinned slash pine at age 40. Forest Prod. J. 47 (7/8):107–109.

Moden, C. 2006. Transverse Anisotropy in Softwoods Licenciate Thesis Stockholm, Sweden 2006.

Moody, R. C. 1970. Tensile strength of fingerjoints in pith-associated and non-pith associated Southern Pine lumber. Res. Pap. FPL-138. Madison, WI:U.S. Department of Agriculture, Forest Service, Forest Products Laboratory. 20pp.

Mott, L., S. M. Shaler, and L. H. Groom 1996. A Novel Technique to Measure Strain Distributions in Single Wood Fibers. Wood and Fiber Sci. 28(4):429-437.

Mott, L., L. Groom, and S. Shaler. 2002. Mechanical properties of individual southern pine fibers. Part II. Comparison of earlywood and latewood fibers with respect to tree height and juvenility. Wood and Fiber Sci. 34(2): 221-237

Munch, E. 1938. Investigations on the harmony of tree shape. Jahrbu¨cher fu¨r wissenschaftliche Botanik 86: 581–673. (Translated by M. H. Zimmermann, 1963).

Murata, K. and Masuda M. 2001. Observation of microscopic swelling behavior of the cell wall. J. Wood Sci. 47:507-509.

Muszynski, L., R. Lopez-Anido and S. M. Shaler. 2000. Image Correlation Analysis Applied to Measurement of Shear Strains in Laminated Composites. in: Proceedings of SEM IX InternationalCongress on Experimental Mechanics, Orando FL, June, 5-7, 2000. 163-166.

Nairn, J. A. 2006. Numerical Simulations of Transverse Compression and Densification in Wood, Wood and Fiber Sci. 38(4):576 – 591.

Navi, P., P. K. Rastogi, V. Gresse, and A. Tolou. 1994. Micromechanics of wood subjected to axial tension. Wood Science and Technology. 29(6):411-429.

Neagu, R. C., E. K. Gamstedt and F. Berthold. 2006. Stiffness contribution of various wood fibers to composite materials, Journal of Composite Materials, 40:(8):663-699

Panshin, A. J., and C. D. Zeeuw. 1980. Textbook of wood technology. McGraw Hill Book Co., New York, NY.

Pearson, R. G. and B. E. Ross. 1984. Growth rate and bending properties of selected loblolly pines. Wood and Fiber Sci. 16:37-47.

Penneru, A. P., K. Jayaramanand, D. Bhattacharyya 2005. Strain analysis in bulk forming of wood Holzforschung, 59:456–458.

Perr´e, P. 2005. Meshpore: A software able to apply image-based meshing techniques to anisotropic and heterogeneous porous media. Dry Technol 239–11:1993–2006.

Persson, K. 2000. Micromechanical Modelling of Wood and Fibre Properties, Doctoral Thesis, Department of Mechanics and Materials, Structural Mechanics, LTH, Lund University, Lund, Sweden.

Price, E.W. 1975 Determining tensile properties of Sweetgum veneer flakes. Forest Prod. J. 26(10): 50-53

Pugel, A. D., E. W. Price, and C. Y. HSE. 1990a. Composites from southern pine juvenile wood. Part I. Panel fabrication and initial properties. Forest Prod. J. 40(1):29-33.

Reiterer, A., H. Lichtenegger, S. Tschegg, and P. Fratzl. 1999. Experimental evidence for a mechanical function of the cellulose microfibril angle in wood cell walls. Philosophical Magazine A, 79(9): 2173-2184.

Sakurada, I, A. Nukushina , T. Ito. 1962. Experimental determination of the elastic modulus of crystalline regions in oriented polymers. J Polymer Sci 57:651–660.

Salmén, L. and de Ruvo, A. 1985. A model for prediction of fiber elasticity *Wood and Fiber Science*, 17, pp. 336 - 350.

Salmén, L., and A. M. Olsson 1998. Interaction between hemicelluloses, lignin and cellulose: structure-property relationships, J. Pulp Pap. Sci. 24(3): 99–103.

Salmén, L. 2004. Micromechanical understanding of the cell-wall structure. Comptes Rendus Biologies 327(9-10): 873-880.

Samarasinghe, S. and G. D. Kulasiri, 2000. Displacement fields of wood in tension based on image processing: Part 1. Tension parallel- and perpendicular-to-grain and comparisons with isotropic behaviour. Silva Fennica 34(3): 251–259.

Samarasinghe, S. and D. Kulasiri, 2004. Stress intensity factor of wood from crack-tip displacement fields obtained from digital image processing. Silva Fennica 38(3): 267–278.

Saliklis, E. P. and R. H. Falk. 2000. Correlating off-axis tension tests to shear modulus of wood-based panels. J. Structural Engineering. 126(5):621-625.

Schuler, A. and C. Adair. 2000. Engineered Wood Products- Production, Trade, Consumption and Outlook. Forest Products Annual Market Review, Chapter 11, FAO/ECE Timber Section. United Nations, NY and Geneva. 131-146 pp.

Serrano, E., and B. Enquist. 2005. Contact-free measurement and non-linear finite element analyses of strain distribution along wood adhesive bonds. Holzforschung 59:641–646.

Shu, J., L. T. Watson, B. G. Zombori, and F. A. Kamke. 2006. WBCSim: an environment for modeling wood-based composites manufacture Engineering with Computers 21: 259–271.

Siddiqui, K. M. 1976. Relationship between cell wall morphologyand chemical composition ofearlywood and latewood in two coniferous species. Pakistan J. For. 26:21–34.

Sjöström, E. 1993. Wood Chemistry, Fundamentals and Applications, second ed. Academic Press, San Diego.

Smith, R. W. and D. G. Briggs. 1986. Juvenile wood:Has it come of age? Pages 1-11 in proc., Juvenile wood: What does it mean to forest management and forest products? Forest Products Research Society, Madison, WI.

Smulski, S. 1997. Engineered wood products, a guide for specifiers, designers and users. PFS Research Foundation. Madison, WI. 294 pp.

Stelmokas, J. W., A. G. Zink, J. L. Loferski, and J.D. Dolan. 1997. Measurement of load distribution among multiple-bolted wood connections. Journal of Testing and Evaluation 25(5):510-515.

Sugimori, M. and F. Lam. 1999. Measuring macro-void distribution in wood composites using computer tomography and image processing techniques. Mohuzai Gakkaishi (J. Japan Wood Res. Soc.) 45(3):254-257.

Sun, Y., J. H. L. Pang, C. K. Wong, and F. Su. 2005. Finite element formulation for a digital image correlation method. Appl. Opt. 44, 7357-7363.

Tang, R. C. and N. N. Hsu. 1973. Analysis of the relationship between microstructure and elastic properties of the cell wall. Wood and Fiber 5, 139–151.

Taylor, F. W. and J. S. Moore, 1981. A comparison of earlywood and latewood tracheid lengths in loblolly pine. Wood and Fiber. 13:159-165.

Uprichard, J. M. 1971. Cellulose and lignin content in *Pinus radiata*D. Don. Within-tree variation in chemical composition, density, and tracheid length. Holzforschung 25:97–105.

Wang, Y. T. and F. Lam. 1998. Computational modeling of material failure for parallel-aligned strand-based wood composites. J. Computational Material Science 11:157-165.

Wasnewski, J. L. 1989. Evaluation of juvenile wood and its effect on Douglas fir structural composite panels. In proc. 23rd Particleboard and Composite Material Symposium, Washington State University, Pullman, WA.

Watanabe, U, M. Norimoto M, T. Ohgama, and M. Fujita. 1999. Tangential Young's modulus of coniferous early wood investigated using cell models. Holzforschung 53:209-214.

Watson, A. J. and H. E. Dadswell. 1964. Influence of fibre morphology on paper properties, 4. Micellar spiral angle. Appita 17,151–156.

Wiener, N. 1938. The homogeneous chaos. Am. J. Math. 60, 897–936.

Wilhelmsson, D., R. C., Neagu, S. L. Bardage, and E. K. Gamstedt. 2006. Finite element modelling of mechanical properties of geometrically characterized wood fibres. 5th Plant Biomechanics Conference, Vol 1, SalménL. (ed.), pp. 181–186. Stockholm: STFI-Packforsk.

Wood, J. R. and D. A. I Goring. 1971. The distribution of lignin in stemand branch wood of Douglas fir. Pulp Pap. Mag. Can. 72:T95–T102.

Wu, Q**.,** and J. N. Lee. 2003. Continuum modeling of engineering constants of oriented strandboard. Wood and Fiber Sci. 35(1):24-40.

Wu, Q., Z. Cai, and J. N. Lee. 2005. Tensile and dimensional properties of wood strands made from plantation southern pine lumber. Forest Prod. J. 52(2):1-6.

Xu, P., A. Lloyd, A. Donaldson, R. Zachary, L. Gergely, and L. A. Staehelin. 2007. Dual-axis electron tomography: a new approachfor investigating the spatial organization of wood cellulose microfibrils Wood Sci Technol 41:101–116.

Ying, L., D. E. Kretschmann, and B. A. Bendtsen. 1994. Longitudinal shrinkage in fast-growth loblolly pine plantation wood. Forest Prod. J. 44(1): 58-62.

Yadama, V., M. P. Wolcott, and L.V. Smith. 2006. Elastic properties of wood-strand composites with undulating strands Composites: Part A 37: 385–392.

Yoshihara, H. and M. Ohta. 2000. Estimation of the shear strength of wood by uniaxial-tension tests of off-axis specimens. J. Wood Sci. 46:159-163.

Zhang, W. and A. Sliker. 1991. Measuring shear moduli in wood with small tension and compression samples. Wood and Fiber Sci. 21(1):58-68.

Zhang, B., Q. Wu, L. Wang, and G Han. 2005. The Influence of In-Plane Density Variation On Engineering Properties of Oriented Strandboard: A Finite Element Simulation. In Proc. the McMat2005 – The 2005 joint ASME/ASCE/SES Conference on Mechanics and Materials. June 1-3, Baton Rouge, LA. Paper 257.

Zink, A. G, R. W. Davidson, and R. B. Hanna. 1995. Strain measurement in wood using a digital image correlation technique. Wood and Fiber Sci. 27(4): 346–359.

Zink, A. G., R. B. Hanna, and J. W. Stelmokas. 1997. Measurement of Poisson's ratios for yellow-poplar. Forest Prod. J. 47(3):78-80.

Zink A. G. and C. Price. 2006. Compression strength parallel to the grain within growth rings of low density hardwoods. *Maderas: Ciencia y Tecnologia* 8(2):117-126.

Chapter 3. Tensile Properties of Earlywood and Latewood from Loblolly Pine (*Pinus taeda*) Using Digital Image Correlation

The goal of this chapter was to measure the elastic properties and strength of earlywood and latewood from growth ring numbers 1-10 and growth ring numbers 11-20. Because of the small specimen size, a contactless strain measurement was applied using a microscope with an appropriate field of view. The tensile properties of the earlywood and latewood were calculated from load data from Minimat tester and coupled with elastic strain data from a digital image correlation (DIC) technique. Incremental loading was applied until specimen failure occurred. Elastic modulus, Poisson ratio, and strength generally increased as the growth ring number increased except for the strength of Latewood showing slightly decreased. Elastic properties and strength were significantly different for different growth ring positions and intra-ring layers. The elastic modulus for earlywood and latewood were best fitted by Weibull distributions regardless of growth ring positions while Poisson ratios were best fitted by Weibull distributions for earlywood 1-10 and latewood 11-20 groups and Gamma distributions for earlywood 11-20 and latewood 1-10 groups. Strain distribution analysis showed non-uniform strain distributions for the four groups and also showed more resistance to load for earlywood and latewood from a higher growth ring position.

Introduction

A large portion of the wood resources for strand-based composites are supplied from plantation grown trees. These plantation grown trees are harvested on a short term rotation, resulting in small diameter logs and a high proportion of juvenile wood (Larson et al. 2001). This situation has placed pressure on the industry to use wood resources more efficiently for strand based composite production. While there is more interest in the efficient utilization of wood resources, there is lack of knowledge on the mechanical behavior of earlywood and latewood layers of loblolly pine (*Pinus taeda*). Different morphological and chemical variations of wood cells for earlywood and latewood produce different physical properties. Comprehensive knowledge of certain physical properties of earlywood and latewood including cell length, chemical composition, microfibril angle, and specific gravity are available from previous work (Taylor and Moore 1980, Bentdsen and Senft 1986, and Larson et al. 2001, and Yeh et al. 2006)

Indeed, it is hardly surprising that previous researchers have measured different mechanical properties between earlywood and latewood. However, there is little information about the effect of the growth ring numbers on the mechanical properties of earlywood and latewood. From pith to bark, there are many changes in anatomical structure including smaller microfibril angles and larger cell diameters (Taylor and Moore 1981, Bentdsen and Senft 1986, and Larson et al. 2001). These changes in earlywood and latewood properties may lead to fundamental changes in wood materials which could affect wood composite production. Therefore, measurement of earlywood and latewood from different growth ring positions can help maximize resource use.

However, elastic properties are difficult to measure for earlywood and latewood bands due to the small specimen size. Since it is difficult to use an extensometer or strain gauge

mounted to the surface of the earlywood and latewood without interference of strain measurement, non-contact methods are required to measure the elastic strain to calculate the elastic modulus. Digital image correlation (DIC) is one of the alternative options for this case since this technique uses images of the surface of test specimens acquired during the testing. Although the DIC is well developed and widely used to measure the strain distribution of materials qualitatively, there is lack of research on measuring elastic strain for wood material quantitatively using DIC. In order to apply DIC to measure the elastic strain, a complex testing set up and many calibrations are needed to have accurate results. In this chapter, earlywood and latewood properties from two different growth ring positions were measured using DIC. Understanding of earlywood and latewood properties from different growth ring positions will allow improved characterization of the constitutive behavior of wood strands and provide a more detailed characterization of the mechanical behavior.

Literature Review

Previous measurement of intra-ring properties

Previous studies have used different test methods to measure elastic properties of earlywood and latewood from different wood species. Table 3.1 provides previous work showing differences in mechanical properties of earlywood and latewood from different species. While Groom et al. (2002) and Mott et al. (2002) measured the properties of single fiber, Kretschmann et al. (2006) and Hindman and Lee (2007) measured the properties of small specimen of earlywood and latewood from loblolly pine (*Pinus taeda*).The presented values are the longitudinal elastic modulus (E_L) of earlywood and latewood and the longitudinal strength (σ_L)

of earlywood and latewood.

Table 3.1 Previous works on intra-ring test showing test conditions and results

Researchers	Species	Loading speed [μm/min]	Earlywood E_L [GPa]	Earlywood σ_L [MPa]	Latewood E_L [GPa]	Latewood σ_L [MPa]
Groom et al. (2002)	Loblolly pine (*Pinus taeda*)	80	N/A	N/A	6.55-27.5	410-1,422
Mott et al. (2002)	Loblolly pine (*Pinus taeda*)	80	14.8	604	N/A	N/A
Kretschmann et al. (2006)	Loblolly pine (*Pinus taeda*)	N/A[1]	3.5[2] 5.1[3]	N/A	8.1[1] 13.0[2]	N/A
Hindman and Lee (2007)	Loblolly pine (*Pinus taeda*)	127	2.71	27.5	6.38	48.8

[1]Not Applicable
[2]Earlywood and latewood at a height of approximately 1.5 m
[3]Earlywood and latewood at a height of approximately 6 m

Groom et al. (2002) measured the modulus of elasticity (MOE) and ultimate tensile strength (UTS) of latewood tracheids of loblolly pine in different growth ring positions and tree heights. The MOE of latewood increased from 6.55 GPa to 27.5 GPa as the ring number increased from pith to mature area. The strength of latewood increased from 410 MPa to 1,422 MPa as the growth ring position moved from pith to mature portion.

Mott et al. (2002) studied mechanical properties of earlywood of loblolly pine using a tensile tester with loading speed of 80 μm/min. The MOE and UTS of juvenile earlywood tracheids were 11.7 GPa and 496 MPa while those of mature earlywood fibers were 17.2 GPa and 648 MPa, respectively. Microfibril angle (MFA) for juvenile wood was 25 to 30 degrees and MFA for mature wood was 5 to 10 degrees. Based on the results, Mott et al. (2002) concluded that the MOE and UTS were dependent upon MFA.

Burgert et al. (2002) combined a video extensometry with a microtensile tester to

determine the MOE and strength of mature spruce fiber in a transition zone between earlywood and latewood. The MOE and UTS were 10 GPa and 530 MPa. Displacement was measured using the video extensometry instead of using cross head movement as specimen deformation. This method provided a more reliable MOE value.

Kretschmann et al. (2006) used a broadband viscoelastic spectroscopy instrument (BVS) to measure the modulus of elasticity and shear modulus of earlywood and latewood of six loblolly pine trees. Samples with the size of 1 mm by 1 mm by 30 mm were obtained from different growth ring numbers and different heights of trees. The MOE of earlywood increased from 3.5 GPa to 5.1 GPa as the height of tree increased from 1.5 m to 6 m. The MOE of latewood increased from 8.1 GPa to 13.0 GPa as the height of tree increased from 1.5 m to 6 m.

Hindman and Lee (2007) measured the MOE and strength of earlywood and latewood bands from loblolly pine using a tensile tester with a loading rate of 127μm/min. Earlywood samples with the size of 0.66 mm by 4.58 mm by 60 mm and latewood samples with the size of 0.66 mm by 3.3 mm by 60 mm were used. The MOE and UTS from earlywood showed 2.71 GPa and 27.5 MPa while those from latewood showed 6.38 GPa and 48.8 MPa.

Previous work to characterize the wood properties of earlywood and latewood has used the cross head movement as deformation of the specimen (Navi et al. 1994, Mott et al. 2002, Groom et al. 2002, and Hindman and Lee 2007). These measurements assumed no slippage in the grips. Also uniform elastic strain through entire span of specimen was assumed. From the result of Burgert et al. (2003), refinement of measurement on displacement of specimen can be found. Due to the size of the specimen used for testing, an accurate measurement of elastic strain is a key component to calculate MOE. Therefore, the elastic strain of earlywood and latewood should be determined from measurement of the center section apart from the edge to avoid edge

effect. One method for measuring elastic strain in the center of a specimen is the digital image correlation (DIC) method. The advantage of the DIC technique is the ability to track the change in position of a point in the field under study.

Digital Image Correlation (DIC) for Strain Measurement

DIC was developed to resolve the displacement on the surface of a specimen by correlating sub-images of a sequence of images - one before loading and several images during loading. Deformation of the material can be achieved by tracking the displacement of markers on the sample's surface. The advantage of DIC is that it can avoid overestimated strain due to the slippage of the clamp and the effect of the low stiffness of the test specimen. Figure 3.1 demonstrates the general scheme of tracking the displacement of the window on the sequence of images. The first step is to locate the interest point, P, in the image of the reference configuration before loading by virtually generating a grid. The virtual fixed grid on the image has information of the exact location of the point, P. After loading, the change in the location of point P is tracked by image correlation using a pattern matching technique. Eight subsets of pixels surrounding the point P in the reference image, called a template or window, are matched with similar sized subsets of pixels within a search window determined by the maximum expected inter-image displacement without marker. Tracking of a sub-image can be achieved by maximizing the cross correlation coefficient between grey value patterns of two images (Sun et al. 2005).

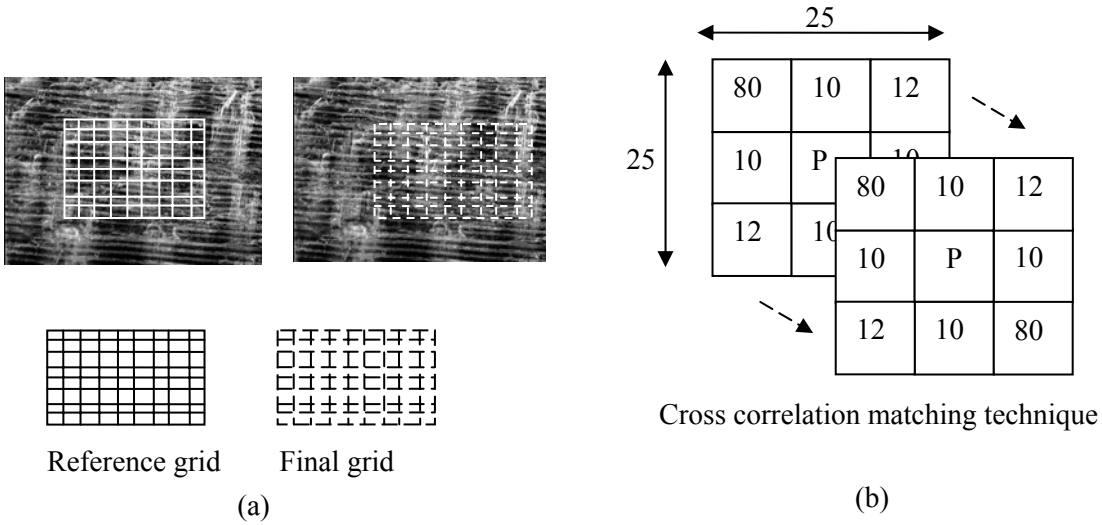

Figure 3.1 Cross correlation techniques for DIC: a) a sequence of images showing the change of grid positions, b) cross correlation matching technique

Many previous researchers have applied DIC to wood and wood-based materials. After the DIC technique was introduced to measure the strain distribution of wood and paper material by Choi et al. (1991), there was a body of DIC applications to wood material (Zink et al. 1995, Mott et al. 1996, Zink et al. 1997, Stelmokas et al. 1997, Muszynski et al. 2000, Murata and Masuda 2001, Danvind 2002, Samarasinghe and Kulasiri 2004, Penneru et al. 2005, Serrano and Enquist 2005, Ljungdahl et al. 2006, and Keunecke and Niemz 2008). While the main application of DIC to wood material was to measure the strain distribution, most DIC applications were not applied to quantify the average strain. Although the strain distribution showed qualitative information, the information could not validate and compare to quantitative properties from other test methods. Therefore, a novel procedure was required to quantify tensile properties of earlywood and latewood.

The objective of this chapter was to measure MOE, Poisson ratio, and UTS of loblolly pine earlywood and latewood from different growth ring positions using DIC. A specific

guideline for using DIC to measure elastic properties of earlywood and latewood from growth ring numbers 1-10 and growth ring numbers 11-20 was developed. Elastic properties of the earlywood and latewood were calculated from load data from Minimat tester coupled with elastic strain data from a digital image correlation (DIC) technique. Strain distribution within the earlywood and latewood samples was also observed.

Materials and Methods

Material Preparation

A twenty-five year old loblolly pine (*Pinus taeda* L.) from Reynolds Homestead Research Center in Patrick County, Virginia was chosen for this study. Four wood disks were cut approximately 0.6 m height from the ground. Wood blocks with a size of 13.9 cm by 13.3 cm by 5.08 cm were taken from growth ring numbers 1 to 10 and growth ring numbers 11 to 20 from pith. Due to the method of strand generation, finer gradiations into discrete growth rings were not obtained. All wood blocks were submerged in water and a vacuum applied to minimize cutting damage. Strands were processed from a flaker located at Brooks Forest Products Center at Virginia Polytechnic Institute and State University. Earlywood and latewood specimens were prepared from aligned strands using a razor knife and a metal ruler. Aligned strands were cut to the size of 55 mm by 10 mm by 0.5 mm of earlywood and latewood from growth ring number 1 to 10 from pith, and the same size of earlywood and latewood from growth ring number 11 to 20 from pith. Four specimen groups were obtained from the same disk. Sample size for each group was 50. Figure 3.2 shows the segmented earlywood and latewood bands from a strand. After extracting the earlywood and latewood separately, both earlywood and latewood bands were

carefully placed into re-closable bags. Strands were kept in an environmental chamber to normalize the moisture content at 6 % for one month.

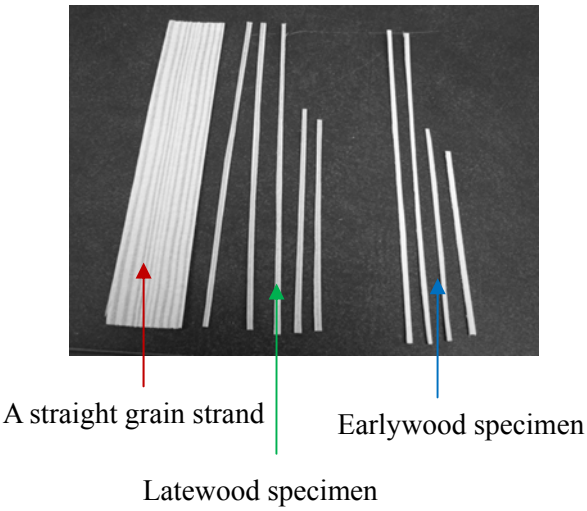

Figure 3.2 Segmentation of earlywood and latewood specimens from a strand

Test Set Up

Specimens were tested using a Minimat tester (Rheometric Scientific, 2000) and a Zeiss microscope with a 10x ocular and 2.5x objective lens. Minimat test frame contained a 200 N load cell and computer controlled displacement with cross head travel range of 100 mm and the sensitivity of 0.15 microns. The Zeiss microscope has a DAGE MTI 72 CCD camera attached to capture the surface of the test specimen. Resolution of the camera was 768 by 493 pixels. Spacial size of the image pixel was calculated using a stage micrometer (100 units in 3 mm) correlated with pixel size of the image in the field of view on the specimen. The spatial resolution of the camera was 11 μm/pixel by 13 μm/pixel. Field of view was calculated to be 4.20 mm (horizontal) by 3.22 mm (vertical). Resolution of the image was 632 by 480 pixels. Pixel size in spatial area was determined to be 6.64 μm by 6.71 μm. However, subpixel was set to 1/1000 pixel to match the displacement of the sequence of images using cross-correlation and bi-cubic

interpolation. Therefore, the pixel resolution can detect a minimum length change of 6.64 by 10^{-3} μm by 6.71 by 10^{-3} μm.

The Minimat test frame was mounted on a newly designed stage, which has a fine level adjustment and two side bars with screws to hold the Minimat tightly (Figure 3.3). The designed stage has two legs in the left side to minimize vibration during testing. Specimens were gripped at both ends using metal jaws. Span length between the grips was 40 mm. Specimens were loaded at a rate of 0.126 mm/min. A preload of 1N was applied to stabilize the specimen and to adjust the focus of the lens. From preliminary testing, this preload represents less than 2% of the failure load, and is well within the elastic range. After adjusting the focus distance, tensile testing continued until the specimen failed. Incremental loading was applied to prevent the capture of distorted images for strain determination. Capture of images during loading can cause strain greater than true strain (Mott et al. 1996). Test was paused for 8 seconds while each image was captured. To have clear contrast for image correlation, a speckle pattern was generated on the surface of the specimen using carbon black particles and a paint brush. Images were taken every 20 seconds for up to 300 seconds. To minimize the influence of light other than a fiber optic lamp, all testing was conducted at night with no room light. All input devices including mouse and keyboard were placed on a different table to avoid creating vibrations while conducting the testing. To analyze the effect of the pause time on relaxation of specimen, images were taken every two seconds up to 120 seconds. The results showed only 1% change in strain compared to the change of strain value for calculating elastic modulus. Therefore, the effect of the 8 second pause time on the strain variation can be ignored.

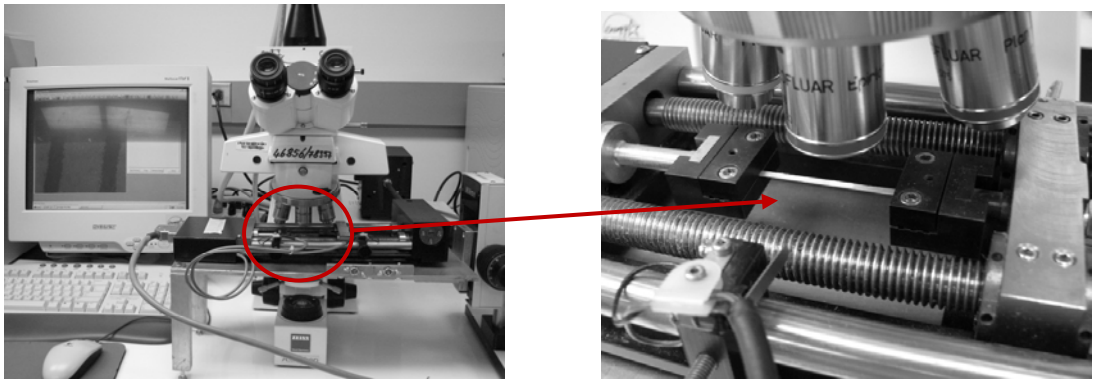

a) Microtensile test set up with a Zeiss b) A tensile specimen at 2.5x magnification

Figure 3.3 Microtensile test set up for applying tensile load and capturing surface images of earlywood and latewood; a) Microtensile test set up with a Zeiss, b) A tensile specimen at 2.5x magnification

Strain Measurement Using Digital Image Correlation (DIC)

Strain was measured from the sequence of specimen images within the elastic range under tension loading using DIC software coded by Eberl et al. (2006). Different window sizes, 200, 100, 50, 25, 15, and 10 pixels were used to check convergence of the strain value. A 25 pixel window size was chosen for the actual image correlation for strain measurement. While image correlation was running, the change of the tracking point was also examined by looking at the sequence of images. The out of range correlation samples were eliminated by visual inspection.

In order to detect a small strain, the conventional DIC considers a homogeneous deformation on the surface of the specimens and uses sub-pixel correlation. A sub-set based correlation compares a sub-set of pixel intensities from the undeformed image with a subset of pixel intensities after loading using interpolation. If the material is not homogeneous, higher order interpolation is required, while homogeneous materials only require zero or first order

interpolation to approximate the variation of the displacement field (Jin and Bruck 2005). In this study, a cubic spline interpolation scheme was employed to represent the inhomogeneous displacement field of wood. Image acquisition and deflection rate were synchronized to evaluate the elastic modulus. A virtual reference grid was generated on the first image before the load was applied, the grid point was tracked by correlated grey scale of the region around the reference point as the image goes from the first to last.

Specific Gravity Measurement

Specific gravity was measured according to ASTM D 2395 (ASTM 2004a). Samples for specific gravity measurement were obtained from untested samples of the same population. To minimize the influence of the environment of room humidity and temperature prior to testing, all samples were kept in the closable bag and handled by forceps when the specimens were mounted on the balance. The balance has a sensitivity of ± 0.00001g. Volume of specimens was measured using micro caliper having a sensitivity of ± 0.001 mm. After measuring the specimen weight, all samples were kept inside petri dishes and covered by a closable bag. To measure the oven-dry weight, the petri dishes were taken out from the closable bag, and put in the oven for twenty-four hours. Specific gravity was measured based on the oven-dry weight and volume at the same condition as during mechanical testing.

Results and Discussion

Experimental Results

Table 3.2 provides a summary of the test results from the four sample groups. Specific

gravity increased as growth ring number increased. The latewood specific gravity from growth ring number 1-10 and from growth ring number 11-20 had 74% and 26% higher than the earlywood specific gravity from growth ring number 1-10 and growth number 11-20. However, for Latewood 1-10 and Latewood 11-20 the specific gravity was slightly decreased from 0.54 to 0.53.

Table 3.2 Physical properties and mechanical properties of earlywood and latewood from growth rings 1-10 and growth rings 11-20

Test groups	SG		MOE (GPa)		UTS (MPa)		Poisson ratio	
	AVE	COV	AVE	COV	AVE	COV	AVE	COV
Earlywood 1-10	0.31	13%	1.92	31%	18.69	35%	0.49	53%
Latewood 1-10	0.54	8%	3.44	31%	34.21	37%	0.59	48%
Earlywood 11-20	0.42	7%	2.48	29%	25.01	29%	0.49	54%
Latewood 11-20	0.53	7%	5.09	36%	33.47	27%	0.80	54%

Latewood 11-20 had the highest MOE of 5.09 GPa with coefficient of variance (COV) of 36% while Earlywood 1-10 had the lowest MOE of 1.92 GPa with COV of 31%. Compare to the MOE of Earlywood 1-10 and Earlywood 11-20, the MOE of Latewood 1-10 and Latewood 11-20 showed 1.79 and 2.05 times higher, respectively. Compared to the MOE of Earlywood 1-10 and Latewood 1-10, the MOE of Earlywood 11-20 and Latewood 11-20 showed 1.29 and 1.48 times higher, respectively.

Latewood 1-10 had the highest UTS of 34.21 MPa with COV of 37% while Earlywood 1-10 had the lowest UTS of 18.69 MPa with COV of 35%. Compared to the UTS of Earlywood 1-10 and Earlywood 11-20, the UTS of Latewood 1-10 and Latewood 11-20 showed 1.83 and 1.33 times higher, respectively. Compared to the UTS of Earlywood 1-10 and Latewood 1-10, the UTS of Earlywood 11-20 and Latewood 11-20 showed 1.33 times higher and 0.97 times lower, respectively.

Latewood 11-20 had the highest Poisson ratio of 0.8 with COV of 54 % while the lowest Poisson ratio found was 0.49 with COV of 53% and with COV of 54% from Earlywood 1-10 and Earlywood 11-20. Compared to the Poisson ratio of Earlywood 1-10 and Earlywood 11-20, the Poisson ratio of Latewood 1-10 and Latewood 11-20 showed 1.20 and 1.63 times higher, respectively. Compared to the Poisson ratio of Earlywood 1-10 and Latewood 1-10, the Poisson ratio of Earlywood 11-20 and Latewood 11-20 showed 1.0 times and 1.35 times higher, respectively

Except for the cases of Latewood 1-10 and Latewood 11-20 UTS, the general trend was as the growth ring number increased, the UTS, MOE, and Poisson ratios also increased. While specific gravity was highly correlated with UTS from earlywood and latewood, specific gravity was weakly correlated with MOE from latewood. Weak correlation between specific gravity and MOE of earlywood and latewood was also found by Cramer et al. (2005) and Kretschmann et al. (2006). Less variation of physical and mechanical properties of earlywood and latewood was found from COV of SG, UTS, and MOE as the growth ring number switched from 1-10 to 11-20. Greater mechanical properties and less variation of earlywood and latewood from a higher growth ring number can be speculated that more mature earlywood and latewood have a more oriented reinforcement to the longitudinal direction. The oriented reinforcement can be associated with the MFA that are more oriented to the fiber axis for a higher growth ring number. Previous results also found that as growth ring number increased, MFA decreased (Groom et al. 2002 and Kretschmann et al. 2006). The less reinforcement to the off-diagonal of the loading direction due to the lower MFA in a higher growth ring position could have resulted in a higher deflection in the transverse direction, which eventually induced a higher Poisson ratio.

Figure 3.4 shows the relationship between tree height and average MOE from earlywood

and latewood from the same species. The average MOE data at growth ring number 1 to 20 from 0.6 m tree height were used from current study. The average MOE data at growth ring number 3, 6, 12, and 18 from 1.5 m and 6 m tree height were obtained from a previous study (Kretschmann et al. 2006). The correlation between MOE of earlywood and height, between MOE of latewood and height, and between the MOE ratio of latewood to earlywood and height showed a strong positive linear relation presenting R^2 of 0.996, 0.995, and 0.931. From the MOE ratio of latewood to earlywood as a function of height, the MOE of latewood increased more than that of earlywood. It can be speculated that in the lower height of tree, earlywood and latewood fiber structures are physiologically adapted to support compression by tree mass and gravity with higher MFA, thicker cell wall diameter, larger cell dimension, and shorter fiber lengths, while in the upper height of tree, earlywood and latewood fiber structures are adapted to support tension by wind and growth stress with lower MFA, thinner cell wall diameter, smaller cell dimension, and longer fiber length (Yeh et al. 2006, Xu et al. 2004, Groom et al. 2002, Mott et al. 2002, Burdon et al. 2003, and Cramer et al. 2005, Kretschmann et al. 2006). These speculations on the anatomical structure adaptations of earlywood and latewood are rather relative comparison for the earlywood and latewood from the three heights of tree and away from bark than the comparison for the individual growth rings at the same height

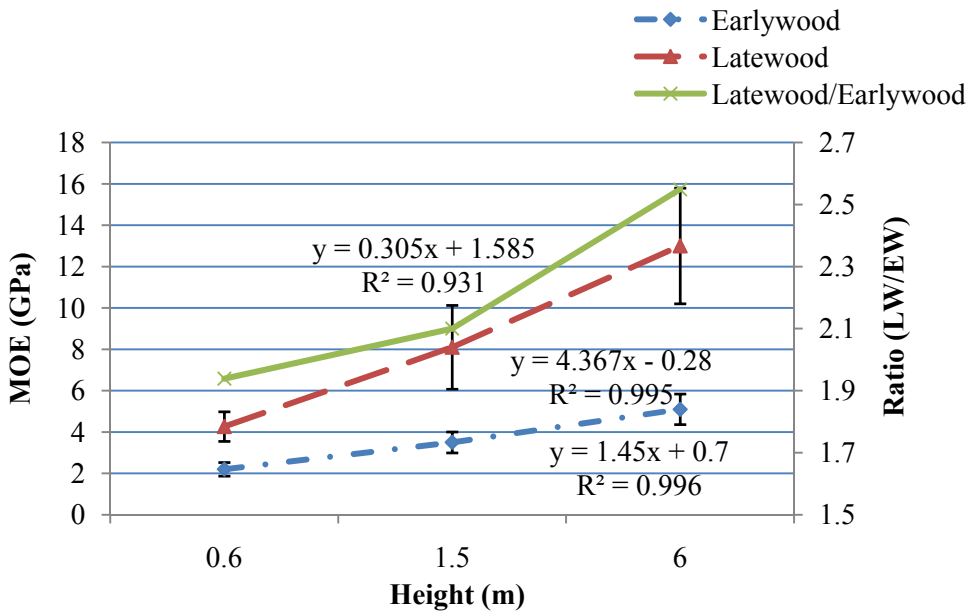

Figure 3.4 Earlywood MOE, latewood MOE, and Ratio of latewood MOE to earlywood MOE as a function of tree heights from current test results including data at 0.6 m height and a previous study by Kretschmann et al. 2006 including data at 1.5 and 6 m height

Table 3.3 shows the summary of the Two-Way ANOVA results considering factors of growth ring and intra-ring position on the MOE, UTS and Poisson ratio from the sample groups. The alpha of 0.05 was used as a significant difference. Although there were many other interaction results between growth ring numbers and intra-ring layers, only the physically meaningful comparisons are shown in Table 3.3. Overall comparison between growth ring number 1-10 and growth ring number 11-20 shows significant differences in MOE, UTS, and Poisson ratio. Overall, comparison between earlywood and latewood also showed significant differences in MOE, UTS, and Poisson ratio. When looking at the detailed comparison of interaction between growth ring numbers and intra-ring layers, all MOE comparisons showed significant differences, which agreed with the results from Table 3.2. For the UTS, only comparison between Latewood 1-10 and Latewood11-20 was not significantly different, which

agreed with results from Table 3.2 showing that 34.21 MPa for Latewood 1-10 with COV of 31% and 33.47 MPa for Latewood 11-20 with COV of 36%. The difference of specific gravity between Latewood 1-10 and Latewood 11-20 was only 1.8%. For Poisson ratio, all comparisons showed significant difference except for the case between Earlywood 1-10 and Earlywood 11-20, which also agrees with the results from Table 3.2.

Table 3.3 Statistical comparison of the tensile properties for earlywood and latewood from two different growth ring positions; growth ring number 1-10 and growth ring number 11-20 (α=0.05)

Variable A	Variable B	p-value for MOE	p-value for UTS	p-value for Poisson ratio
Growth ring position 1-10	Growth ring position 11-20	<0.0001	0.006	0.030
Earlywood	Latewood	<0.0001	<0.0001	<0.0001
Earlywood 1-10	Earlywood 11-20	0.006	0.0003	0.440
Earlywood 1-10	Latewood 1-10	<0.0001	<0.0001	0.017
Earlywood 11-20	Latewood 11-20	<0.0001	<0.0001	<0.0001
Latewood 1-10	Latewood 11-20	<0.0001	0.831	0.028

Table 3.4 shows the distribution fitting for MOE, UTS, and Poisson's ratio from four groups. The alpha value of 0.05 was used to find the best fitting curve for the MOE, UTS, and Poisson's ratio from normal, lognormal, Weibull, and Gamma distribution using SAS 9.1 (SAS Institute Inc. 2004). The distribution fitting was examined by Kolmogorov-Smimov (K-S) and Chi-square test. Visual inspection also conducted for estimating the best fitting curve. Based on the p-value from K-S and Chi-square test and visual inspection, the Weibull distributions were decided to be the best fitting curve with the three estimated parameters. The best fitting curves for UTS of Earlywood 1-10 and Latewood 1-10 were Weibull distribution while Earlywood 11-20 and Latewood 11-20 group were lognormal. However, for Earlywood 11-20 group, Chi-

square test was below p-value of 0.05. For the Poisson ratio, Earlywood 1-10 and Latewood 11-20 groups were fitted best with the Weibull distribution while the Latewood 1-10 and Earlywood 11-20 followed with the Gamma distribution. Analytical distribution of mechanical properties for earlywood and latewood from different growth ring number could be used for numerical modeling.

Table 3.4 Distribution fitting for tensile properties of earlywood and latewood from growth ring numbers 1-10 and growth ring numbers 11-20 (α=0.05)

Test groups	Normal		Lognormal		Weibull		Gamma	
MOE	K-S	Chi-square	K-S	Chi-square	K-S	Chi-square	K-S	Chi-square
Earlywood 1-10	0.14	0.32	0.25	0.26	0.11	0.31	0.09	0.30
Latewood 1-10	0.15	0.29	0.25	0.26	0.25	0.51	0.25	0.36
Earlywood 11-20	0.15	0.15	0.50	0.05	0.5	0.08	0.02	0.08
Latewood 11-20	0.06	0.28	0.5	0.71	0.5	0.85	0.5	0.79
UTS	K-S	Chi-square	K-S	Chi-square	K-S	Chi-square	K-S	Chi-square
Earlywood 1-10	0.15	0.23	0.25	0.17	0.5	0.22	0.25	0.22
Latewood 1-10	0.13	0.14	0.23	0.75	0.14	0.40	0.25	0.67
Earlywood 11-20	0.08	0.001	0.25	0.01	NA	0.001	0.25	0.004
Latewood 11-20	0.15	0.07	0.23	0.05	0.25	0.04	N/A	N/A
Poisson Ratio	K-S	Chi-square	K-S	Chi-square	K-S	Chi-square	K-S	Chi-square
Earlywood 1-10	0.15	0.03	0.04	N/A	0.5	0.50	0.25	0.59
Latewood 1-10	0.02	0.001	0.04	0.17	0.06	0.05	0.25	0.17
Earlywood 11-20	0.01	0.001	0.03	0.13	0.007	0.04	0.06	0.09
Latewood 11-20	0.01	0.001	0.25	0.11	0.25	0.25	0.13	0.04

Strain Distribution of Earlywood and Latewood from growth ring number 1-10 and 11-20

Representative strain distributions of one sample from each test group are shown in Figure 3.5 and Figure 3.6. The strain distribution in x is the direction parallel to the load direction, while strain distribution in y direction is the direction perpendicular to the loading direction. To compare the strain distribution for earlywood and latewood from different growth ring positions at a similar stress level, a sequence from images correlation is shown here; the

seventh image for Earlywood 1-10, the fourth image for Latewood 1-10, the sixth image for Earlywood 11-20, and the second image for Latewood 11-20, which were under elastic range. Normally failure of earlywood and latewood occurred at least after the tenth image was taken for all groups.

Figure 3.5 shows the strain distribution of sample number 45 from Earlywood 1-10 and sample number 50 from Latewood 1-10. The strain distributions in x and y directions for the Latewood 1-10 showed more resistance under similar stress level, showing that approximately one magnitude smaller strain occurred. The Latewood 1-10 strain distribution showed higher proportions of negative strain distributions in the x-direction to the positive strain by applied load and higher proportions of negative strain distributions in the y-direction to the negative strain by applied load. Due to the strain distribution of earlywood and latewood, Latewood 1-10 had higher MOE and Poisson ratio found from Table 3.2.

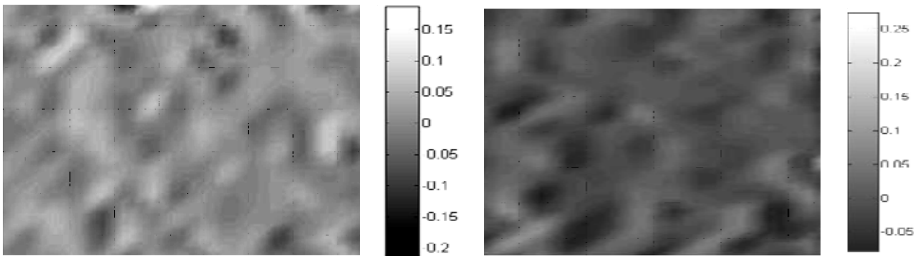

a) Strain x of Earlywood 1-10 b) Strain y of Earlywood 1-10

c) Strain x of Latewood 1-10 d) Strain y of Latewood 1-10

Figure 3.5 Strain distribution of earlywood and latewood from growth ring numbers 1-10 (Specimen number 45 under 19.6 MPa, Specimen number 50 under 21.9 MPa)

Figure 3.6 shows the strain distribution of specimen number 50 for the Earlywood 11-20 and specimen number 50 for the Latewood 11-20. The magnitude of the strain distributions was much lower for earlywood and latewood from growth ring number 11-20, which can be interpreted as more oriented structure to the load direction for growth ring number 11-20 group. Compared to growth ring number 1-10, a higher MOE value for growth ring number 11-20 can be seen from the strain distribution in x showing much lower magnitude in strain x of earlywood 11-20 and Latewood 11-20. Under the same stress level, Latewood 11-20 showed the most distinctive pattern for negative strain in x and negative strain in y from growth ring number 11-20 resulted in the highest Poisson ratio among the groups.

Regardless of intra-ring layer and growth ring positions, non-uniform strain distribution occurred in both directions during the testing. The average strain value used for the calculation of elastic modulus and Poisson ratio was in the 10^{-3} range; however, high oscillations of the strain distributions were observed on the cross section. This is an interesting point that non-uniform strains occur in the middle of the cross section away from the edge since uniform strain distribution within the gauge length is one of the assumptions made for ASTM D143 (ASTM 2004b) for tension and compression tests. However, from the results, the earlywood and latewood structure responds differently under a given load. Therefore, the elastic moduli of wood defined from ASTM D143 are actually effective moduli of the average of a set of individual fibers.

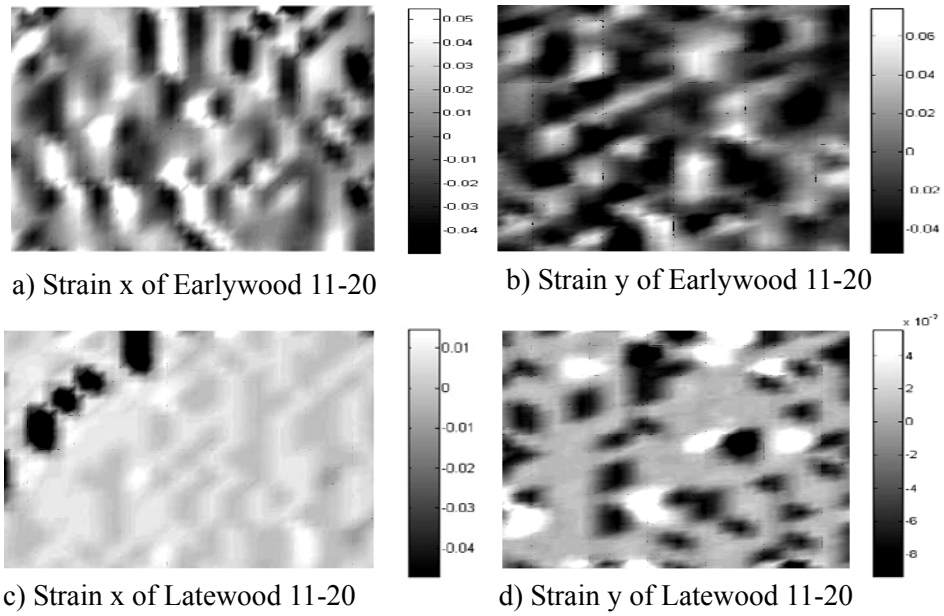

a) Strain x of Earlywood 11-20 b) Strain y of Earlywood 11-20

c) Strain x of Latewood 11-20 d) Strain y of Latewood 11-20

Figure 3.6 Strain distribution of earlywood and latewood from growth ring number 11-20 (Specimen number 50 under 19.4 MPa and Specimen number 50 under 19.8 MPa)

Conclusions

The physical and mechanical properties of earlywood and latewood from two different growth ring positions showed different values. The general trend was that specific gravity, MOE, UTS, and Poisson ratio generally increased with the increment of the growth ring positions except for specific gravity and UTS from latewood. While the MOE for earlywood and latewood was not dependent on the specific gravity, UTS for earlywood and latewood was highly dependent on specific gravity. From comparison between current results and a previous study, MOE from earlywood and latewood showed a positive relationship with the height of tree. Statistical comparisons showed that the MOE and UTS had a significant difference by both growth ring and intra-ring positions. Distribution fitting showed that MOE for four groups were

best fitted by Weibull distribution while Poisson' ratio were best fitted by Weibull distribution for Earlywood 1-10 and Latewood 11-20 groups and Gamma distribution for Earlywood 11-20 and Latewood 1-10 groups. Strain distribution showed non-uniform distributions for four groups. Compared to Earlywood 1-10 and Latewood 1-10, Earlywood 11-20 and Latewood 11-20 showed more resistance to the load.

Acknowledgements

This work was funded by the USDA National Research Initiative Competitive Grants Program (2005-35504-16115). Their financial contribution to this work is greatly acknowledged.

References

ASTM. 2004a. Standard Test Methods for Specific Gravity of Wood and Wood-Based Materials. ASTM D 2395. Annual Book of ASTM Standard. Vol. 4.10 Wood. ASTM, West Conshohocken, PA.

ASTM. 2004b. Standard Test Methods for Small Clear Specimens of Timber. ASTM D 143. Annual Book of ASTM Standards. Vol. 4.10 Wood. ASTM, West Conshohocken, PA.

Bendtsen, B. A. and J. Senft. 1986. Mechanical and anatomical properties in individual growth rings of plantation-grown Eastern cottonwood and loblolly pine. Wood and Fiber Sci. 18:23–38.

Burdon, R. D., R. P. Kibblewhite, J. C. F. Walker, R. A. Megraw, R. Evans, and D. J. Cown. 2004. Juvenile versus mature wood: a new concept, orthogonal to corewood versus outerwood, with special reference to *Pinus radiata* and *P. taeda*. Forest Sci. 50:399-415.

Burgert I, Fruhmann K, Keckes J, Fratzl P, Stanzl-Tschegg SE (2003) Microtensile testing of wood fibers combined with video extensometry for efficient strain detection. Holzforschung. 57:661-664

Choi, D., J. L. Thorpe and R. B. Hanna. 1991. Image analysis to measure strain in wood and paper. Wood Science and Technology 25(2):251-262.

Cramer, S. M., D. E. Kretschmann, R. Lakes, and T. Schmidt. 2005. Earlywood and latewood elastic properties in loblolly pine. Holzforschung. 59:531-538.

Danvind, J. 2002. Methods for Collecting and analysing simultaneous strain and moisture data during wood drying; Licenciate Thesis in the Division of Wood Physics, Skelleftea Campus:

Skelleftea, Sweden, Lulea University of Technology

Eberl C., R. Thompson, and D. Gianola. 2006. Digital image correlation and tracking with Matlab. Matlab Central. http://www.mathworks.com/matlabcentral/fileexchange/loadFile.do?objectId=12413&objectType=FILE (27 September 2006).

Groom, L., L. Mott., and S. Shaler. 2002. Mechanical properties of individual southern pine fibers. Part I. Determination and variability of stress-strain curves with respect to tree height and juvenility. Wood and Fiber Sci. 34(1):14-27.

Hindman D. P. and J. N. Lee. 2007. Modeling wood strands as multi-layer composites: bending and tension loads. Wood and Fiber Sci. 39(4):515-526.

Jin H. and H. A. Bruck. 2005. Theoretical development for pointwise digital image correlation. Optical Engineering, Volume 44, pp

Keunecke D, Niemz P (2008) Axial stiffness and selected structural properties of yew and spruce microtensile specimens. Wood Research 53:1-14

Kretschmann, D. E., S. M. Cramer, R. Lakes, and T. Schmidt. 2006. Selected mesostructure properties in loblolly pine from Arkansas plantations. Characterization of the Cellulosic Cell Wall. Ames, Iowa : Blackwell Pub., 149-170 pp.

Larson, P. R., D. E. Kretschmann, A. Clark III, and J. G. Isebrands. 2001. Juvenile wood formation and properties in southern pine. General Technical Report FPL-GTR-129. Madison, Wisconsin: US Department of Agriculture, Forest Service, Forest Products Laboratory

Ljungdahl J. L. A. Berglund, and M. Burman. 2006. Transverse anisotropy of compressive failure in European oak-a digital speckle photography study. Holzforschung, 60:190-195

Mott, L., L. Groom, and S. Shaler. 2002. Mechanical properties of individual southern pine fibers. Part II. Comparison of earlywood and latewood fibers with respect to tree height and juvenility. Wood and Fiber Sci. 34(2): 221-237.

Mott, L., S. M. Shaler, and L. H. Groom. 1996. A novel technique to measure strain distributions in single wood fibers. Wood and Fiber Sci. 28(4):429-437.

Muszynski, L., R. Lopez-Anido, and S. M. Shaler. 2000. Image correlation analysis applied to measurement of shear strains in laminated composites. In: Proceedings of SEM IX International Congress on Experimental Mechanics, Orlando FL, June, 5-7, 2000. 163-166.

Penneru A. P., K. Jayaramanand, and D. Bhattacharyya. 2005. Strain analysis in bulk forming of wood. Holzforschung, 59:456–458

Samarasinghe, S. and D. Kulasiri. 2004. Stress intensity factor of wood from crack-tip displacement fields obtained from digital image processing. Silva Fennica 38(3):267–278.

Serrano, E., and B. Enquist. 2005. Contact-free measurement and non-linear finite element analyses of strain distribution along wood adhesive bonds. Holzforschung 59:641–646.

SAS Institute Inc. 2004. SAS/STAT® 9.1 User's Guide. Cary, NC: SAS Institute Inc.

Stelmokas, J. W., A. G. Zink, J. L. Loferski, and J. D. Dolan. 1997. Measurement of load distribution among multiple-bolted wood connections. Journal of Testing and Evaluation 25(5):510-515

Sun Y, Pang JHL, Wong CK, Su F (2005) Finite element formulation for a digital image correlation method. Appl. Opt. 44:7357-7363

Taylor, F. W. and J. S. Moore. 1981. A comparison of earlywood and latewood tracheid lengths in loblolly pine. Wood and Fiber. 13:159-165

Xu P., L. Donaldson, J. Walker, R. Evans, and G. Downes. 2004. Effects of density and microfibril orientation on the vertical variation of low-stiffness wood in radiate pine butt logs. Holzforschung. 58:673-677.

Yeh T. F., J. L. Braun, B. Goldfarb, H. M. Chang, and J. F. Kadla. 2006. Morphological and chemical variations between juvenile wood, mature wood, and compression wood of loblolly pine (*Pinus taeda* L.). Holzforschung. 60:1-8.

Zink, A. G, R. W. Davidson, and R. B. Hanna. 1995. Strain measurement in wood using a digital image correlation technique. Wood and Fiber Sci. 27(4):346–359.

Zink, A. G., R. B. Hanna, and J. W. Stelmokas. 1997. Measurement of Poisson's ratios for yellow-poplar. Forest Prod. J. 47(3):78-80.

Chapter 4. Comparison of Longitudinal Tensile Properties of Different Orientation Strands from Loblolly Pine (*Pinus taeda*)

The goal of this chapter was to measure the tensile properties of different orientations of loblolly pine strands from growth ring numbers 1-10 and growth ring numbers 11-20 using digital image correlation (DIC). A series of images was captured for strain measurement and synchronized with loading data for calculation of modulus of elasticity (MOE) and Poisson ratio. Ultimate tensile strength (UTS) was also measured. The general trend for straight grain orientation strands and tangential grain orientation strands was that MOE and UTS increased as the growth ring numbers increased. Statistical comparison showed no significant difference of MOE between the two different orientations of wood strands, and no significant difference of Poisson ratio between the two growth ring numbers. The UTS comparison between straight grain orientation strands from inner growth ring number 1-10 and straight grain orientation strands from outer growth ring number 11-20 were significantly different. The UTS comparison between straight and tangential grain orientation strands from outer growth ring number 11-20 showed a significant difference. Strands from higher growth ring number showed more consistent tensile failure behavior.

Introduction

In the U.S., the use of softwood strands has been growing as oriented strand board (OSB) and structural composite lumber (SCL) production increases. The impetus for development of a variety of SCL products has been decreasing access to large high quality logs, and industry commitments to better utilization of harvests. Development of SCL has many advantages, which are to use smaller trees, to use waste wood from other processing, to remove defects, to create more uniform components, to develop composites that improve some mechanical properties compared to solid wood, and to have higher yield from logs with bark compared to solid sawn lumber (Schuler and Adair 2000, and Balatinecz and Kretschmann 2001).

Although SCLs and OSB have several advantages over solid lumber, there is little research analyzing the material properties of wood strands. Wood has an orientation developed by the arrangement of earlywood and latewood. Earlywood and latewood properties vary throughout different growth ring numbers. Growth rings closer to pith contain higher proportions of juvenile wood than growth rings closer to bark. Juvenile wood differs from mature wood in that it has a higher microfibril orientation, a high percentage of compression wood, distorted grain patterns, and a lower percentage of latewood (Larson et al. 2001). The effects of orientation and growth ring numbers on mechanical properties of wood strands are not well known.

This chapter focuses on the effect of the growth ring number and orientation of wood strands on tensile properties of wood strands. Tensile testing was conducted with digital image correlation (DIC). Two-dimensional measurements were carried out to measure longitudinal strain as well as transverse strain. A better understanding of the mechanical properties of wood strands can lead better mechanical properties of wood products (Wu et al. 2005). This chapter can serve as a tool for manufacturing engineers to develop better performing material. The

knowledge of wood strands properties can maximize the use of wood resources.

Literature Review

Previous studies used different test set-ups to evaluate the modulus of elasticity (MOE) and strength of strands from different species. Comprehensive results from previous research can be found in Jeong et al. (2008). Literature review from this study focuses on the effect of testing arrangement on mechanical properties of wood strands from different wood species.

Price (1975) studied the effect of gage length on the MOE and UTS of sweetgum (*Liquidambar styraciflua L.)* flakes using a tensile test with the strain rate of 0.0127 cm/cm/min. Four different gage lengths (1.27 cm, 1.90 cm, 2.54 cm and 3.17 cm) were used in this study. UTS increased with an increase of gage length while MOE decreased with an increase of gage length. MOE of flake specimens was less than that of solid wood for the same species.

Geimer et al. (1985) measured the tensile stiffness and strength of two different grades of Douglas-fir (*Pseudotsuga menziesii)* strands. The grade of strands was determined by damage conditions. The test set-up was 3.81 cm gage length and used cross head movement to calculate strain in the flakes. The test speed was 0.0127 cm/min. Boards made from higher grade strands had 55% higher tensile strength compared to boards made from lower grade strands. MOE and UTS of the strands were 50% and 28% of the reported value for northern interior Douglas-fir (*Pseudotsuga menziesii).*

Deomano and Zink-Sharp (2004) conducted three point bending to calculate MOE and modulus of rupture (MOR) of 25 mm by 5.0 mm by 0.6 mm flakes from three different species including southern pine (*Pinus spp.*), sweetgum (*Liquidambar styraciflua L.*), and yellow-poplar (*Liriodendron tulipifera L.*) with different test conditioning (three different temperatures, two

cutting directions). The loading rate was 2.54 mm/min. Higher drying temperature lowered mechanical properties of flakes and tangentially cut specimens had higher mechanical properties compared to radially cut specimens. The average MOE of radial and tangential cutting direction specimen was 4.3 GPa and 5.2 GPa. The MOR of radial and tangential cutting direction specimens was 69.1 MPa and 86.7 MPa.

Cai et al. (2007) extended the work of Wu et al. (2005) by adding more species - willow (*Salix spp*.), yellow-poplar (*Liriodendron tulipifera L*.), red oak (*Quercus spp*.), and loblolly pine (*Pinus taeda*). The tensile properties of wood strands were significantly lower than those of solid wood. Compared to the tensile strength of solid woods (USDA 1999), that of wood strands from the various species was lower 31.1%, 44.2%, 36.2% , 73.4 % for willow, yellow-poplar, red oak, and loblolly pine, respectively.

Hindman and Lee (2007) tested different orientations (straight, angle, arbitrary) of wood strands for MOE and UTS using tension and bending tests. The results showed that both MOE and UTS were different from different orientations of wood strands. For MOE and UTS from tension test, the highest values were found from straight grain orientation strands, while the lowest values were found from the arbitrary grain orientation strands. For MOE and UTS from bending tests, the highest values were found from straight grain orientation strands while the lowest values were found from angle grain strands.

Jeong et al. (2008) noted that previous research on measurement of mechanical properties from wood strands cannot be directly comparable due to different testing arrangements. To investigate the effect of the testing arrangement on mechanical properties of wood strands, a different loading rate and different thickness of wood strands were used. While there was no significant difference of MOE and UTS by different loading rate, there was a significant

difference of MOE and UTS by different thickness. The trends showed that as thickness increased, MOE and UTS increased. Appropriate loading rate and thickness of wood strands for tensile testing were suggested.

From previous studies, two key issues for measurement of MOE and UTS of wood strands are the mechanical testing set-up and material preparation. For testing set-up, the importance of application of correct gage length and loading speed to measure MOE was noted by Price (1975). For material preparation, different thickness, grade, and cutting direction are important parameters for the determination of mechanical properties of wood strands (Geimer et al. 1985, Deomano and Zink-Sharp 2004, Cai et al. 2007, Hindman and Lee 2007, and Jeong et al. 2008).

In processing wood strands, understanding the effect of the orientation and growth ring numbers on the mechanical properties is crucial to maximize the properties for the end use. Segregation of different strands into discrete categories can maximize the benefits of use. Understanding the effect of the growth ring numbers on mechanical properties of wood strands can lead to better utilization of resources. The purpose of this chapter was to measure tensile properties of different grain orientation strands from growth ring number 1-10 and growth ring number 11-20. The MOE, UTS, and Poisson ratios from strands were obtained using tension tests incorporated with DIC.

Material and Methods

Specimen preparation

Two representative grain orientation strands for radial and tangential surfaces from two

different growth ring numbers were prepared from a loblolly pine disk. Figure 4.1 shows the schematic illustration of a wood disk with the coordinate of the disk, two different orientations of wood blocks, and the final wood strand geometry with dimension. Wood blocks A and B of size 127 mm by 133.4 mm by 25.4 mm were wood sliced from the loblolly pine disk using a band saw. After all wood blocks were marked to notify the growth ring number, the blocks were soaked in water and placed under a vacuum overnight to minimize surface damage during flaking. Radial grain orientation strands were flaked from wood blocks sliced from A samples. Tangential grain orientation strands were obtained from wood blocks sliced from B samples.

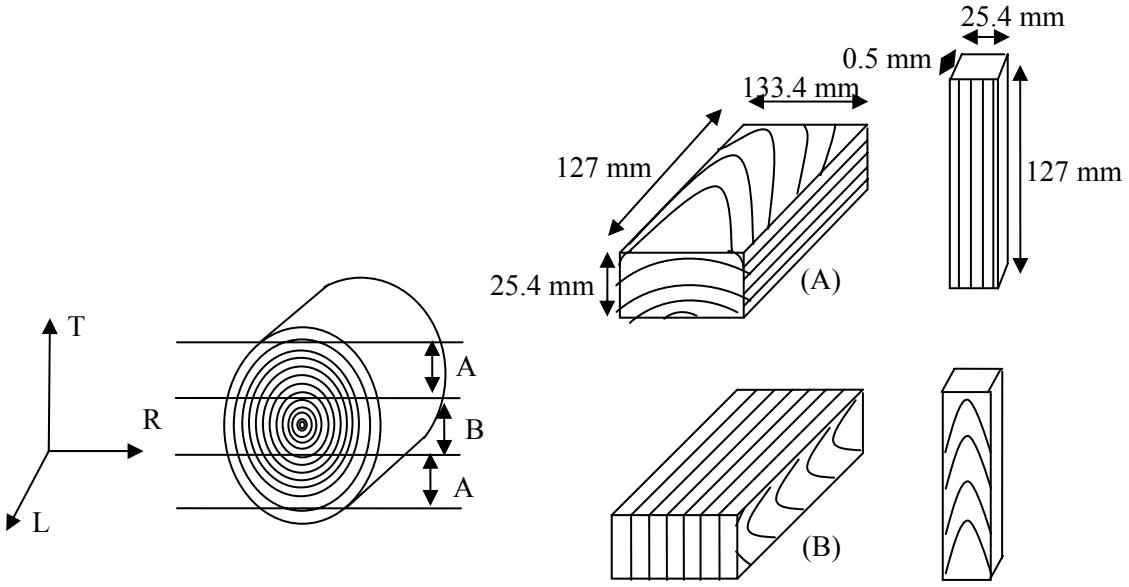

Figure 4.1 Strands generated from different cutting positions of the loblolly pine disk. (A) radial specimen and (B) tangential specimen

Strands were processed from a flaker located at Brook Forest Center laboratory at Virginia Polytechnic Institute and State University. All strands were processed to a size of 127 mm by 25.4 mm by 0.5 mm from growth ring number 1 to 10 from pith, and the same size from growth ring number 11 to 20 from pith. Table 4.1 shows sample size for each tension test. All

strands were conditioned to stabilize at 6% moisture content in the environment chamber for one month before testing.

Table 4.1 Nomenclatures and sample sizes for different orientations of wood strands from different growth ring numbers

Orientation	Growth Ring number	Nomenclatures	Sample sizes
Radial Grain[1]	1-10	Radial 1-10	30
Radial Grain	11-20	Radial 11-20	30
Tangential Grain[2]	1-20	Tangential 1-10	30
Tangential Grain	11-20	Tangential 11-20	30

[1] Radial grain from A
[2] Tangential grain from B

Test Methods

Tension tests used an MTS machine incorporated with digital image correlation (DIC) to calculate elastic properties of wood strands. The test set up for the strand test is shown in Figure 4.2. The MTS machine with 889 N load cell was used for tension test. Loading speed was 0.025 cm/min. Span for tension test was 10.16 cm. A 22.24 N preload was applied to prevent slippage of the grip. Load was intermittently applied at 44.48 N increments and paused for 5 seconds for image capture.

Optem Zoom 70 lens with the magnification of 0.75x attached to a camera was used in this test. To give a light source for the lens and to minimize the influence by the light, a fiber optic light was used during the test. Sequence images of the strands during the test were captured using a CCD camera (Model PL-A662) from Pixel Link Megapixel Firewire Camera. The CCD camera was mounted on a stage with a macro adjustable driver. The distance between lens and object was adjusted for the test to have a clear image. Camera set up was placed on a desk which

was apart from the MTS machine to prevent the vibration while the images were taken.

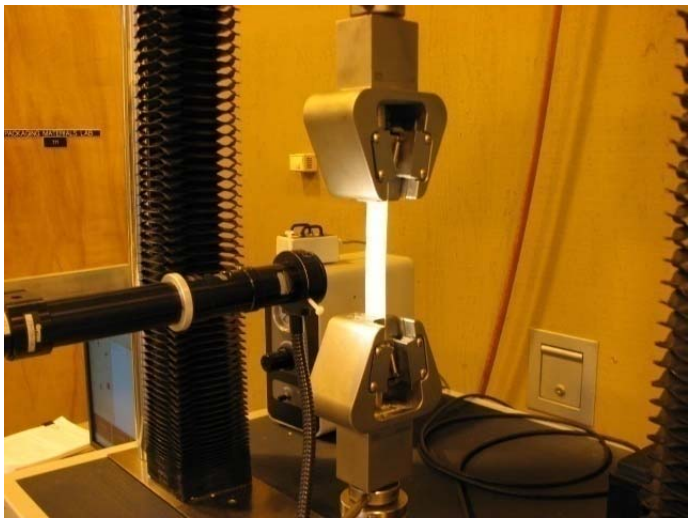

Figure 4.2 Experimental tensile testing set up showing camera for DIC

Resolution of the camera was 1280 by 1024 pixels with an 8-bit grey level. Pixel size of the image was 1280 by 1024. The pixel size was converted to spatial size for the determination of displacement. Horizontal and vertical length of the image taken was 10 mm and 8 mm, respectively. Spatial size of the pixel was calculated to be 9.765 μm/pixel by 6.25 μm/pixel. An aluminum bar with the same dimensions as the strands was used to evaluate strain measurement using DIC coded by Eberl *et al*. (2006). Tensile testing was performed for an aluminum bar with an extensometer to calculate the longitudinal elastic property with the loading speed of 0.025 mm/min. Tensile testing was then performed under the same conditions using DIC. The window size for image correlation was defined as 25 by 25 pixels since the results converged from this window size. Experimental results were calculated using measured elastic strains and a maximum load of 2.20 KN, which was a load within the elastic range. The difference between strain from DIC and strain from the extensometer was only 1.1%. The results prove the accuracy of the strain measurement using DIC.

To validate DIC for calculating MOE of wood strands, specimens were tested with

speckle pattern and without speckle pattern on the surface of the wood strands and compared to the results from extensometer. The difference was 5% between results from DIC with no speckle and results from extensometer. The difference was 4% between results from DIC with speckle and results from extensometer. Therefore, in this study, a speckle pattern was generated on the surface of wood strands with carbon black particles and a paint brush. To minimize the influence of light other than from the fiber optic lamp, all testing was conducted at night with no direct room light. Rubber pads were put under the stage to reduce the vibration. Different loading increments (22.2 N, 44.4 N, and 66.7 N) and loading speeds (0.00254 cm/min and 0.0254 cm/min) were used to determine the testing conditions for measuring the elastic properties of straight grain orientation of wood strands. Preliminary testing found that a 44.4 N loading increment and 0.0254 cm/min load rate were best for the elastic property measurements of strands.

Baxter and Graham (2000) and Baxter et al. (2001) proposed a moving window generalized method of cells (MW-GMC) to characterize material properties of composite materials based on digitized images of local microstructure of the material. The statistical variability of material properties of composite material is dependent upon the window size. Larger window sizes produced smaller variance of material properties. However, if window size becomes too large, the variability of material properties approaches zero. A smaller window size produces noisier fields. Also a smaller window size requires higher computational effort. The choice of window size was emphasized to represent the local material properties. Therefore, the proper window size for wood and wood based material should be used to represent the local material properties. A 25 by 25 pixel size (0.244 mm by 0.156 mm) of window was chosen to represent the local material properties of strands. The grid was generated on the digital image of

the surface of the wood strands before a load was applied. The position of the grid was recorded as x, y coordinate of the pixel position on the image. Figure 4.3 describes the grid generated on the reference digital image of a strand.

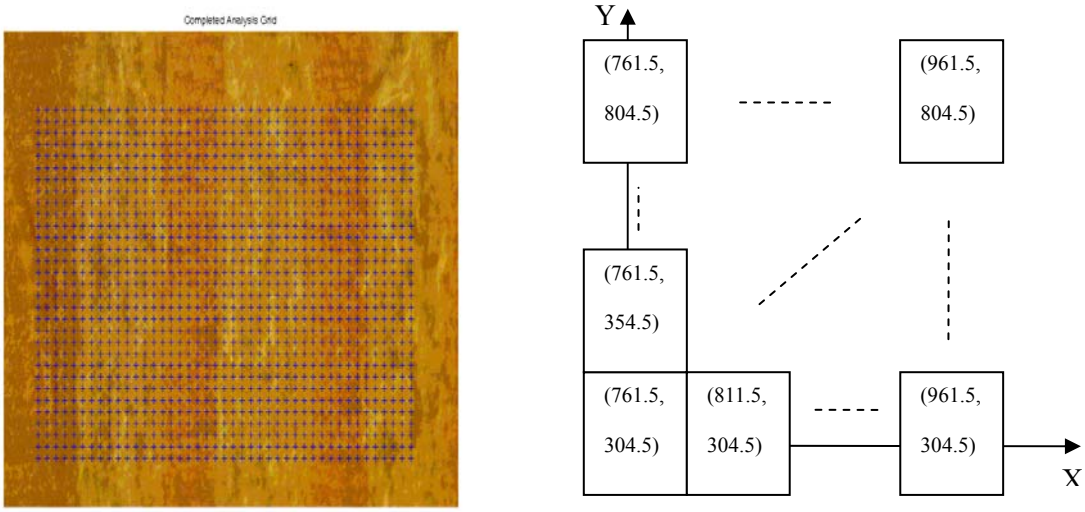

Figure 4.3 Generating a grid on the image from the surface of a strand

MOE (E_L) for both radial grain and tangential grain specimens was obtained using Equation 1. UTS (σ_{LMAX}) for both radial grain and tangential grain specimens was obtained using Equation 2. From straight grain specimens, strain parallel (ε_L) to the direction of load and strain perpendicular (ε_R) to the direction of load was calculated from the change of grid point on the sequence of images during loading. Poisson ratio (υ_{LR}) was calculated from the ratio of the compression strain perpendicular to the load to expansion strain parallel to the load (Equation 4.3). From tangential grain specimens, strain parallel (ε_L) to the direction of load and strain perpendicular (ε_T) to the direction of load was calculated from the change of grid point on the sequence of images during loading. Poisson ratio (υ_{LT}) was calculated from the ratio of the compression strain perpendicular to the load to expansion strain parallel to the load (Equation 4.4).

$$E_L = \frac{\sigma_L}{\varepsilon_L} = \left(\frac{P}{\Delta L}\right)\frac{L}{A} \quad (4.1)$$

$$\sigma_{LMAX} = \frac{P_{LMAX}}{A} \quad (4.2)$$

$$\nu_{LR} = \frac{\varepsilon_R}{\varepsilon_L} \quad (4.3)$$

$$\nu_{LT} = \frac{\varepsilon_T}{\varepsilon_L} \quad (4.4)$$

Where,
ε_L: longitudinal strain in loading to the longitudinal direction of wood.
L: span length in longitudinal direction of wood
ε_R: radial strain in loading to the longitudinal direction of wood
P_{LMAX}: maximum load in loading to the longitudinal direction of wood.
A: area of cross section of specimens
$\frac{P}{\Delta L}$: slope of load-displacement curve under elastic range

Moisture content and specific gravity measurement

Moisture content and specific gravity were measured according to ASTM D 4442 (ASTM 2004a) and ASTM D 2395 (ASTM 2004b). Samples for both testing methods were obtained from the same populations using untested strands. To minimize the influence of the environment of the room humidity and temperature, all samples were kept in a closable bag and handled by a forcep when the specimens were mounted on the balance. The balance has a sensitivity of measurement up to five decimal points in grams. Specimen volume was measured using a micro caliper having a sensitivity of three decimal points in millimeters. After measuring the specimen weight and volume, all samples were kept in a closable bag. To measure the oven-dry weight, samples were put in the oven for twenty four hours. The specific gravity was measured based on the oven-dry weight and volume at the same condition with mechanical testing.

Results and Discussion

Physical and mechanical test results

Table 4.2 presents a summary of the physical and mechanical test results. Moisture contents for four strands were quite similar with the Radial 1-10 having the lowest moisture content of 7.37% with coefficient of variance (COV) of 4% while Radial 11-20 had the highest moisture content of 7.69% with COV of 3%. COV for the moisture contents indicates the low variability for both within the groups and between the groups. Specific gravity increased as the growth ring number increased. However, specific gravity for the four groups was quite varied and the lowest specific gravity of 0.33 occurred in the Radial 1-10 with COV of 12% while the highest specific gravity of 0.43 was found in the Tangential 11-20 with COV of 15%.

Table 4.2 Summary of physical properties and elastic properties of four strands from growth ring number 1-10 and growth ring number 11-20

Growth ring number 1-10	Radial 1-10					Tangential 1-10				
	MC (%)	SG	MOE (GPa)	UTS (MPa)	ν_{LR}	MC (%)	SG	MOE (GPa)	UTS (MPa)	ν_{LT}
AVE	7.37%	0.33	2.41	20.5	0.66	7.49%	0.37	2.47	17.0	0.95
COV	4%	12%	27%	37%	77%	2%	8%	23%	25%	42%
Growth ring number 11-20	Radial 11-20					Tangential 11-20				
	MC (%)	SG	MOE (GPa)	UTS (MPa)	ν_{LR}	MC (%)	SG	MOE (GPa)	UTS (MPa)	ν_{LT}
AVE	7.69%	0.41	2.75	29.0	0.60	7.41%	0.43	2.53	17.4	1.31
COV	3%	5%	14%	24%	36%	2%	15%	32%	31%	43%

The highest MOE of 2.75 GPa was obtained from Radial 11-20 with COV of 14% while the lowest MOE of 2.41 GPa was obtained from Radial 1-10 with COV of 27%, which explains the mechanical properties was more correlated with grain orientations than specific gravity. For

the growth ring number 1-10 the Radial 1-10 had a lower MOE than Tangential 1-10 while for the growth ring number 11-20 the Radial 11-20 had a higher MOE than Tangential 11-20. While the COV from MOE of Straight 1-10 showed 48% higher than that of SO, the COV from Tangential 1-10 showed 39% lower than that of Tangential 11-20.

The highest UTS of 29.03 GPa was obtained from Radial 11-20 with COV of 24 % while the lowest UTS of 17.04 GPa was obtained from Tangential 1-10 with COV of 25%. The COV of UTS from Radial 1-10 had 35% higher than that of SO while the COV of UTS from Tangential 1-10 showed 24 % lower than Tangential 11-20. For the growth ring number 1-10 the Radial 1-10 had a lower UTS than Tangential 1-10 while for the growth ring number 11-20 the Radial 11-20 had a higher UTS than Tangential 11-20. This explains more mature wood strands had a more oriented reinforcement to the longitudinal direction.

Poisson ratios (υ_{LR}) found from the Radial 1-10 and Radial 11-20 while Poisson ratios (υ_{LT}) found from the Tangential 1-10 and Tangential 11-20. The lowest Poisson ratio of 0.60 was obtained from Radial 11-20 with COV of 36% while the highest Poisson ratio of 1.31 was obtained from Tangential 11-20 with COV of 43 %. Poisson ratio from Radial 1-10 had 53.7% higher COV than that of Radial 11-20 while Poisson ratio from Tangential 1-10 was very slightly different from that of Tangential 11-20. At the same growth ring number Poisson ratio from Radial 1-10 had 43% lower than that of Tangential 1-10 and Poisson ratio from Radial 11-20 had 118% lower than that from Tangential 11-20. Under the elastic loading parallel to the longitudinal direction, the negative radial strain perpendicular to the loading showed a higher resistance than the tangential direction.

Failure Modes

Table 4.3 shows the failure behavior of the four different wood strand groups. All four groups had a different percentage of three particular failure behaviors. Shear failure describes the failure around at 45 degree orientations. Brittle failure describes the failure like tearing in the middle with no distinctive orientation. Wedge failure describes the failure showing crack propagation along the grain. No grip failure was recorded for any group. These failure modes were adapted from ASTM D 143 (2005b) testing of compression specimens. For the Radial 1-10, the wedge failure had 40% followed by 30% for Shear and 30% for Brittle failure. For the Radial 11-20, shear failure mode was dominant rating 70% while brittle failure had 26.67% and wedge failure had only 3.33%. For Tangential 1-10, the highest failure mode occurred 56.25% in shear followed by brittle 40.63%. The wedge failure had only 3.13%. For the Tangential 11-20, the highest failure mode was found in Brittle 53.13% followed by shear 37.5%. The wedge failure mode had 9.38%. A trend can be seen from the Radial 1-10 and Radial 11-20 failure mode showing more uniform failure types that could indicate more oriented structure. However, for Tangential 1-10 and Tangential 11-20 failure mode showed more susceptibility to the orientation of grain.

Table 4.3 Failure behavior of wood strands

Sample	Shear	Brittle	Wedge
Radial 1-10	30.00%	30.00%	40.00%
Radial 11-20	70.00%	26.67%	3.33%
Tangential 1-10	56.25%	40.63%	3.13%
Tangential 11-20	37.50%	53.13%	9.38%

Statistical comparison

Table 4.4 shows the results from One-Way ANOVA to analyze the effect of the growth ring numbers and two different geometries on MOE, UTS, and Poisson ratio. An alpha value of 0.05 was used. Strands from different growth ring numbers showed different mechanical properties. While straight grain orientation strands showed a significant difference on MOE and UTS between two growth ring numbers, tangential grain orientation wood strands did not have a significant difference on MOE, UTS, and Poisson ratio between the growth ring numbers.

At the same growth ring numbers, a comparison between the two different orientations showed different trends. While comparison between Radial 1-10 and Tangential 1-10 for MOE and UTS was not significantly different, the Poisson ratio comparison between Radial 1-10 and Tangential 1-10 was significantly different. The comparison of MOE between Radial 11-20 and Tangential 11-20 showed no significant difference while the comparison of UTS and Poisson ratio showed a significant difference.

The statistical comparison of MOE for four groups explained that there was not significant difference between the different grain orientations. This implies that MOE for wood strands doesn't change by strand cutting direction at the same growth ring number. The statistical comparison of UTS for four groups showed no consistent trend from growth ring number and from orientation of strands. However, it can be speculated that UTS for straight grain was not significantly different by growth ring numbers and that UTS for two different orientation strands from growth ring number 11-20 was not significantly different. The statistical comparison of Poisson ratio for four groups explained that there was not a significant difference between the different growth ring numbers while there was a significant difference between the different orientations. This is not surprising that as Poisson ratio is calculated from two different strain

direction, the geometry of strands are highly sensitive to the two strain distribution.

Table 4.4 Statistical comparison of MOE, UTS, and Poisson's ratios for the radial grain strands and tangential grain strands from two different growth ring numbers [1]

Growth ring numbers effect		MOE p-value	UTS p-value	Poisson ratio p-value
Radial 1-10	Radial 11-20	0.01	<.0001	1.00
Tangential 1-10	Tangential 11-20	0.75	0.57	0.40
Orientation effect		MOE p-value	UTS p-value	Poisson ratio p-value
Radial 1-10	Tangential 1-10	0.69	0.96	0.02
Radial 11-20	Tangential 11-20	0.15	<.0001	<.0001

[1] ($\alpha = 0.05$)

Distribution Fitting

Table 4.5 shows the statistical distribution fitting for MOE, UTS, and Poisson ratio. Normal, lognormal, Weibull, and Gamma distributions were used to fit the experimental results from the four test groups. Kolmogorov-Smirnov (K-S), Chi-square statistical tests and visual inspection were used to verify a particular distribution fitting with alpha value of 0.05. For MOE, except for Tangential 1-10 followed Gamma distribution, the rest of three strand groups were best fitted with Weibull distribution. While UTS from Radial 1-10 and Tangential 1-10 group followed Weibull and Gamma distribution, Radial 11-20 and Tangential 11-20 did not follow any distributions. For Poisson ratio, Radial 11-20 did not match with any distribution curve. Radial 1-10, Tangential 1-10, and Tangential 11-20 followed Lognormal, Gamma, and Weibull distribution, respectively. This statistical distribution can be used as input data to simulate the strand based composites.

Table 4.5 Distribution fitting for MOE, UTS, and Poisson's ratio for Radial 1-10, Radial 11-20, Tangential 1-10, and Tangential 11-20 groups[1]

Test Groups	Normal		Lognormal		Weibull		Gamma	
MOE	K-S	Chi-square	K-S	Chi-square	K-S	Chi-square	K-S	Chi-square
Radial 1-10	0.150	0.043	0.093	0.014	0.25	0.058	0.144	0.005
Radial 11-20	0.109	0.805	0.017	0.644	0.25	0.929	0.049	0.532
Tangential 1-10	0.031	0.001	0.5	0.354	N/A	0.232	0.5	0.273
Tangential 11-20	0.150	0.277	0.5	0.222	0.5	0.255	0.5	0.276
UTS								
Radial 1-10	0.150	0.511	0.250	0.496	0.25	0.601	0.144	0.005
Radial 11-20	0.150	0.018	0.052	0.007	0.5	0.032	0.049	0.532
Tangential 1-10	0.150	0.391	0.5	0.353	0.5	0.367	0.5	0.438
Tangential 11-20	0.01	0.001	0.014	0.105	0.01	0.001	0.006	0.059
Poisson Ratio								
Radial 1-10	0.01	0.001	0.148	0.2	N/A	0.112	N/A	N/A
Radial 11-20	0.011	0.012	0.009	0.001	0.006	0.004	0.007	0.004
Tangential 1-10	0.1	0.087	0.192	0.191	0.112	0.130	0.192	0.157
Tangential 11-20	0.150	0.598	0.125	0.391	0.5	0.667	N/A	N/A

[1]($\alpha = 0.05$)

Comparison of MOE and UTS from previous studies with current test results

Figure 4.4 shows a comparison between the results from previous researchers and current test results from Radial 11-20 samples describing MOE and UTS as a function of specific gravity. Although the same species were tested from previous studies (Cai et al. 2007, Hindman and Lee 2007), the location and the height where the samples were obtained were different or not identifiable. In addition, different loading speeds and thicknesses were used for the determination of the UTS and MOE. Two previous studies had a similar specific gravity ranged from 0.539 to 0.55 while the current test specimens had specific gravity of 0.41. The current specimen was obtained from growth ring number 11-20 below 1 m height from the ground, which is still having a large portion of juvenile wood (Larson et al. 2001). Linear correlation for MOE and specific gravity of two previous studies and current work shows moderately positive relationship presenting R^2 of 0.541. Linear correlation for UTS and specific gravity of three studies shows

that strong positive relationship presenting R^2 of 0.798. A previous study also showed a poor correlation found between specific gravity and MOE while a strong correlation was found between specific gravity and strength (Zhang 1997).

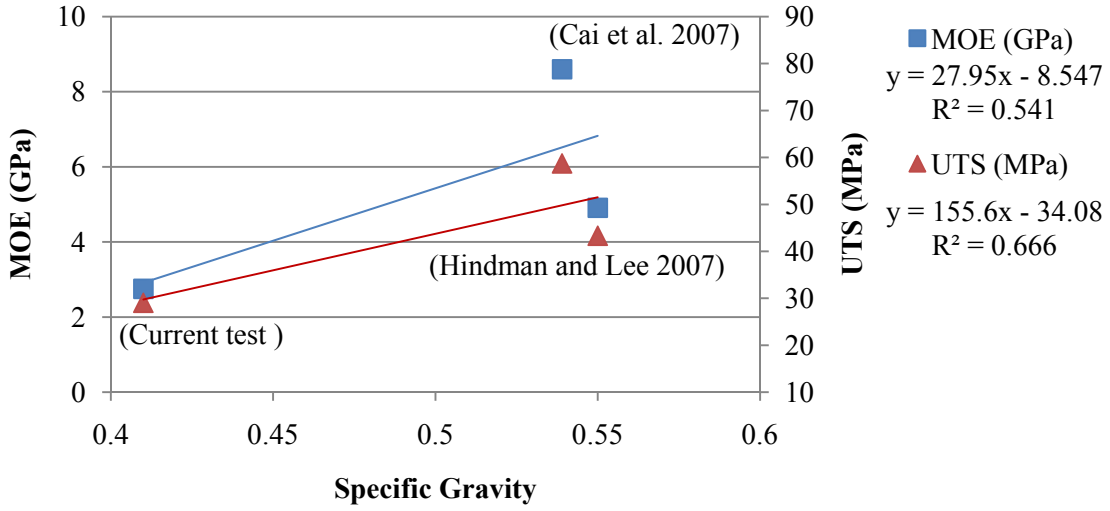

Figure 4.4 Relationship between specific gravity and tensile properties of MOE and UTS of current data and previous studies.

Figure 4.5 shows a comparison between the results from the previous studies and current test results from Radial 11-20 samples describing MOE and UTS as a function of thickness. Linear correlation for MOE and thickness of two previous studies and current work shows strong positive relationship presenting R^2 of 0.992. Linear correlation for UTS and thickness of three studies shows that strong positive relationship presenting R^2 of 0.954. A previous study also showed the positive relationship between thickness and MOE, and between thickness and UTS, respectively (Jeong et al. 2008). It can be speculated that the proportional surface damage on thicker strands is relative lower than thinner strands, which resulted in higher MOE and UTS values for thicker strands. This could be a reason for a higher MOE and strength of OSB produced from proportionally less damaged strands by Geimer et al. (1985).

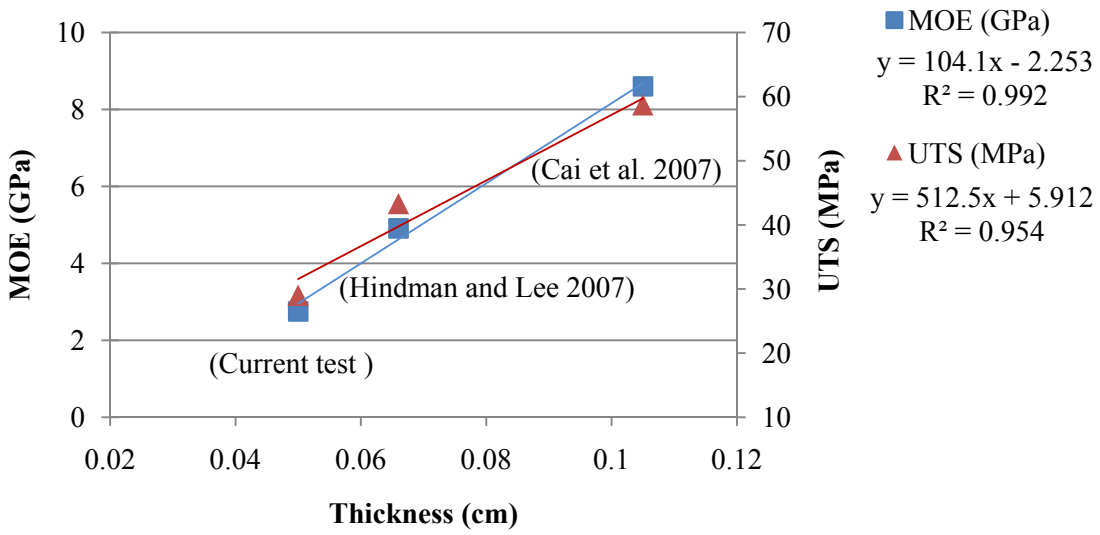

Figure 4.5 Relationship between thickness and tensile properties of MOE and UTS of current data and previous studies.

Conclusions

Tensile properties of two different grain orientations of wood strands from growth ring number 1-10 and growth ring number 11-20 were examined using DIC. The following are conclusions from this chapter:

- As growth ring number increased, modulus of elasticity (MOE) and ultimate tensile strength (UTS) from two different orientation strands increased. For the growth ring number 1-10 the Radial 1-10 had a lower MOE and UTS than Tangential 1-10. For the growth ring number 11-20 the Radial 11-20 had a higher MOE and UTS than Tangential 11-20. For Poisson ratios, tangential grain orientation strands had higher Poisson ratios than straight grain orientation strands.
- From the failure mode, although all four groups had a different percentage of three particular failure behaviors, more mature wood had a more organized structure to show

more consistent failure behavior.

- Statistical comparisons of MOE and UTS from straight grain orientation strands were significantly different between growth ring numbers, while MOE and UTS from tangential grain orientation strands were not significantly different between growth ring numbers.
- Statistical comparisons also showed that there was no significant difference of MOE between two different orientation wood strands. For UTS, the comparison between Radial 1-10 and Radial 11-20 were significantly different as well as the comparison between Radial 11-20 and Tangential 11-20.
- For distribution fitting from MOE, except for Tangential 1-10, the rest of three strand groups were best fitted with Weibull distribution. For UTS, while Radial 1-10 and Radial 11-20 group followed Weibull distribution, Gamma distribution for Tangential 1-10 and Lognormal distribution for Tangential 11-20 were best fitted curve. For Poisson ratio, Radial 11-20 did not match with any distribution curve. Radial 1-10, Tangential 1-10, and Tangential 11-20 followed Lognormal, Gamma, and Weibull distribution, respectively.
- From comparison between previous studies and current test results, MOE and UTS of wood strands were more linearly correlated with thickness than specific gravity.

Acknowledgements

This work was funded by the USDA National Research Initiative Competitive Grants Program (2005-35504-16115). Their financial contribution to this work is greatly acknowledged.

Reference

American Society for Testing and Materials (ASTM). 2004a. ASTM D 4442. Standard Test Methods for Direct Moisture Content Measurement of Wood and Wood-Base Materials *In*: Annual Book of ASTM Standard, Section 4, Vol. 04.10 Wood. ASTM, West Conshohocken, PA.

American Society for Testing and Materials (ASTM). 2004b. ASTM D 2395. Standard Test Methods for Specific Gravity of Wood and Wood-Based Materials. *In*: Annual Book of ASTM Standard, Section 4, Vol. 04.10 Wood. ASTM, West Conshohocken, PA.

Balatinecz, J. J., and D. E. Kretschmann. 2001. Properties and utilization of poplar wood. In Poplar Culture in North America. Part A, Chapter 9. Edited by D.I. Dickmann, J.G. Isebrands,

J.E. Eckenwalder, and J. Richardson. NRC Research Press, National Research Council of Canada, Ottawa, ON KIA OR6, Canada. 277-291 pp.

Baxter S. C. and L. L. Graham. 2000. Characterization of random composites using a moving window technique, ASCE J. Eng. Mech**. 126** (4):389–404

Baxter S. C., M. I. Hossain, and L. L. Graham. 2001. Micromechanics based random material property fields for particulate reinforced composites, Int. J. Solids Struct. **38**: 9209–9220

Cai, Z., Q. Wu, G. Han, and J. N. Lee. 2007. Tensile and thickness swelling properties of strands from Southern hardwoods and Southern pine: Effect of hot-pressing and resin application. Forest Prod. J. 57(5):36-40.

Deomano E. C., and A. Zink-Sharp 2005. Effect of species, cutting direction, dimensions, and temperature on flake drying. Forest Prod. J. 55(9):31-36

Geimer, R. L., R. J. Mahoney, S. P. Loehnertz, and R. W. Meyer. 1985. Influence of processing-induced damage on the strength properties of oriented strand wood products. Forest Prod. J. 50(11/12):33-42.

Hindman D. P. and J. N. Lee. 2007. Modeling wood strands as multi-layer composites: bending and tension loads. Wood and Fiber Sci.39(4):515-526.

Jeong, G. Y**.**, D. P. Hindman, D. Finkenbinder, J. N. Lee, and Z. Lyne. 2008. Evaluation of loading rate and thickness effect on stiffness and strength of wood strands. Forest Prod. J. in process

Larson, P. R., D. E. Kretschmann, A. Clark III, and J. G. Isebrands. 2001. Juvenile wood formation and properties in southern pine. General technical report FPL-GTR-129. Madison, Wisconsin: USDA, Forest Service, Forest Products Laboratory

Price E.W. 1975. Determining tensile properties of sweetgum veneer flakes. Forest Prod. J. 26(10):50-53

Schuler, A. and C. Adair. 2000. Engineered wood products- production, trade, consumption and outlook. Forest products annual market review, Chapter 11, FAO/ECE Timber section. United Nations, NY and Geneva. 131-146 pp.

United Stated Department of Agriculture. 1999. *Wood Handbook: Wood as an engineering material*. Forest Products Society. FPL-GTR-113. Madison, WI. 463 p.

Wu, Q., Z. Cai, and J. N. Lee. 2005. Tensile and dimensional properties of wood strands made from plantation southern pine lumber. Forest Prod. J. 52(2):1-6

Zhang S. Y. 1997. Wood specific gravity-mechanical property relationship at species level. Wood Sci. and Technology. 31:181-191

Chapter 5. Shear and Transverse Properties of Loblolly Pine (*Pinus taeda*) Strands Using Tension Test Incorporating Digital Image Correlation (DIC)

Shear and transverse properties of different orientation loblolly pine strands from growth ring number 1-10 and growth ring number 11-20 were determined using tension tests incorporating digital image correlation. From angled grain orientation strands, longitudinal properties and shear properties for loblolly pine strands from different growth ring numbers were evaluated. Transverse tension properties were evaluated from cross-grain strands. Modulus of elasticity (MOE), shear modulus, and ultimate tensile strength (UTS) from angled grain strands increased as the growth ring number increased. However, Poisson ratio and shear strength from angled grain strands decreased as the growth ring number increased. MOE and UTS from cross-grain strands decreased as the growth ring number increased, while Poisson ratio from cross grain orientation strands increased as the growth ring number increased. The failure modes indicated that the strands from growth ring number 11-20 showed more oriented structures to the loading direction. From the results, grain orientations of strands were a strong indicator of mechanical properties of wood strands.

Introduction

Efficient uses of wood resources are needed to maximize material production, lower costs, and produce environmentally responsible products. These pressures have resulted in increased use of oriented strand board (OSB) and structural composite lumber (SCL). However, the fundamental study for measuring material properties of the main component of the products such as wood strands has not been completed. If OSB and SCL can be designed based on known material properties of the constituent, specific targeted properties could be achieved with minimal time and resources.

A previous research (Jeong et al. 2008a) found differences of modulus of elasticity (MOE), ultimate tensile strength (UTS), and Poisson ratio of different grain strands from growth ring number 1-10 and growth ring number 11-20. Those different material properties were reasoned to be structural differences of wood fibers between the two growth ring numbers. However, off-axis properties of wood strands have not been evaluated yet.

Shear modulus of wood is an important property for analyzing elastic properties and strength of strand based composites. However, shear properties are difficult to obtain for wood materials especially for thin specimens. Due to the low stiffness and high aspect ratio of wood strands, most shear modulus testing listed in ASTM and other literature cannot be applied. One possible test method is the off-axis tension test. Due to the coupling between normal strain and shear strain in the axis of loading, multi-axial deformation occurs. However, typical extensometers or strain gauges cannot measure such a deformation.

Measurement of transverse elastic modulus is also hard due to the low stiffness of cross grain wood strands. Cross-grain strands can be easily broken or damaged by an attempt to attach an extensometer. The low strength cannot support the extensometer during cross-head movement.

Strain gauges use adhesive to attach the strain gauge on low stiffness material and can alter the mechanical properties of specimens.

An alternative strain measurement is the digital image correlation (DIC) that uses the surface image of specimens to measure strain. Since DIC uses the image of specimens, DIC can measure two dimensional strain distributions with no interference of specimen properties. A tension test incorporating DIC was used to measure MOE and shear properties from angled grain orientation strands and transverse properties from cross-grain orientation strands.

Literature Review

Previous researchers have discussed off-axis tension tests to measure shear properties and transverse properties of different materials. The off-axis tension test is one way to evaluate shear properties from unidirectional laminates under uniform loading in y-direction at an angle from the fiber orientation. Transverse direction of wood is considered to be an off-axis angle of 90 degrees between load direction and grain orientation. This literature review focuses on off-axis angle tension tests for wood material.

Zhang and Sliker (1991) measured shear modulus from different species - redwood (*Sequoia sempervirens*), sugar pine (*Pinus lambertiana*), white pine (*Pinus strobes*), basswood (*Tilia americana*), cottonwood (*Populus deltoides*), white ash (*Fraxinus americana*), and yellow poplar (*Liriodendron tulipifera*) using off-axis tension and compression tests. Compared to off-axis compression tests, shear modulus measurements from off-axis tension test were better due to lack of distortion by crosshead. Different grain angle (10, 20, and 45 degrees) specimens were tested. From the off-axis tension and compression tests, angles of 14 to 35 degrees between the grain direction and loading direction were recommended to measure the shear modulus.

Yoshihara and Ohta (2000) measured the shear strength of Sitka spruce (*Picea sitchensis* Carr.) and katsura (*Cercidiphyllum japonicum* Sieb. a Zucc.). Off-axis tension tests were conducted with different grain orientation specimens from the two species. Shear properties obtained from grain orientations between 15 and 30 degree specimens agreed well with results from torsion tests. Yoshihara and Ohta (2000) noted that shear properties determined using off-axis tension tests are highly influenced by other stresses due to the off-axis loading compared to the torsion test.

Jernkvist and Thuvander (2001) measured elastic properties (E_R, E_T, G_{RT}, ν_{TR}) of Norway spruce (*Picea abies*) along growth ring positions from the radial tension test incorporated with digital speckle photography (DSP). The strain values from earlywood had two times higher than strains from latewood. The averaged elastic properties (E_R and E_T) found to be two times higher than corresponding values from conventional experimental test with macro size, while the average shear modulus was two time lower than shear modulus from conventional experimental test.

Liu (2002) analyzed the effect of the Poisson ratio and shear coupling coefficient on stress distribution by changing the grain angle of Sitka spruce (*Picea sitchensis Carr.*). The principal stresses of grain direction at grain orientations ranged from 3 to 45 degree were more influenced by shear coupling coefficient than Poisson ratio. For the principal stress of radial direction at the grain orientation up to 67 degrees, shear coupling coefficient had a positive influence, while Poisson ratio had a negative influence. Up to grain orientation of 30 degrees, shear coupling coefficient dominantly controlled the shear stress compared to the Poisson ratio.

Galicki and Czech (2005) measured the ultimate tensile strength (UTS) of four different grain angles (0, 30, 45, and 90 degrees) from scots pine (*Pinus silvestris*). The UTS from grain

angles up to 25 degree was dependent upon density showing a transverse rupture in latewood band and earlywood band. However, the UTS of 30, 45, and 90 degree grain angle strands were not related with density showing failure only within earlywood band.

From the previous study, the interaction between grain angle and stress distribution and between grain angle and failure behavior of wood strands were recognized. Correct grain angle and strain measurement were key components to have accurate the elastic properties and strength of wood strands. The goal of this chapter was to measure shear and transverse properties of different orientation loblolly pine strands from growth ring number 1-10 and growth ring number 11-20. Tension tests incorporated with DIC were used to measure strain in both parallel to the loading direction and perpendicular to the loading direction. MOE and Poisson ratios at different orientation strands were evaluated. Shear properties were obtained from angle grain orientation strands while transverse properties were obtained from cross grain strands.

Materials and Methods

Specimen preparation

Figure 5.1 shows the two different orientations of wood blocks, and the final wood strand orientation with dimensions. A size of 127 mm by 133.4 mm by 25.4 mm wood blocks were sliced in portion of A and B from a wood disk using a band saw. After all wood blocks were marked to notify the growth ring position, the blocks were submerged in water and a vacuum applied overnight to minimize the surface damage during the flaking. For best results in evaluation of shear modulus (Zhang and Sliker 1991), angle grain orientation strands were cut to thirty degree grain angle (θ).

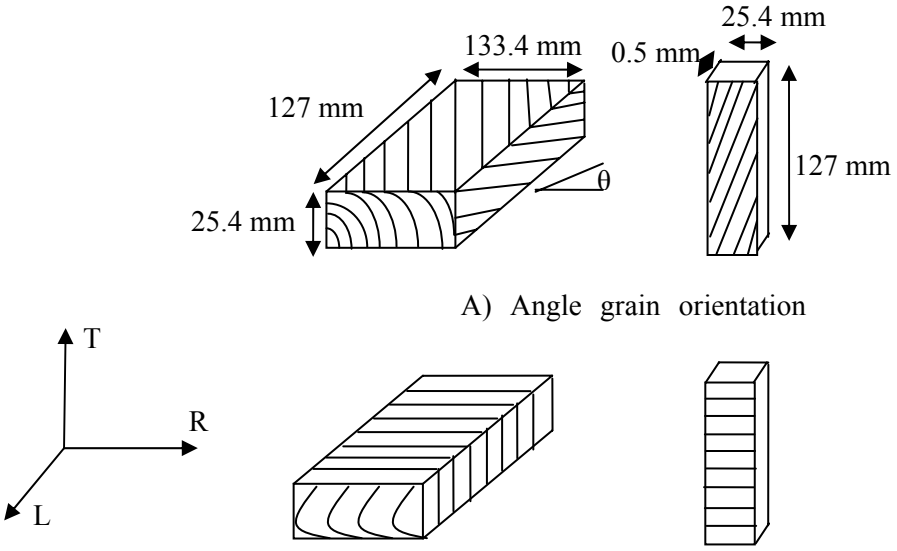

Figure 5.1 Two different grain orientation strands used in testing. A) Angle grain orientation, B) Cross grain orientation

Strands were processed from a flaker located at Brooks Forest Product Center laboratory at Virginia Polytechnic Institute and State University. Final strand size was 127 mm long, 25.4 mm wide, and 0.5 mm thick. Table 5.1 shows nomenclatures and sample sizes for each growth ring number and grain orientation. All strands were conditioned to stabilize at 6% moisture content in the environment chamber for one month before testing.

Table 5.1 Nomenclatures and sample sizes for two different orientation wood strands from growth ring number 1-10 and growth ring number 11-20.

Name	Strand orientation	Growth ring number	Number of samples
AI	Angle	1-10	30
AO	Angle	11-20	30
CI	Cross	1-10	30
CO	Cross	11-20	30

Test Methods

Figure 5.2 shows the testing arrangement for off-axis properties of strands from different growth ring numbers. Tension testing used a MTS machine incorporating DIC. Loading data were obtained from the MTS. The strain measurement was obtained from DIC using a program developed by Eberl *et al*. (2006). The loading speed was 0.25 mm/min. Distance between grips was 10.16 cm. For angled grain strands, a 22.24 N preload was applied to prevent slippage of the grip. Load was intermittently applied at 22.24 N increments and paused for 5 seconds for image capture. For cross-grain strands, a 4.44 N preload was applied to prevent slippage of the grip. Load was intermittently applied at 4.44N increments and paused for 5 seconds for image capture. Camera set up for DIC and synchronization for loading and strain used the same arrangement from previous study (Jeong et al. 2008).

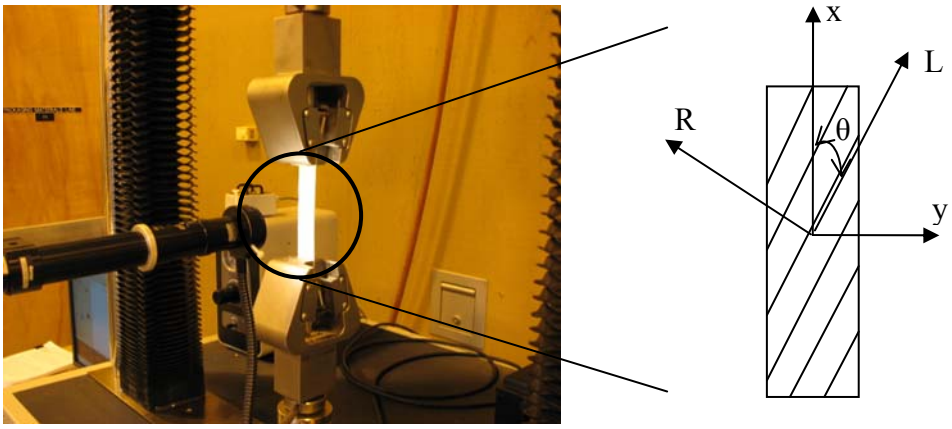

Figure 5.2 Tensile test set up for off-axis tension test showing the global axis (x and y), the principal material axis (L and R), and angle (θ) between x and L

After all tests finished, elastic modulus at θ degree (E_θ) and UTS of angled grain strands from growth ring number 1-10 and growth ring number 11-20 were calculated. Radial elastic modulus (E_R) and UTS of cross grain orientation strands from growth ring number 1-10 and

growth ring number 11-20 were also calculated. Poisson ratios for four groups were obtained from the ratio of strain parallel to the loading direction to the strain perpendicular to the loading direction. Shear modulus was calculated using Equation 5.1 (Jones 1975). Since wood strands had a high slenderness ratio, the deformation of wood strands was assumed to show no distortion. That is, St. Venant end effects can be ignored in the area away from the grips. The E_θ were obtained from angled grain strands while E_R was obtained from cross-grain strands. E_L and Poisson ratio (ν_{LR}) were obtained from the same population (Jeong et al. 2008). With the average grain angle of 30 degree, the shear modulus for loblolly pine strands from growth ring number 1-10 and growth ring number 11-20 were calculated. Shear strength was also measured from off-axis tension test using Equation 5.2 (Jones 1975). UTS for the four groups were determined using Equation 5.3.

$$G_{LR} = \frac{1}{(-\frac{1}{E_L}cos^4\theta - \frac{1}{E_R}sin^4\theta + \frac{1}{E_\theta})\frac{1}{sin^2\theta cos^2\theta} + \frac{2\nu_{LR}}{E_L}} \tag{5.1}$$

$$\tau_{xy} = \sigma_{LMAX} sin\theta cos\theta \tag{5.2}$$

$$UTS = \frac{P_{LMAX}}{A} \tag{5.3}$$

Where,
θ: angle between global axis and grain direction
E_L: Longitudinal elastic modulus from Jeong et al. (2008a)
E_R: Radial elastic modulus from cross grain strands
A: area of cross section of specimen
P_{LMAX}: Peak load
υ_{LR}: Poisson ratio from Jeong et al. (2008a)

After all elastic properties and strength from experimental test were determined, elastic properties and strength were evaluated using orthotropic theory. Elastic modulus of strands was calculated with respect to the grain angle using Equation 5.4 (Jones 1975). The UTS of strands was also calculated using Tsai-Hill criterion to analyze the tensile strength as a function of grain orientation using Equation 5.5 (Jones 1975).

$$E_x = \frac{1}{\frac{1}{E_L}cos^4\theta + \left(\frac{1}{G_{LR}} - \frac{2\upsilon_{LR}}{E_L}\right)sin^2\theta cos^2\theta + \frac{1}{E_R}sin^4\theta} \tag{5.4}$$

$$\sigma_x = \frac{1}{\sqrt{\frac{cos^4\theta}{X^2} + \left(\frac{1}{S^2} - \frac{1}{X^2}\right)cos^2\theta sin^2\theta + \frac{sin^4\theta}{Y^2}}} \tag{5.5}$$

Where,
X: Longitudinal strength
Y: Transverse strength
S: Shear strength

Moisture content and specific gravity measurement

Moisture content and specific gravity were measured according to ASTM D 4442 (ASTM 2004a) and ASTM D 2395 (ASTM 2004b). Samples for both testing methods were obtained from the same populations using untested strands. To minimize the influence of the environment of the room humidity and temperature, all samples were kept in a reclosable bag and handled by forceps when the specimens were mounted on the balance. The balance has a sensitivity of ±0.00001 g. After measuring the specimen weight, all samples were kept in the reclosable bag. To measure the oven-dry weight, samples were put in the oven for twenty four hours. The specific gravity was measured based on the oven-dry weight and volume at the same condition as during mechanical testing.

Results and Discussion

Table 5.2 shows the moisture content (MC) and specific gravity (SG) of angled grain strands and cross-grain strands from growth ring number 1-10 and growth ring number 11-20. It can be speculated that the average specific gravity is not dependent upon growth ring position and cutting direction in this arrangement. However, the variation of specific gravity was dependent upon growth ring position.

Table 5.2 Physical properties of angled and cross-grain strands from growth ring number 1-10 and growth ring number 11-20

Name	MC (%), (COV)	SG, (COV)
AI	6.97% (1.75%)	0.44 (7.23%)
AO	6.74% (3.46%)	0.41 (8.08%)
CI	6.47% (7.67%)	0.39 (11.1%)
CO	6.50% (6.62%)	0.43 (15.1%)

Table 5.3 shows the mechanical properties of angled grain strands and cross-grain strands from growth ring number 1-10 and growth ring number 11-20. While MOE from angled grain strands (AI and AO) increased about 25% from growth ring number 1-10 to growth ring number 11-20, MOE from cross-grain strands (CI and CO) decreased 1% from growth ring number 1-10 to growth ring number 11-20. The distinctive difference of MOE between these two different orientation strands showed that the fiber orientation of strands was a strong indicator on mechanical properties of wood strands.

AO had the highest ultimate tensile strength (UTS) of 16.96 MPa with a COV of 19% while CO had the lowest UTS of 2.52 MPa with a COV of 33%. The UTS from angle grain

orientation strands increased as the growth ring number increased. However, The UTS from cross grain orientation strands decreased as the growth ring number increased, which could indicate UTS from cross grain orientation strands is not dependent upon the growth ring positions.

Shear moduli were calculated from Equation 5.1. The longitudinal elastic modulus and Poisson ratio were obtained from previous research (Jeong et al. 2008a). The shear modulus increased as the growth ring number increased. However, shear strength decreased as the growth ring number increased. This counter-intuitive result can be speculated that shear strength is more sensitive to the structure of earlywood and latewood bands. The higher ratio of latewood MOE to earlywood MOE could result in lower shear strength as growth ring number increases (Jeong et al. 2008b). The higher ratio of MOE could cause stress concentrations between the boundaries resulting in a lower strength value. Shear modulus, however, was measured by average elastic properties of earlywood and latewood band rather than elastic ratio of earlywood and latewood band.

Poisson ratios from angled grain strands decreased as the growth ring number increased. From the Poisson ratio (ν_{RT}) of 1.07 for CI and 1.10 for CO, the smaller radial strain over tangential strain can be interpreted as a higher reinforcement in the radial direction compared to that in the tangential direction. COV values of Poisson ratio from four groups decreased as growth ring number increased.

Although specific gravity from AI shows a higher value than AO, AO had higher MOE and UTS values than AI. AO showed lower COV values for MOE and UTS compared to AI. Although specific gravity from CI was lower than CO, CI had higher MOE and UTS values than CO. Compared to CI, CO showed lower COV values for MOE and UTS. With the lower COV

values, a less variation of strand structures in a higher growth ring number can be speculated. The results showed that specific gravity was not a main control factor on mechanical properties of angled grain strands from two different growth ring positions. The morphology of wood structure from two strands group could be speculated as a main control factor including grain orientation, microfibril angles, and anatomical structure.

Table 5.3 Mechanical properties from angled grain and cross-grain strands from growth ring number 1-10 and growth ring number 11-20

Name	Angle, θ (COV)	MOE, GPa (COV)	UTS, MPa (COV)	Shear Modulus[1], GPa	Shear Strength, MPa (COV)	Poisson ratio (COV)
AI	33.46 (16.7%)	1.97 (27.2%)	13.58 (23.7%)	0.89	4.67 (27.2%)	1.04 (45.1%)
AO	23.53 (16.0%)	2.46 (22.9%)	16.96 (18.8%)	1.11	4.09 (26.2%)	0.72 (36.5%)
CI	90	0.89 (44.5%)	2.94 (42.1%)	N/A[2]	N/A	1.07 (70.8%)
CO	90	0.88 (44.7%)	2.52 (33.1%)	N/A	N/A	1.10 (56.7%)

[1] Calculated values of shear modulus based on average test values
[2] Not applicable

Table 5.4 shows the statistical distribution fitting for shear strength, MOE, UTS, and Poisson ratio. Normal, Lognormal, Weibull, and Gamma distribution were used to fit the experimental results from four groups. Kolmogorov-Smirnov (K-S) and Chi-square were used to verify a particular distribution fitting with alpha value of 0.05. Along with these two criteria, visual inspection was also conducted to find the best fit. From two criteria and visual inspection, the best fitting curves for mechanical properties of each group were estimated. Shaded values indicated the best fitting curve for each mechanical value. Shear strength values from AI and AO were best fitted with Gamma distribution. MOE values from AI, AO, and CO followed

Lognormal distribution, while MOE values from CI followed Weibull distribution. UTS values from all four groups didn't follow any specific distribution. Poisson ratio values from AI, CI, and CO were best fitted with Normal distribution, while Poisson ratio values from AO followed Lognormal distribution. This statistical distribution can be used as input data to simulate mechanical properties of strand based composites.

Table 5.4 Statistical distribution of shear strength, MOE, UTS, and Poisson ratio from two different orientation strands generated from two different growth ring positions

	Normal		Lognormal		Weibull		Gamma	
	K-S	Chi-square	K-S	Chi-square	K-S	Chi-square	K-S	Chi-square
Shear strength								
AI	0.08	0.037	0.250	0.075	0.244	0.063	0.232	0.081
AO	0.150	0.003	0.144	0.352	0.054	0.003	0.250	0.326
MOE								
AI	<0.001	0.013	0.250	0.263	N/A	0.388	N/A	N/A
AO	0.150	0.701	0.150	0.777	0.250	0.636	0.250	0.759
CI	0.150	0.253	0.162	0.208	0.250	0.310	0.242	0.255
CO	0.019	0.006	0.250	0.359	0.140	0.143	0.137	0.222
UTS								
AI	<0.001	0.054	<0.001	0.114	0.023	0.045	0.005	0.090
AO	0.018	0.035	0.079	0.038	0.02	0.033	0.045	0.031
CI	0.01	0.190	0.015	0.189	0.039	0.309	0.026	0.237
CO	0.01	0.069	0.01	0.026	0.01	0.07	0.02	0.056
Poisson ratio								
AI	0.150	0.225	<0.001	<0.001	0.049	0.042	0.011	0.005
AO	<0.001	<0.001	0.150	0.157	<0.001	<0.001	0.126	<0.001
CI	0.150	0.183	0.067	0.015	0.054	0.157	0.110	0.143
CO	0.150	0.482	0.01	0.002	0.037	0.171	0.009	0.069

Table 5.5 shows the failure modes of strands from two different orientations and growth ring positions. Three different failure modes were observed visually. Shear failure mode included a crack propagating along the boundary between earlywood and latewood. Brittle failure mode included failure with crack at no specific angles. Shear against grain angle failure mode

describes crack propagating cross grain direction. The dominant failure mode for AI was 46.8% of brittle failure and followed by 34.3% of shear failure. Interestingly 18.75% of shear against grain angle failure mode occurred, indicating that grain angle direction was not dominant factor controlling the stress propagation. For AO, the shear against failure mode did not occur. The most dominant failure mode for AO was 93.5% of shear failure and followed by only 6.45% of brittle failure. For cross grain orientation strands, brittle failure occurred in earlywood band while shear failure occurred in boundary between earlywood and latewood band. CI had 66.6% of brittle failure and followed by 33.33% of shear failure. CO had mostly shear failure with only 16.67% brittle failure. The failure mode showed quite difference between growth ring numbers. Based on the results, more mature wood (growth ring number 11-20) had more directional reinforcement to the grain direction while more juvenile wood (growth ring number 1-10) had more variation on the orientation of its structure.

Table 5.5 Failure behavior of different grain orientation strands from growth ring number 1-10 and growth ring number 11-20

Sample	Shear failure	Brittle failure	Shear against grain angle failure
AI	34.3%	46.8%	18.7%
AO	93.5%	6.45%	0%
CI	33.3%	66.6%	0%
CO	83.3%	16.6%	0%

Table 5.6 shows MOE, UTS, and shear strength values from experimental tests and predicted MOE using Equation 5.4, predicted UTS Equation 5.5, and predicted shear strength Equation 3 as a function of grain angles. Experimental results were obtained from each thirty strand for growth ring number 1-10 and growth ring number 11-20. Predicted values were

obtained at an average grain angle of 33.46 degree for strands from growth ring number 1-10 and an average grain angle of 23.53 degree for strands from growth ring number 11-20.

Both experimental and predicted MOE values had the same trends that MOE increased as the grain angle increased. However, the predicted MOE values were more conservative showing 23.8% and 22.3% higher for strands from growth ring number 1-10 and growth ring number 11-20, respectively. This could be because the Equation 5.4 was derived from orthotropic transformation considering only the grain orientation while the anatomical structure of strands includes fiber orientation, microfibril angle (MFA), and chemical orientation that could reinforce the structure in other than one material axis. From an engineering point of view, wood is normally assumed as an orthotropic material that fiber orientations, MFA, and chemical orientation were identical with the material axis. Due to the limitation of orthotropic transformation and lack of information on orientation of anatomical structures, orthotropic transformation of micro-level and nano-level wood structure is ignored. Therefore the material property prediction from orthotropic transformation should be considered as a conservative approximation.

Tsai-Hill criterion (Equation 5.5) was used to predict UTS of strands as a function of different grain angles. Predicted strength values were followed the trends from experimental results that UTS decreased as the growth ring number increased. However, the difference between UTS from experimental test and predicted UTS was 43.4% and 39.3% for strands from growth ring number 1-10 and growth ring number 11-20, respectively. The predicted UTS value was used to calculate the shear strength using Equation 3. From the comparison between shear strength from experimental and predicted shear strength, the predicted shear strength was more conservative showing 38.1% and 27.6% higher for strands from growth ring number 1-10 and

growth ring number 11-20, respectively. These different values for UTS and shear strength from the two different growth ring positions can be speculated that the anatomical structure may influence the final strength value. Similar to the MOE prediction, strength predictions using orthotropic transformation are sensitive to the direction of structure and structure variation resulting in multi-axial stress distribution.

Table 5.6 The MOE, UTS, and shear strength of strands from growth ring number 1-10 and growth ring number 11-20

	MOE (GPa)			UTS (MPa)			Shear strength (MPa)		
	Ex[1]	Pr[2]	Diff[3]	Ex	Pr	Diff	Ex	Pr	Diff
Growth ring number 1-10	1.97	1.50	23.8%	10.47	5.92	43.4%	4.66	2.88	38.1%
Growth ring number 11-20	2.46	1.91	22.3%	11.27	6.83	39.3%	4.09	2.96	27.6%

[1]Experimental
[2]Predicted
[3]Diff= (experimental-predicted)/experimental*100%

Conclusions

Elastic and strength properties of loblolly pine strands from growth ring number 1-10 and growth ring number 11-20 were measured using tension test incorporating DIC. The following are conclusions from this study:

- MOE of angled grain strands increased as the growth ring number increased while MOE of cross-grain strands decreased 1% as the growth ring number increased. MOE was more sensitive to the orientation compared to specific gravity.
- UTS of angled grain strands increased as the growth ring number increased, while UTS of cross-grain strands decreased as the growth ring number increased. The UTS was dependent upon grain orientations of strands rather than specific gravity.

- Shear modulus increased as the growth ring number increased, but shear strength decreased as the growth ring number increased. Lower shear strength values can be speculated as a higher elastic constant ratio of strands from growth ring number 11-20.
- Poisson ratio from angled grain strands decreased with increasing growth ring numbers. However, Poisson ratio from cross-grain strands slightly increased with the increment of growth ring numbers.
- COV values from MOE, UTS, Poisson ratio, and shear strength decreased as growth ring number increased. From the results, a less variation in structure of strands from growth ring number 11-20 can be speculated.
- Statistical distribution fitting showed that shear strength values were best fitted with Gamma distribution. MOE values from AI, AO, and CO followed Lognormal distribution, while MOE values from CI followed Weibull distribution. UTS values from four groups didn't follow any specific distribution. Poisson ratio values from AI, CI, and CO followed Normal distribution, while AO followed Lognormal distribution.
- Although four groups of strands showed the mixed failure modes, strands from growth ring number 11-20 showed a more consistent failure mode. The failure mode indicated that strands from growth ring number 11-20 showed more oriented structures compared to the strands from growth ring number 1-10.
- From the comparison of MOE, UTS, shear strength from experimental and from orthotropic transformation, conservative predicted values for all values were obtained.

References

American Society for Testing and Materials (ASTM). 2004a. ASTM D 4442. Standard Test Methods for Direct Moisture Content Measurement of Wood and Wood-Base Materials *In*: Annual Book of ASTM Standard, Section 4, Vol. 04.10 Wood. ASTM, West Conshohocken, PA.

American Society for Testing and Materials (ASTM). 2004b. ASTM D 2395. Standard Test Methods for Specific Gravity of Wood and Wood-Based Materials. *In*: Annual Book of ASTM Standard, Section 4, Vol. 04.10 Wood. ASTM, West Conshohocken, PA.

American Society for Testing and Materials (ASTM). 2004c. Standard Test Methods for Shear Modulus of Wood-Based Structural Panels. Standard D 3044-94. *In*: Annual Book of ASTM Standard, Section 4, Vol. 04.10 Wood. ASTM, West Conshohocken, PA.

Chang B. W., D. H. Huang, and D. G. Smith. 1984. A pinned-end fixture for off-axis testing. Experimental Tech. 28-30 (June)

Eberl C., R. Thompson, and D. Gianola. 2006. Digital image correlation and tracking with matlab. Matlab Central. http://www.mathworks.com/matlabcentral/fileexchange/loadFile.do?objectId=12413&objectType=FILE (27 September 2006).

Galicki J. and M. Czech. 2005. Tensile strength of softwood in LR orthotropy plane. Mechanics of Materials. 37:677-686

Jernkvist L. O. and F. Thuvander. 2001. Experimental determination of stiffness variation across growth rings in Picea abies. Holzforschung. 55(3):309-317

Jeong G. Y., A. Zink-Sharp, and D. P. Hindman. 2008a. Comparison of longitudinal tensile properties of different grain orientation strands from loblolly pine (Pinus taeda). In review, Wood and Fiber Sci.

Jeong G. Y., D. P. Hindman, and A. Zink-Sharp. 2008b. Tensile properties of earlywood and latewood from loblolly pine (Pinus taeda) using digital image correlation. In review, Wood and Fiber Sci.

Jones R. M. 1975. *Mechanics of Composite Materials*. McGraw-Hill, New York. 55-79 pp.

Liu J. Y. 2002. Analysis of off-axis tension test of wood specimens. Wood and Fiber Sci. 34(2):205-211.

Yoshihara H. and M. Ohta. 2000. Estimation of the shear strength of wood by uniaxial-tension tests of off-axis specimens. J. Wood Sci. 46:159-163.

Zhang W. and A. Sliker. 1991. Measuring shear moduli in wood with small tension and compression samples. Wood and Fiber Sci. 21(1):58-68.

Chapter 6. Evaluation on Effective Modulus of Elasticity of Loblolly Pine Strands Using Stochastic Finite Element Method

Wood as a biological material has variations in structure leading to variations in material properties. Previous modeling of wood and wood based composites has used average elastic constants for estimating the mechanical behavior. The variation of wood material properties should be accounted for to produce more reliable results. In this chapter, Monte-Carlo simulation based stochastic finite element method (SFEM) was used to model the stiffness of wood strands including intra-ring property variation and three different grain orientations (radial grain, tangential grain, and angled grain). Homogenized models were used as a control to compare the results from the deterministic layer finite element method (FEM) and SFEM models. The homogeneous model predicted the average effective MOE well for radial and tangential grain strands from growth ring number 1-10 but provided unrealistic physical strain distributions. Except for the radial grain orientation models from growth ring number 11-20, the cumulative probability curves from experimental tests and SFEM results agreed well. The difference of average effective MOE between experimental results and SFEM results ranged from 0.96% to 22.31% for different grain orientation strands. From a sensitivity analysis, earlywood MOE was the most important variable affecting the effective MOE.

Introduction

Although there are many models of mechanical behavior of wood at different length scales, little research has explored the variations of mechanical properties in earlywood, latewood, and wood strands. Earlywood is the layer of wood created by growth during the early growing season, characterized by thin cell walls and large lumens. Latewood is the layer of wood created by growth during the late growing season, characterized by thick cell walls and small lumens. Due to the anatomical structural differences, the mechanical properties of these two layers are also different. Previous studies have shown that latewood MOE was about two times greater than earlywood MOE (Groom et al. 2002, Mott et al. 2002, Cramer et al. 2005, and Jeong et al. 2008a). Growth rings closer to pith contain higher proportions of juvenile wood than growth rings closer to bark. Juvenile wood differs from mature wood in that it has a higher microfibril angles, a high percentage of compression wood, distorted grain patterns, and a lower percentage of latewood (Larson et al. 2001). Variations of material properties of earlywood and latewood were found in different growth ring positions (Cramer et al. 2005 and Jeong et al. 2008a). However, previous modeling work on strand based composites assumed wood as a homogeneous material (Wang and Lam 1997, Clouston and Lam 2002, and Clouston 2007).

The mechanical properties of wood strands are different by the intra-ring properties and grain orientations (Hindman and Lee 2007). However, the intra-ring properties and the orientation of grain are uncertain factors. The material properties of wood are random in nature and the grain orientation of strands may be varied due to indeterministic cutting (Jeong et al. 2008b and Jeong et al. 2008c). Therefore, it is desirable to investigate the effect of the uncertain variables of intra-ring properties and grain angle on the mechanical behavior of wood strands. Random properties of wood strands will affect not only modulus of elasticity (MOE) changes of

wood strands, but also the strain distribution, which is important for analyzing the effect of the inputs on mechanical behavior of wood strands. These research topics have not been discussed in the previous studies.

Stochastic finite element method (SFEM) is used to account for the uncertainties of material properties from the earlywood and latewood as inputs to model the different grain angles of loblolly pine wood strands. SFEM can solve for the variability associated with wood strands as known probabilities of material properties. SFEM can take advantage of the existing finite element method (FEM) for deterministic problems combined with uncertainty variables. The fundamental principle of the SFEM technique fits well for the high uncertainties of wood structure.

Literature Review

Although many previous researchers have studied the mechanical behavior of strand based composites, only one article was found to be related to strand modeling (Hindman and Lee 2007). Among many strand based composite modeling studies, three representative studies were present, which account for the randomness of material properties of wood as inputs for model.

Wang and Lam (1997) used SFEM to predict the tensile strength of parallel aligned multi layer strand based wood composites. Based on the strength of multi layers from experimental test, strength modification factors were evaluated using Weibull-weakest-link theory and size effect. The results associated with strength modification factors from models were agreed with the results from experimental test.

Clouston and Lam (2002) used SFEM to predict the strength of angle ply laminates ($[\pm 15]_s$ and $[\pm 30]_s$). Tsai-Wu failure criteria associated with flow rule was used to calculate the

failure index. The failure index was modified by size effect and loading configuration effect between tension and bending. The difference of strength between simulation and experimental test results ranged from 3.8% to 9.8%. The difference of stiffness between simulation and experimental test results ranged from 6.1% to 14.8%.

Clouston (2007) expanded the previous work to predict mechanical behavior of parallel strand lumber made from Douglas fir (*Pseudotsuga menziesii)*. Statistical variation of void area and grain angle in PSL were counted as random variables for model to predict the strength from tension, compression, and bending. The results were well agreed with the experimental tests showing 5.5% difference for tension, 3.3% difference for compression, and 6.4% difference for bending.

Hindman and Lee (2007) predicted the elastic properties of different orientation strands from loblolly pine (*Pinus taeda*) using FEM that incorporated the elastic properties of earlywood and latewood as inputs. Hindman and Lee (2007) used cellular FEM models and solid FEM models to predict the modulus of elasticity (MOE) of different orientation strands under tension and bending loading condition. Homogeneous models were also constructed to compare the prediction of MOE from the layered models. The inputs for the models were average longitudinal elastic moduli of earlywood and latewood from experimental test. The cellular models had a better prediction of MOE from different orientation strands over solid models. The difference of MOE between experimental results and layer cellular model results ranged from 1.7% to 20.4%.

While the three SFEM models (Wang and Lam 1997, Clouston and Lam 2002, and Clouston 2007) were used for predicting the mechanical properties of strand based composite using strand properties, the models did not consider the variability of mechanical properties of earlywood and latewood. Although Hindman and Lee (2007) modeled different orientated

strands using earlywood and latewood properties, the results of the models were limited by the deterministic inputs to predict the mechanical properties of wood strands. The variability of mechanical properties of earlywood and latewood must be considered in modeling to represent the true nature of wood as a biological composite material.

In order to have more rigorous data on earlywood and latewood properties, Jeong et al. (2008a) measured the mechanical properties of earlywood and latewood from growth ring number 1-10 and growth ring number 11-20 using tension testing incorporated with digital image correlation (DIC). The results showed that MOE and Poisson ratio increased as the growth ring number increased. Statistical comparisons showed that the MOE and UTS had a significant difference by both growth ring positions and intra-ring. Based on testing results, probability density functions for MOE, Poisson ratios, and UTS were examined using Kolmogorov-Smimov (K-S), Chi-square test, and visual inspection. These results were used as inputs for the current modeling work.

Jeong et al. (2008b) and Jeong et al. (2008c) measured the tensile properties of different orientation loblolly pine (*Pinus taeda*) strands from growth ring number 1-10 and growth ring number 11-20. Three different oriented strands (radial, tangential, and angled orientation strands) showed MOE and UTS of wood strands increased as growth ring number increased. Statistical comparison showed that the growth ring position and grain angle can impact the mechanical properties of the wood strands. The MOE of three different oriented strands from the two different growth ring positions were used as a validation of the current model.

The goal of this chapter was to analyze the effect of the intra-ring properties and grain angles on the MOE of wood strands with respect to these variables. Monte Carlo simulation based SFEM used the results from the earlywood and latewood testing as inputs to model the

mechanical property variation of loblolly pine wood strands. A sensitivity analysis of the input parameters in the SFEM model was conducted to analyze the most important parameters related to mechanical response.

Methods

SFEM models were constructed using ANSYS 11.0v program. Before the SFEM models were constructed, the following assumptions were applied.

1. Wood strands behaved in a linear elastic manner.
2. No slippage occurred between earlywood and latewood under uniform loading.
3. Loading was assumed to be deterministic
4. MOE of earlywood and latewood were assumed to be random variables with known distribution.
5. Poisson ratio for earlywood and latewood were assumed to be random variables with known distribution.

Figure 6.1 shows four different wood strand models, dimensions of the model analogs, and the loading conditions. While models A, B, and C consider variation of intra-ring properties and grain angles, model D does not consider the intra-ring property variation and grain angle effect. Model A shows radial grain orientation model. Model B shows tangential grain orientation model. Model C shows angled grain orientation model. Model D shows a homogenized model. The dimensions for all SFEM models were 10.0 cm in length, 2.54 cm in width and 0.6 mm in thickness. The ratio of earlywood to latewood was defined to be 2.0:1.0. Uniform tension pressure was applied at the top end of the strands and the bottom of the strands was fixed in both x and y directions. To generate the random field for describing the properties of

earlywood and latewood of different orientation models, 2900 elements for radial grain orientation models, 14683 elements for tangential grain orientation models, and 4187 elements for angled grain orientation models were generated. Different element numbers for the different strand models were assigned after convergence checks that stress and strain values converged to less than 1%.

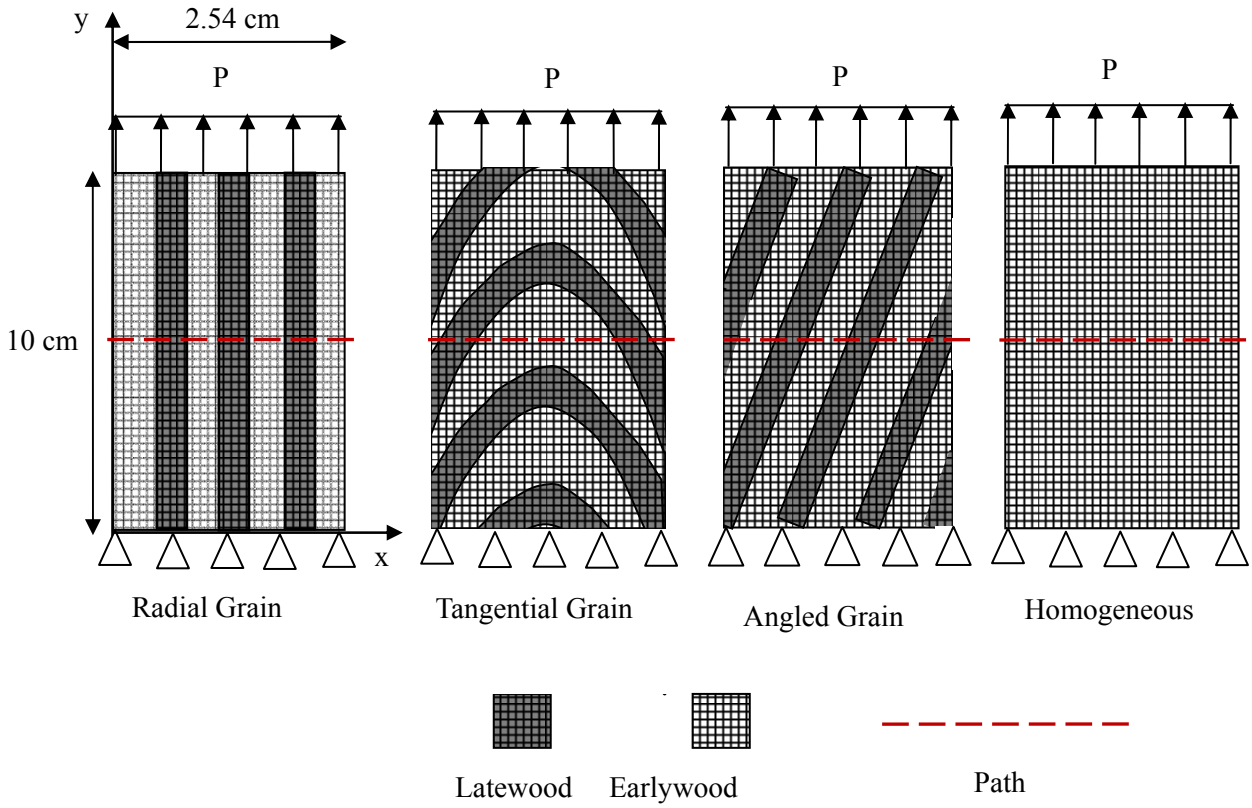

Figure 6.1 Structural analog of strand orientation models

Model Property Generation

Earlywood and latewood are defined as transverse iso-tropic materials considering in-plane properties only. For random material property generation, only E_L and υ_{LR} were counted.

The elastic properties of E_L, E_R, and G_{LR} were all expressed in terms of E_L using reciprocal relationships. This process was based on the assumption that longitudinal elastic modulus (E_L), transverse elastic modulus (E_R), longitudinal elastic modulus (E_L), and shear modulus (G_{LR}) are linearly correlated (Bodig and Goodman 1973). Kretschmann et al. (2006) found the ratio of E_L:G_{LR} for latewood and for earlywood 3.5:1.0 regardless of growth ring position. This ratio was used to calculate G_{LR} for earlywood and latewood layers for the current model. Also the ratio of E_L:E_R for earlywood and for latewood from the two different growth ring positions was indirectly calculated from transverse tension testing of cross grain strands (Jeong et al. 2008c). The E_L:E_R ratio of 2.72:1.0 was used to calculate the E_R for earlywood and latewood from growth ring number 1-10, and the E_L: E_R ratio of 3.12:1.0 was used to calculate the E_R for earlywood and latewood from growth ring number 11-20.

Table 6.1 shows the average E_L and υ_{LR} from experimental test with the distribution type and parameters (Jeong et al. 2008a). For homogeneous model, representative material properties for E_L and υ_{LR} for growth ring number 1-10 and growth ring number 11-20 were calculated by combining average E_L of earlywood and latewood based on experimental test using the Rule of Mixtures and combining the average υ_{LR} of earlywood and latewood from experimental test using the Rule of Mixtures. Based upon the E_L and υ_{LR}, the rest of properties were generated using the reciprocal relationships described above.

For deterministic layer FEM, material properties of earlywood and latewood from growth ring number 1-10 and growth ring number 11-20 were calculated based on the reciprocal relationship with the E/G ratio. For probabilistic SFEM, Monte Carlo simulation associated with Latin Hypercube Sampling (LHS) technique used for generating random properties of earlywood and latewood characterized by the distribution type and by the distribution parameters. Table 6.1

shows the exact statistical distribution type and parameters for MOE and Poisson ratio of earlywood and latewood from growth ring number 1-10 and growth ring number 11-20. These uncertain properties were randomly distributed on a discretized mesh for the distribution of earlywood and latewood. Two different random stiffness matrices for earlywood and latewood were simulated and assembled to formulate the different grain orientation models in Figure 6.1. One thousand analysis loops were executed to compute the random outputs as a function of the set of random input variables.

Table 6.1 Distribution types and parameters for MOE of earlywood and latewood from growth ring positions (Jeong et al. 2008a).

Groups	Average E_L (GPa)	Fitted Distribution	Theta	Scale	Shape
Earlywood 1-10	1.92	Weibull	0.077	2.049	3.410
Latewood 1-10	3.44	Weibull	1.699	1.947	1.697
Earlywood 11-20	2.48	Weibull	1.0	1.670	2.200
Latewood 11-20	5.09	Weibull	2.248	3.149	1.534
Poisson ratio	Average υ_{LR}	Fitted Distribution	Theta	Scale	Shape
Earlywood 1-10	0.49	Weibull	0	0.161	3.004
Latewood 1-10	0.59	Gamma	0	0.144	4.105
Earlywood 11-20	0.49	Gamma	0	0.144	3.429
Latewood 11-20	0.8	Weibull	0	0.841	2.359

After all simulations were executed, the nodal displacement was used to obtain effective MOE of different grain orientation models. From deterministic FEM, strain distributions for different grain strand models were examined as defining the path through the width at the center of the specimen. Along the path sixty points were marked to collect the strain values. From probabilistic SFEM, all results were exported to Excel to fit the cumulative probability of effective MOE and conduct probabilistic sensitivity analysis using Pearson linear correlation between input variables and effective MOE for different grain orientation strands from different

growth ring positions. The Pearson correlation coefficient was calculated using Equation 6.1.

$$r = \frac{n(\sum XY) - (\sum X)(\sum Y)}{\sqrt{[n\sum X^2 - (\sum X)^2][n\sum Y^2 - (\sum Y)^2]}} \quad (6.1)$$

Where,

r: Pearson correlation coefficient

n: Number of samples

X: Random input variable

Y:MOE outputs

XY: Covariance between random input variable and MOE output.

Results and Discussion

Comparison of experimental results to model results

Figure 6.2 shows the comparison of the averaged effective MOE values from experimental testing (Jeong et al. 2008b and Jeong et al. 2008c) and results from models. The homogeneous models (H) for Radial 1-10 and Tangential 1-10 have differences of -0.64% and 8.57%, respectively from the experimental results. Predictions of effective MOE of Radial 11-20, Tangential 11-20, Angled 1-10, and Angled 11-20 from the homogeneous models were not as accurate as the Radial 1-10 and Tangential 1-10 ranging from -21.75% to -35.96%. The deterministic layer FEM and probabilistic SFEM models were relatively good for all orientations of wood strands tested, ranging from -0.8% to -22.31%. The highest three difference between

experimental results and model results were found in Radial 11-20, Tangential 11-20, and Angled 11-20. For growth ring number 11-20, a higher ratio of latewood MOE to earlywood MOE and a higher ratio of latewood Poisson ratio to earlywood Poisson ratio may cause the slippage between earlywood and latewood, which may result in lower MOE values than current model results.

For the prediction of effective MOE for Radial 1-10 and Radial 11-20, homogeneous, deterministic FEM, and probabilistic SFEM had little difference as shown in Figure 6.2. From the analogy of laminate theory, radial grain orientation models were not influenced by the different mechanical properties of earlywood and latewood due to the iso-strain movement along the y-axis. Since input for homogeneous model was applied using the Rule of Mixtures based on earlywood and latewood properties, the homogeneous models for radial grain orientation strands should be the same strain value obtained from the corresponding deterministic FEM models. However, effective MOE from tangential and angled grain orientation models were influenced by different strain distributions caused by differences between the loading direction and the orientation of earlywood and latewood. The homogeneous model cannot represent the different orientation of earlywood and latewood other than loading direction, which resulted in a greater effective MOE for the tangential and angled grain orientation models than the experimental results.

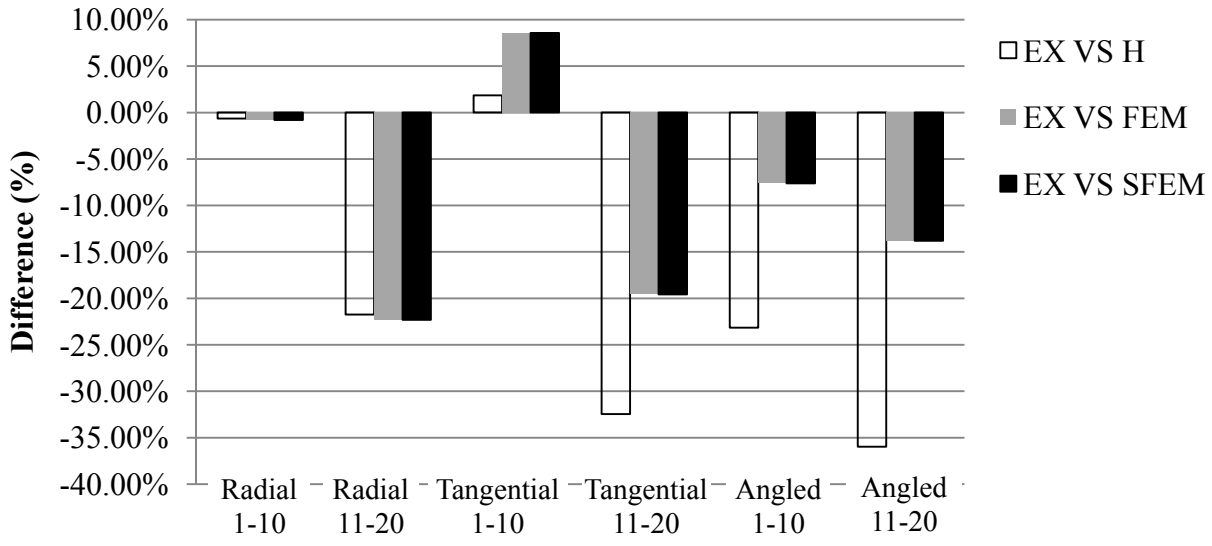

Figure 6.2 Differences between the average MOE from experimental tests (Jeong et al. 2008a and Jeong et al. 2008b) and the average MOE from models ((Difference (%)=Experimental-simulation/experimental)*100%)

Strain distribution from different orientation models from growth ring number 1-10 and growth ring number 11-20

Figure 6.3, 6.4, and 6.5 show the normalized longitudinal strain y, transverse strain x, and shear strain xy distribution through the center of the strand models (Figure 6.1), respectively. Earlywood and latewood bands change position with the different orientations through the path. For the radial, tangential, angled grain strand models, a smaller band plateau strain distribution indicates the latewood band and a larger band plateau indicates the earlywood band.

Figure 6.3 shows the strain y distribution of different orientation models from different growth ring positions. Homogeneous and radial grain orientation models showed a uniform strain distribution through the width and overlapped each other. From iso-strain behavior from homogeneous models and radial grain models, effective MOE from the two models was similar

(Figure 6.2). Tangential grain models and angled grain models showed non-uniform strain y distribution because the orientation of grain was not parallel to the loading direction. For tangential grain models, the strain y distribution showed a peak near the edge and generally smoothed out to the middle width. For angled grain models, the strain y distribution in earlywood was greater than latewood, since the latewood had a greater stiffness that produced less strain at the same load level. All strand models from growth ring number 11-20 showed a lower magnitude strain y distribution compared to strand models from growth ring number 1-10.

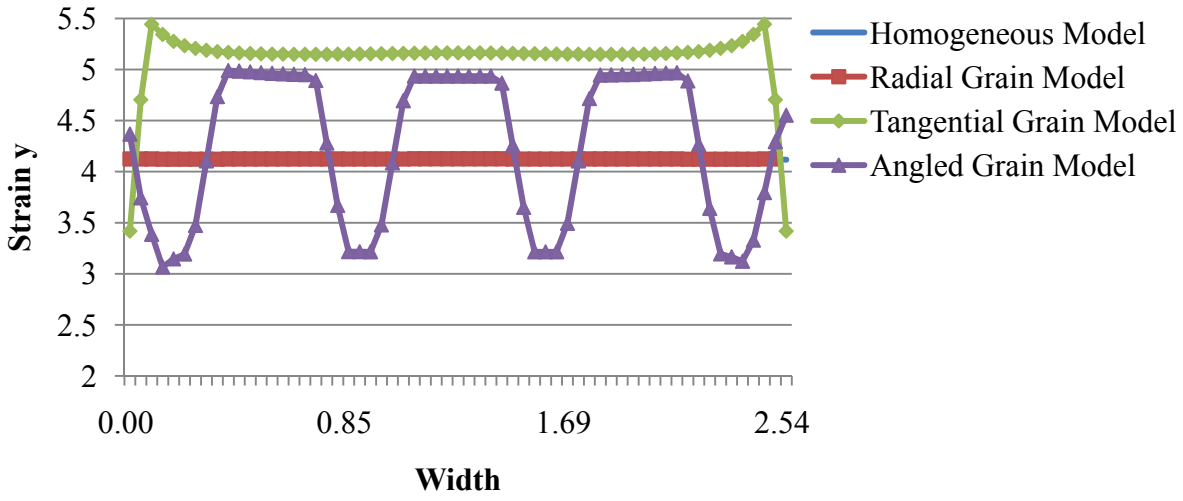

a) Growth ring number 1-10

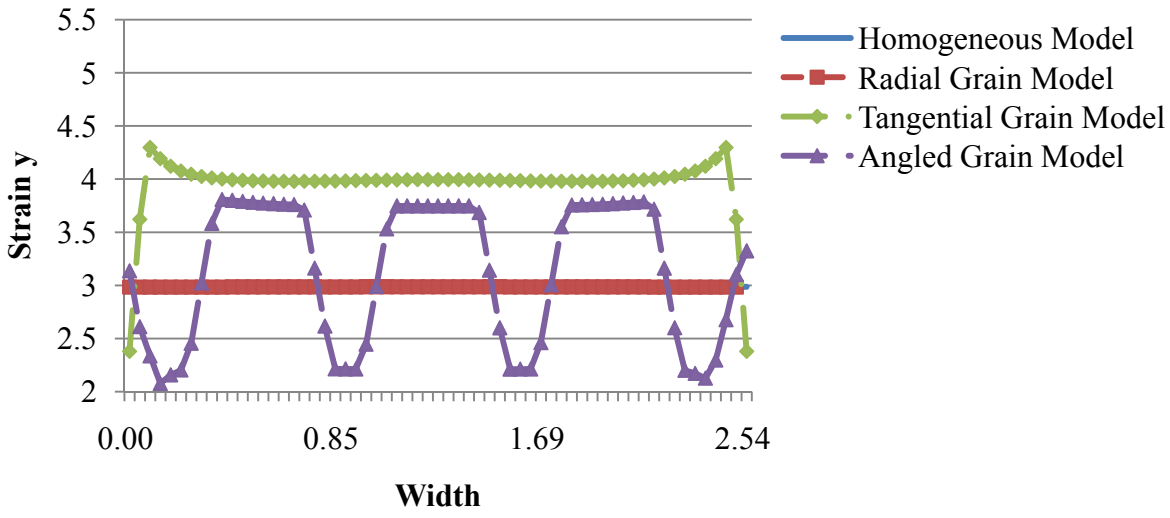

b) Growth ring number 11-20

Figure 6.3 Strain y distribution from simulation models considering grain orientations and growth ring positions. a) Growth ring number 1-10, b) Growth ring number 11-20

Figure 6.4 shows the strain x distributions of different strand models from different growth ring positions. The homogenous models showed uniform strain x distribution through the width of models, the radial, tangential, and angled grain orientation models showed non-uniform strain distributions. The radial grain orientation models showed a greater compressive strain in latewood band compared to the earlywood band because latewood MOE was greater than earlywood MOE. The tangential grain models had the greatest negative strain, which occurred near the edge of the model and generally decreased to the middle width due to the alignment direction of earlywood and latewood. The angled grain models showed trends of both the radial and tangential models, with a change in strain between earlywood bands and latewood bands, and with a frequency similar to the radial grain orientation model but with a greater amplitude.

The off-axis angle of earlywood and latewood bands to the global x axis caused a greater strain x distribution for earlywood and latewood bands from angled grain orientation models. Compared to the strain distribution of different orientation models from growth ring numbers 1-10, the strain distribution from growth ring numbers 11-20 showed a lower amplitude in general for all strand simulations, which was reasonable to expect that a greater elastic properties of strands from a higher growth ring numbers 11-20 had a greater resistance to the load.

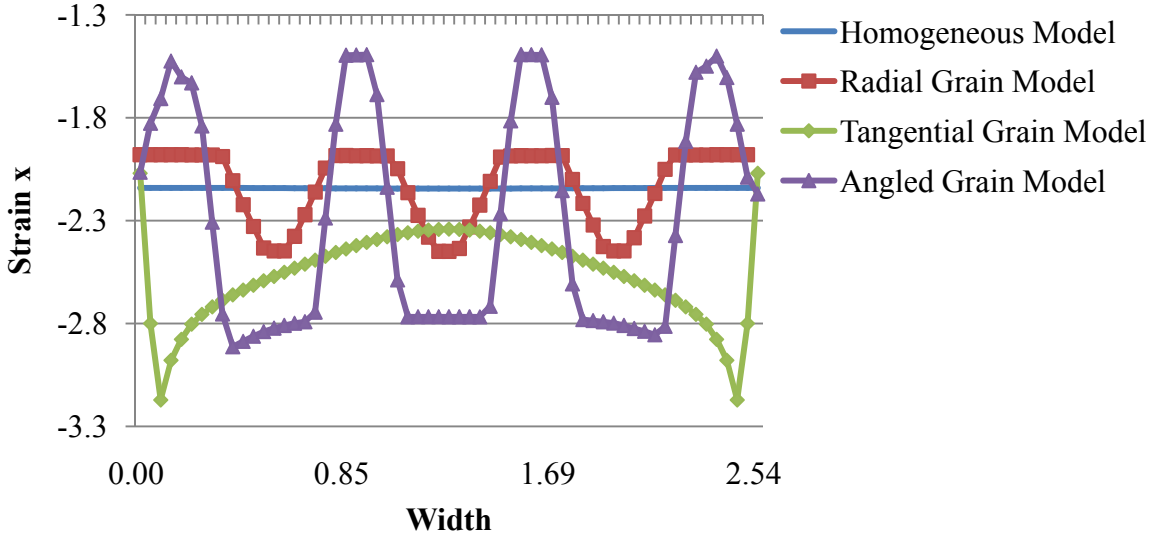

a) Growth ring number 1-10

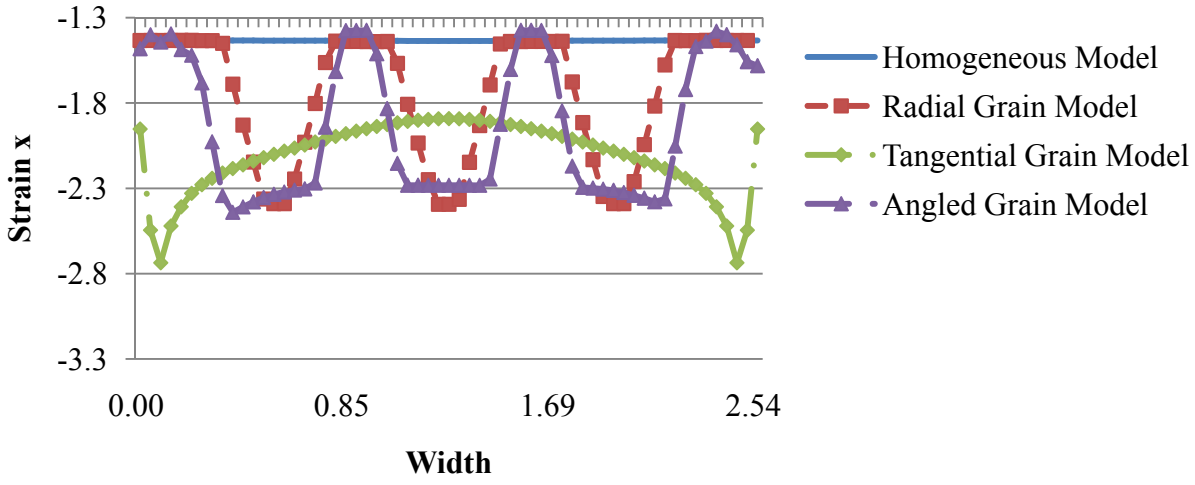

b) Growth ring number 11-20

Figure 6.4 Strain x distribution from simulation models considering grain orientations and growth ring positions. a) Growth ring number 1-10, b) Growth ring number 11-20

Figure 6.5 shows the shear strain distribution of different models from different growth ring positions. The homogeneous and radial grain orientation models showed a uniform shear strain distribution through the width of models relative to the other grain orientation models. The magnitude of shear strain distribution from the homogeneous and radial models was 100 times lower than the shear strain from the tangential and angled grain orientation models. The shear strain distributions from the homogeneous and radial grain orientation models appeared to be overlapped. The tangential grain orientation models showed the maximum negative shear strain, near the earlywood and latewood boundary at the left side, and continuously increased, crossing zero at the center, and forming an anti-symmetric distribution in the other half. The angled grain orientation models had shear strain distribution oscillated between earlywood and latewood bands. A positive shear strain occurred from earlywood band while a negative shear strain occurred from latewood band due to the higher MOE value in latewood and the lower value in

earlywood. There was no noticeable shear strain distribution and magnitude difference between different growth ring numbers.

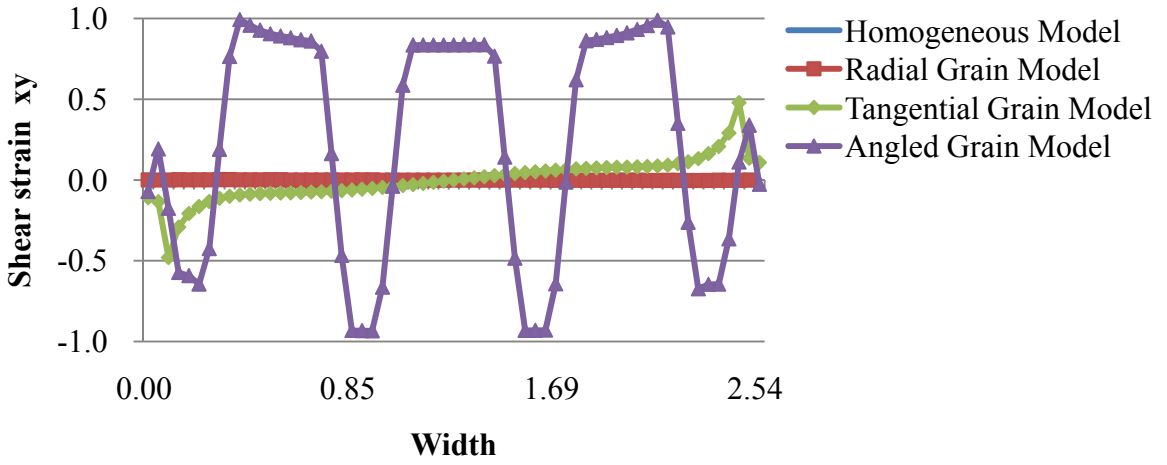

a) Growth ring number 1-10

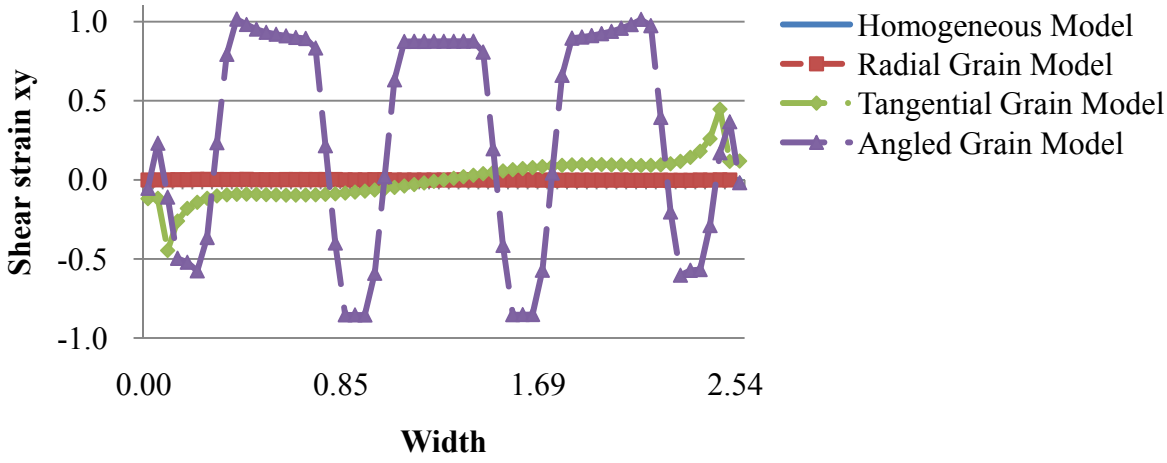

b) Growth ring number 11-20

Figure 6.5 Shear strain xy from simulation models considering grain orientations and growth ring positions. a) Growth ring number 1-10, b) Growth ring number 11-20

Statistical distribution of the effective MOE of different orientation of wood strands from different growth ring positions.

Figure 6.6 shows the cumulative probability of the effective MOE of radial, tangential, and angled grain orientation SFEM models and experimental testing from Jeong et al. (2008b and 2008c). A minimum of thirty test results was fitted from the experimental MOE results while one thousand simulation results were fitted for the SFEM results. Kolmogorov-Smimov (K-S) tests with 95% confidence interval showed the comparison between experimental results and SFEM results was not significantly different (p-value 0.999 for Radial 1-10, 0.973 for Tangential 1-10, 0.198 for Tangential 11-20, 0.855 for Angled 1-10, 0.275 for Angled 11-20 comparison) except for the comparison for radial grain strands from growth ring number 11-20 (p-value 0.001 for Radial 11-20 comparison).

Although general agreement between experimental results and corresponding SFEM results were made, some of the differences of MOE values between the experimental results and the SFEM results are discussed. The highest effective MOE value of radial orientation strand from growth ring numbers 11-20 obtained from experimental test was 3.48 GPa while the highest values of 5.29 GPa was obtained from SFEM using the combination of input variables within the distribution of experimental test data (Figure 6.6a). The lowest effective MOE value of tangential orientation strands from growth ring number 11-20 from experimental was 1.35 GPa and from SFEM model was 1.53 GPa (Figure 6.6b). The highest effective MOE value of the angled orientation stands from growth ring number 11-20 from experimental was 3.42 GPa while the corresponding SFEM model predicted 4.28 GPa (Figure 6.6c). The trends of the difference showed that SFEM results were more conservative than experimental results. Possible improvements in this modeling may provide for direct input of the volume fraction of earlywood

and latewood for each strand and also account for slippage between the earlywood and latewood bands

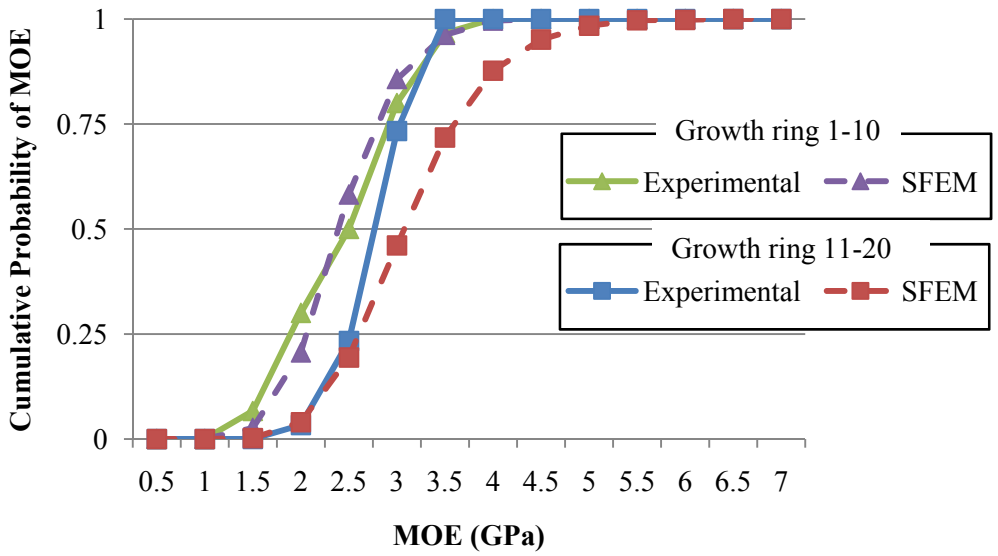

a) Comparison for MOE of radial grain orientation strands from experimental and SFEM

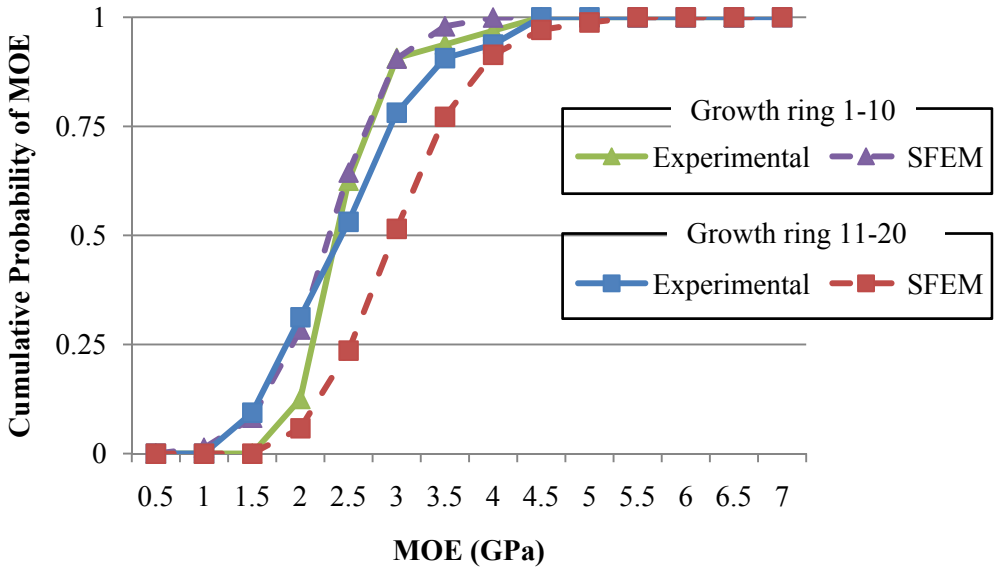

b) Comparison for MOE of tangential grain orientation strands from experimental and SFEM

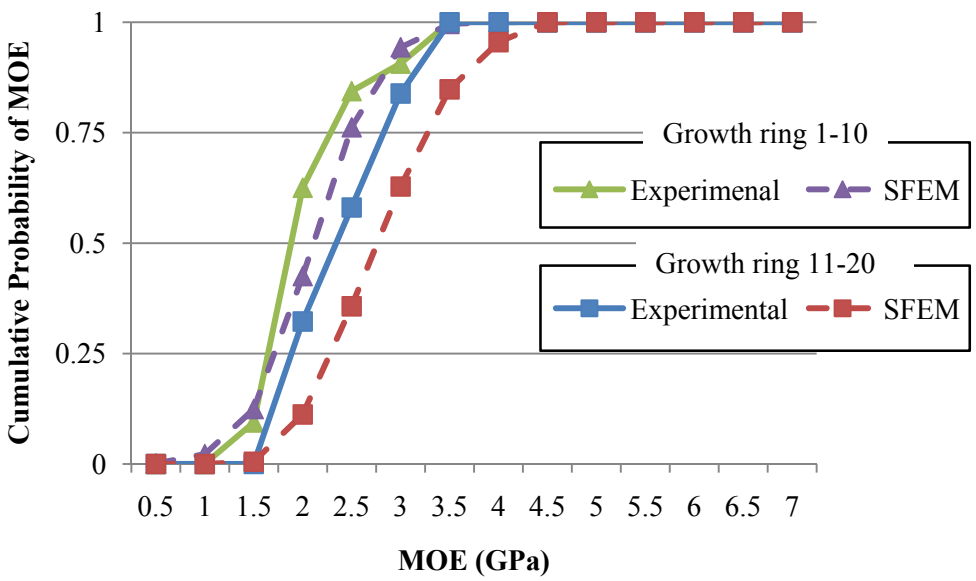

c) Comparison for MOE of angled grain orientation strands from experimental and SFEM

Figure 6.6 Comparison between cumulative probability of MOE from experimental and that from SFEM; a) radial grain orientation strands comparison, b) tangential grain orientation strands comparison, c) angled grain orientation strands comparison

Sensitivity of input variables for the effective MOE of different orientation strand models

Table 6.2 shows the sensitivity of input variables (MOE for earlywood and latewood from growth ring numbers 1-10 and growth ring numbers 11-20, Poisson ratio for earlywood and latewood from growth ring numbers 1-10 and growth ring numbers 11-20) on the effective MOE from the SFEM models of growth ring numbers 1-10 and growth ring numbers 11-20. The shaded cells represent a strong correlation of Pearson linear correlation coefficient, defined as greater than 0.5, between an input variable and effective MOE of strand models (Equation 6.1).

For growth ring numbers 1-10, earlywood MOE and earlywood Poisson ratio were strongly correlated with effective MOE from tangential and angled orientation strand models, while only earlywood MOE was strongly correlated with effective MOE from radial orientation

strand models. Latewood MOE and latewood Poisson ratio were strongly correlated with effective MOE of the radial orientation model. For growth ring numbers 11-20, earlywood MOE and earlywood Poisson ratio had high correlations with the effective MOE of tangential and angled orientation strand models, while earlywood MOE was strongly correlated with the effective MOE of radial orientation strand models. Latewood MOE was strongly correlated with the effective MOE of radial orientation model. Regardless of growth ring number, earlywood and latewood MOE had greater correlations with the effective MOE of different orientation strand models than the Poisson ratios.

Table 6.2 Sensitivity analysis of input variables on MOE of different grain orientation strands from growth ring number 1-10 and growth ring number 11-20 showing the Pearson linear correlation coefficient (r)

Growth ring Number 1-10	Variables	Radial	Tangential	Angle
Earlywood	MOE	0.734	0.916	0.952
	Poisson ratio	0.410	0.551	0.598
Latewood	MOE	0.662	0.259	0.255
	Poisson ratio	0.571	0.168	0.194
Growth ring number 11-20	Variables	Radial	Tangential	Angle
Earlywood	MOE	0.603	0.899	0.936
	Poisson ratio	0.400	0.563	0.543
Latewood	MOE	0.809	0.385	0.269
	Poisson ratio	0.452	0.256	0.192

The sensitivity of earlywood and latewood variables changed with varying orientation of strands and growth ring number. While correlation between earlywood MOE and effective MOE of different orientation strand models increased as orientation of strands switched from radial to tangential to angle, the correlation between latewood MOE and effective MOE of different

orientation strand models decreased, which can be explained by the fact that the tangential and angled orientation strand models had a different strain distribution through the width. In the earlywood band, greater strains occurred while lower strains occurred in latewood band (Figure 6.3). With the same MOE value of latewood, increment of MOE of earlywood will significantly increase the stiffness of the tangential and angled orientation strands.

As orientation of strands switched from radial to tangential to angle, correlation between earlywood Poisson ratio and effective MOE of the different orientation strand models increased. However, as orientation of strands switched from radial to tangential to angle, correlation between latewood Poisson ratio and the effective MOE of the different orientation strand models decreased. The correlation between Poisson ratio from earlywood and latewood and effective MOE of different orientation wood strands can be explained by different strain x distribution associated with strain y distribution (Figure 6.3 and Figure 6.4). From the superimposed strain x and strain y distribution, radial strands had a greater magnitude of Poisson ratio in latewood bands while tangential and angled strands had a greater magnitude of Poisson ratio in earlywood bands. Poisson ratio can increase by increment of strain x and decrement of strain y. Therefore, the effective MOE of radial strands had a positive correlation with Poisson ratio of latewood while the effective MOE of tangential and angled strands had a positive correlation with Poisson ratio of earlywood. The sensitivity of earlywood and latewood variables on effective MOE of different orientation wood strands was changed by different strain distribution that was highly related to growth ring number, orientation of strands, and interaction of variables. Regardless of growth ring number and orientation, earlywood MOE was a dominant factor that controlled effective MOE of different orientation wood strands.

Conclusions

Tensile properties of different orientation wood strands were evaluated using deterministic finite element method (FEM) models and probabilistic stochastic finite element method (SFEM) models. While the deterministic FEM models used average material properties of earlywood and latewood, SFEM models used the distribution of material properties of earlywood and latewood from growth ring number 1-10 and growth ring number 11-20. While the homogeneous model predicted the average effective MOE well for radial and tangential orientation strand from growth ring number 1-10, the physical strain distribution showed unrealistic behavior. Compared to deterministic homogeneous model, deterministic layer FEM and SFEM models predicted the average effective MOE of the rest orientation strands better. From strain distribution analysis, different strain distribution for earlywood and latewood layers occurred in different grain orientations. Homogeneous and radial orientation models, however, showed iso-strain distribution in longitudinal y direction, which resulted in the same MOE values. Comparison of cumulative probability curves from experimental test and SFEM was agreed well. The difference of variation of MOE from different grain strands between experimental results (Jeong et al. 2008b and Jeong et al. 2008c) and SFEM results ranged from 0.96% to 22.31%. From sensitivity analysis, earlywood and latewood participated differently to effective MOE of different grain orientation strand models, which was highly associated with the strain distribution caused by different orientation strands and interaction of input parameters. In general, earlywood MOE had a greater effect on effective MOE of wood strands than other input parameters.

References

Bodig, J. and J. R. Goodman. 1973. Prediction of elastic parameters for wood. Wood Sci. 5(4):

249-264.

Clouston, P. and F. Lam, 2002. A stochastic plasticity approach to strength modeling of strand-based wood composites. Composites Science and Technology, 62:1381-1395.

Clouston P. 2007. Characterization and strength modeling of parallel-strand lumber. Holzforschung, 61:394-399.

Cramer, S. M., D. E. Kretschmann, R. Lakes, and T. Schmidt. 2005. Earlywood and latewood elastic properties in loblolly pine. Holzforschung. 59:531-538.

Groom, L., L. Mott., and S. Shaler. 2002. Mechanical properties of individual southern pine fibers. Part I. Determination and variability of stress-strain curves with respect to tree height and juvenility. Wood and Fiber Sci. 34(1):14-27.

Hindman D. P. and J. N. Lee. 2007. Modeling wood strands as multi-layer composites: bending and tension loads. Wood and Fiber Sci. 39(4):515-526.

Jeong G. Y., D. P. Hindman, and A. Zink-Sharp. 2008a. Tensile properties of earlywood and latewood from loblolly pine (*Pinus taeda*) using digital image correlation.

Jeong G. Y., A. Zink-Sharp, and D. P. Hindman. 2008b. Comparison of longitudinal tensile properties of different grain orientation strands from loblolly pine (*Pinus taeda*).

Jeong G. Y., D. P. Hindman, and A. Zink-Sharp. 2008c. Shear and transverse properties of loblolly pine (*Pinus taeda*) strands using tension test incorporated with digital image correlation (DIC).

Kretschmann, D. E., S. M. Cramer, R. Lakes, and T. Schmidt. 2006. Selected mesostructure properties in loblolly pine from Arkansas plantations Characterization of the cellulosic cell wall. Ames, Iowa : Blackwell Pub., 149-170 pp.

Larson, P. R., D. E. Kretschmann, A. Clark III, and J. G. Isebrands. 2001. Juvenile wood formation and properties in southern pine. General Technical Report FPL-GTR-129. Madison, Wisconsin: US Department of Agriculture, Forest Service, Forest Products Laboratory

Mott, L., L. Groom, and S. Shaler. 2002. Mechanical properties of individual southern pine fibers. Part II. Comparison of earlywood and latewood fibers with respect to tree height and juvenility. Wood and Fiber Sci. 34(2): 221-237.

Wang, Y. T. and F. Lam. 1998. Computational modeling of material failure for parallel-aligned strand-based wood composites. J. Computational Material Science 11:157-165.

Chapter 7. Evaluation on Ultimate Tensile Strength of Loblolly Pine Strands Using Stochastic Finite Element Method

The purpose of the chapter was to predict the failure strength of different orientation of wood strands from different growth ring positions under tension loading. Stochastic models were constructed to account for the uncertainty of material properties. The Tsai-Hill criteria were used to predict the ultimate tensile strength (UTS). The UTS results from experimental testing were used to validate the results from models. The difference of UTS between experimental and SFEM ranged from 0.09% to 11.09%. Stress distributions showed the different stress distributions for the different orientation strand models while uniform stress distribution for homogeneous models. The magnitude of the stress distribution was higher for strands from the growth ring number 11-20. Sensitivity analysis showed that grain orientation and growth ring number influenced the UTS of strands. UTS of strands from growth ring number 1-10 showed strength indexes (X_t, Y_t, and S) a dominant factor while UTS of strands from growth ring number 11-20 showed both strength indexes and stress components (σ_1, σ_2, and τ_{12}) a dominant factor.

Introduction

The use of wood strand based composites in structural applications has been increasing. Most wood strands have been prepared from plantation grown trees. Plantation grown trees have a short-term rotation time, which results in high production of juvenile wood. Juvenile wood located near the pith has a higher microfibril angle and a thinner cell wall while mature wood located near the bark has a lower microfibril angle and a thicker cell wall (Larson et al. 2001). Values for tensile strength, bending modulus of rupture (MOR), and bending modulus of elasticity (MOE) of juvenile wood were less than mature wood due to higher fibril angle, shorter tracheid length, and lower specific gravity (Bendtsen 1978, Panshin and de Zeeuw 1980, Smith and Briggs 1986, Cave and Walker 1994). Prior to analyzing the effect of juvenile wood strands on the mechanical properties of wood strand based composites, the rigorous analysis of mechanical properties of wood strands from plantations is required maximizing wood resources.

Strength of wood materials shows large variation due to the complexity of structure, interaction of failure modes, inherent inhomogenity, anisotropy, and orientation of grain (Jeong et al. 2008a, Jeong et al 2008b, and Jeong et al. 2008c). A deterministic approach, however, cannot predict the scatter range of the variables and the use of deterministic analysis can lead to serious misinterpretation including overestimation of strength, underestimation of strength, and inconclusive reliability level. A probability based failure prediction of wood is more appropriate to overcome the limitation of deterministic approach. Random properties of wood strands will affect not only stiffness changes of wood strands, but also the evaluation of stresses in principal material directions, which are important for failure estimation of wood strands.

A great deal of failure criteria used in composite materials are empirical. Therefore, the failure criteria for wood strands should be developed based on physical failure behavior of wood

strands to avoid underestimating strength. Failure stresses for either earlywood or latewood layers present in wood strands are not acceptable since wood strands usually fail by a combination of earlywood and latewood layer failure. Lumped or averaged strength of earlywood and latewood may provide a more realistic assessment of the failure envelope. To have a more reliable prediction of wood strand strength, the variation of material properties of wood strands should be accounted for as well as statistical variation of failure strength. Kasal and Leichti (2005) proposed "The problem of finding the failure probability can be reduced to finding parameters of a multivariate distribution.".

Deterministic finite element method (FEM) and stochastic finite element method (SFEM) were employed to analyze the effect of the variation of earlywood and latewood properties and grain orientations on mechanical behavior of wood strands. Homogeneous models were also employed as control for layer models. SFEM counted the variations of earlywood and latewood material properties, and the variation of the wood strengths as random variables for stochastic processing.

Literature Review

The computation of the stochastic field of nodal displacements (u) from the random stiffness matrix (K) is the main objective of the SFEM. There are many representative methods to solve the SFEM including perturbation, Monte Carlo simulation, Neumann expansion, and Karhunen-Loeve decomposition (Wang and Lam 1998, Ghanem and Spanos 1991, Kleiber and Hien 1992, Ghanem 1999, Kaminski 2000, Chkraborty and Dey 2000, Clouston and Lam 2002, Chung et al. 2005, and Eiermann et al. 2005). This study focuses on Monte Carlo simulation method to generate the random stiffness matrix (K). The stochastic field of nodal displacements

(u) can be expressed in response to the stiffness matrix. Although there was no previous research on strength prediction of wood strands using SFEM, studies for prediction of strength of strand based composite were available. Therefore, literature review was focused on the prediction of strength of strand based composite.

Wang and Lam (1997) constructed a Monte Carlo simulation based SFEM to predict UTS of parallel strand based wood composite. Strength modification factors for different layer models were obtained using Weibull-weakest-link theory and size effect to fit the strength from experimental results. The results associated with strength modification factors from models were agreed with the results from experimental test.

Clouston and Lam (2002) used the SFEM to predict the strength of angle ply laminates ($[\pm 15]_s$ and $[\pm 30]_s$). The SFEM had a capable of the prediction of failure indexes for the different angle laminates using Tsai-Wu failure criteria associated with flow rule. The failure index was modified by size effect and loading configuration effect between tension and bending. The difference of strength between simulation and experimental test results ranged from 3.8% to 9.8%. Clouston (2007) expanded the model to count statistical variation of void area and grain angle in parallel strand lumber (PSL) made from Douglas fir (*Pseudotsuga menziesii)*. The difference between model and experimental results for tension, compression, and bending strength of the PSL was 5.5%, 3.3%, and 6.4%, respectively.

Kasal and Leichti (2005) summarized the previous studies on application of various failure criteria on wood material. Most deterministic stress analysis assumed wood materials as a homogeneous and isotropic material that violated the real physical structure of wood material. Such simplifications were only acceptable for obtaining primitive results assuming uniaxial stresses involved. Some stochastic analysis application on strength of wood material including

first order second moment method, Monte Carlo simulation method, and Binomial distribution method were summarized.

Jeong et al. (2008d) constructed SFEM models to predict the MOE values for different orientation wood strands from growth ring number 1-10 and growth ring number 11-20. The inputs for the models were distribution of elastic properties of earlywood and latewood from the two different growth ring position (Jeong et al. 2008a). The model results had a good agreement with the experimental results ranging from 0.96% to 22.31%. The constructed models were used in this current study.

Jeong et al. (2008b and 2008c) measured the strength of different orientation of wood strands from the two different growth ring positions and found the specific distribution of strength values including longitudinal strength, transverse strength, and shear strength. The distribution of strength of wood strands was used to generate the random strength indexes to predict the ultimate tensile strength (UTS) of different orientation wood strands. The average of the strength values from experimental test were used to validate the predicted UTS from the current models.

The goal of this chapter was to predict the UTS of different grain orientation strands from growth ring number 1-10 and growth ring number 11-20 using SFEM considering the variability of material properties. Uncertainties of strength indexes were implemented using Monte Carlo simulation with known probabilities of UTS of different grain orientation strands from experimental test result. The sensitivity analysis was conducted to analyze the effect of input random variables on the UTS of different orientation wood strands.

Model Development

Figure 7.1 shows the flowchart describing the key steps to compute UTS and sensitivity for the different orientation of wood strands. Jeong and Hindman (2008d) constructed eight SFEM models for different orientation wood strands from growth ring number 1-10 and growth ring number 11-20. The previous constructed models used random inputs (MOE, υ_{LR} of earlywood and latewood) from Jeong et al. (2008a) to count the variability of mechanical properties of earlywood and latewood band to analyze the mechanical behavior of different orientation wood strands. Three strength components (X_t, Y_t, S) were used to count the variability of strength of wood strands (Jeong et al. 2008b and Jeong et al. 2008c). With the assigned distributions of the random variables, stress components and strength indexes were generated using Monte Carlo simulation method associated with Latin Hypercube Sampling. One thousand loops were used to predict the UTS of different orientation strands. The UTS were predicted from the strength and stress components using Tsai-Hill failure criteria. This method can be applied due to the brittle failure behavior. From SFEM generated stress-displacement relationships, UTS can be predicted associated with strength value from experimental test. Newton-Raphson iteration method was used to find roots for the critical stress components to calculate UTS.

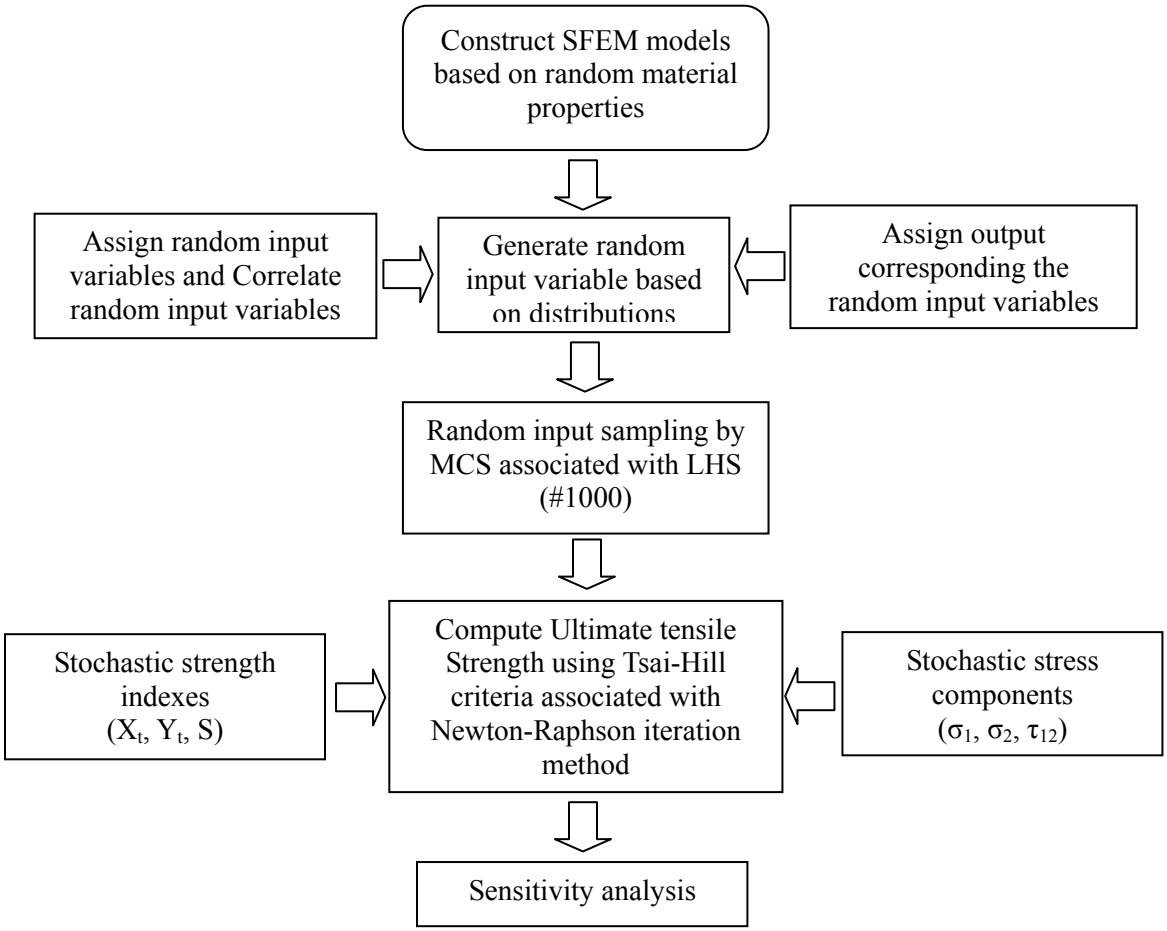

Figure 7.1 Flowchart for the SFEM procedure

Figure 7.2 shows the four different orientation wood strand models, dimensions of the model analogs, and the loading conditions. While models A, B, and C were considered variation of intra-ring properties and grain angles, model D did not include intra-ring property variation and grain angle effect. The dimension for all SFEM models was 10.0 cm in length, 2.54 cm in width and 0.6 mm in thickness. The ratio of latewood and earlywood was defined to be 0.5. Uniform tension displacement applied at the top end of the strands and at the bottom of the strands was fixed in both x and y direction.

The following assumptions were made to predict UTS of different orientation strands.

1. Strength indexes are random and independent

2. Stress components increase linearly with the increment of displacement.

3. Strength and stress components are not correlated

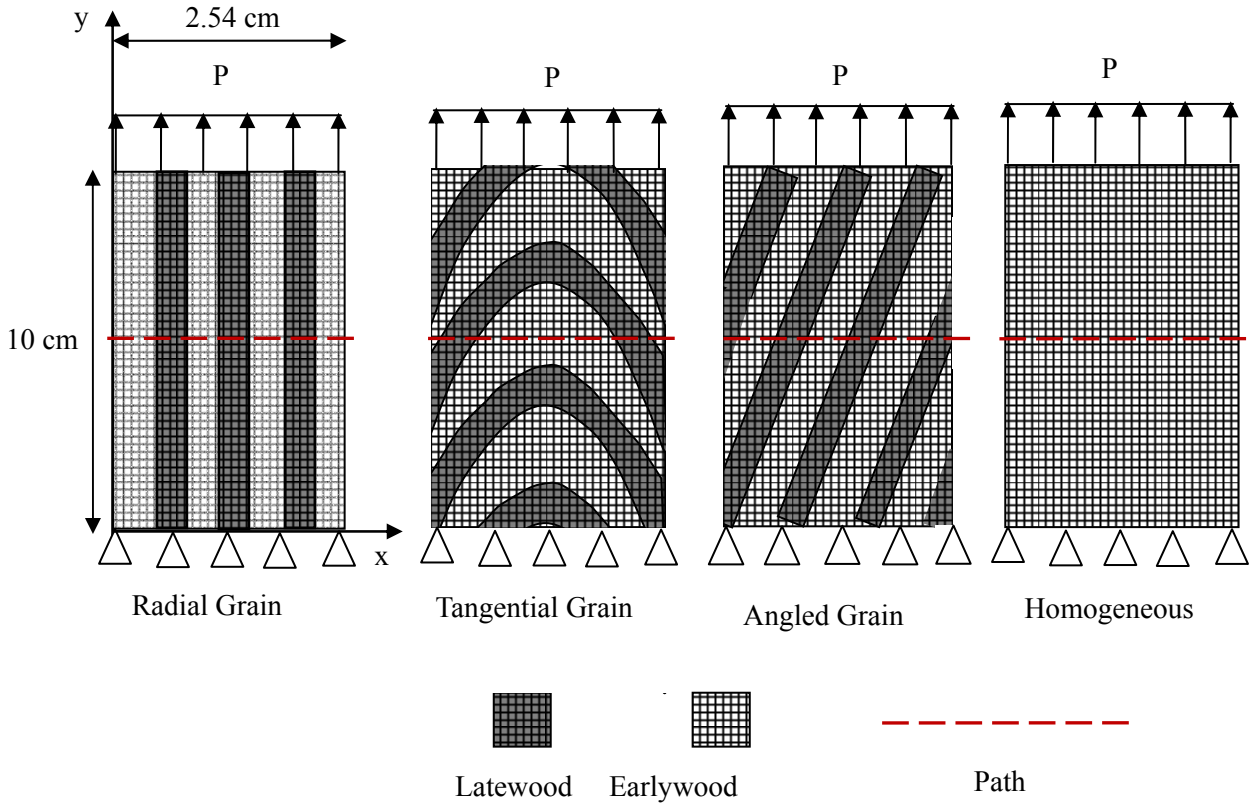

Figure 7.2 Structural analog of strand orientation models

The probabilistic failure stress was predicted using Equation 7.1 showing the Tsai-Hill failure criteria. Based on analytical distribution of three parameters (X_t, Y_t, S), random strength indexes were generated using Monte Carlo simulation method. The distributions of stress components (σ_1, σ_2, τ_{12}) were obtained from the SFEM.

$$\frac{\sigma_1^2}{X_t^2} + \frac{\sigma_2^2}{Y_t^2} + \frac{\tau_{12}^2}{S^2} - \frac{\sigma_1 \sigma_2}{Y_t^2} \leq 1 \qquad (7.1)$$

Where,

σ_1: Principal stress in radial direction

σ_2: Principal stress in longitudinal direction

τ_{12}: Principal shear stress

X_t: Transverse strength

Y_t: Longitudinal strength

S: Shear strength

Regardless of grain orientation and growth ring positions, most strands failed in a brittle manner. From the stress-displacement, extrapolation of slope would meet the peak load, which can be assumed from the experimental results (Jeong et al. 2008b and 2008c). The maximum stress can be considered a function of deflection due to the lack of non-linear deformation. With the slope, stress components were generated for model results. From the slope of stress and displacement relationship, the three stresses components could be summarized as a function of displacement and values of slope for the three stress components.

$$\sigma_1 = aX \qquad (7.2a)$$

$$\sigma_2 = bX \qquad (7.2b)$$

$$\tau_{12} = cX \qquad (7.2c)$$

Where,

X : Given displacement (Δ)

a: slope between σ_1 and X

b: slope between σ_2 and X

c: slope between τ_{12} and X

Substitute Equations 7.2a, 7.2b, 7.2c into Equation 7.1, Equation 7.1 can be summarized as

$$X^2\left(\frac{a^2}{X_t^2}+\frac{b^2}{Y_t^2}+\frac{c^2}{S^2}-\frac{ab}{Y_t^2}\right)-1\leq 0 \qquad (7.3)$$

From Equation 7.3, the strength of different grain orientation strands can be predicted as a function of stochastic constants of a, b, and c, and stochastic constants of strength indexes. To solve Equation 7.3, Newton-Raphson iteration method was used with an established tolerance of 1×10^{-7}.

Deterministic FEM and Probabilistic SFEM Stress Components and Strength Indexes Generation

Table 7.1 shows the best fitted distribution for strength indexes (X_t, Y_t, and S) from two growth ring numbers with distribution parameters (Jeong et al. 2008b and Jeong et al. 2008c). The average strength values and standard deviation from experimental and the distribution were also shown. The X_t represented transverse strength, Y_t represented longitudinal strength, and S represented shear strength.

For deterministic layer FEM, stress components were generated using the average material properties for earlywood and latewood from growth ring number 1-10 and growth ring

number 11-20. Average strength component for the deterministic models were used to predict the UTS of different orientation strands. For homogeneous model, average stress components were calculated using representative material properties for E_L and υ_{LR} for growth ring number 1-10 and growth ring number 11-20 that were calculated combining average E_L of earlywood and latewood based on experimental test using rule of mixture and combining average υ_{LR} of earlywood and latewood from experimental test using rule of mixture.

For probabilistic SFEM, Monte Carlo Simulation associated with Latin Hypercube Sampling technique used for generating random stress components and strength indexes of different orientation strands characterized by the distribution type and by the distribution parameters. Table 7.1 shows the exact statistical distribution type and parameters for the three strength indexes from growth ring number 1-10 and growth ring number 11-20. These uncertain properties were randomly distributed on the discretized mesh for the distribution of earlywood and latewood (Figure 7.1). One thousand analysis loops were executed to generate random stress components and strength indexes for different orientation strands to predict UTS.

Table 7.1 Distribution of strength indexes from Jeong et al. (2008c) and Jeong et al. (2008d)

Growth ring number 1-10	Estimated Average (MPa)	Estimated Standard deviation (MPa)	Predicted Average (MPa)	Predicted Standard deviation (MPa)	Fitted Distribution	Theta	Scale	Shape
Y_t	20.52	7.56	20.50	7.48	Weibull	6.55	15.72	1.94
X_t	2.94	1.24	2.95	1.20	Weibull	0	3.32	2.64
S	4.66	1.26	4.73	1.24	Gamma	1.04	0.42	8.80
Growth ring number 11-20	Estimated Average (MPa)	Estimated Standard deviation (MPa)	Predicted Average (MPa)	Predicted Standard deviation (MPa)	Fitted Distribution	Theta	Scale	Shape
Y_t	29.03	6.85	29.06	6.45	Weibull	0	31.59	5.17
X_t	2.53	0.83	2.52	0.85	Weibull	0	2.81	3.25
S	4.09	1.07	4.09	1.01	Gamma	0	0.25	16.26

After all simulations executed, from deterministic FEM, stress distributions for different grain strand models were examined as defining the path through the width at the center of the specimen. Along the path sixty points were marked to collect the stress values. All results from probabilistic SFEM were exported to Excel to fit the cumulative probability distribution of UTS and conduct sensitivity analysis using the Spearman rank correlation coefficient (r) defined in Equation 4 between input variables and UTS for different grain orientation strands from different growth ring positions.

$$r = 1 - \frac{6\sum_{i=1}^{n} d_i^2}{n^3 - n} \tag{7.4}$$

Where,

d_i: distance in ranks between an input variable and UTS

n: number of simulation (1000)

Results and Discussion

Table 7.2 shows the percent difference of model and experimental results from Jeong et al. (2008b and 2008c). Homogeneous models for radial grain orientation strands from growth ring number 1-10 (Radial 1-10), growth ring number 11-20 (Radial 11-20), and for tangential grain orientation strands from growth ring number 1-10 (Tangential 1-10) agreed well with the experimental results (0.15%, 0.20%, and 0.41% difference, respectively). However, the UTS predictions of other oriented strands were not accurate with the homogeneous model ranging from -23.24% to -157.06%. The homogeneous model predicted the strength of radial grain

orientation strands well due to the fact that the strength of strands was determined as a system failure rather than either individual earlywood band or latewood band in different orientation wood strands. Since input for the homogeneous model was applied using Rule of Mixture based on earlywood and latewood properties, the homogeneous model for Radial 1-10 and Radial 11-20 should be the same average stress value obtained from the corresponding layer FEM model.

The deterministic layer FEM models and SFEM models had the same average UTS values for the different orientation strands. In general, both deterministic layer FEM and SFEM models predicted well for the different grain orientation wood strands ranged from 0.09% to 11.09%. Radial grain orientation strands were influenced little by the orientation of earlywood and latewood due to the prediction of system failure, where a failure of the strand would involve multiple layers of both earlywood and latewood. The highest difference of 11.09% between UTS and predicted UTS from FEM and SFEM for tangential grain orientation models was found. Tangential grain orientation strand models were difficult to model since the geometry of earlywood and latewood bands were created by cutting the tangent to the earlywood and latewood boundary when the wood disk assumed a tapered cylinder (Figure 7.2). However, the wood strands show variation in the actual earlywood and latewood bands present in the strands, which may influence the volume fraction of earlywood and latewood as well as the specific geometry associated with the mesh for the tangential grain orientation model in Figure 2.

The highest difference of 95.7% and 157.06% between UTS and predicted UTS from the homogeneous models for angled grain orientation models of growth ring numbers 1-10 and 11-20 was found, respectively. Since the geometry of the homogeneous models could not mimic the complicated stress distributions induced by the combination of loading direction with orientation of earlywood and latewood for angled grain orientation strands. However, the mimicked

geometry of layered FEM and SFEM for angled grain orientation strands could show the stress distribution in earlywood and latewood bands that were important to predict the UTS. The difference of UTS between experimental and model results was ranged from 0.34% for Angled 1-10 and 1.60% for Angled 11-20

Table 7.2 Comparison of average ultimate tensile strengths of wood strands from current SFEM and previous experimental tests from Jeong et al. (2008b and 2008c).

Notation	Ex (MPa)	H (MPa)	FEM (MPa)	SFEM (MPa)	Ex vs H (%)[1]	Ex vs FEM (%)	Ex vs SFEM (%)
Radial 1-10	20.52	20.51	20.50	20.50	0.15	0.09	0.09
Radial 11-20	29.03	29.07	29.06	29.06	0.20	-0.14	-0.14
Tangential 1-10	20.58	20.51	19.43	19.43	0.41	5.55	5.55
Tangential 11-20	23.51	29.07	26.11	26.11	-23.24	-11.09	-11.09
Angled 1-10	10.47	20.51	10.50	10.50	-95.70	-0.34	-0.34
Angled 11-20	11.27	29.07	11.08	11.08	-157.06	1.60	1.60

[1]Difference (%) = (experimental result-model results)/experimental results *100%

Stress distributions from different strands

Figure 7.3, 7.4, and 7.5 show the normalized longitudinal stress y, transverse stress x, and shear stress xy distribution through the width of the center of the strand models (Figure 7.2), respectively. Earlywood and latewood bands change position with the different orientation through the path. Earlywood bands are two times wider than the latewood bands. For radial, tangential, and angled grain strand models, a smaller band plateau stress distribution indicates the latewood band and a larger band plateau indicates the earlywood band.

Figure 7.3 shows the longitudinal stress y distribution of different orientation models for different growth ring positions. The stress distribution of the homogenous model was uniform throughout the width of the strand regardless of growth ring positions. Radial grain orientation models showed the distinctive stress y distribution showing lower stress in earlywood and

greater stress in latewood due to the lower longitudinal elastic modulus of earlywood and the greater longitudinal elastic modulus of latewood. Tangential grain orientation models showed greater stress in latewood at both edge and lower stress in earlywood. Although tangential grain orientation model had a different stress distribution between earlywood and latewood, the magnitude of difference between two bands were lowest compared to the radial and angled grain orientation models. The angled grain orientation models showed lower stress in earlywood bands than the latewood bands. The magnitude of the stress difference between earlywood and latewood for angled grain model was lower than that of radial grain model. Compared to the stress x distribution, the magnitude of stress y distribution was about twenty times greater for growth ring numbers 1-10 and about fifteen times greater for growth ring numbers 11-20. The general trend for stress distribution from different growth ring positions were similar but greater magnitude stress in strands from a higher growth ring positions.

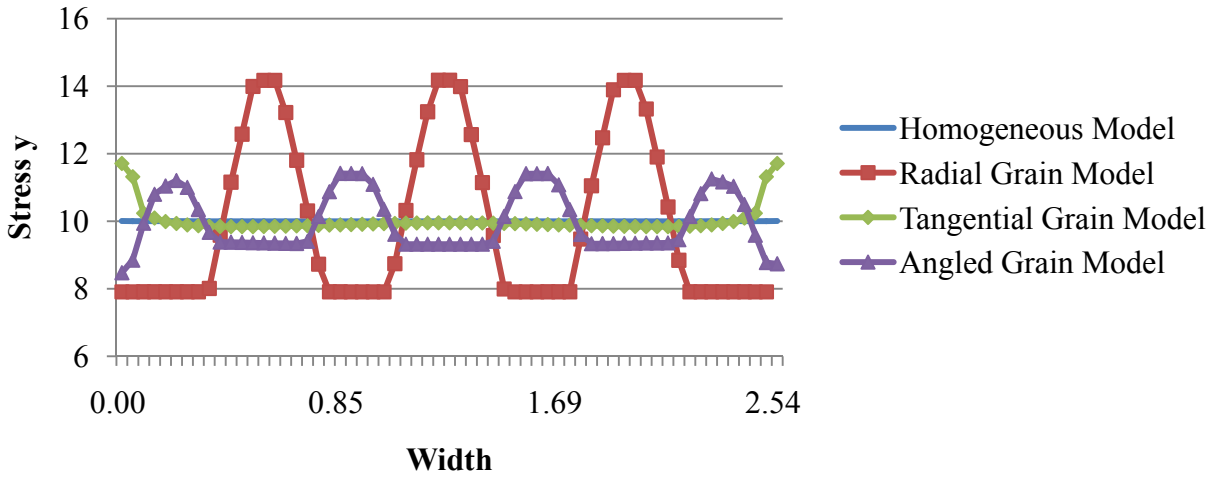

a) Growth ring number 1-10

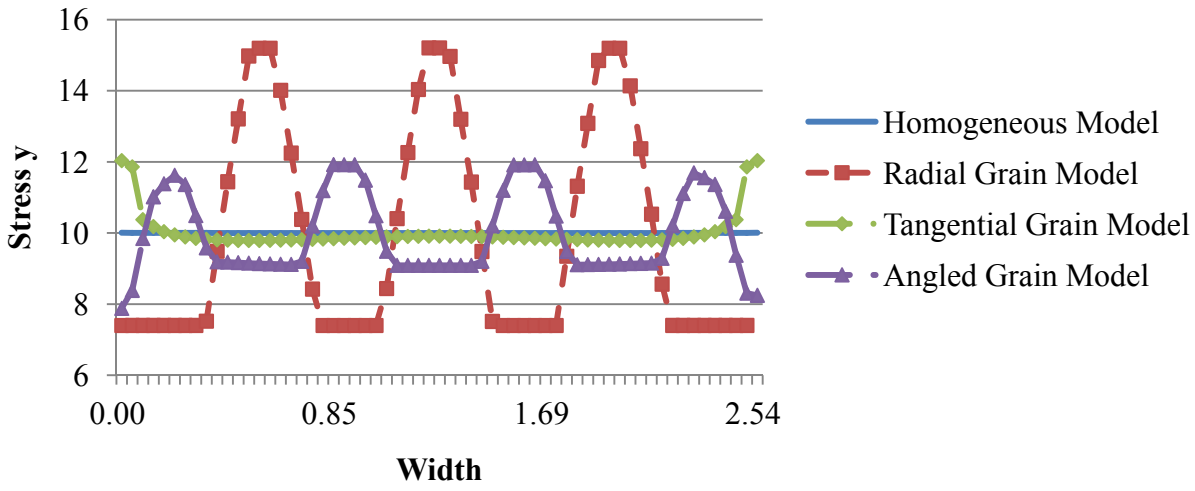

b) Growth ring number 11-20

Figure 7.3 Stress y distribution from simulation models considering grain orientations and growth ring positions. a) Growth ring numbers 1-10, b) Growth ring numbers 11-20

Figure 7.4 shows the transverse stress x distribution from different orientation models for different growth ring positions. Homogeneous models and radial grain orientation models showed relatively uniform stress x distribution and overlapped each other while the tangential and angled grain orientation models showed a distinctive non-uniform stress distribution through the width of model. Strictly speaking, the homogeneous and radial grain orientation strands showed the negative parabolic stress distributions. The magnitude of stress distribution from the homogeneous and radial grain orientation strands was 1×10^{-2} times the stress x distribution from the tangential and angled grain orientation strands. The stress distribution for tangential grain models showed stress x generally increased to the middle width and decreased symmetrically. The stress distribution for angled grain orientation strands showed oscillating stress distribution through the width, with tension stress for latewood layers and compressive stress for earlywood layers. The stress distributions for tangential and angled grain orientation models from growth

ring numbers 11-20 had a greater magnitude than those from growth ring numbers 1-10.

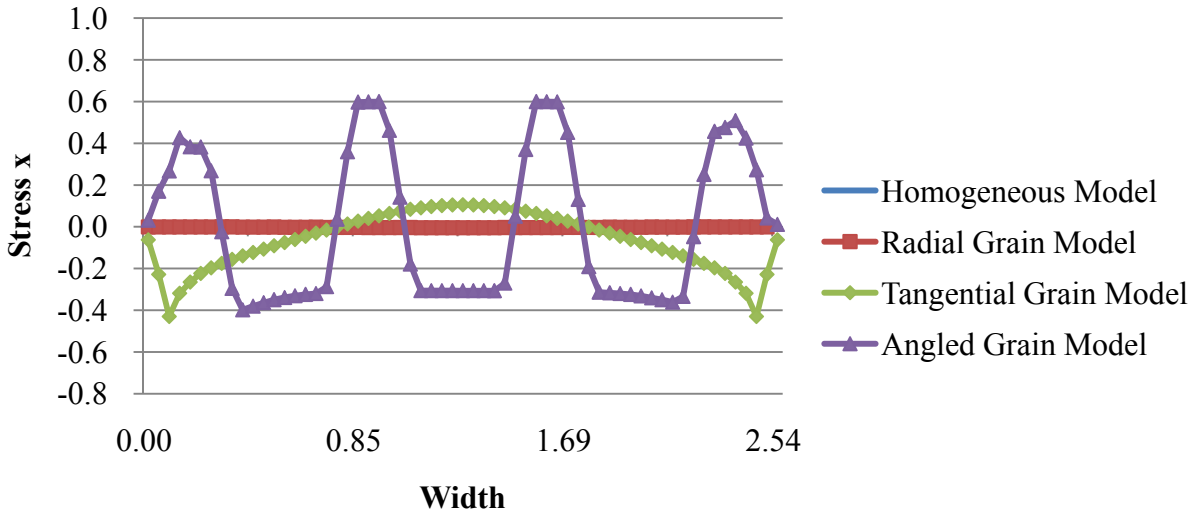

a) Growth ring numbers 1-10

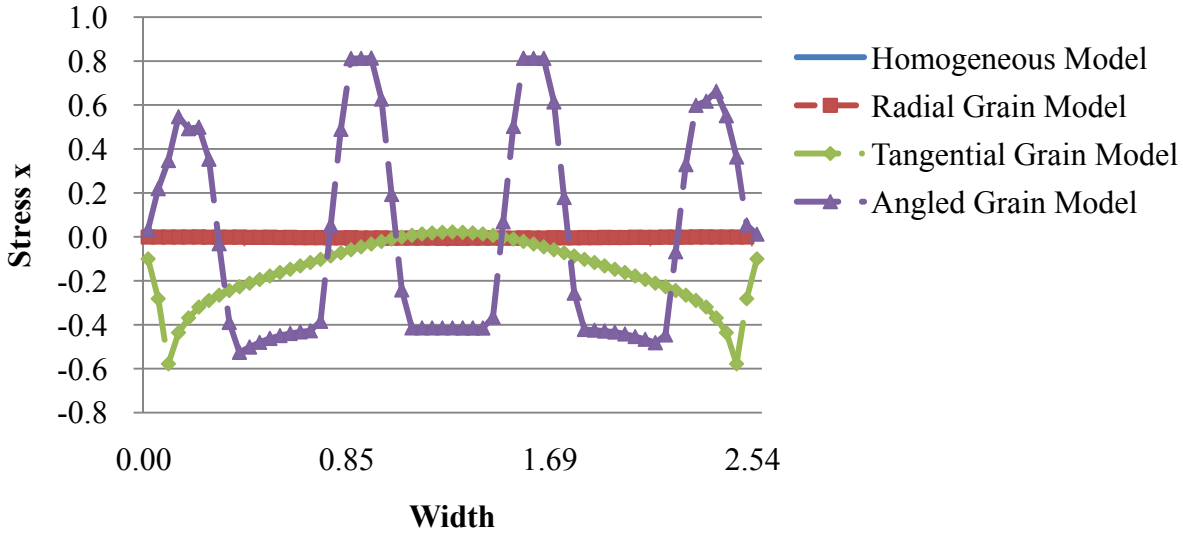

b) Growth ring numbers 11-20

Figure 7.4 Stress x distribution from simulation models considering grain orientations and growth ring positions. a) Growth ring numbers 1-10, b) Growth ring numbers 11-20

Figure 7.5 shows shear stress distribution of different orientation models from different growth ring positions. The homogeneous and radial grain orientation models showed the

relatively uniform shear stress distribution while tangential and angled grain orientation models showed the non-uniform shear stress distribution. The magnitude of shear stress distributions from homogeneous and radial grain orientation strands was 1×10^{-2} times the shear stress from the tangential and angled grain orientation models. The shear stress distributions from homogeneous and radial grain orientation models appeared to be overlapped. The material principal direction of homogeneous and radial grain models was parallel to the loading direction that caused nearly zero shear stress while tangential and angled grain orientation models had different directions between grain orientation and loading direction that caused relative greater shear stress distributions. The tangential grain orientation models had the greatest negative shear stress near the left edge and showed the anti-symmetric distribution through the width of the strand, with zero shear stress at the center and a maximum positive shear stress near the right edge. The greatest shear stress near the right and left edge occurred due to the boundary between earlywood and latewood. The shear stress of the angled grain orientation models showed a distinctive pattern between earlywood and latewood band including the negative shear stress in latewood band and positive shear stress in earlywood band. Greater MOE and shear modulus from latewood induced negative and greater magnitude shear stress while lower MOE and shear modulus from earlywood induced positive and lower magnitude shear stress. The general trend for shear stress distribution from different growth ring positions was similar but greater magnitude shear stress in strands from a higher growth ring positions.

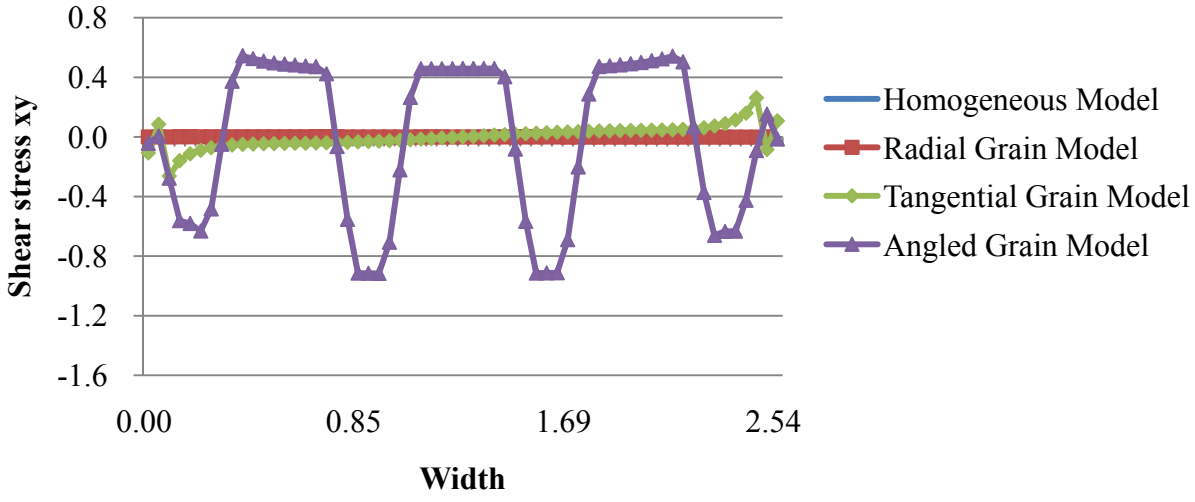

a) Growth ring numbers 1-10

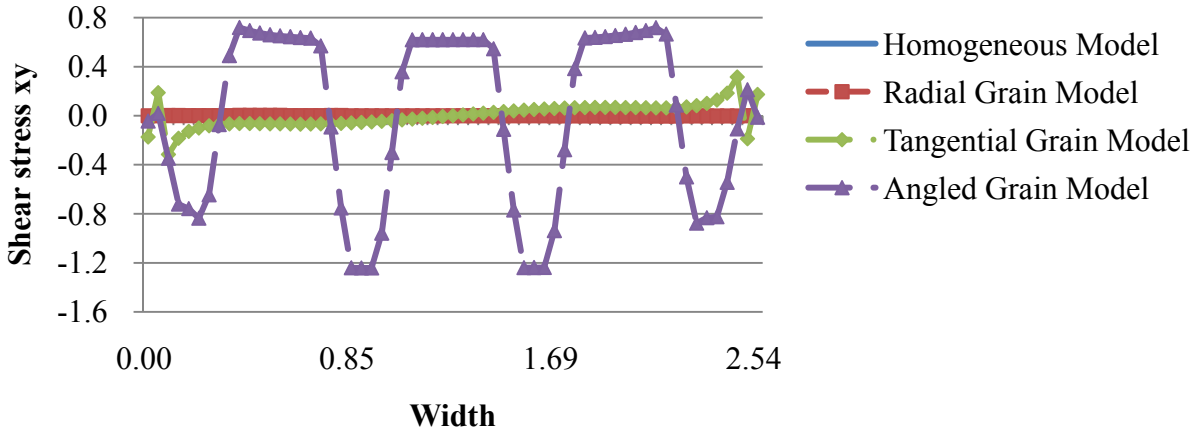

b) Growth ring numbers 11-20

Figure 7.5 Shear stress distribution from simulation models considering grain orientations and growth ring positions. a) Growth ring numbers 1-10, b) Growth ring numbers 11-20

Statistical distribution of the UTS of different orientation of wood strands from different growth ring positions.

Figure 7.6 shows the comparison between cumulative probability of UTS of radial grain orientation models from experimental (Jeong et al. 2008b and Jeong et al. 2008c) and predicted UTS from SFEM. A minimum of thirty test results were fitted for experimental cumulative

probability of UTS while one thousand simulation results were fitted for SFEM cumulative probability of predicted UTS. Kolmogorov-Smimov (K-S) test with 95% confidence interval showed that all comparisons between experimental and SFEM were not significantly different.

The two highest differences of 5.55% and 11.09% were found from the comparison for tangential grain orientation strands from growth ring numbers 1-10 and growth ring numbers 11-20, respectively (Figure 7.6b), which was also shown in Table 7.2. The difference for the rest of models ranged from 0.09% to -1.39%. The two extreme differences were found from the maximum UTS of angled grain orientation strands from growth ring numbers 1-10 and the minimum predicted UTS of angled grain orientation strands from growth ring numbers 11-20 (Figure 7.6c). While experimental results had maximum UTS of 15.2 MPa from the angled grain orientation strands from growth ring numbers 1-10, simulation results had maximum predicted UTS of 21.5 MPa. The minimum UTS of angled grain orientation strands from growth ring numbers 11-20 had 8.2 MPa while the simulation results had minimum predicted UTS of 2.2 MPa. SFEM models showed more conservative predicted UTS values that covered lowest and highest UTS values from experimental tests.

Radial and tangential grain orientation models showed differences between the 1-10 and 11-20 growth ring numbers for the cumulative probability of predicted UTS while the angled grain orientation models showed no significant difference. The differences of UTS from radial grain orientation models between the 1-10 and 11-20 growth ring numbers and tangential grain orientation models between the 1-10 and 11-20 growth ring numbers could be interpreted as the differences of earlywood and latewood properties between the two growth ring numbers mainly affected the cumulative probability of UTS. UTS values from the angled grain orientation model were not much affected by the difference of earlywood and latewood properties between the two

growth ring numbers but grain orientation did affect the cumulative probability of UTS, which explained grain orientation dominantly affecting the UTS of angled grain orientation while the predicted UTS from radial and tangential grain orientation were mainly affected by earlywood and latewood properties

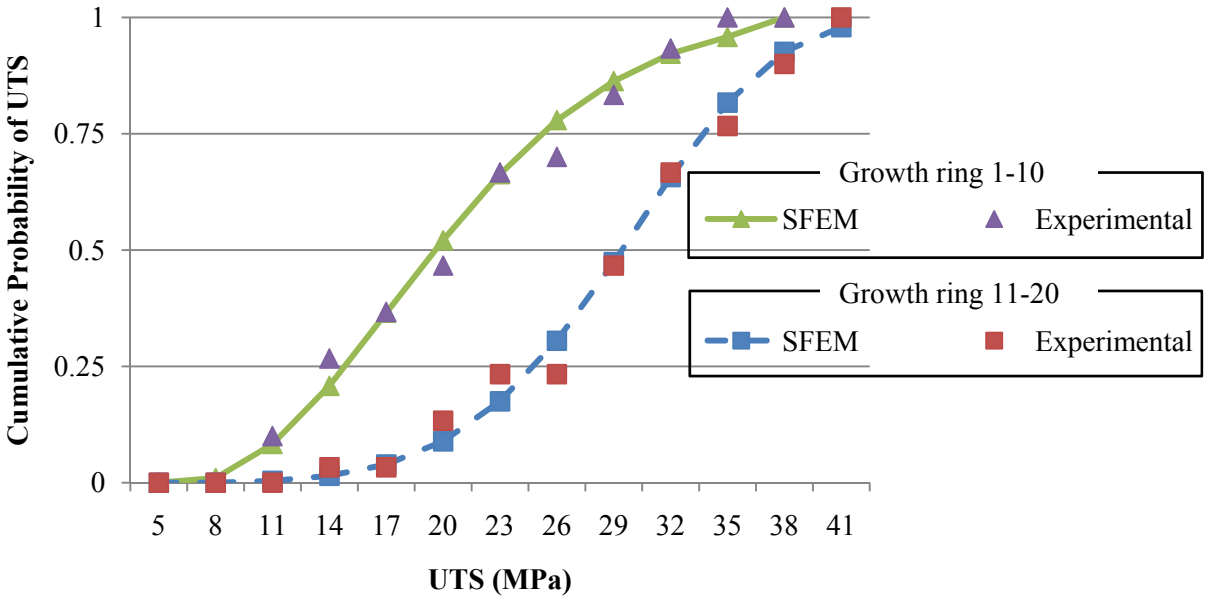

a) Comparison for UTS of radial grain orientation strands from experimental and SFEM

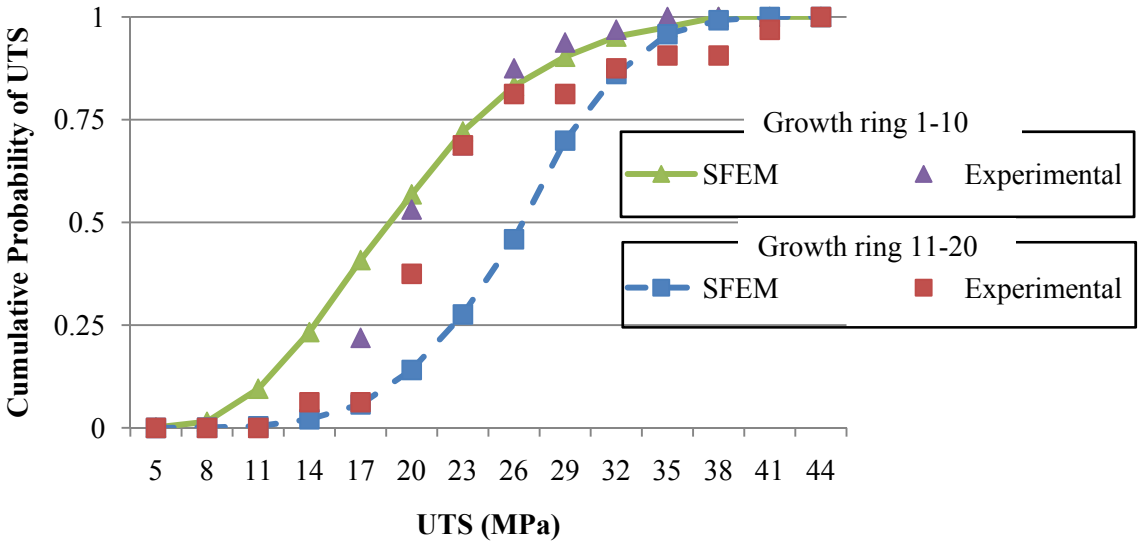

b) Comparison for UTS of tangential grain orientation strands from experimental and SFEM

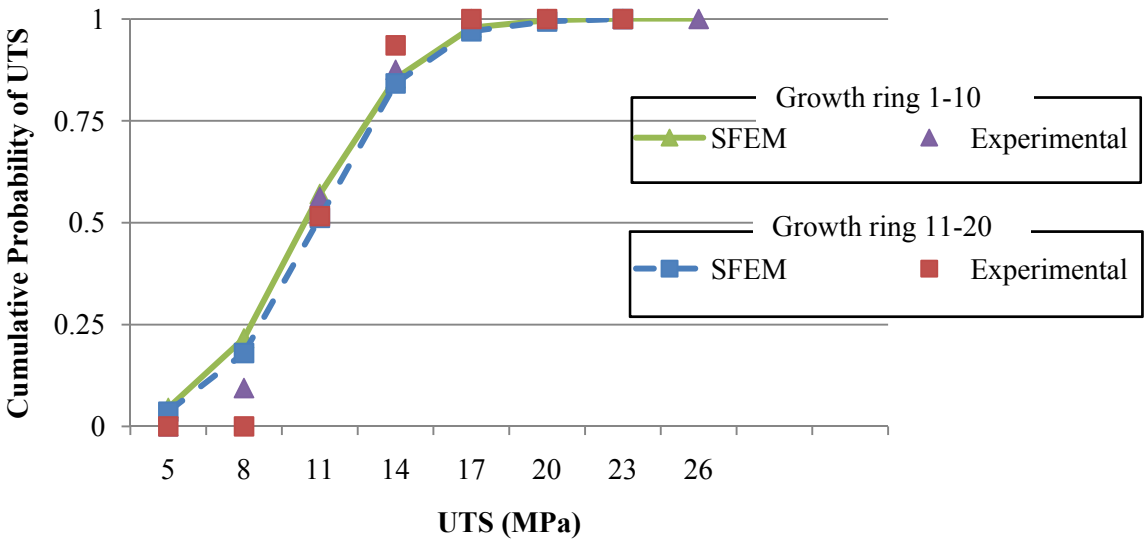

c) Comparison for UTS of angled grain orientation strands from experimental and SFEM

Figure 7.6 Comparison between cumulative probability of UTS from experimental and that from SFEM; a) radial grain orientation strands comparison, b) tangential grain orientation strands comparison, c) angled grain orientation strands comparison

Sensitivity analysis for UTS of different grain orientation strands

Table 7.3 shows Spearman rank correlation coefficient (r) indicating the strength of linear relationship between the random input variables and UTS (Equation 7.4). The shaded cells indicate a correlation above 0.5 between the corresponding input variable and UTS. For growth ring number 1-10, UTS from radial grain strands was highly correlated with the longitudinal tension strength (Y_t). UTS from the tangential grain strands was highly correlated with earlywood MOE, latewood Poisson ratio, σ_y, Y_t. UTS from angled grain strands was highly correlated with transverse tension strength (X_t). For growth ring number 11-20, UTS from radial grain strands was correlated with the latewood MOE, latewood Poisson ratio, σ_x, σ_y, τ_{xy}, and Y_t. UTS from tangential grain strands was correlated with the earlywood MOE, earlywood Poisson ratio, σ_x, σ_y, τ_{xy}, and Y_t. UTS from angled strands was correlated with latewood MOE, latewood

Poisson ratio, σ_x, σ_y, τ_{xy}, and X_t.

The UTS values associated with the different strand orientations and growth ring numbers showed different responses to the input variables. Strands from growth ring number 1-10 had a higher correlation between the strength indexes and UTS values. Strands from growth ring number 11-20 had a higher correlation between the stress components and UTS. Material properties of earlywood and latewood from growth ring number 11-20 had higher values than from growth ring number 1-10, which caused greater stress x and y, and shear stress distributions (Figure 7.3, 7.4, and 7.5). Longitudinal strength index (Y_t) of growth ring number 11-20 was 41% greater than growth ring number 1-10, which was much greater change than the growth ring number 11-20 values of X_t and S, which were 16.2% and 13.9% less, respectively (Table 7.1). This change in the Y_t value caused the increase of sensitivity of stress components by minimizing the solution and predicted UTS from Equation 7.3.

Table 7.3 Sensitivity analysis of input variables on UTS of different orientation strands showing the Spearman rank correlation coefficient (r)

Sample	Earlywood		Latewood		Stress Components			Strength Indexes		
Growth ring number 1-10	E_L	ν_{LR}	E_L	ν_{LR}	σ_x	σ_y	τ_{xy}	X_t	Y_t	S
Radial 1-10	-0.28	-0.24	-0.41	-0.37	-0.45	-0.49	0.43	-0.01	0.84	0.01
Tangential 1-10	-0.48	-0.41	-0.18	-0.18	-0.09	-0.52	0.01	0.11	0.79	-0.02
Angled 1-10	-0.27	-0.26	-0.19	-0.16	-0.09	-0.31	-0.28	0.76	0.41	0.07
Growth ring number 11-20	E_L	ν_{LR}	E_L	ν_{LR}	σ_x	σ_y	τ_{xy}	X_t	Y_t	S
Radial 11-20	-0.27	-0.23	-0.69	-0.63	-0.58	-0.74	0.57	-0.02	0.62	0.03
Tangential 11-20	-0.74	-0.71	-0.24	-0.23	-0.66	-0.79	-0.74	0.19	0.51	0.07
Angled 11-20	-0.28	-0.27	-0.57	-0.64	-0.72	-0.68	-0.55	0.60	0.11	0.06

Latewood MOE and Poisson ratio had higher correlation with UTS of radial and angled orientation strand models from growth ring numbers 11-20. Earlywood MOE and Poisson ratio,

however, had higher correlation with the UTS of tangential orientation strand model. Compared to the other orientation models, the physical geometry of tangential orientation strand models showed that one individual latewood or earlywood band failure was more susceptible in similar stress level to cause strand failure. The smallest longitudinal stress difference between earlywood band and latewood band was shown in the tangential orientation models that evidenced the high sensitivity of earlywood material properties on the UTS (Figure 7.3). Longitudinal strength index (Y_t) had a strong correlation with the UTS of radial and tangential orientation models because the loading direction and fiber orientation were coincident. The transverse strength index (X_t) had a strong correlation with the UTS of angled orientation models because the loading direction and fiber orientation were not coincident.

Conclusions

Ultimate tensile strength (UTS) of different orientation wood strands was predicted from homogeneous model, deterministic layer FEM models, and probabilistic SFEM models. Comparison of average UTS from experimental and models indicated that homogeneous models were not as accurate as layered FEM and SFEM models. Stress distributions associated with the homogenous models were not representative for physical wood structures that composed of earlywood and latewood bands. Tangential and angled grain orientation models showed greater stress x distributions in earlywood bands and lower transverse stress distributions in latewood bands. Radial, tangential, and angled grain orientation models showed lower longitudinal stress distributions in earlywood bands and greater longitudinal stress distributions in latewood bands, except for homogeneous models. The magnitude of shear stress from homogeneous and radial grain orientation models showed 100 times lower than the shear stress from the tangential and

angled grain orientation models while tangential and angled grain orientation models showed lower shear stress distributions in earlywood bands and greater stress distributions in latewood bands. Comparison between cumulative probability of UTS from experimental test and that of predicted UTS from SFEM found no significant difference. UTS of radial, tangential, and angled orientation strands from the two different growth ring numbers showed a quite different sensitivity on input variables showing that UTS from strands from growth ring number 1-10 had a high sensitivity on strength indexes while UTS from strands from growth ring number 11-20 had a high sensitivity on stress components and strength indexes. Different grain orientation also affected the sensitivity of UTS of different orientation strands. Longitudinal strength index (Y_t) had a strong correlation with UTS of radial and tangential orientation strands while transverse strength index (X_t) had a strong correlation with UTS of angled orientation strand.

References

Bendtsen, B.A. 1978. Properties of wood from improved and intensively managed stands. Forest Prod. J. 28(10):61-72.

Cave, I.D., J.C.F. Walker, 1994. Stiffness of wood in fast grownplantation softwoods: the influence of microfibril angle. Forest Prod. J. 44 (5): 43–48.

Chakraborty S. and S. S. Dey 2000. Stochastic finite element simulation of uncertain structures subjected to earthquake. Shock and Vibration. 7(5):309 -320

Chung D. B., M. A. Gutiérrez and R. D. Borst. 2005. Object-oriented stochastic finite element analysis of fibre metal laminates. Computer Methods in Applied Mechanics and Engineering 194(12-16):1427-1446

Clouston, P. and F. Lam, 2002. A stochastic plasticity approach to strength modeling of strand-based wood composites. Composites Science and Technology, 62:1381-1395.

Clouston P. 2007. Characterization and strength modeling of parallel-strand lumber. Holzforschung, 61:394-399.

Eiermann M., O. G. Ernst and E. Ullmann. 2005. Computational aspects of the stochastic finite

element method. Proceeding of algoritmy. pp. 1-10.

Ghanem R. G., P. D. Spanos. 1991. Stochastic Finite Elements: A Spectral Approach, Springer-Verlag.

Ghanem R. G. 1999. Higher order sensitivity of heat conduction problems to random data using the spectral stochastic finite element method, ASME Journal of Heat Transfer, 121:290–299.

Jeong G. Y., D. P. Hindman, and A. Zink-Sharp. 2008a. Tensile properties of earlywood and latewood from loblolly pine (*Pinus taeda*) using digital image correlation.

Jeong G. Y., A. Zink-Sharp, and D. P. Hindman. 2008b. Comparison of longitudinal tensile properties of different grain orientation strands from loblolly pine (*Pinus taeda*).

Jeong G. Y., D. P. Hindman, and A. Zink-Sharp. 2008c. Shear and transverse properties of loblolly pine (*Pinus taeda*) strands using tension test incorporated with digital image correlation (DIC).

Jeong G. Y., D. P. Hindman. 2008d.Evaluation of effective elastic modulus of different orientation wood strands using stochastic finite element method.

Jones R. M. 1975. Mechanics of composite materials. McGraw-Hill, New York

Kasal B. and R. J. Leichti. 2005. State of the art in multiaxial phenomenological failure criteria for wood members. Progress in Structural Engineering and Materials 7(1):3-13

Kaminski M. 2002. Stochastic problem of fiber-reinforced composite with interface defects. Engineering computations. 19 (7) :854-868

Kleiber M., T. Hien, 1992. The Stochastic Finite Element Method. Basic Perturbation Technique and Computer Implementation. John Willey & Sons.

Larson, P. R., D. E. Kretschmann, A. Clark III, and J. G. Isebrands. 2001. Juvenile wood formation and properties in southern pine. Gen Tech Rep FPL-GTR-129.: USDA Forest Prod Lab, Madison, WI

Panshin, A. J., and C. D. Zeeuw. 1980. Textbook of wood technology. McGraw Hill Book Co., New York, NY.

Smith, R. W., and D. G. Briggs. 1986. Juvenile wood:Has it come of age? Pages 1-11 in proc., Juvenile wood: What does it mean to forest management and forest products? Forest Products Research Society, Madison, WI.

Wang, Y. T. and F. Lam. 1998. Computational modeling of material failure for parallel-aligned strand-based wood composites. J. Computational Material Science 11:157-165.

Chapter 8. Summary and Conclusion

The results from this study demonstrated the effect of intra-ring properties on the mechanical behavior of wood strands incorporating strand cutting orientations and growth ring positions. Each Chapter has a specific contribution to this dissertation. Chapter 1 shows the background and goal of this project. A comprehensive literature from Chapter 2 serves as the basis of the literature reviews in Chapters 3 through 7. Loblolly pine earlywood and latewood properties from growth ring numbers 1-10 and growth ring numbers 11-20 were measured in Chapter 3. Mechanical properties of radial, tangential, angled, and cross grain orientation strands from the two growth ring numbers were measured in Chapter 4 and 5. The results from Chapter 3 are used as input variables for development of stochastic finite element method (SFEM) models for different orientation strands (radial, tangential, and angled grain orientation) in Chapter 6 and 7. The results from Chapter 4 and 5 are used as validation of predictions from Chapter 6 and 7. Effective elastic modulus of the different orientation strands and sensitivity of the input variables are evaluated in Chapter 6. Ultimate tensile strength of the different orientation strands and sensitivity of the input variables are evaluated in Chapter 7. The following conclusions have been made based on the results from Chapter 3 to Chapter 7.

Tensile Properties of Earlywood and Latewood Using DIC (Chapter 3)

The physical and mechanical properties of earlywood and latewood from the two different growth ring positions were measured using DIC.

- In general, specific gravity, MOE, UTS, and Poisson ratio generally increased with the increment of the growth ring positions except for specific gravity and UTS from

latewood.

- While the MOE for earlywood and latewood was not dependent on specific gravity, UTS for earlywood and latewood was highly dependent on specific gravity.
- Combining current results and Kretschmann et al. (2006), MOE from earlywood and latewood showed a positive relationship with the height of material in the tree.
- Statistical comparisons showed that the MOE and UTS had a significant difference from the factor of growth ring number and intra-ring position.
- Distribution fitting of MOE for Earlywood 1-10, Latewood 1-10, Earlywood 11-20, and Latewood 11-20 was best fitted by the Weibull distribution. Poisson ratios were best fitted by Weibull distribution for Earlywood 1-10 and Latewood 11-20 groups and Gamma distribution for Earlywood 11-20 and Latewood 1-10 groups.
- Strain distribution showed non-uniform distributions for the four groups. Compared to Earlywood 1-10 and Latewood 1-10, Earlywood 11-20 and Latewood 11-20 showed more resistance to the load indicating more oriented structure and reinforcement to the longitudinal direction.

Longitudinal Elastic Properties of Different Orientation Loblolly Pine Strands (Chapter 4)

Tensile properties of radial and tangential grain orientations of wood strands from growth ring numbers 1-10 and growth ring numbers 11-20 were measured using DIC.

- As growth ring number increased, MOE and UTS from radial and tangential grain orientation strands increased.
- Radial 1-10 strands had a lower MOE and UTS than Tangential 1-10 strands. Radial 11-20 strands had a higher MOE and UTS than Tangential 11-20 strands.

- Tangential grain orientation strands had higher Poisson ratios than radial grain orientation strands.
- Although Radial 1-10, Radial 11-20, Tangential 1-10, and Tangential 11-20 strands had a different percentage of three particular failure behaviors, more mature wood had a more organized structure to show more consistent failure behavior.
- Statistical comparisons of MOE and UTS from radial grain orientation strands were significantly different between growth ring numbers, while MOE and UTS from tangential grain orientation strands were not significantly different between growth ring numbers.
- Statistical comparisons also showed that there was no significant difference of MOE between the radial and tangential orientation strands. For UTS, the comparisons between Radial 1-10 and Radial 11-20 strands and the comparison between Radial 11-20 and Tangential 11-20 strands were significantly different.
- For distribution fitting from MOE, Radial 1-10, Radial 11-20, and Tangential 11-20 strands were best fitted with Weibull distribution except for Tangential 1-10 fitted with Lognormal distribution. For UTS, while Radial 1-10 and Radial 11-20 group followed Weibull distribution, Gamma distribution for Tangential 1-10 and Lognormal distribution for Tangential 11-20 were best fitted curve. For Poisson ratio, Radial 11-20 strands did not match with any distribution curve. Radial 1-10, Tangential 1-10, and Tangential 11-20 strands followed Lognormal, Gamma, and Weibull distribution, respectively.
- Comparing current test results to Cai et al. (2007) and Hindman and Lee (2007), MOE and UTS of wood strands had higher correlations with thickness than specific gravity.

Transverse and Shear Properties of Loblolly Pine Strands (Chapter 5)

Transverse elastic properties, shear properties, and UTS of loblolly pine strands from growth ring numbers 1-10 and growth ring numbers 11-20 were measured using tension test incorporating DIC.

- MOE of angled grain strands increased as the growth ring number increased while MOE of cross-grain strands decreased 1% as the growth ring number increased. MOE of cross grain strands was more sensitive to the orientation of strands than specific gravity.
- UTS of angled grain strands increased as the growth ring number increased, while UTS of cross-grain strands decreased as the growth ring number increased. The UTS was dependent upon grain orientations of strands rather than specific gravity.
- Shear modulus increased as the growth ring number increased, but shear strength decreased as the growth ring number increased. Lower shear strength values can be speculated as a higher elastic constant ratio of strands from growth ring numbers 11-20.
- Poisson ratio from angled grain strands decreased with increasing growth ring numbers. However, Poisson ratio from cross-grain strands slightly increased with the increment of growth ring numbers.
- COV values from MOE, UTS, Poisson ratio, and shear strength decreased as growth ring number increased. Based on the lower variation of mechanical properties, more uniform structure of strands from growth ring numbers 11-20 can be speculated.
- Statistical distribution fitting showed that shear strength values were best fitted with Gamma distribution. MOE values from Angled 1-10, Angled 11-20, and Cross 11-20 followed Lognormal distributions, while MOE values from Cross 1-10 followed a Weibull distribution. UTS values from four groups did not follow any specific

distribution. Poisson ratio values from Angled 1-10, Cross 1-10, and Cross 11-20 followed Normal distribution, while Angled 11-20 followed Lognormal distribution.

- Although four groups of strands showed mixed failure modes, strands from growth ring numbers 11-20 showed a more consistent failure mode. The consistency in failure mode indicated that strands from growth ring numbers 11-20 showed less variations in structures compared to the strands from growth ring numbers 1-10.
- Comparing the MOE, UTS, and shear strength from both experimental and orthotropic transformation, conservative predicted values from the orthotropic transformation were obtained.

Effective Elastic Modulus of Different Orientation Strands Using SFEM (Chapter 6)

Tensile properties of different orientation wood strands were evaluated using deterministic FEM and SFEM models. While the deterministic models used average material properties of earlywood and latewood, SFEM models used the distribution of material properties of earlywood and latewood from growth ring numbers 1-10 and growth ring numbers 11-20.

- While the homogeneous model predicted the average MOE well for radial and tangential grain orientation strand from growth ring numbers 1-10, the physical strain distribution showed an unrealistic behavior.
- In general, the predicted average MOE of strands from the deterministic layer FEM and SFEM was better than the homogeneous models.
- From strain distribution analysis, different strain distribution for earlywood and latewood layers occurred by different grain orientations. Homogeneous and radial orientation models, however, showed iso-strain distribution in y direction, which resulted in the

same MOE values.

- Comparison of cumulative probability curves from experimental test and SFEM agreed well. The difference of variation of MOE from different grain strands between experimental results (Chapter 4 and Chapter 5) and SFEM results ranged from 0.96% to 22.31%.
- From sensitivity analysis, earlywood and latewood participated differently to MOE of different grain orientation strand models, which is highly associated with the strain distribution caused by different orientation strands and interaction of input parameters.
- In general, earlywood MOE had a greater effect on MOE of wood strands than other input parameters.

Ultimate Tensile Strength (UTS) of Different Orientation Strands Using SFEM (Chapter 7)

Ultimate tensile strength (UTS) of different orientation wood strands was predicted from homogeneous model, deterministic layer FEM models, and probabilistic SFEM models.

- Comparison of average UTS from experimental and models indicated that homogeneous models were not as accurate as layered FEM and SFEM models.
- Stress distributions associated with the homogenous models were not representative for physical wood structures that composed of earlywood and latewood bands.
- Comparison between experimental and SFEM agreed well with the UTS from different orientation strands ranging from 0.09% and 11.09%.
- UTS of different orientation strands from the two different growth ring numbers showed a quite different sensitivity on input variables showing that UTS from strands from growth ring number 1-10 had a high sensitivity on strength indexes while UTS from

strands from growth ring number 11-20 had a high sensitivity on stress components and strength indexes.

- Different grain orientation also affected the sensitivity of UTS of different orientation strands. Longitudinal strength index (Y_t) had a strong correlation with UTS of radial and tangential orientation strands while transverse strength index (X_t) had a strong correlation with UTS of angled orientation strand.

Overall Conclusions of Research

Different elastic properties of earlywood and latewood from the two different growth ring positions affected the mechanical properties of strands. Mechanical properties of strands were influenced by different orientation wood strands and growth ring numbers. With the difference of earlywood and latewood and the different orientation, stress and strain distributions of strands showed a distinctive pattern. Homogeneous models could not represent the physical stress and strain distributions while SFEM for different orientation strand models incorporating the variation of the mechanical properties of earlywood and latewood could represent the physical stress and strain behavior of wood strands. With the different stress and strain distribution sensitivity of mechanical properties of wood strands was changed. Earlywood MOE was the most important parameter to maximize the effective MOE of strands. Longitudinal strength index (Y_t) had a strong correlation with UTS of radial and tangential orientation strands while transverse strength index (X_t) had a strong correlation with UTS of angled orientation strand. This hierarchical approach showed if material properties of earlywood and latewood, and orientation of wood strands can be manipulated, the final MOE and UTS of wood strands can be controlled.

Limitations

The following limitations were found from the scope of this study.

- DIC measured only longitudinal elastic properties and one major Poisson ratio from earlywood and latewood while microfibril angle (MFA) and other physical structure of earlywood and latewood were cited from previous studies.
- Six elastic properties (E_L, E_R, G_{LR}, υ_{LR}, υ_{LT}, and υ_{RT}) and three strengthes (σ_L, σ_R, and τ_{LR}) were measured and three elastic properties (E_T, G_{LT} and G_{RT}) and three strengthes (σ_T, τ_{LT}, and τ_{RT}) were missed.
- SFEM used analytical distributions from the experimental results rather the exact distribution from the experimental tests.
- SFEM used a plane stress assumption, which could be expanded to a three dimensional orthotropic problem with measured material properties.
- SFEM model used an average volume fraction and assumed no slippage between the earlywood and latewood bands.
- SFEM model for prediction of UTS assumed that the strength indexes were independent each other, which could have some correlation between strength indexes.

Recommendations for Future Research

This study was originally initiated to establish the link between mechanical behavior of loblolly pine strands and the mechanical properties of earlywood and latewood by developing different orientation strand models and measuring earlywood and latewood properties. With the developed models and newly designed testing methods, this research could be directly expanded to evaluate the mechanical properties of other wood species and natural fiber sources. A novel

DIC testing set up could be expanded to examine a similar micro-scale analysis such as the mechanical behavior of glue lines, micromechanical fracture testing, micromechanical shear testing, and other micromechanical testings. Also this testing set-up has the capability of adding other devices such as the Raman microscope which could examine the relationship between major chemical components of wood (cellulose, hemicelluloses, and lignin) with mechanical properties of wood. The developed DIC testing set-up for strands could measure nine elastic properties including elastic modulus (E_L, E_R, and E_T), Poisson ratio (ν_{LR} ν_{RL} and ν_{RT}), and shear modulus (G_{LR}, G_{LT}, and G_{RT}) of different wood species. The DIC testing set-up could expand for fracture testing, connection testing, and other macro size testings. Although this research has connected one length scale to other length scale, there are still many missing links between different length scales. This research could be expanded to examine how properties of earlywood and latewood affect the mechanical properties of strand based composites. This research could also be expanded to understand how silvicultural activities affect earlywood and latewood, wood strands, and strand based composite properties.

Appendix 1.

Comparison of Elastic Constants Generated from Plate Tests to Bending Tests

Gi Young Jeong
Graduate Research Assistant
Department of Wood Science and Forest Products
Virginia Polytechnic Institute and State University
Brooks Forest Products Center
1650 Ramble Road
Blacksburg, VA 24061-0503

Daniel P. Hindman
Assistant Professor
Department of Wood Science and Forest Products
Virginia Polytechnic Institute and State University
Brooks Forest Products Center
1650 Ramble Road
Blacksburg, VA 24061-0503

Notice - Appendix 1 appears in the Forest Product Journal, 58(9):53-58.

Abstract

Many different test methods have been used to evaluate the elastic constants and elastic constant ratios of solid sawn lumber and structural composite lumber (SCL). Previous work has noted that the elastic constant ratios of solid sawn lumber and SCL are different. However, no direct comparison of current bending test methods and previously used plate bending and twisting methods has been performed. This study conducted plate bending and twisting tests to determine the longitudinal modulus of elasticity and in-plane shear modulus of MSR and PSL materials. Samples were taken from the same material previously tested by Hindman *et al*. (2006) The E:G ratios from MSR plate testing were 40% less than values from ASTM D 198 Bending and the five point bending test (FPBT), while the E:G ratios from PSL plate testing showed no consistent trend. Statistical comparisons of the E and G values found that the MSR E values for all three tests and the PSL G values from plate testing and ASTM D 198 Bending were not significantly different. The differences in elastic constant ratios and comparison of the elastic constants indicate that the elastic behavior of MSR and PSL is different. Therefore, elastic constant ratios derived from plate testing methods for MSR and PSL are not directly comparable to elastic constant ratios derived from structural sized bending tests.

Previous researchers have found differences in the elastic constants and elastic constant ratios of structural size solid-sawn lumber and SCL materials using a variety of bending and torsion test methods. These test methods have been compared to elastic constant ratio of 16:1 found in the Wood Handbook (USDA 1999) and Bodig and Jayne (1982). This value is an average of many different wood species tested using plate bending and twisting tests (Bodig and Goodman 1973). Plate bending and twisting tests were performed on clear sections of wood laminated together to achieve different directional orientations (Bodig and Goodman 1973). Recent studies to evaluate the shear modulus of solid-sawn lumber and SCL materials have focused on structural sized lumber only. The discrepancy between small sized samples from plate bending and twisting compared to structural sized samples in bending has not been previously explored.

Currently, there is no specific guideline to determine the material properties of SCL products. ASTM D 5456 (ASTM 2005a) is the standard governing SCL products and gives no guidance on the test methods to use for shear modulus evaluation. The only mention of test methods is a reference to ASTM D 198 (ASTM 2005b), which is the test standard for structural sized lumber. Previous findings (Janowiak et al. 2001, Hindman et al. 2006, Harrison and Hindman 2007) have recommended that the shear modulus test method be similar to the intended loading of the member. While these previous studies compared the shear modulus and elastic constant ratios developed to solid wood results from Bodig and Goodman (1973), no testing of equivalent materials using the plate bending and plate twisting test methods was performed.

Table 1 shows the modulus of elasticity and shear modulus values determined from different studies for solid wood, solid-sawn lumber and parallel strand lumber (PSL). Bodig and Goodman (1973) performed plate bending and plate twisting tests on an extensive number of

softwood and hardwood specimens. These test results are summarized by Bodig and Jayne (1982) and in the Wood Handbook (USDA 1999).

Table 1. MSR and PSL Elastic and Shear Modulus Values from Previous Studies

Researcher	Material	Test Method	Average E, GPa (10^6 psi)	Average G, GPa (10^6 psi)
Bodig and Goodman 1972	Loblolly pine (*P. taeda*)	Plate bending/twisting	11.1 (1.61)	0.903 (0.131)
Bodig and Goodman 1973	Longleaf pine (*P. palustris*)	Plate bending/twisting	14.6 (2.12)	1.04 (0.151)
Bodig and Goodman 1973	Slash pine (*P. elliottii*)	Plate bending/twisting	16.0 (2.317)	0.883 (0.128)
Hindman 2006	MSR lumber (*Pinus spp.*)	FPBT	16.1 (2.35)	0.748 (0.109)
Hindman 2006	MSR lumber (*Pinus spp.*)	ASTM D 198 Bending	17.2 (2.51)	0.800 (0.16)
Harrison and Hindman 2007	MSR lumber (*Pinus spp.*)	ASTM D 198 Bending	17.4 (2.53)	0.903 (0.131)
Harrison and Hindman 2007	MSR lumber (*Pinus spp.*)	ASTM D 198 Torsion	N/A	1.16 (0.168)
Harrison and Hindman 2007	MSR lumber (*Pinus spp.*)	FPBT	17.5 (2.54)	0.789 (0.114)
Hindman et al. 2006	PSL (*Pinus spp.*)	FPBT	13.4 (1.96)	0.727 (0.106)
Hindman et al. 2006	PSL (*Pinus spp.*)	ASTM D 198 Bending	12.4 (1.81)	1.03 (0.149)

Recent research comparing the elastic modulus, shear modulus and elastic constant ratios from different test methods has been performed by Hindman et al. (2006) and Harrison and Hindman (2007). Hindman et al. (2006) compared results from ASTM D 198 Bending and five point bending test (FPBT) to determine the elastic constants of SCLs and to compare the test methods. The ASTM D 198 (2005b) bending test consists of testing three-point bending specimens at different length to height aspect ratios to determine the elastic and shear modulus simultaneously. The FPBT is a novel test method proposed by Bradtmueller et al. (1994) as an

alternative method for shear modulus measurement. Harrison and Hindman (2007) compared the ASTM D 198 Bending, ASTM D 198 Torsion and the FPBT for MSR lumber and LVL. ASTM D 198 Torsion is another ASTM D 198 (2005b) method to measure shear modulus that uses a torsion loading and angle measurement. Trends from both of these papers demonstrated that there is no consistent pattern of equivalency between the elastic constants and elastic constant ratios measured using different test methods.

The results in Table 1 demonstrate some of the trends previously observed in the study of solid wood, solid-sawn lumber and parallel strand lumber (PSL). While it is difficult to make a direct comparison between the results of Bodig and Goodman (1973) and current species group assignments used for solid-sawn lumber, three of the four species currently included in the southern pine species group are given. From Bodig and Goodman (1973), the modulus of elasticity values ranged from 11.1 GPa to 16.0 GPa (1.61×10^6 psi to 2.32×10^6 psi) and the shear modulus values ranged from 903 MPa to 1.04 GPa (1.28×10^5 psi to 1.51×10^5 psi). Comparing the range of Bodig and Goodman (1973) values to the ASTM D 198 Bending, the modulus of elasticity values were greater than the range, while the shear modulus values were within the range or slightly below it. Comparing the range of Bodig and Goodman (1973) values to the FPBT results, the modulus of elasticity was within or greater than the range of values, while the shear modulus was less than the range. The ASTM D 198 Torsion value was much higher than the range of values from Bodig and Goodman (1973). Due to the differences in the loading conditions, the different test methods may not produce the same results. This study measured the elastic and shear modulus of MSR lumber and PSL materials using plate bending and ASTM D 3044 plate twisting test for comparison to previous testing results of ASTM D 198 Bending and FPBT from Hindman et al. (2006).

Materials and Methods

MSR and PSL materials used for this testing were taken from an untested subset of the material used by Hindman et al. (2006). MSR lumber was southern pine (*Pinus spp.*) 2250f-1.9E with a modulus of elasticity of 13.1 GPa (1.90 x 10^6 psi). PSL was 2.0E rated southern pine (*Pinus spp.*) with a modulus of elasticity of 13.8 GPa (2.0 x 10^6 psi). Specimens were cut to 40.6 cm long by 20.3 cm wide by 8.89 mm high (16.0 in by 8.0 in by 0.35 in) for the plate bending test. Ten specimens from each material were tested. After the plate bending test was complete, the specimens were cut in half to a size of 20.3 cm long by 20.3 cm wide by 8.89 mm high (8.0 in x 8.0 in x 0.35 in) for ASTM D 3044 plate twisting test (ASTM 2005c). All specimens were labeled and stored in an environmental chamber at 20 degrees C and 65% relative humidity. After plate twisting testing was completed, moisture content and specific gravity samples were measured according to ASTM D 2395 (ASTM 2005d) and ASTM D 4442 (ASTM 2005e). Table 2 summarizes the rated modulus of elasticity as well as the resultant moisture content and specific gravity. Materials tested by Hindman et al. (2006) have a specific gravity of 0.56 for MSR and 0.66 for PSL, demonstrating that these materials are similar to those previously tested.

Table 2. Summary of test materials

Test material	Rated E, GPa (psi)	Moisture content (%), (COV)	Specific gravity, (COV)
2250f-1.9E Southern Pine MSR	13.1 (1.9 x 10^6)	11.6 (3.10%)	0.62 (8.15 %)
2.0E Southern Pine PSL	13.8 (2.0 x 10^6)	11.0 (3.05 %)	0.71 (5.12 %)

Plate Bending Test

The determination of orthotropic elastic constants using plate bending and plate twisting methods was originally developed by Witt et al. (1953). The plate bending test uses a three point loading on the top of the plate and a three point support on the bottom of the plate placed in an anti - symmetric pattern. Figure 1 shows a schematic drawing of the plate bending samples indicating the position of the loading, support and deflection measurement points. This configuration allows the plate to have a constant bending moment in the center and no bending moment at the three supports. Due to the large difference in stiffness between the parallel to grain direction and perpendicular to grain direction, a correction factor must be applied using an alternative beam theory (Gunnerson et al. 1972).

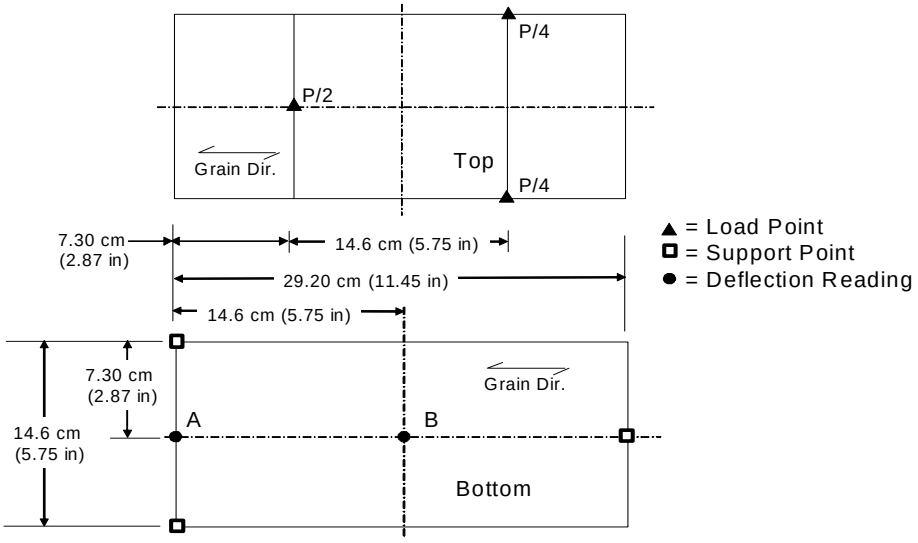

Figure 1. Schematic Drawing of Plate Bending Sample

Figure 2 shows a plate bending specimen being tested. The loading speed was set to 0.0762 cm/min (0.03 in/min). Two Trans-Tek 351-0000 linear variable differential transformers

(LVDT) (range of 5.08 mm (0.20 in.) and sensitivity of 0.0091 mm (0.0025 in.)) were used to measure the displacement at the point A and B under elastic range for the calculation of elastic modulus of plate.

Equation 1 shows the calculation of the modulus of elasticity. The load P is the total load applied to the plate. The deflection Δ is equal to the deflection at B minus one half of deflection at A. This is the correction factor discussed by Gunnerson et al. (1972). The length L is the span of the plate, or 29.20 cm (11.45 in.).

$$E = \left(\frac{P}{\Delta}\right)\left(\frac{11L^3}{768I}\right) \tag{1}$$

where

P/Δ= load-deflection curve

L = span length of plate

I = moment of inertia = width * height$^{3}/12$

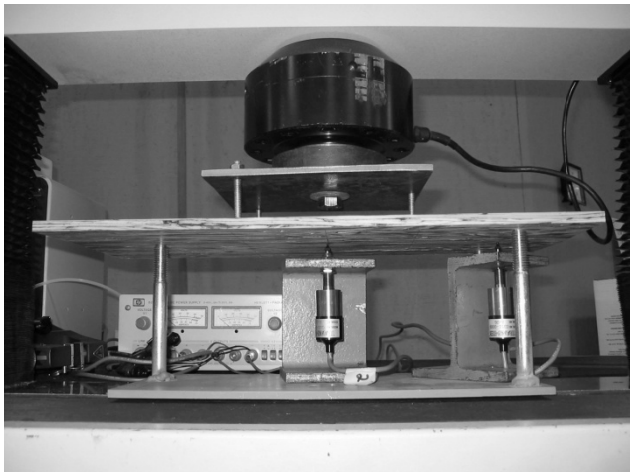

Figure 2. Plate Bending Sample During Testing

ASTM D 3044 Plate twisting

Plate twisting test procedures are detailed in ASTM D 3044 (ASTM 2005c). Figure 3 shows the anticlastic plate twisting, where two diagonal corners of a square plate are supported and the other two diagonal corners are loaded. To avoid edge damage from the concentrated loads at each corner, small metal plates were clamped to the top and bottom of each corner. An MTS test machine applied a displacement rate of 0.0762 cm/min (0.03 in/min) to the specimen. Deflection was taken as the difference of the movement between the two diagonals as described in ASTM D 3044 (ASTM 2005c). Deflection was measured using an LVDT (range of 5.08 mm (0.20 in.) and sensitivity of 0.0091 mm (0.0025 in.)) attached to a metal jig to measure the difference between the diagonal deflections. Equation 2 shows the calculation of the shear modulus.

$$G = \left(\frac{P}{\Delta}\right)\left(\frac{1.5u^2}{h^3}\right) \tag{2}$$

where

P/Δ = load-deflection curve

u = distance from the center of plate to the point where the deflection was measured.

h= thickness of plate

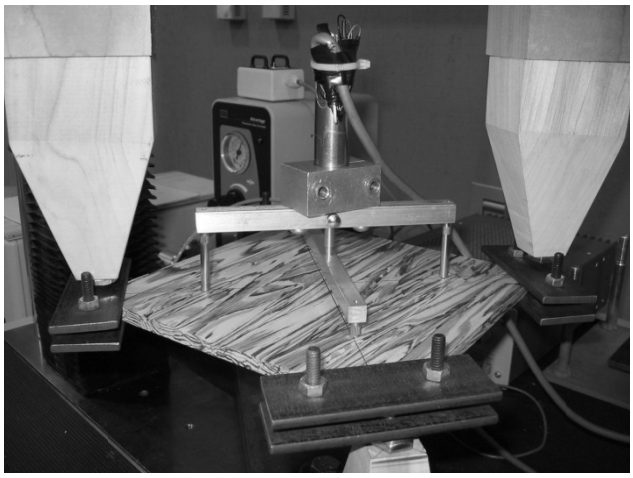

Figure 3. ASTM D 3044 Plate Twisting Specimen Under Load

Load and deflection information were collected using the TEST WORK 3.09 software for both plate bending and plate twisting test methods. All test data were exported to Microsoft Excel to plot the load-deflection (P/Δ) curve. Three loading repetitions were applied to each specimen and the load-deflection curves were averaged. To ensure all loads were within the elastic range of the specimens, several plywood specimens of similar stiffness were tested to define the maximum loading. For the plate bending test, the maximum load and deflection of crosshead were limited to 444.8N (100 lb) and 0.254cm (0.1 in), respectively. For the plate twisting test, the maximum load and deflection of crosshead were limited to 44.4N (10 lb) and 0.254cm (0.1 in), respectively.

Results and Discussion

Plate bending and ASTM D 3044 plate twisting results

Table 3 summarizes the modulus of elasticity and shear modulus values including coefficient of variation from the plate bending and ASTM D 3044 plate twisting tests. The modulus of elasticity of PSL was higher than that of MSR while the shear modulus of PSL is

much lower than that of MSR. The modulus of elasticity COV values of MSR and PSL were 18.8% and 11.48 %, respectively, while the shear modulus COV values for MSR and PSL were 11.34% and 7.58%, respectively. For both elastic constants, the COV of the MSR value was greater than the PSL value. The E:G ratio for MSR was 12.9 while the E:G ratio for PSL was 17.8. The measured moduli of elasticity were greater than the rated E for both materials.

Table 3. Test results from plate bending and plate twisting test

Material	Modulus of Elasticity[1], GPa (10^6 psi) [COV]	Shear Modulus[2], GPa (10^6 psi) [COV]	E:G ratio[3]
MSR	14.7 (2.15) [18.8]	1.13 (0.165) [11.3]	12.9:1
PSL	15.2 (2.22) [11. 5]	0.85 (0.124) [7.58]	17.8:1

[1] Modulus of elasticity was measured using plate bending test methods.
[2] Shear modulus was measured using plate twisting test methods.
[3] E:G ratio refers to the E_1:G_{12} ratio.

Comparison of E:G Ratios with Previous Results

Table 4 shows the comparison of the E:G ratio of MSR and PSL from plate testing with the results from Hindman et. al (2006). These results are directly comparable since the test materials of both studies were sampled from the same population. For MSR, the E:G ratio from plate testing was 40.1% less than the FPBT ratio and 40.4% less than the ASTM D 198 Bending ratio. For PSL, the E:G ratio from plate testing was 3.83% less than the FPBT ratio and 46.8% greater than the ASTM D 198 Bending ratio. The plate testing results shows a different elastic relationship for MSR lumber and PSL material. The MSR E:G ratio from plate testing is consistently 40% less than the other test method ratios from structural-sized bending tests, while the PSL has a different relationship. Hindman et al. (2006) and Harrison and Hindman (2007) reasoned that the change in E:G ratio was caused by differences in stress distribution combined

and the vertical density profile for wood composites. Gunnerson et al. (1972) demonstrated that the stress distribution of the plate bending specimen is different from a simple beam due to the high orthotropy of wood materials.

Table 4. Comparison of the measured E_1:G_{12} ratios and Hindman et al. (2006)

Material	Plate Testing E:G Ratio	Hindman et al. (2006)		% Difference of Plate Testing and FPBT[1]	% Difference of Plate Testing and ASTM D 198 Bending[2]
		FPBT E:G Ratio	ASTM D 198 Bending E:G Ratio		
MSR	12.9:1	21.6:1	21.7:1	-40.1%	-40.4%
PSL	17.8:1	18.5:1	12.1:1	-3.83%	46.8%

[1]% Difference = (Plate test – FPBT)/FPBT * 100%

[2]% Difference = (Plate test – ASTM D 198 Bending)/ASTM D 198 Bending * 100%

Table 5 presents the statistical comparison of the elastic modulus and shear modulus results comparing previous research to plate bending results. The analysis of variance (ANOVA) statistical test used an alpha of 0.05 for comparing three different test methods with different sample sizes. The null hypothesis was not rejected for the MSR E values from the three test methods. The Plate Testing vs. ASTM Bending comparison for the PSL G value also did not reject the null hypothesis. In general, the trend of the shear modulus values and modulus of elasticity from PSL was to reject the null hypothesis, indicating that the elastic constant values from the different test methods were significantly different. This statistical comparison demonstrates that the elastic behavior of MSR lumber is different from PSL, which was previously noted by Janowiak et al. (2001).

Table 5. Statistical comparison of E_1 and G_{12} from three different test methods (α=0.05)

Tests for Comparison	Material	p-value for E	p-value for G
Plate Tests vs. FPBT[1]	MSR	0.262	0.000
	PSL	0.037	0.000
Plate Tests vs. ASTM Bending[2]	MSR	0.204	0.010
	PSL	0.000	0.182
Plate Tests vs, FBPT vs. ASTM Bending	MSR	0.369	0.000
	PSL	0.001	0.004

[1] Sixteen data points from Hindman *et al*. (2006)

[2] Eight data points from Hindman *et al*. (2006)

Comparison of MSR Lumber with Previous Plate Testing Results

Table 6 shows the comparison of selected southern pine species test results from Bodig and Goodman (1973) with the results from this study. The elastic constants of longleaf pine (P. *palustris*) were the closest to the test results, with a modulus of elasticity 7.4% less than the average MSR value and a shear modulus 8.7% less than the average MSR value. The E_1:G_{12} ratio for three southern pine groups varied from 12.27 to 18.08. The E_1:G_{12} ratio of MSR was in the range of the ratios given by Bodig and Goodman (1973). .

Table 6 Comparison of the test results to Bodig and Goodman (1973)

Elastic Property	Current MSR Value	Loblolly Pine (*P. taeda*)		Longleaf Pine (*P. palustris*)		Slash Pine (*P. elliottii*)	
		Value[1]	% Diff.[2]	Value[1]	% Diff.[2]	Value[1]	% Diff.[2]
E_1	14.7 GPa	11.1 GPa	-24.8%	14.6 GPa	-7.4%	16.0 GPa	8.2%
G_{12}	1.13 GPa	903 MPa	-20.6%	1.04 GPa	-8.7%	883 MPa	-22.3%
E_1:G_{12}	13.0:1.0	12.3:1.0	-5.3%	14.1:1.0	8.7%	18.1:1.0	39.5%

[1] values from Bodig and Goodman (1973)

[2] % Difference = (Previous Result-MSR)/MSR*100%

Conclusions

This research studied the elastic constants measured from plate testing methods versus ASTM D 198 Bending and the five-point bending test for MSR lumber and PSL. The elastic constant ratios of MSR lumber from the plate testing methods demonstrated a consistent difference with both the ASTM D 198 Bending and FPBT test methods. PSL elastic constant ratios from the plate testing methods did not show a consistent relationship between the two test methods, indicating that the MSR lumber and PSL demonstrate different elastic behaviors possibly due to the manufacture of PSL materials. Statistical comparisons of the modulus of elasticity and shear modulus values indicated that the three test methods produce values that are not significantly different for the MSR modulus of elasticity values and between the plate testing and ASTM Bending for the PSL shear modulus. Except for the above comparisons, the three test methods produced values that were significantly different for the MSR shear modulus and for the PSL modulus of elasticity and shear modulus. Therefore, elastic constant ratios derived from plate testing methods for MSR and PSL are not directly comparable to elastic constant ratios derived from structural sized bending tests. Comparing the MSR lumber values to Bodig and Goodman (1973), the MSR lumber elastic constants were similar to longleaf pine (*P. palustris*).

References

American Society for Testing and Materials (ASTM). 2005a. Standard Specification for Evaluation of Structural Composite Lumber Products. Standard D 5456-03. *In*: Annual Book of ASTM Standard, Section 4, Vol. 04.10 Wood. ASTM, West Conshohocken, PA.

American Society for Testing and Materials (ASTM). 2005b. Standard Test Methods of Static Tests of Lumber in Structural Sizes. Standard D 198-02. *In*: Annual Book of ASTM Standard, Section 4, Vol. 04.10 Wood. ASTM, West Conshohocken, PA.

American Society for Testing and Materials (ASTM). 2005c. Standard Test Methods for Shear Modulus of Wood-Based Structural Panels. Standard D 3044-94. *In*: Annual Book of ASTM Standard, Section 4, Vol. 04.10 Wood. ASTM, West Conshohocken, PA.

American Society for Testing and Materials (ASTM). 2005d. Standard Test Methods for Specific Gravity of Wood and Wood-Based Materials. Standard D 2395-02. *In*: Annual Book of ASTM Standard, Section 4, Vol. 04.10 Wood. ASTM, West Conshohocken, PA

American Society for Testing and Materials (ASTM). 2005e. Standard Test Methods for Direct Moisture Content Measurement of Wood and Wood-Based Materials. Standard D 4442-92. *In*: Annual Book of ASTM Standard, Section 4, Vol. 04.10 Wood. ASTM, West Conshohocken, PA.

Bodig, J. and , J. R. Goodman. 1973. Prediction of elastic parameters for wood. Wood Sci. 5(4): 249-264.

Bodig, J. and B. A. Jayne. 1982. *Mechanics of Wood and Wood Composites*. Van Nostrand Reinhold Company, New York, NY. 714 pp.

Bradtmueller, J. P., M. O. Hunt, K. J. Fridley and G. P. McCabe. 1994. Development of the five-point bending test to determine shear moduli of wood composites. Forest Prod. J. 44(5):17-26.

Gunnerson, R. A., J. R. Goodman and J. Bodig. 1972. Plate Tests for Determination of Elastic Parameters of Wood. Wood Sci. 5(4): 241-248.

Harrison, S. K. and D. P. Hindman. 2007. Test Method Comparison of Shear Modulus Evaluation of MSR and SCL Products. Forest Prod. J. 57 (7). In Press.

Hindman, D. P., J. J.Janowiak and H. B. Manbeck. 2006. Comparison of ASTM D 198 and five-point bending for elastic constant ratio determination. Forest Prod. J. 56(7):85-90.

Janowiak, J. J., D. P. Hindman, H. B. Manbeck. 2001. Orthotropic behavior of lumber composite materials. Wood and Fiber Sci. 33(4):580-594.

USDA Forest Service, Forest Products Laboratory. 1999. *Wood Handbook: Wood as an engineering material.* Forest Prod. Soc., Madison, WI. 463 pp.

Witt, R. K., W. H. Hoppmann, and R. S. Buxbaum. 1953. Determination of Elastic Constants of Orthotropic Materials with Special Reference to Laminates. ASTM Bulletin: 53-57

Appendix 2.

Effect of loading rate and thickness on the tensile properties of wood strands

Gi Young Jeong
Graduate Research Assistant
Department of Wood Science and Forest Products
Virginia Polytechnic Institute and State University
Brooks Forest Products Center
1650 Ramble Road
Blacksburg, VA 24061-0503

Daniel P. Hindman*
Assistant Professor
Department of Wood Science and Forest Products
Virginia Polytechnic Institute and State University
Brooks Forest Products Center
1650 Ramble Road
Blacksburg, VA 24061-0503

David Finkenbinder
Graduate Research Assistant
Department of Wood Science and Forest Products
Virginia Polytechnic Institute and State University
Brooks Forest Products Center
1650 Ramble Road
Blacksburg, VA 24061-0503

Jong N. Lee
Staff Engineer
APA-The Engineered Wood Association
7011 South 19th St.
Tacoma, WA 98466

Zhiyuan Lin
Graduate Research Assistant
Department of Wood Science and Forest Products
Virginia Polytechnic Institute and State University
Brooks Forest Products Center
1650 Ramble Road
Blacksburg, VA 24061-0503

Notice –This appendix appears in the Forest Product Journal, 58(10):33-37.

Abstract

Previous studies evaluating the tensile properties of wood strands used different test conditions and different wood species. Direct comparison of these results cannot be performed. Guidelines for the standardized testing of wood strands are not currently available. Specifically, there is no information on the effect of different loading rates and strand sizes for the tensile properties of wood strands. The goal of this paper was to investigate the effect of loading rate and strand thickness on tensile modulus of elasticity (MOE) and ultimate tensile strength (UTS) of southern pine (*Pinus spp.*) strands. Tensile testing used three different loading rates (0.0102 cm/min, 0.0254 cm/min, and 0.0406 cm/min) and four different specimen thicknesses (0.0381 cm, 0.0794 cm, 0.191 cm, and 0.381 cm). Results showed the UTS and MOE of wood strands generally increased as the thickness increased except for the 0.381 cm thick strands. All of the 0.381 cm strands showed slippage in the grip areas of the specimens, which caused lower average MOE value for this group. Statistical analysis showed that the MOE and UTS from different loading rates were not significantly different, while the MOE and UTS from different strand thicknesses were significantly different. Results of Tukey's HSD comparisons found that MOE and UTS values from the 0.0794 cm and 0.191 cm thick strands were not significantly different. To decrease variability of test results, the authors recommend testing strands at 0.0254 cm/min and a strand thickness between 0.0794 cm and 0.191 cm.

Wood strands are the main constituents of engineered wood products (EWP) including laminated strand lumber (LSL), parallel strand lumber (PSL), oriented strand lumber (OSL) and oriented strand board (OSB). Strand thickness for these EWPs can vary from 0.76 mm to 3.0 mm (Smulski 1997). Currently, there is no test protocol for measurement of the tensile properties of wood strands. While previous studies have measured tensile properties of strands, these results cannot be directly compared because of differences in specimen size, loading rate and wood species. The strand geometry and test methods may affect the tensile properties of wood strands. This study investigates the effect of loading rate and strand thickness on the tensile properties of wood strands.

While there are no ASTM standards for the tensile testing of wood strands, several previous researchers have measured the tensile properties. Table 1 lists previous tensile testing results including the parent wood species, dimensions, loading rate, specific gravity, ultimate tensile strength (UTS) and modulus of elasticity (MOE). As can be seen from Table 1, the loading rate, dimension of the specimens, and parent wood species vary. The loading rate ranged from 0.0127 cm/min to 0.19 cm/min and the thickness of wood strands ranged from 0.038 cm to 0.105 cm.

Table.1 Previous research on the tensile properties of wood strands from different species

Researcher	Species	Dimensions (cm×cm×cm)	Loading rate (cm/min)	Specific gravity	UTS (MPa)	MOE (GPa)
Price (1975)	Sweetgum (*Liquidambar styraciflua L.)*	7.62×0.95× 0.038	0.016[1]	0.58	54.4	4.65
Geimer et al. (1985)	Douglas-fir (*Pseudotsuga menziesii)*	5.71×1.27× 0.038	0.019	0.46	36.8	6.16
Hunt et al. (1989)	Yellow-poplar (*Liriodendron tulipifera L.)*	30.48×1.27× 0.079	0.19	0.50	70.3	11.8
Wu et al. (2005)	Southern pine (*Pinus spp*.)	15.24×2.54× 0.38	0.0127	0.58	49.98	12.84
Hindman and Lee (2007)	Loblolly pine (*Pinus taeda*)	6.0×0.507× 0.066	0.0127	0.55	43.3	4.91
Cai et al. (2007)	Yellow-poplar (*Liriodendron tulipifera L.*)	15.24×2.54× 0.105	0.0127	0.459	48.5	8.71
Cai et al. (2007)	Loblolly pine (*Pinus taeda*)	15.24×2.54× 0.105	0.0127	0.539	58.7	8.60

[1] Tension properties were measured at a gage length of 3.81 cm (1.25 in).

Price (1975) studied the effect of gage length on the stiffness and strength of sweetgum flakes. The average UTS value increased as the gage length increased while the average MOE value decreased as the gage length increased. Geimer et al (1985) measured the MOE and UTS of two different grades of Douglas-fir strands. Hunt et al. (1989) measured the MOE and UTS as well as a stress wave MOE for yellow poplar strands. Good correlation was found between the tensile MOE and stress wave MOE. Wu et al. (2005) measured the MOE and UTS of southern pine strands and found that these properties were similar to solid wood. Hindman and Lee (2007) measured the MOE and UTS of loblolly pine strands. Cai et al. (2007) extended the work of Wu et al. (2005) by testing willow, yellow-poplar, red oak, and southern pine strands using the

same methods as Wu et al. (2005).

Table 1 demonstrates the variability of test conditions and test results found by previous researchers. For example, comparing the loblolly pine results of Hindman and Lee (2007) and Cai et al. (2007), the MOE is 75% greater and UTS is 36% greater from Cai et al. (2007). Similarly, the yellow-poplar results of Hunt et al. (1989) are 37% greater for MOE and 20% greater for UTS than the results from Cai et al (2007). These comparisons are complicated by different strand sizes and loading rates.

Although many researchers have measured the MOE and UTS of wood strands, the results are not directly comparable because of different loading conditions and different wood species. Specific guidelines for testing wood strands would allow comparison of different test methods. The goal of this paper is to compare the MOE and UTS results of southern pine strands (*Pinus spp.*) under different loading rates and strand thickness.

Materials and Methods

Clear, straight grained rectangular strand specimens were cut from a single piece of southern pine (*Pinus spp.*) lumber using a disc flaker. The average strand dimensions were 13.97 cm long by 2.54 cm wide. Strand thickness varied between four different levels : 0.0381 cm, 0.0794 cm, 0.1905 cm, and 0.381 cm. All strands were conditioned in an environmental chamber at 25.4 degrees C and 36% RH, resulting in an equilibrium moisture content of 7.0%. The strands were stored for two weeks of conditioning in reclosable plastic bags which were sealed during testing to prevent moisture loss when the samples were outside of the environmental chamber.

Table 2 shows the experimental plan used for testing. Three different loading rates and

four different strand sizes were evaluated in a split-plot design. The different loading rates were chosen so correspond to strain rates of 0.002 cm/cm/min, 0.005 cm/cm/min and 0.008 cm/cm/min. The different thicknesses of strands were chosen based upon the range of strand thicknesses from the previous research in Table 1. A minimum of 30 specimens were tested for each combination of specimen thickness and loading rate used, with Table 2 giving the exact numbers for each test factor.

Table 2. Experimental Plan for Evaluating Tensile Properties

Loading Rate	Strand Thickness			
	0.0381 cm	0.0794 cm	0.191 cm	0.381 cm
0.0102 cm/min		31		
0.0254 cm/min	32	31	30	30
0.0406 cm/min		30		

Strands were loaded in tension parallel to grain, in accordance with the provisions of ASTM D 1037 (ASTM 2005a). Testing equipment included an MTS universal testing machine with a 44.5 kN load cell, pressure-driven tension grips and a clip extensometer, as shown in Figure 1. The test span was 10.2 cm from grip to grip. The clip extensometer was a DSST-II (Measurement Technology Inc.) with a gage length of 5.08 cm that was centered between the grips to limit end effects.

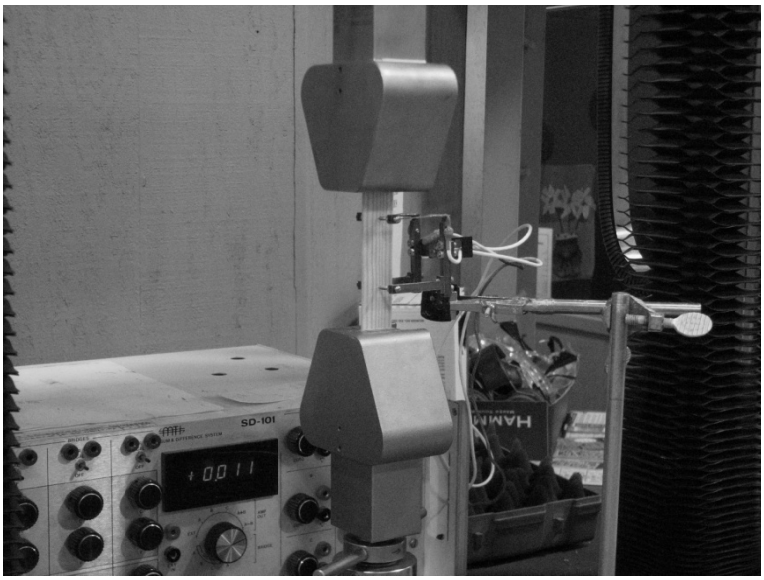

Figure 1. Tensile Testing of Wood Strands

Commercial data acquisition software recorded the load-deflection curve for each sample. The MOE and UTS were calculated from the load-deflection curve and maximum load value, respectively, according to procedures included in ASTM D 1037 (ASTM 2005a). After failure occurred, the wood strands were visually inspected for the failure mode.

Figure 2 shows five different failure modes associated with wood strands under tension. These failure modes were adapted from ASTM D 143 (2005b) testing of compression specimens, with the removal of the crushing and brooming failures and the addition of grip-related failures. The shear failure mode has a crack propagating at a 45 degree angle across the width of the strand. The wedge split failure mode has a transverse crack with or without longitudinal cracking. The grip failure mode shows a fracture at the edge of the area of the specimen contained in the grip. Grip failures are often thought of as failures that occur before the maximum load of the specimen is achieved. Statistical analysis of a subset of strands tested demonstrated no difference in the strength and stiffness of strands with and without grip failures.

The splitting failure mode shows splitting in the longitudinal direction. The slippage failure mode shows a crosshatched pattern and a reduced thickness of the sections held within the grips, which may occur along with one of the other failure modes.

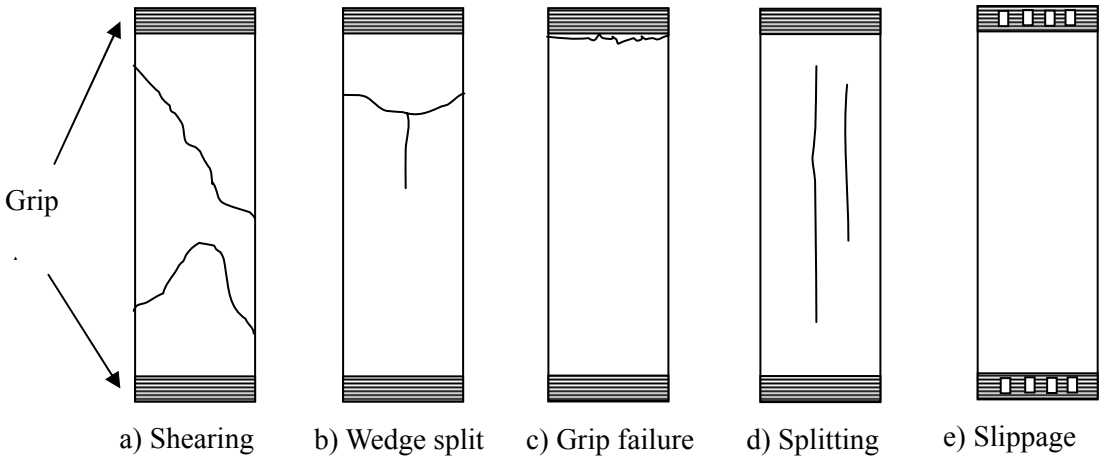

Figure 2. Failure Modes of Wood Strands under Tensile Loading

Untested specimens were selected from the 0.381 cm thickness for moisture content and specific gravity measurement. The largest size strand was chosen for ease of measurement. Since all specimens were flaked from the same board and all strands were conditioned in the same environmental chamber, the moisture content and specific gravity from this subset were assumed to be equal for the set of strands tested. Measurement of moisture content followed Method A of ASTM D 4442 (ASTM 2005c) and measurement of specific gravity followed Method A in ASTM D 2395 (ASTM 2005d).

Results and Discussion

Table 3 shows the moisture content and specific gravity values. The specific gravity determined from these strands was identical to the specific gravity assumed in the National Design Specification for Wood Construction (NDS) (AF&PA 2005) for the Southern Pine species group.

Table 3. Moisture Content and Specific Gravity from Untested 0.381 cm Strands

Thickness of Strand	Moisture Content, % (COV)	Specific Gravity, (COV)
0.381 cm	7.8% (1.2%)	0.55 (3.4%)

Table 4 shows the average MOE and UTS measured from each strand group. The MOE COV values ranged from 10.7% to 18.9%, and the UTS COV values ranged from 11.6% to 25.1%. The Wood Handbook (USDA 1999) predicts that the COV associated with the tensile testing of solid wood is 25%. The average MOE and UTS values are similar for all strand thickness sizes, except for the 0.381 cm thick specimens.

Table 4. Modulus of Elasticity and Tensile Strength Results from Strand Testing

Strand Thickness, cm	Loading Rate, cm/min	MOE, GPa (COV)	UTS, MPa (COV)
0.0381	0.0254	11.4 (15.6%)	37.3 (21.3%)
0.0794	0.0102	12.1 (15.0%)	50.0 (24.3%)
0.0794	0.0254	12.9 (12.0%)	47.2 (18.2%)
0.0794	0.0406	13.2 (18.9%)	52.2 (25.1%)
0.191	0.0254	13.5 (13.4%)	46.0 (14.5%)
0.381	0.0254	0.22 (10.7%)	73.8 (11.6%)

Table 5 shows the strand failure modes from Figure 2 in terms of the percentage of sample size for each loading rate and strand thickness. Comparing the 0.0794 cm results at different loading rates, shear failures were 61.3-83.9% of the failures, wedge failures were 12.9-

29.0% of the failures, grip and splitting failures accounted for 10.0% or less of the failures, and no slip failures were noted. Comparing the 0.0254 cm/min results at different strand thicknesses, specimens with 0.191 cm or less thickness exhibited similar trends in failure mode percentages, while the 0.381 cm specimens differed significantly. For 0.381 cm thick specimens, slip failures occurred in all of the specimens, regardless of the presence of other failure types. The differences in the 0.381 cm specimens from Table 5 correspond with an observed lower MOE value in Table 4 for this group. The slippage observed indicates that this test arrangement may not be suitable for testing strands with a thickness of 0.381 cm.

Table 5. Summary of Failure Mode Occurrences

Loading Rate	Thickness	Failure (% of set)				
cm/min	cm	Shear	Wedge	Grip	Splitting	Slip
0.0102	0.0794	83.9%	12.9%	0.0%	3.2%	0.0%
0.0254	0.0381	71.9%	21.9%	0.0%	6.3%	0.0%
	0.0794	61.3%	29.0%	3.2%	6.5%	0.0%
	0.191	83.3%	6.7%	0.0%	10.0%	0.0%
	0.381	16.7%	6.7%	3.3%	20.0%	100.0%
0.0406	0.0794	76.7%	13.3%	10.0%	0.0%	0.0%

Figure 5 shows the average MOE and UTS values of wood strands with varying load rate and a thickness of 0.0254 cm. The error bars in Figure 5 represent one standard deviation positive and negative to the average value. The average MOE value increases slightly as loading rate increases. The MOE error bars for different loading rates overlap. The average UTS value for the 0.0254 cm/min loading rate is less than the average UTS of the other two loading rates. The UTS error bars for different load rates overlap.

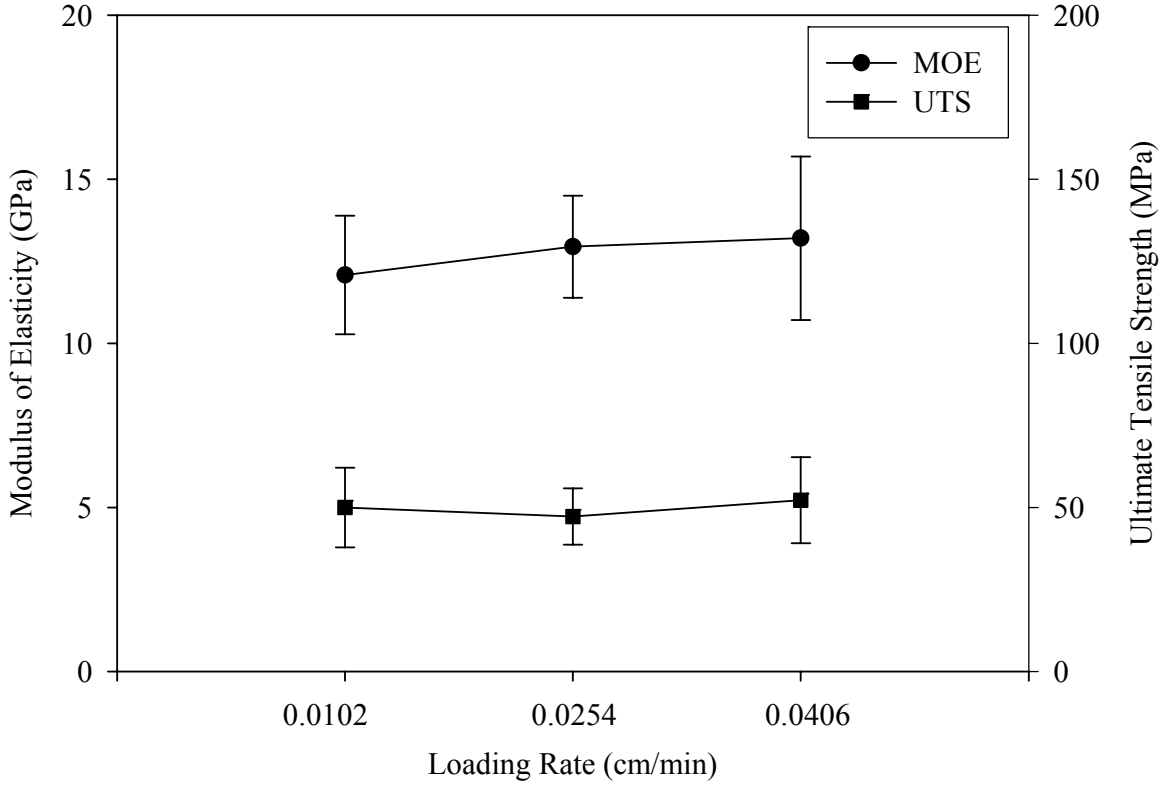

Figure 5. MOE and UTS of wood strands at different loading rates and constant thickness (0.0254 cm)

Figure 6 shows the MOE and UTS values of wood strands with varying thickness at a loading rate of 0.0254 cm/min. The error bars in Figure 6 represent one standard deviation positive and negative to the average value. The average MOE value increases as thickness increases, except for the 0.381 cm size. The lower average MOE value for the 0.381 cm thickness corresponds to the slippage failures from Table 5. The error bars of the MOE values at different thicknesses overlap, except for the 0.381 cm value. The average UTS value increases

as thickness increases, except for the 0.191 cm thickness, which had a UTS value similar to the 0.0794 cm thickness. The UTS results from the varying thickness do not appear to be affected by the slippage failures at the 0.381 cm thickness. The error bars for the three smaller thicknesses overlap for the UTS values.

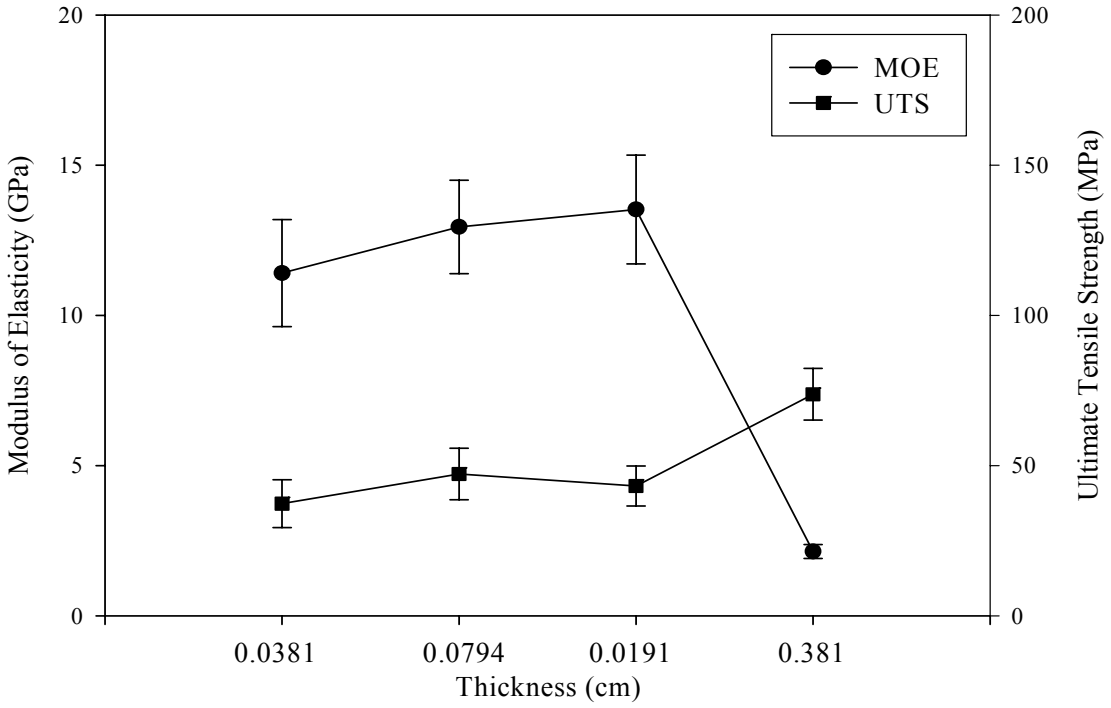

Figure 6. MOE and UTS of wood strands at different strand thicknesses and constant load rate (0.0254 cm/min).

Table 6 shows the analysis of variance (ANOVA) results for the statistical comparison of the MOE and UTS values considering different loading rates and strand thickness. Comparing the different loading rates, both MOE and UTS had p-values greater than an alpha of 0.05, indicating no statistical difference. Comparing the different strand thicknesses, both MOE and UTS had p-values less than an alpha of 0.05, indicating a statistical difference. For these

different strand thicknesses, subsequent Tukey's Honestly Significant Difference (HSD) multiple comparison analysis was performed to determine the relationship of the statistical difference. The MOE values from the 0.381 cm thick specimens were significantly less than all other tested thicknesses due to the slippage in the grips. The UTS values from the 0.381 cm thick specimens were significantly greater than all other tested thicknesses. The MOE values from the 0.0381 cm thick specimens were significantly less than the 0.0794 cm and 0.191 cm thick specimens. The UTS values from the 0.0381 cm thick specimens were significantly less than the other tested thickness. No difference was detected between the MOE and UTS values at the 0.0794 cm and 0.191 cm thicknesses. These results correspond with the error bar trends noted in Figure 5 and Figure 6.

Table 6 Analysis of variance (ANOVA) comparisons of MOE and UTS

Variable	Property Comparison	p-value[c]
Loading Rate[a]	Modulus of elasticity	0.0740
Loading Rate[a]	Tensile strength	0.2380
Specimen Thickness[b]	Modulus of elasticity	0.0000
Specimen Thickness[b]	Tensile strength	0.0000

[a]Constant specimen thickness = 0.76 mm

[b]Constant loading rate = 0.254 mm/mm/min

[c]$\alpha = 0.05$

The increase of MOE and UTS with increasing thickness seems counter-intuitive compared to current solid-sawn lumber design. In the NDS, no modification of reference MOE values is made for changes in cross-section, while there is a size factor (C_F) applied to the reference strength terms which increases the strength as the specimen width decreases (AWC 2005). The size factor for solid-sawn lumber accounts for the increased probability of knots and

other defects in larger cross-sections that could act as strength-reducing characteristics. All samples for this testing were clear, straight grained, and free of defects, negating this kind of a size factor. A survey of current strand testing literature has not found any results on the thickness effect associated with the MOE and UTS of wood strands to support or contradict these findings. The 0.381 cm thickness seems to be a limiting value for this testing arrangement for stiffness measurement.

Based on the results of this testing, the authors recommend that the loading rate in the range of 0.0102 cm/min to 0.0406 cm/min did not significantly affect the MOE and UTS values found. However, the MOE and UTS showed a general increase in value with increasing strand size. Caution should be exercised in using thick strands greater than 0.191 cm for MOE measurement to prevent slippage of the specimens in the grips. Based upon the COV values of the results in Table 4 and the results of the Tukey's HSD, the 0.0254 cm/min with a strand thickness between 0.0794 cm and 0.191 cm is recommended.

Conclusions

The effect of different loading rate and strand thickness upon the MOE and UTS of southern pine (*Pinus spp.*) strands was studied. With a constant strand thickness of 0.0794 cm, changes in the loading rate in the range of 0.0102 cm/min to 0.0406 cm/min did not produce significantly different MOE and UTS values at a level of α=0.05. At the thickest strand size of 0.381 cm, all of the strands had slippage in the grips, which produced a lowered MOE value. Over the range of strand sizes tested, the MOE and UTS values were significantly different. Using Tukey's HSD comparisons, the MOE and UTS values were not significantly different for strand thicknesses of 0.0794 cm and 0.191 cm. Based upon these results, the authors recommend

testing strands at 0.0254 cm/min (0.005 cm/cm/min) and between a thickness of 0.0794 cm and 0.191 cm to reduce variability.

References

American Forest and Paper Association. 2005. National Design Specification for Wood Construction. American Forest and Paper Association.

American Society for Testing and Materials (ASTM). 2005a. ASTM D 1037 Standard Test Methods for Evaluating Properties of Wood-Base Fiber and Particle Panel Materials. *In*: Annual Book of ASTM Standard, Section 4, Vol. 04.10 Wood. ASTM, West Conshohocken, PA.

American Society for Testing and Materials (ASTM). 2005b. ASTM D 143 Standard Test Methods for Small Clear Specimens of Timber. *In*: Annual Book of ASTM Standard, Section 4, Vol. 04.10 Wood. ASTM, West Conshohocken, PA.

American Society for Testing and Materials (ASTM). 2005c. ASTM D 4442. Standard Test Methods for Direct Moisture Content Measurement of Wood and Wood-Base Materials *In*: Annual Book of ASTM Standard, Section 4, Vol. 04.10 Wood. ASTM, West Conshohocken, PA.

American Society for Testing and Materials (ASTM). 2005d. ASTM D 2395. Standard Test Methods for Specific Gravity of Wood and Wood-Based Materials. *In*: Annual Book of ASTM Standard, Section 4, Vol. 04.10 Wood. ASTM, West Conshohocken, PA.

Cai, Z., Q. Wu, G. Han, and J. N. Lee. 2007. Tensile and thickness swelling properties of strands from Southern hardwoods and Southern pine: Effect of hot-pressing and resin application. Forest Prod. J. 57(5):36-40.

Geimer, R. L., R. J. Mahoney, S. P. Loehnertz, and R. W. Meyer. 1985. Influence of processing induced damage on the strength properties of oriented strand wood products. Forest Prod. J. 50(11/12):33-42.

Hindman, D. P. and J. N. Lee. 2007. Modeling wood strands as multi-layer composites: bending and tension loads. Wood and Fiber Sci. in Process.

Hunt, M. O., M. H. Triche, G. P. McCabe, and W. L. Hoover. 1989. Tensile properties of yellow-poplar veneer strands. Forest Prod. J. 39(9).

Price E. W. 1975 Determining tensile properties of Sweetgum veneer flakes. Forest Prod. J. 26(10): 50-53.

Smulski, S. 1997. *Engineered wood products, a guide for specifiers, designers and users.* PFS Research Foundation. Madison, WI. 294 p.

United Stated Department of Agriculture. 1999. *Wood Handbook: Wood as an engineering material*. Forest Products Society. FPL-GTR-113. Madison, WI. 463 p.

Wu, Q., Z. Cai, and J. N. Lee. 2005. Tensile and dimensional properties of wood strands made from plantation southern pine lumber. Forest Prod. J. 52(2):1-6